The Geological Society of America Bulletin

Volume 72 March 1961 Number 3

CONTENTS

Age and stratigraphic relations of the Formosa reef limestone (Middle Devonian) of southwestern Ontario . . . . . *J. A. Fagerstrom* 341–350

Precambrian rocks and their relationship to Laramide structure along the east flank of Bighorn Mountains near Buffalo, Wyoming . . . . . *Richard A. Hoppin* 351–368

Hydrothermal magnetite . . . . . *William T. Holser and Cecil J. Schneer* 369–386

Welded tuffs and flows in the rhyolite plateau of Yellowstone Park, Wyoming . . . . . *Francis R. Boyd* 387–426

Limnology, sedimentation, and microorganisms of the Salton Sea, California. . . . . *Robert E. Arnal* 427–478

SHORT NOTES

Method for predicting line-of-sight capabilities: preliminary investigations . . *Joan B. Snell* 479–484

Bald Mountain limestone, New York: new facts and interpretations relative to Taconic geology. . . . . *John E. Sanders, Lucian Platt, and R. W. Powers* 485–488

Ground-water contamination in the Rocky Mountain Arsenal area, Denver, Colorado . . . . . *Theodore R. Walker* 489–494

Experimental deformation of viscous layers in oblique stress fields . . . . . *A. R. McBirney and Myron G. Best* 495–498

Subscriptions $15.00 per year. Printing Office: Burlington, Vt. Second-class postage paid at Burlington, Vermont. Published monthly.

Communications regarding publications should be addressed to The Geological Society of America, Dr. Frederick Betz, Jr., Secretary, 419 West 117 Street, New York 27, N. Y.

Please give notice of change of address 4 weeks in advance. Claims for nonreceipt of the Bulletin of a given month must be sent to the Secretary of the Society before the end of the second succeeding month.

PAPERS IN PRESS FOR FORTHCOMING ISSUES

THE STRATIGRAPHIC PANORAMA (An Inquiry into the Bases for Age Determination and Age Classification of the Earth's Rock Strata). Hollis D. Hedberg

PALEOTEMPERATURE ANALYSIS OF THE PLIO-PLEISTOCENE SECTION AT LE CASTELLA, CALABRIA, SOUTHERN ITALY. C. Emiliani, T. Mayeda, and R. Selli

SEISMIC EVIDENCE SUPPORTING A NEW INTERPRETATION OF THE CODY TERRACE NEAR CODY, WYOMING. John H. Moss and William E. Bonini

LUNAR FEATURES AND LUNAR PROBLEMS. L. W. LeRoy

STRUCTURE OF THE GLENARM SERIES IN CHESTER COUNTY, PENNSYLVANIA. Hugh McKinstry

PATTERNS AND ORIGIN OF RADIAL DIKE SWARMS ASSOCIATED WITH WEST SPANISH PEAK AND DIKE MOUNTAIN, SOUTH-CENTRAL COLORADO. Ross B. Johnson

LIMNOLOGY AND AMINO-ACID CONTENT OF SOME LAKE DEPOSITS IN MINNESOTA, MONTANA, NEVADA, AND LOUISIANA. Frederick M. Swain

ALGODONES DUNES OF SOUTHEASTERN CALIFORNIA. Robert M. Norris and Kenneth S. Norris

NEW FOREIGN BIBLIOGRAPHY

BIBLIOGRAPHY AND INDEX OF GEOLOGY EXCLUSIVE OF NORTH AMERICA. Volume 23. Marie Siegrist, Mary C. Grier, and others

Price, $13.00
Special price to Fellows and Members of GSA, $8.50

NEW MEMOIRS

82. OLIGOCENE PLANTS FROM THE UPPER RUBY RIVER BASIN, SOUTHWESTERN MONTANA. Herman F. Becker

Description of a well-preserved flora (37 families, 61 genera, and 82 identifiable species, 25 of which are new) from Tertiary fossiliferous shales of the Ruby River basin. The author uses the flora to interpret the paleoecology and paleoclimatology and suggests that the Ruby and Florissant assemblages represent a single botanical province.

128 pages, 4 figures, 32 photographic plates
Price, $4.25
Special price to Fellows and Members of GSA, $3.00

83. BIOSTRATIGRAPHIC STUDIES IN THE COMANCHE (CRETACEOUS) SERIES OF NORTHERN MEXICO AND TEXAS. Bob F. Perkins

The author relates the biostratigraphy of the Aurora limestone of southwestern Coahuila to the type Aurora and to the type Lower Cretaceous of northern Texas and reports stratigraphic revisions of the Fredericksburg and Washita groups of north Texas. He describes a fauna of larger invertebrates from the upper member of the Aurora and on paleontological evidence correlates the member with the Fort Worth limestone and Grayson marl. He concludes that the Aurora limestone is of epineritic origin, deposited far from any source of terrigenous clastic material.

138 pages, 26 figures, 3 maps in color, 29 photographic plates
Price, $6.00
Special price to Fellows and Members of GSA, $4.50

J. A. FAGERSTROM *Dept. Geology, University of Nebraska, Lincoln, Nebr.*

Age and Stratigraphic Relations of the Formosa Reef Limestone (Middle Devonian) of Southwestern Ontario, Canada

Abstract: The Formosa reef limestone consists of a localized three-dimensional cluster of very pure, massive limestone reefs (bioherms) outcropping as irregular knobs in a roughly elliptical area in southern Bruce and northern Huron counties, Ontario. Outcrop and subsurface evidence indicates that the reefs are small, numerous, scattered over an outcrop area of about 150 square miles, and occur through a stratigraphic interval of approximately 200 feet within the brown, bituminously laminated dolomite of the Detroit River group (undifferentiated), which is about 240 feet thick in the area.

CONTENTS

Introduction 341
Stratigraphy 342
Regional relations 342
Stratigraphic nomenclature 344
Formosa reef limestone 344
Definition 344
Lithologic description 346
Thickness and lateral extent 346
Stratigraphic position 346
Conclusions 348
References cited 349

Figure
1. Generalized geologic map showing the outcrop area of the Formosa reef limestone in southwestern Ontario 343

Table
1. Summary of the historical development of stratigraphic nomenclature of the Devonian rocks in southwestern Ontario and the stratigraphic position of the Formosa reef limestone as inferred by the writer 345
2. Description of upper part of section from J. B. McKenzie No. 1 well 348

INTRODUCTION

Although the reefs outcropping in the area around Formosa, Ontario, have been known in geological literature since 1863 (Logan, 1863, p. 371), their age and stratigraphic relations have been the subject of considerable controversy since Stauffer (1915, p. 10) equated their fauna with that of the Alpena limestone of Michigan. Since Stauffer's work these reefs have been included in the Onondaga limestone (Pohl, 1930, p. 59), the Delaware limestone (Cooper *et al.*, 1942, p. 1754), the Norfolk formation of Caley (1943, p. 47), and the Detroit River group (Best, 1953, Ph.D. thesis, Univ. Wisconsin, p. 3). (*See* Table 1.)

Before Best's detailed study of the pre-Hamilton Devonian rocks of southwestern Ontario, most evidence for the age of the reefs was based on supposed similarities of their fauna with better known faunas of Michigan (Alpena limestone), New York (Onondaga limestone), and Ohio (Delaware limestone). Since the contacts between the reefs and the adjacent beds are rather inaccessible and poorly exposed, correlation by stratigraphic position was largely overlooked or subordinated to faunal correlation, although Stauffer (1915, p. 146), Goudge (1938, p. 211), and Caley (1943, p. 49) reported seeing the contact between the reefs and the underlying dolomite.

Field work by the writer during July 1958 and the examination of cuttings from a well which penetrated a subsurface reef have confirmed the unpublished (Ehlers, personal communication; Best, 1953, Ph.D. thesis, Univ. Wisconsin) stratigraphic placement of these reefs as a three-dimensional cluster within the

Geological Society of America Bulletin, v. 72, p. 341–350, 1 fig., March 1961

Detroit River group. Whether they are restricted to either the Lucas or Amherstburg formations or occur in both, as Best suggests (1953, p. 145), has not been satisfactorily determined.

The present writer investigated the problem of determining the age of the reefs by both lithostratigraphic and paleontologic methods; the lithostratigraphic evidence is the subject of this paper, and the paleontologic evidence will be reviewed in a detailed report on the reef fauna (Fagerstrom, 1961). The lithostratigraphic evidence is much more conclusive than the paleontologic evidence, since the fauna contains many new species, long ranging species known previously from beds of Bois Blanc to early Hamilton age, and only four species restricted to the Detroit River group. The value of even these four in correlation is somewhat doubtful. (*See* Fagerstrom, 1961.) The previous errors in paleontologic correlation of the reefs (Stauffer, 1915, p. 10; Cooper *et al.*, 1942, p. 1754) may be largely attributed to a misunderstanding of the peculiarities inherent in the fauna of the entire Detroit River group and the relations of these rocks with the adjacent formations. The peculiarities of the fauna are evident from the fact that Lane *et al.* (1909) believed that the group was of late Silurian age. Until the Detroit River fauna and stratigraphy are understood in more detail the exact age of the Formosa reefs will remain uncertain.

This manuscript has been critically reviewed by E. C. Stumm, L. I. Briggs, J. A. Dorr, E. N. Goddard, and D. F. Eschman. To all the above the writer is most grateful. Part of the field expense was borne by a grant from the Graduate Student Research Fund at the University of Michigan.

STRATIGRAPHY

Regional Relations

The dominant tectonic features controlling the environment of deposition and the present-day distribution of the Devonian sedimentary rocks in this region are the Michigan basin on the west and Allegheny synclinorium on the east, separated approximately along the axis of the southwestern Ontario peninsula by the Findlay arch. Across the axis of this arch there is a transverse trough toward which the surface and near-surface rocks dip; this feature is called the Chatham sag (Figure 1). The Devonian formations outcrop as broad, irregular arcs striking nearly parallel to the trend of the axis of the Chatham sag from Lake Erie on the south to Lake Huron on the northwest. The youngest Devonian strata (Kettle Point formation) occur in an area approximately coincident with the Chatham sag; successively older beds outcrop on both sides of the Kettle Point formation toward Windsor on the southwest and Woodstock on the northeast.

The Detroit River group is one of these pre-Kettle Point stratigraphic units having equivalents on both sides of the sag. The type section of the group is along the Detroit River in southwestern Ontario, southeastern Michigan, and northwestern Ohio where it contains four formations; in ascending order these are the Sylvania sandstone, Amherstburg dolomite, Lucas dolomite, and Anderdon limestone (Ehlers, Stumm, and Kesling, 1951, p. 24).

Best's study (1953, Ph.D. thesis, Univ. Wisconsin) included only the pre-Hamilton Devonian rocks northeast of the Chatham sag occurring in a broad arc from Fort Erie on the east, through London and Stratford, to Port Elgin on the north. Within this area he recognized two contrasting lithologic facies in the rocks of the Detroit River group (Best, 1953, p. 1395). In the quarries around Ingersoll, Best (1953, Ph.D. thesis, Univ. Wisconsin, p. 108–116) identified the Lucas and Amherstburg formations, both consisting of limestone which he combined under the term "southern facies." To the north in the Brussels-Wingham-Teeswater area the dominant lithology of the group is dolomite (Best, 1953, Ph.D. thesis, Univ. Wisconsin, p. 121–129), which he was unable to subdivide into individual formations. At St. Mary's the limestones of the "southern facies" and the dolomites to the north interfinger, so that the Detroit River section here consists of about equal amounts of each lithology. Because of this very gradual facies change and his inability to differentiate the Lucas and Amherstburg formations outside the Ingersoll area, Best mapped the Detroit River group as one unit over his entire area of study.

In Landes' report (1951, p. 15) on the subsurface aspects of the Detroit River group in the Michigan basin, he also recognized only the Lucas and Amherstburg formations and included the Sylvania sandstone as the lower member of the Amherstburg, limited in its occurrence to the central and southeastern portions of the basin. As noted by Cooper *et al.* (1942, p. 1754–1755), the stratigraphic relations of the Anderdon limestone are very poorly known, since it has not been recognized outside the type area.

The discrepancies indicated in Table 1 for

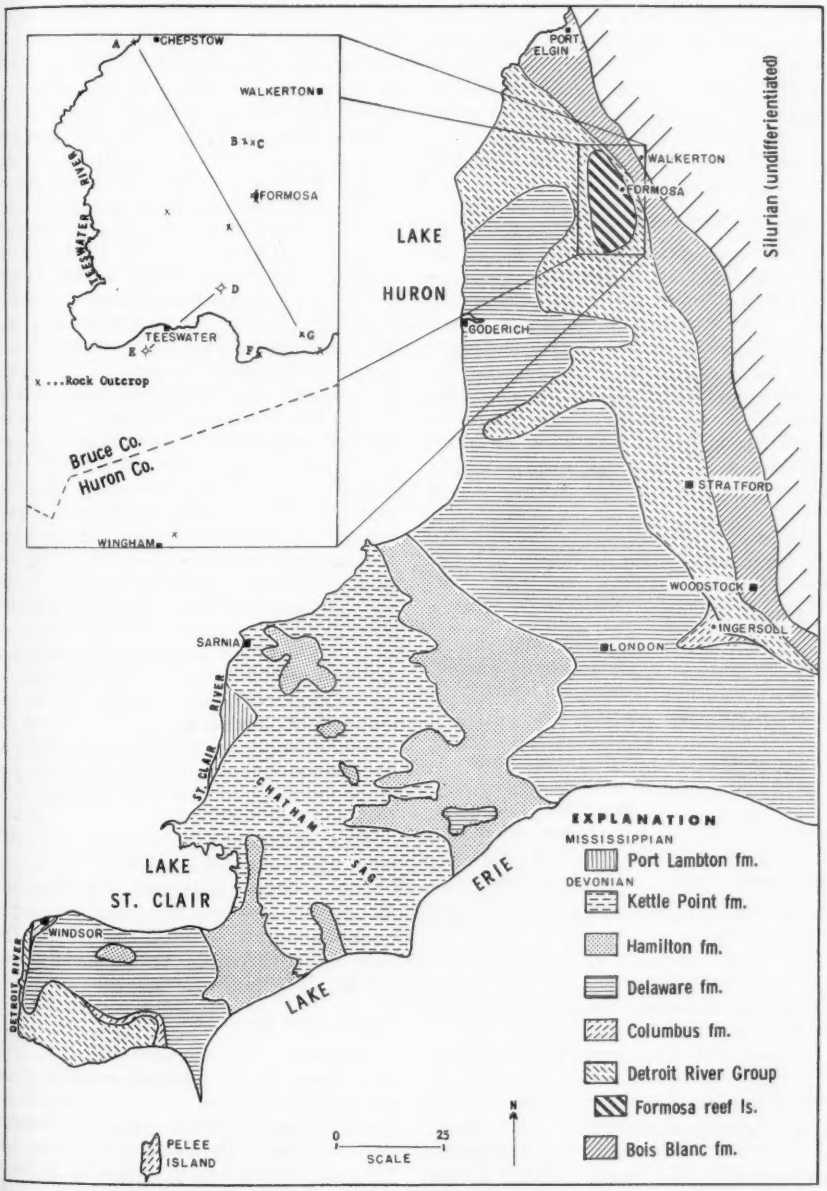

Figure 1. Generalized geologic map showing the outcrop area of the Formosa reef limestone in southwestern Ontario (Adapted from Sanford, 1958)

the age of the Detroit River group are not so great as they may appear, since they are in part due to the placement of the boundary between the Lower and Middle Devonian. Cooper *et al.* (1942) include the Detroit River group in the Lower Devonian, and Ehlers, Stumm, and Kesling (1951) place it in the Middle Devonian. Regardless of whether the Detroit River group is Lower or Middle Devonian, it is nonetheless equivalent in age to part of the Onondaga limestone of New York.

Stratigraphic Nomenclature

The history of the Devonian stratigraphic nomenclature in southwestern Ontario has been thoroughly discussed by Best (1953, Ph.D. thesis, Univ. Wisconsin, p. 4–12) and is summarized in part in Table 1. Logan (1863) gave one of the first Devonian geologic columns for southwestern Ontario which included from oldest to youngest the Oriskany sandstone, Corniferous limestone, and Hamilton shale; these units had all been established previously and named by the New York State Geological Survey.

Lane *et al.* (1909) introduced the term Detroit River series for the upper part of Lane's Monroe formation (*in* Wadsworth, 1893, p. 66) and gave the following tabulation (p. 556):

	Lucas dolomite
Upper Monroe	Amherstburg dolomite
or	Anderdon limestone
Detroit River series	Flat Rock
	Disconformity
Middle Monroe	Sylvania sandstone
	Disconformity
	Raisin River dolomite
Lower Monroe	Put-in-bay dolomite
or	Tymochtee beds
Bass Islands series	Greenfield dolomite

The complete Monroe group was considered to be of late Silurian age.

This same tabulation was duplicated by Grabau and Sherzer (1910, p. 27). The Monroe thus included all beds between the Salina group and the Dundee limestone.

Nattress (1912) first asserted that the Detroit River group is Devonian rather than Upper Silurian. He based his argument on chemical and stratigraphic characteristics of the Anderdon limestone which have very questionable validity (p. 281–282). Stauffer (1916, p. 77) discussed the possibility of a Devonian age for the Detroit River rocks; however, the relations between the Detroit River and the Oriskany as suggested by Stauffer are quite erroneous. Williams (1919, p. 18) declared the Detroit River to be Devonian and supported his claim by faunal evidence (p. 19–20) for the first time. Williams, like Stauffer, confused the relations between the Oriskany and the Detroit River by incorrectly correlating the unconformity below the Oriskany with the unconformity above the Detroit River. This error persisted until as late as 1938 when Goudge (p. 8) also placed the Oriskany above the Detroit River.

The modern concept of the stratigraphic relations of the Detroit River group is embodied in two reports by Ehlers (1945; 1950) and one by Ehlers and Stumm (1951). In 1945, Ehlers (p. 35, 107) recognized that his new Bois Blanc formation underlay the Detroit River group and correlated the Bois Blanc with the lower part of the Onondaga limestone of New York. He also correctly established that his new Garden Island formation was equivalent to the Oriskany sandstone of New York and Ontario (p. 75) and also that it was older than the Detroit River (p. 35). In 1950, Ehlers (p. 1455-1456) corrected the errors in the stratigraphic sequence of formations in the Detroit River group as listed by Lane *et al.* (1909, p. 556) and eliminated the use of their Flat Rock formation. The revised Detroit River thus included from oldest to youngest the Sylvania sandstone, Amherstburg dolomite, Lucas dolomite, and Anderdon limestone in the type area. In 1951 Ehlers and Stumm reported the discovery of the Columbus limestone overlying the Detroit River group near Ingersoll, Ontario. The Columbus is equivalent to the upper part of the Onondaga of New York (Cooper *et al.*, 1942, p. 1774).

Thus the stratigraphic sequence was established which was used in the latest map by the Geological Survey of Canada of southwestern Ontario; the Devonian formations are listed in ascending order as Oriskany, Bois Blanc, Detroit River, Columbus, Delaware, Hamilton, and Kettle Point (Sanford, 1958).

Formosa Reef Limestone

Definition. The abundant limestone reefs outcropping in the region of southern Bruce and northern Huron counties, Ontario, especially in and around the village of Formosa, are herein named the Formosa reef limestone. The type locality is designated as the highway road cut 2½ miles north of Formosa, which includes the eastern edge of Lot 72, Concession IS, Greenock Township, and the western edge

TABLE 1.—SUMMARY OF THE HISTORICAL DEVELOPMENT OF STRATIGRAPHIC NOMENCLATURE OF THE DEVONIAN ROCKS IN SOUTHWESTERN ONTARIO AND

TABLE 1.—SUMMARY OF THE HISTORICAL DEVELOPMENT OF STRATIGRAPHIC NOMENCLATURE OF THE DEVONIAN ROCKS IN SOUTHWESTERN ONTARIO AND THE STRATIGRAPHIC POSITION OF THE FORMOSA REEF LIMESTONE AS INFERRED BY THE WRITER

		BEST (1953)	COOPER ET AL (1942)	EHLERS & STUMM (1951)	CALEY (1943)	POHL (1930)	STAUFFER (1915)	LOGAN (1863)
UPPER DEVONIAN	SENECAN		KETTLE POINT BLACK SH.		KETTLE POINT FM.	SENECA CHEMUNG	PORT LAMBTON BEDS	PORTAGE AND CHEMUNG GROUP
						GENESEE	HURON SH.	
MIDDLE DEVONIAN	ERIAN		FINGER LAKS			ERIE	HAMILTON FM. FRL	HAMILTON FM.
			TAGHANIC		HAMILTON	WIDDER "ENCRINAL LS."		
			TIOUGHNIOGA	DELAWARE LS.		"OLENTANGY SH."	DELAWARE LS.	
			UPPERWASH LS.	COLUMBUS LS.		ULSTER		CORNIFEROUS LS. FRL
			PETROLIA SH.	DETROIT RIVER GROUP	NORFOLK FRL	"ALPENA LS." FRL	ONONDAGA LS.	
			WIDDER SH.			ONONDAGA		
			HUNGRY HOLLOW					
		DELAWARE FM.	ARKONA SH.			ORISKANY	ORISKANY SS.	ORISKANY SS.
			CAZENOVIA DELWARE LS. FRL	ONONDAGA LS.		ORISKANY		
LOWER DEVONIAN	ULSTERIAN	*COLUMBUS FM.	ONESQUETHAW		FM.			
		LUCAS FM. FRL	ONONDAGA LS.					
		AMHERSTBURG	SPRINGVALE SS.					
		BOIS BLANC FM.	DEERPARK			DETROIT RIV.	HELDERBERGIAN	
		* ORISKANY FM.	ORISKANY SS.			LUCAS AMHERSTBURG ANDERSON FLAT ROCK		
		*(MISSING IN FORMOSA AREA)	HELDERBERG		FRL=FORMOSA REEF LS.	HELDERBERG		

of Lot A, Concession IIIS, Brant Township, Bruce County (Fig. 1, outcrop B).

The outcrops of these reefs occur within a roughly elliptical area extending north-south for about 22 miles from Chepstow in Bruce County to just northeast of Wingham in Huron County. The maximum diameter of the area is about 9 miles from west of Teeswater to northeast of Belmore in Bruce County. This area of outcrop has been designated on the maps of Stauffer (1915), Caley (1943), and Best (1953, Ph.D. thesis, Univ. Wisconsin), although only Stauffer indicated it by a separate color pattern.

The most numerous exposures of this limestone occur within the village of Formosa and in the area of the Falls of the Teeswater River (Fig. 1, outcrop F) from Lot 5, Concession III, Culross Township, upstream for about 1 mile. The reefs are exposed in nine other localities, but in most of these the outcrops are rather small sections (2–5 feet) of minor stratigraphic importance.

Lithologic description. The lithology of the Formosa reef limestone has been suitably described by Stauffer (1915, p. 138), Caley (1943, p. 47), and Best (1953, Ph.D. thesis, Univ. Wisconsin, p. 105) but for convenience is herein redescribed.

As indicated by Goudge (1938, p. 213–214) the limestone is extremely pure; the average calcium carbonate content of four samples is 99.13 per cent. The unweathered surface is light gray weathering to a dull blue gray. The massive reef character of the limestone is apparent from the absence of bedding and the mound-shaped outcrops, which occur as resistant hills and cliffs. The reef framework consists of thin, flat, laminar stromatoporoid and tabulate coral colonies which locally constitute more than half of the rock mass. The limestone between the organic materials is locally dense and fine-grained or coarsely crystalline and has an almost brecciated appearance due to secondary recrystallization. Vugs are particularly abundant and are concentrated in the more fossiliferous parts of the rock. In many places the vugs apparently have grown from the internal cavities between the valves of brachiopods. Many specimens show partial recrystallization; the cavity is lined by singly terminated calcite crystals, much like a small geode, and part of the valve is gaping, as though separated by growth of the crystals. This relation between vugs and fossils was also noted by Stauffer (1915, p. 143) and agrees well with Bassler's ideas on geode formation (1908, p. 134) in the Mississippian limestones of Kentucky.

In most outcrops the flank beds have been removed by erosion, with the notable exception of the type locality where they are exposed toward the north end of the road cut. The flanks are characteristically very uneven, thin beds of brownish, dolomitic limestone weathering to irregular chips and generally barren of identifiable fossil remains.

Thickness and lateral extent. The thickness of the Formosa reef limestone varies considerably from reef to reef and within any one reef ranges from a feather edge to a maximum near the center. Since the outcrops in the Falls of the Teeswater River area are scattered, a precise measurement of the total thickness of any one of the reefs is impossible, although Stauffer (1915, p. 138) suggests as much as 40 feet in this area. The maximum thickness at the type locality is 29½ feet (Best, 1953, Ph.D. thesis, Univ. Wisconsin, p. 103).

Subsurface evidence from a well drilled just west of Teeswater indicates a thickness of reef limestone of 51 feet, which is the maximum known at present.

Stauffer (1915, p. 138), Goudge (1938, p. 31), and Caley (1943, p. 49) treated the Formosa reef limestone as though all the outcrops were part of a single reef once covering the entire area and occurring at one stratigraphic level. However, more recent study by Best (1953, Ph.D. thesis, Univ. Wisconsin, p. 106) and the writer indicates that there are several (perhaps as many as 100) reefs of the platform (Fairbridge, 1950, p. 345–347), table or patch (Cloud, 1952, p. 2128) varieties, none of which is more than 1000 feet in diameter. They average about 400–600 feet in diameter and occur within a stratigraphic interval of at least 200 feet within the Detroit River group.

Stratigraphic position of the Formosa reefs. Since Logan's initial correlation of the Formosa reefs with the Corniferous (Onondaga in modern usage) limestone (1863, p. 371), five other authors have attempted correlations ranging in age from the Detroit River group to the Alpena limestone. These various opinions are tabulated in Table 1.

The results of detailed field investigations in the Formosa, Teeswater, and Chepstow areas by Best (1953, Ph.D. thesis, Univ. Wisconsin) and the writer leave little doubt that the reefs are overlain and underlain by typical brown to buff, bituminous laminated dolomite of the

Detroit River group. However, in no case to date have fossils restricted to the Detroit River group, such as *Prosserella*, been collected from either the adjacent dolomite or from the reef limestones. The Detroit River age of the reefs is based solely on presumed lithologic correlations of the adjacent beds.

The sections wherein these stratigraphic relations between the reefs and the Detroit River dolomite can be demonstrated are summarized as follows:

(1) Lot 8, Con. VI, Greenock Twp., Bruce Co., Ont. (Fig. 1, outcrop A)

At low water, outcrops along the banks of the Teeswater River half a mile west of Chepstow from the highway bridge upstream for about 1000 feet, reveal 13.4 feet of Detroit River group dolomite underlying 1.2 feet of Formosa reef limestone (Best, 1953, Ph.D. thesis, Univ. Wisconsin, p. 129). Contact is sharp between the two lithologic units.

(2) Lot B, Con. III, Carrick Twp., Bruce Co., Ont. (Fig. 1, outcrop C)

An abandoned quarry of the Ontario Hydro-Electric Company is located a quarter of a mile east of the type locality 2½ miles north of Formosa. Approximately 200 feet north of the quarry face a small test pit has been excavated and about 20 feet of the Detroit River group exposed. Although the contact with overlying reef limestone cannot be determined, it occurs within a 5- to 10-foot covered interval.

In 1938 Goudge (p. 211) reported this locality and correctly identified the rocks below the reef as Detroit River but erred in following Stauffer's (1915) identification of the reefs as Alpena limestone.

(3) Lot 4, Con. III, and Lot 4, Con. IV, Culross Twp., Bruce Co., Ont. (Fig. 1, outcrop F)

The Falls of the Teeswater River contains numerous outcrops of the Formosa reef limestone and the Detroit River group. At the falls the river divides into two channels cut through a group of reefs and drops over a 5-foot ledge of reef limestone in a series of rapids and falls. About 300 feet downstream from the falls on the south bank an isolated outcrop exposes a 20-foot section of Detroit River dolomite. Topographically, the lower 5 feet of this outcrop lies below the base of the falls, and the remaining 15 feet is on the same level as the reef limestone at the falls and in the walls of the gorge above. On the south side of the valley about 500 feet farther downstream another section of reef limestone about 5 feet thick outcrops topographically higher than all other outcrops in the area.

These topographic relations indicate that the reef limestones occur above, below, and at the same stratigraphic level as the outcrop of the Detroit River dolomite. Best (1953, Ph.D. thesis, Univ. Wisconsin, p. 141) reported dips up to 24° in this area; however, these measurements probably are localized primary dips of the reef flank beds.

(4) Lot 18, Con. V, Culross Twp., Bruce Co., Ont. (Fig. 1, point E)

In addition to the outcrop evidence for the stratigraphic position of the reefs, there was one important well (J. B. McKenzie No. 1 of the Dominion Natural Gas Co., Ltd.) drilled just southwest of Teeswater which penetrated a subsurface reef of the same lithology as those at the outcrop.

Table 2 gives a brief description of the upper portion of the section.

The decision to include this subsurface reef as part of the Formosa reef limestone is based on a study of the local rock structure in relation to the topographic occurrence of a few representative reefs. In addition to the McKenzie No. 1 well, another well—Armstrong No. 1, E. P. Rowe Co. (Fig. 1, point D)—was drilled on Lot 5, Concession VIII, of Culross Township. These wells are about 4 miles apart, and the line (Fig. 1, D-E) joining them is about parallel to the regional dip. In the McKenzie well the Detroit River—Bois Blanc contact occurs at an elevation of 768 feet; the same contact in the Armstrong well is at 816 feet (Louis I. Briggs, personal communication). These relations give a dip in this area of about 12 feet per mile into the Michigan basin. This is much less than the structural relief cited by Landes (1951, p. 14) for the base of the Lucas formation in the southern peninsula of Michigan (35 feet per mile).

Two reef outcrop areas occur along the Teeswater River about 3 miles southeast of the line joining the above cited wells; these areas are critical for the proper understanding of the stratigraphic relations of the Formosa reef limestone. The reefs at the Falls of the Teeswater River (Fig. 1, outcrop F) occur at an elevation of approximately 1000 feet; another reef on Lot A, Concession A, of Carrick Township (Fig. 1, outcrop G), 1¾ miles east of the falls, is at about 1100 feet. If these two reefs were at the same stratigraphic level the dip of this horizon would be nearly five times the dip determined from the wells 3 miles away, or

about 57 feet per mile. These relations demonstrate that the Formosa reefs do not occur at the same stratigraphic level within the Detroit River group.

The reef in the bank of the Teeswater River just west of Chepstow occurs at the lowest elevation (900 feet) of any exposed reef in the Formosa area. The direction of a line (Fig. 1, A-G) joining this locality and the reef in the stratigraphic relations of the Detroit River group has been a slow process, and at present these relations are still imperfectly known. Perhaps one of the major factors in this confusion has been the problems arising from the lateral lithologic variation of the group between incomplete and widely scattered outcrop areas. The general scarcity and poor preservation of the fossils in the dolomitic portions has made

Table 2.—Description of Upper Part of Section from J. B. McKenzie No. 1 Well

Elevation (in feet)	*Thickness (in feet)*	*Formation*	*Lithologic description*
1039–1006	33		Glacial drift
1006–881	125	Detroit River group	Dolomite, brown to buff, dense and fine-grained becoming a dolomitic limestone calcarenite in the lower 4 feet
881–830	51	Formosa reef limestone	Limestone, light gray, sugary texture with abundant stromatoporoids and *Favosites*
830–798	32		Limestone calcarenite, light gray, becoming dolomitic toward base, with a few rounded quartz sand grains
798–768	30	Detroit River group	Dolomite, dark brown, sugary texture with thin wavy bituminous bands and increasing amounts of light-gray chert toward base
768–589	179	Bois Blanc formation	Chert, white to light gray, with 25–50 per cent brown dolomite

Carrick Township noted in the previous paragraph is nearly parallel to the regional strike, so that the difference in elevation of about 200 feet between these two reefs is probably not an effect of dip and lends support to the assumption that the reefs are not all the same age. Since most evidence supports this assumption there can be no objection to including a reef just 20 feet below the level of the Chepstow locality as part of the Formosa reef limestone, even though it is wholly in the subsurface and cannot be studied faunally.

This entire cluster of exposed and subsurface reefs is related to a long episode of intermittent reef building in this region. Perhaps additional drilling will reveal more reefs of this type in adjacent areas and thus extend the sphere of reef development both laterally and vertically.

CONCLUSIONS

As noted by Best (1953, Ph.D. thesis, Univ. Wisconsin, p. 100–103) the understanding of paleontologic correlation both difficult and hazardous.

Thus in the entire area of his study Best (1953, Ph.D. thesis, Univ. Wisconsin) was able to apply the formation names of the Detroit River group as used in the type area only around Ingersoll. Similarly the stratigraphic relations of the Formosa reef limestone with Best's "southern facies" (1953, Ph.D. thesis, Univ. Wisconsin, p. 104) and with the type area are as yet unknown and await more detailed study. Perhaps additional subsurface and careful stratigraphic and paleontologic study will eventually solve the problem. Reefs occur locally in the Amherstburg and Anderdon formations outcropping in the type area, and other reefs may occur in the Detroit River group around Beachville, Ontario. However, correlation of the Formosa reefs with any of these on the basis of present knowledge would be quite uncertain. (*Cf.* Briggs, 1959, p. 52.)

REFERENCES CITED

Bassler, R. S., 1908, The formation of geodes, with remarks on the silicification of fossils: U. S. Natl. Mus. Proc., v. 35, p. 133–154

Best, E. W., 1953, Pre-Hamilton Devonian stratigraphy, southwestern Ontario, Canada (Abstract): Geol. Soc. America Bull., v. 64, p. 1395

Briggs, L. I., 1959, Physical stratigraphy of Lower Middle Devonian rocks in the Michigan basin: Mich. Basin Geol. Soc. Field Trip Guidebook, 63 p.

Caley, J. F., 1943, Paleozoic geology of the London area, Ontario: Canada Geol. Survey Mem. 237, 171p.

Cloud, P. E., Jr., 1952, Facies relationships of organic reefs: Am. Assoc. Petroleum Geologists Bull., v. 36, p. 2125–2149

Cooper, G. Arthur, *et al.*, 1942, Correlation of the Devonian sedimentary formation of North America: Geol. Soc. America Bull., v. 53, p. 1729–1794

Ehlers, G. M., 1945, Stratigraphy of the surface formations of the Mackinac Straits region: Dept. Conserv. (Mich.), Geol. Survey Div. Pub. 44, Geol. Ser. 37, p. 19–120

— 1950, Revised classification of the Middle Devonian Detroit River group (Abstract): Geol. Soc. America Bull., v. 61, p. 1455–1456

Ehlers, G. M., and Stumm, E. C., 1951, Middle Devonian Columbus limestone near Ingersoll, Ontario, Canada: Am. Assoc. Petroleum Geologists Bull., v. 35, p. 1879–1888

Ehlers, G. M., Stumm, E. C., and Kesling, R. V., 1951, Devonian rocks of southeastern Michigan and northwestern Ohio: Geol. Soc. America Field Trip Guidebook (Detroit), 40 p.

Fagerstrom, J. A., 1961, The fauna of the Middle Devonian Formosa reef limestone of southwestern Ontario: Jour. Paleontology, v. 35, p. 1–48, 14 Pls.

Fairbridge, R. W., 1950, Recent and Pleistocene coral reefs of Australia: Jour. Geology, v. 58, p. 330–401

Goudge, M. F., 1938, Limestones of Canada; Part IV, Ontario: Canada Bur. Mines, Dept. Mines and Resources, no. 781, 362 p.

Grabau, A. W., and Sherzer, W. H., 1910, The Monroe formation of southern Michigan and adjoining regions: Mich. Geol. and Biol. Survey Pub. 2, Geol. Ser. 1, 248 p., 32 Pls.

Landes, K. K., 1951, Detroit River group in the Michigan basin: U. S. Geol. Survey Circ. 133, 23 p.

Lane, A. C., Prosser, C. R., Sherzer, W. H., and Grabau, A. W., 1909, Nomenclature and subdivision of the upper Siluric strata of Michigan, Ohio, and western New York: Geol. Soc. America Bull., v. 19, p. 553–556

Logan, W. E., 1863, Report on the geology of Canada: Can. Geol. Survey Rept. of Progress to 1863, 983 p.

Nattress, T., 1912, Geology of the Detroit River area: Ont. Bur. Mines 21st Ann. Rept., v. 21, pt. 1, p. 281–287

Pohl, E. R., 1930, Devonian formations of the Mississippi basin: Jour. Tenn. Acad. Sci., v. 5, p. 54–63

Sanford, B. V., 1958, Geological map of southwestern Ontario showing oil and natural gas producing areas: Can. Geol. Survey Map 1062A

Stauffer, C. R., 1915, The Devonian of southwestern Ontario: Canada Geol. Survey Mem. 36, 341 p.

— 1916, Relative age of the Detroit River series: Geol. Soc. America Bull., v. 27, p. 72–77

Wadsworth, M. E., 1893, Report of the state geologist for 1891–1892: Rept. State board of Geol. Survey (Mich.) for 1891 and 1892, p. 59–73

Williams, M. Y., 1919, The Silurian geology and faunas of Ontario peninsula, and Manitoulin and adjacent islands: Can. Geol. Survey Mem. 111, 195 p., 34 Pls.

Manuscript Received by the Secretary of the Society, September 21, 1959

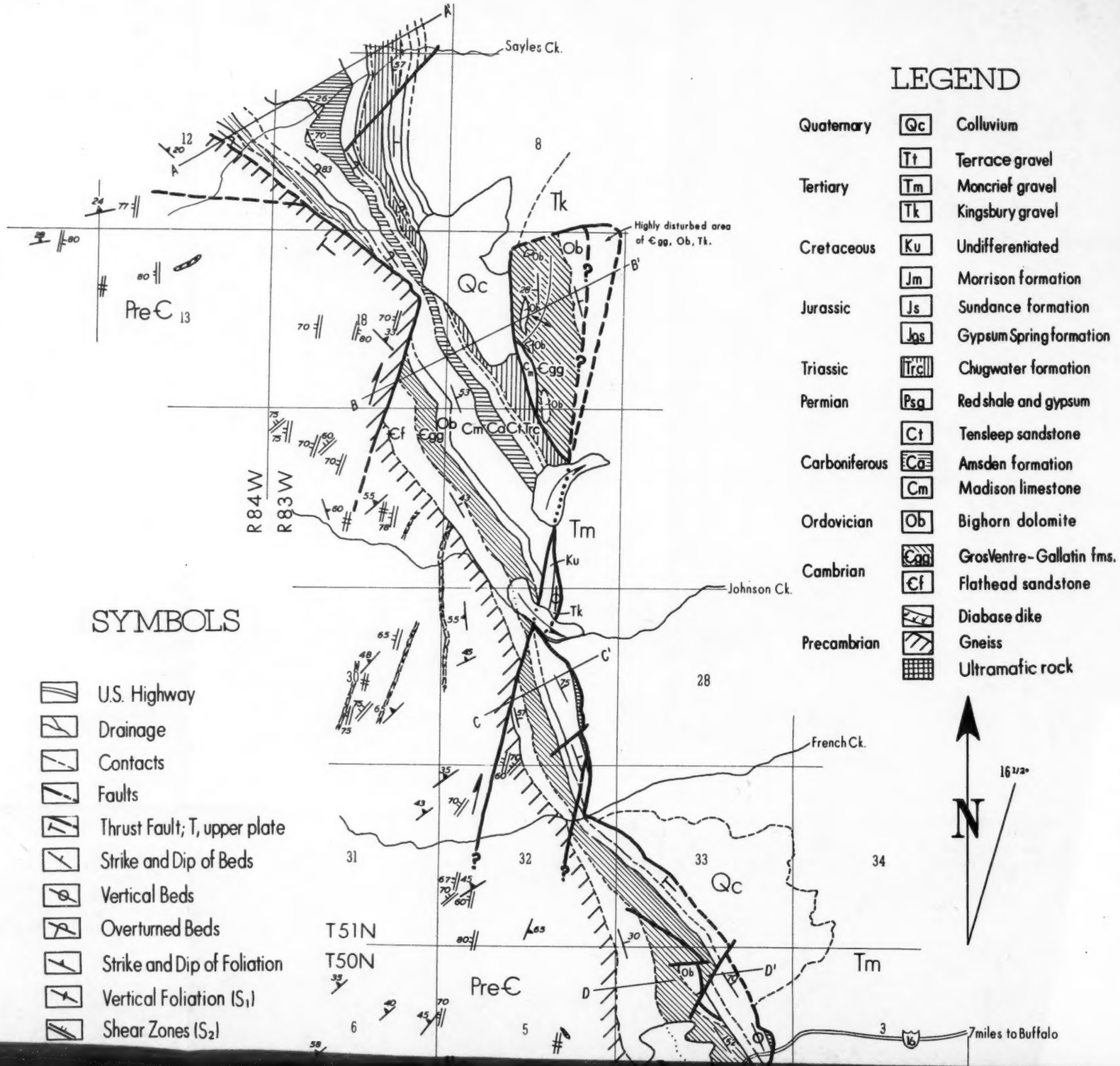
Sayles Ck.
Highly disturbed area of €gg, Ob, Tk.
Johnson Ck.
French Ck.
7miles to Buffalo
Pre€
Qc
Tk
Tm
Ku
Ob
Cm
Ca
Ct
Trc
€gg
€f
R84W
R83W
T51N
T50N
16 1/2°
N
LEGEND
Quaternary
Qc Colluvium
Tt Terrace gravel
Tertiary
Tm Moncrief gravel
Tk Kingsbury gravel
Cretaceous
Ku Undifferentiated
Jm Morrison formation
Jurassic
Js Sundance formation
Jgs Gypsum Spring formation
Triassic
Trc Chugwater formation
Permian
Psg Red shale and gypsum
Ct Tensleep sandstone
Carboniferous
Ca Amsden formation
Cm Madison limestone
Ordovician
Ob Bighorn dolomite
Cambrian
€gg Gros Ventre-Gallatin fms.
€f Flathead sandstone
Precambrian
Diabase dike
Gneiss
Ultramafic rock
SYMBOLS
U.S. Highway
Drainage
Contacts
Faults
Thrust Fault; T, upper plate
Strike and Dip of Beds
Vertical Beds
Overturned Beds
Strike and Dip of Foliation
Vertical Foliation (S1)
Shear Zones (S2)

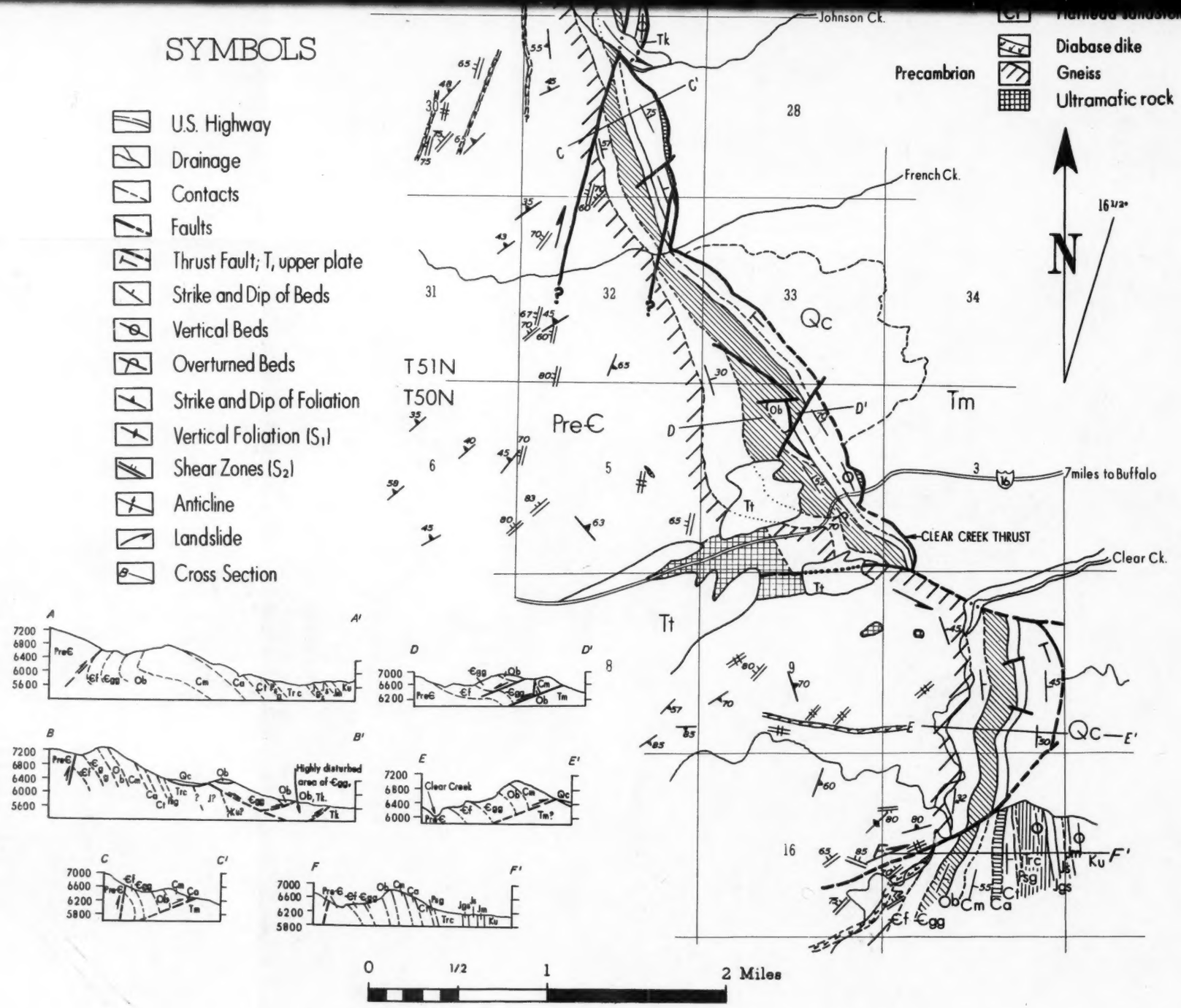

GEOLOGIC MAP AND CROSS SECTIONS, CLEAR CREEK THRUST AREA

NEAR BUFFALO, WYOMING

HOPPIN, PLATE 1
Geological Society of America Bulletin, volume 72

RICHARD A. HOPPIN *Dept. Geology, State University of Iowa, Iowa City, Iowa*

Precambrian Rocks and their Relationship to Laramide Structure along the East Flank of the Bighorn Mountains near Buffalo, Wyoming

Abstract: Precambrian crystalline rocks and younger sedimentary rocks were involved in Laramide deformation in the western part of the United States. Near Buffalo, Wyoming, two high-angle dextral faults striking N. 10° E. cut both the upturned sedimentary rocks and the crystalline basement. As this trend does not correspond to directions of transcurrent faulting expected with east–northeast-west–southwest compression (indicated by the north–northwest-trending Clear Creek thrust and upturned sedimentary rocks), the writer studied Precambrian rocks to see if basement structure controlled the strike of the N. 10° E. faults.

The Precambrian complex consists of quartz-biotite-plagioclase gneiss and migmatite with minor hornblende gneiss and amphibolite. These rocks are greatly deformed and partly granitized. Mafic dikes and small ultramafic bodies cut the complex. Early foliation and layering are obscured by later shear fracturing. Three prominent directions of high-angle fractures are N. 10° E., N. 45° E., and N. 75°–80° W.

In the sedimentary rocks, N. 45° E. and N. 75° E.–N. 75° W. fracture sets are well developed; the N. 10° E. set is poorly developed.

The pronounced development of the N. 10° E. fractures and shear zones in the Precambrian rocks and absence of these structure trends in the sedimentary rocks suggest that these fractures and shears were formed during a Precambrian deformation and provided zones of weakness which controlled Laramide tear faulting. Three diabase dikes in the Precambrian rocks between the faults also follow this direction.

The other two trends cutting both the gneisses and the sedimentary rocks are probably Laramide in age, although an east-west dike and a northeast-trending dike in the south end of the area suggest that movement was reactivated along older Precambrian fractures.

CONTENTS

Introduction 352
Acknowledgments 352
Previous work in the Bighorn Mountains 352
Geologic setting 352
Scope and method of study 353
Precambrian rocks 356
General statement 356
Structures in the gneiss 356
Microscopic features of the gneiss 357
Other rock types 359
Coarse feldspathic bodies and pegmatites. . . 359
Amphibolite 359
Ultramafic rocks 359
Mafic dikes 360
Summary of Precambrian events 360
Fracture analysis 360
General statement 360
Area north of Johnson Creek 362
Area between Johnson Creek and Highway 16 . 362
Area south of Highway 16 363
Sisters Hill area 364
Summary 365
Problems of regional control and the forces responsible for uplift 365
Conclusion 366
References cited 366

Figure
1. Index map of the Bighorn Mountains area, Wyoming 353
2. Geologic map of the Sisters Hill area, Wyoming 354
3. Diagrammatic sketch showing relationship of the N. 10° E. wrench faults to the expected directions of shear for a maximum principal stress acting along a N. 65° E. direction. 355
4. Fracture distribution diagrams of Clear Creek area, Wyoming 361
5. Fracture distribution diagrams of Sisters Hill area, Wyoming 364

Plate Facing
1. Geologic map and cross sections, Clear Creek thrust area near Buffalo, Wyoming . . . 351
2. Clear Creek thrust and Johnson Creek wrench fault, Wyoming. 356
3. Precambrian rocks from Clear Creek thrust area near Buffalo, Wyoming 357
4. Photomicrographs of gneisses from Clear Creek thrust area near Buffalo, Wyoming . . . 358
5. Shearing in sedimentary rocks in ridge north of Johnson Creek, Wyoming 359

Geological Society of America Bulletin, v. 72, p. 351–368, 5 figs., 5 pls., March 1961

INTRODUCTION

Various investigators, notably Bucher,Chamberlin, and Thom (1933), Bucher, Thom, and Chamberlin (1934), and Cloos and Cloos (1934), believed that lines of weakness in Precambrian crystalline rocks of the Western United States exerted a strong control on the Laramide deformation there. Chamberlin (1945) clearly summarized these views. Bucher, Thom, and Chamberlin (1934) posed a number of problems concerning this postulated control that are still appropriate. Unfortunately, many of the investigations they suggested were not carried out.

Three questions summarize the problems of the origin of mountain ranges such as the Bighorn, Beartooth, and Wind River ranges. These are: (1) Did Precambrian structures in any way control the trends of Laramide faults and minor folds? (2) Did the Precambrian structures control the regional trends of the ranges; or were the trends controlled more by a strong Laramide stress system? (3) Were the uplifts due dominantly to vertical forces or to horizontal compression?

Many writers have attempted to answer these questions, but in most cases they have not substantiated their conclusions by study of the Precambrian rocks. Writers have credited or discredited the crystalline basement for many things without making a detailed investigation of it (*See* Beckwith, 1941, for example). Detailed work has been undertaken only in recent years, particularly by Poldervaart and his coworkers in the Beartooth Mountains, by Spencer in the Madison Range, and by me and my students in the Bighorn Mountains. This study is concentrating on the petrography, petrology, structure, and history of the Precambrian core. Also involved are supporting studies in the sedimentary formations along the margins of the range. Hopefully these studies will clarify the structural evolution of the Bighorn Mountains.

This paper presents data and interpretations dealing with the first of the three problems noted and brief comments relating to the other two.

ACKNOWLEDGMENTS

This study was made possible through support by the Penrose Bequest of The Geological Society of America. R. F. Hudson and G. S. Stone assisted in the field, and K. A. Sargent drafted the illustrations. I am particularly grateful for stimulating discussions with J. J. Prucha, Jr,. D. U. Wise, E. W. Spencer, and R. P. Nickelsen.

PREVIOUS WORK IN THE BIGHORN MOUNTAINS

Darton (1906a; 1906b) did the first major mapping of the Bighorn Mountains. His reports still serve as the basic source material for the geology of the range as a whole.

Wilson (1934) studied fracturing in the Precambrian rocks of the Five Springs Creek area in the northwest part of the range. He based his interpretations mainly on granite tectonics and presented no petrographic data. I have collected samples of rocks in that area and found them to be metamorphic gneisses and granitization granites very much like the rocks elsewhere in the core of the range; the area must be reexamined and re-evaluated.

Demorest (1941) mapped the east flank of the range in more detail than had Darton. Sharp (1948) clarified the relationships between the two lower Tertiary gravels along the east flank and added to our knowledge of the tectonic events of the Laramide.

Osterwald (1949; 1955; 1959) provided the first detailed petrologic study of Precambrian rocks of the northern Bighorn Mountains. This work was carried out at the north end of the crystalline core west of Sheridan, Wyoming. He also mapped foliation and mentioned the existence of fractures and shear zones. Osterwald's 1959 report contains a map of the central part of the range, but the supporting data are too scattered to be of other than reconnaissance value.

Hose (1954; 1955) and Maple (1954) mapped parts of the east fllank. Their reports are mainly concerned, however, with the geology of the adjacent parts of the Powder River Basin and currently are the best sources of published stratigraphic information for the area.

GEOLOGIC SETTING

The Bighorn Mountains (Fig. 1) extend for 120 miles from the Bridger Mountains in the south to a synclinal basin in the north. The range averages 25–30 miles in width. Elevations range from 10,000–13,000 feet along the crest to 7000–8000 feet on the subsummit surface. Elevations in the basins adjacent to the range are between 4500 and 5000 feet.

Darton (1906a, p. 13) described the range as a simple anticlinal flexure with the sedimentary rocks draped more or less passively over the rising anticlinal arch. Thom (1947, p. 176) be

lieves that the range is made up of several elevated and tilted blocks. He divides the Bighorn Mountains into four units: (1) a northern block, extending from the Montana-Wyoming state line to the north end of the range: (2) a north-central segment with reverse faults on the northwest flank; (3) a south-central segment which includes the Piney and Clear Creek thrusts with upper plates thrust eastward and extends south to the Crazy Woman fault; and (4) the south Bighorn block in which the movement of the hanging walls of reverse faults was toward the west.

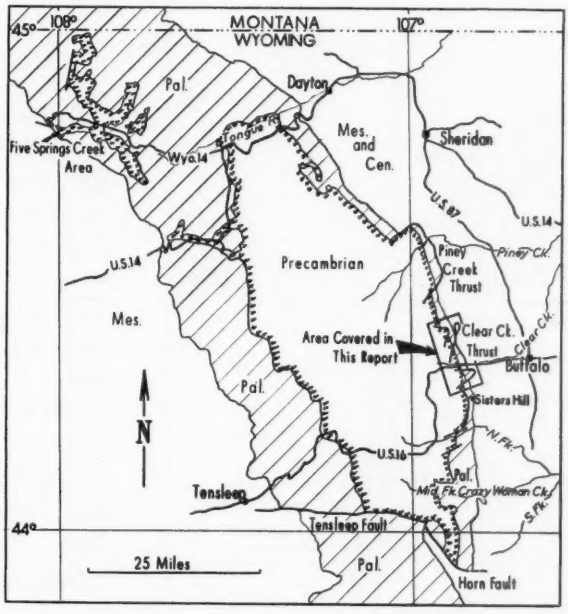

Figure 1. Index map of the Bighorn Mountains area, Wyoming

The area of this report (Fig. 1; Pl. 1) lies along a portion of the east flank of the south-central segment. It includes the Clear Creek thrust and several prominent wrench faults. The Paleozoic sedimentary rocks (about 2350 feet thick) forming the frontal parapets dip steeply to the east; locally their dips are vertical or overturned to the west. At the southeast and northeast ends of the area, some of the Triassic and Jurassic rocks (about 1650 feet thick) of the basin are vertical or overturned. Thick accumulations of Tertiary gravels lie directly east of the Clear Creek thrust (Sharp, 1948). These gravels are present only immediately ahead of this thrust and the Piney thrust to the north. These two salients must have been very active during the Laramide. The movements culminated with the thrusting of the Paleozoic formations onto the gravels.

Four miles south of the Clear Creek thrust just north of Sisters Hill, a small wedge of the Precambrian was thrust over the Flathead and Gros Ventre formations. The sedimentary rocks are greatly overturned and locally faulted in the vicinity of this wedge. This small area was mapped (Fig. 2) and analyzed in the same manner as the main area.

SCOPE AND METHOD OF STUDY

The most logical first step in the study of the possible control of later deformation by Precambrian structure is to deal with the margins of the range where both the Precambrian core and the overlying sedimentary formations were involved in Laramide movements. The area chosen for this study (Fig. 1) lies along the east flank of the range 4 miles west of Buffalo,

Wyoming. It extends 12 miles from the south end of the Clear Creek thrust (Pl. 2, fig. 1) north to Sayles Creek. The strip is 1–3 miles in width.

This area was selected because of the presence of several prominent high-angle wrench faults which displace the contact of the Precambrian and Flathead (Middle Cambrian) rocks. Of special interest are two dextral wrench faults (Pl. 2, fig. 2) in the north part of the area (Pl. 1) which trend N. 10°–15° E. These two faults appear to have anomalous directions if we assume that the local Laramide stresses responsible for the thrust and upturned flank of the range were applied essentially horizontally along a N. 65° E. direction. Wrench faults would be expected along conjugate shear directions making angles of 30° or less with the principal stress direction, such as the two offsets at the south end of the Clear Creek thrust. The two faults trending N. 10°–15° E. fall outside of the expected directions (Fig. 3). This sug-

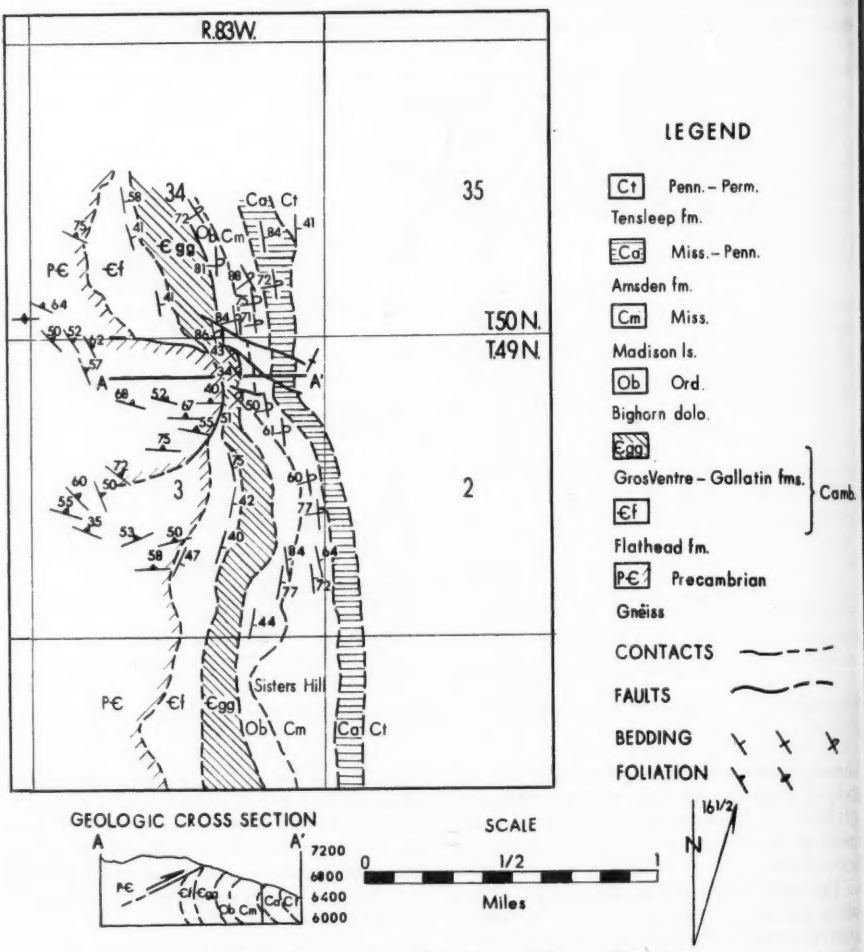

Figure 2. Geologic map of the Sisters Hill area, Wyoming

gests that here wrench faulting, although due to Laramide stresses, may have actually occurred along a favorably oriented Precambrian structure.

The areal geology was first mapped on topographic maps (scale, 1:24,000) of the Bureau of Reclamation Powder River Basin Survey (1946). Two sets of aerial photographs were available. One set (scale, 1:48,000) was particularly valuable for observation of regional trends; the other (scale, 1:20,000) was used for plotting of station locations.

The collection, representation, and interpretation of fracture data are always a problem. Some investigators (Spencer, 1959) measure the attitudes of a given number of fractures for each exposure, having chosen the exposures on the basis of a selected sampling pattern. They plot the measurements on a stereographic projection and interpret the origins of the fractures and even the stress distribution responsible for the fractures on the basis of the statistical distributions. Such purely statistical approaches do not take fracture spacing into account; nor does it appear that any attempt at interpretation of origin is made in the field. Osterwald (1959, p. 33) has attempted to consider joint spacing by applying a "spacing factor" to each joint set in an outcrop. Rocks may contain primary tectonic joints representing more than one period, kind, and depth of deformation. Finally, there are secondary fractures related to local movements along faults (Pl. 3, fig. 6) or local tension joints developed in competent sedimentary units due to slippage between adjacent beds; such fractures are only indirectly related to the regional stress patterns.

In order to overcome the disadvantages of the purely statistical approach, this investigation was conducted as follows. At each exposure examined a number of readings were made of fracture and foliation directions and the average of the attitudes of each structural feature recorded in the notes, along with notations as to spacing and such interpretations of the nature and origin of the fractures as could be made. Figures 4 and 5 are fracture-distribution diagrams made from these averages and should be considered only in this light. These diagrams show that certain trends stand out. These trends can be related to observations made at field stations that the fractures having these trends were closely spaced, were the most prominent surfaces, and so on.

It may be argued that this approach to the study of fractures is too open to bias. A method such as this requires that the investigator carefully study the rocks both in the field and in the laboratory. I believe that interpretations of fractures using this technique are more sound

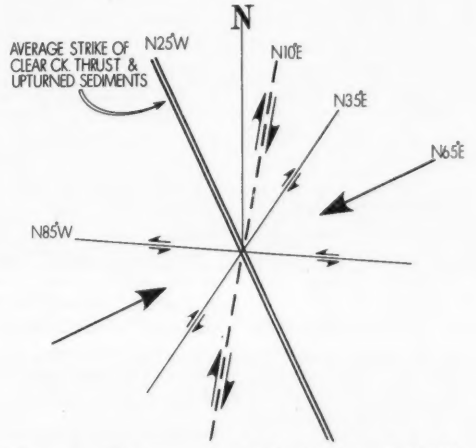

Figure 3. Diagrammatic sketch showing relationship of the N. 10° E. wrench faults to the expected directions of shear for a maximum principal stress acting along a N. 65° E. direction.

than interpretations based only on distribution diagrams of fractures of various ages and origins, particularly where the maxima on such diagrams are related to a single hypothetical stress system which in turn is then used to classify the fractures as due to shear or tension.

The Precambrian rocks were studied in detail for a distance of 1 or 2 miles west of the contact with the Flathead sandstone. Although the area is heavily forested, there are many exposures, and most of these were examined. Measurements and observations were recorded for a total of 210 stations in the Precambrian rocks. Data were also obtained along traverses between stations. The field data were supplemented by laboratory study of hand specimens and of 120 thin sections.

Inasmuch as the sedimentary rocks were also affected by Laramide movements, fracturing and other structures were studied in the competent zones; these included the Flathead, Gallatin, Bighorn, Madison, and Tensleep formations, and a few exposures of competent units in the Amsden, Gypsum Spring, Sundance, and Morrison formations.

Mapping of structures in the sedimentary rocks is necessary because these units have been affected predominantly by only the Laramide orogeny. The Precambrian rocks, on the other hand, bear the impress of not only Laramide deformation, but of several Precambrian deformations and of several lesser uplifts during the Paleozoic and Mesozoic.

A first premise, therefore, is that in order to consider the possibility of Precambrian structural control, the truly Precambrian structures must be distinguished from later ones in the crystalline rocks. This means that sedimentary structures must also be mapped.

The second basic premise arising from this study, and from reconnaissance elsewhere in the Precambrian core of the Bighorns, is that the petrology and structure of crystalline rocks are so intimately associated that they should be studied simultaneously. Our approach, therefore, is to have one man study both the petrology and the structure in a given area rather than to have two or three men, each studying only one phase in the same area, work more or less independently.

R. F. Hudson has completed a similar study in the vicinity of the Piney thrust, north of the area of the report. The basic premises noted here are being tested further by J. C. Palmquist in the Horn area and by L. O. Williams in an east-west strip across the range from the north fork of Crazy Woman Creek to Tensleep.

PRECAMBRIAN ROCKS

General Statement

Gneisses are by far the most abundant rock type in the crystalline core. Darton (1906b, p. 3) considered these to be granites, although he noted an incipient tendency toward schistosity. He emphasized the variations in color from red to gray but found the different kinds of granite to be so irregularly distributed that he did not find it possible to indicate their limits on the map. He believed that all the granite was part of one great mass of batholithic nature.

Detailed study shows that these gneisses are actually metamorphic rocks. Their textures are crystalloblastic. Osterwald (1955) arrived at the same conclusion from his studies at the northern end of the Precambrian core.

Occurrences of pegmatite, amphibolite, ultramafic rocks, and mafic dikes are relatively minor.

Obviously such a small area as is involved in this study cannot provide all the information needed to complete the petrological story. However, reconnaissance in other parts of the core and continuing detailed studies to the west of the map area indicate that the nature of the rocks is much the same.

Structures in the Gneiss

The gneisses are quite varied in appearance. They range from dark gray to light gray to pink. Where a megascopic preferred orientation is poorly developed, they appear quite homogeneous. In many places, however, they are quite heterogeneous and can be termed migmatites (Pl. 3, fig. 1). There are no true banded gneisses. Two kinds of *S*-structure were mapped in the field. One is a poorly developed foliation and mineralogical layering, and is designated S_1. The other is a later shear structure and is designated S_2. In many parts of the area S_1 was so difficult to detect, or so contorted, as in the migmatitic parts, that it was impossible to obtain consistent measurements; this accounts for the relatively small number of symbols on the map. Thin sections cut at right angles to S_1 revealed evidence of granulation. This foliation is more prominent in the Sisters Hill area. In some gneisses S_2 is expressed by augen structure (Pl. 4), in others by closely spaced shear surfaces (Pl. 4, figs. 1–3). In some zones (3–12 feet wide) the shearing was so intense that the rock was mylonitized; later recrystallization of mica along these surfaces requires that these rocks be termed phyllonites.

Figure 1. Clear Creek thrust. View looking north at road cut along U.S. Highway 16. Vertical beds of Madison limestone (Cm) thrust on Moncrief gravels (Tm).

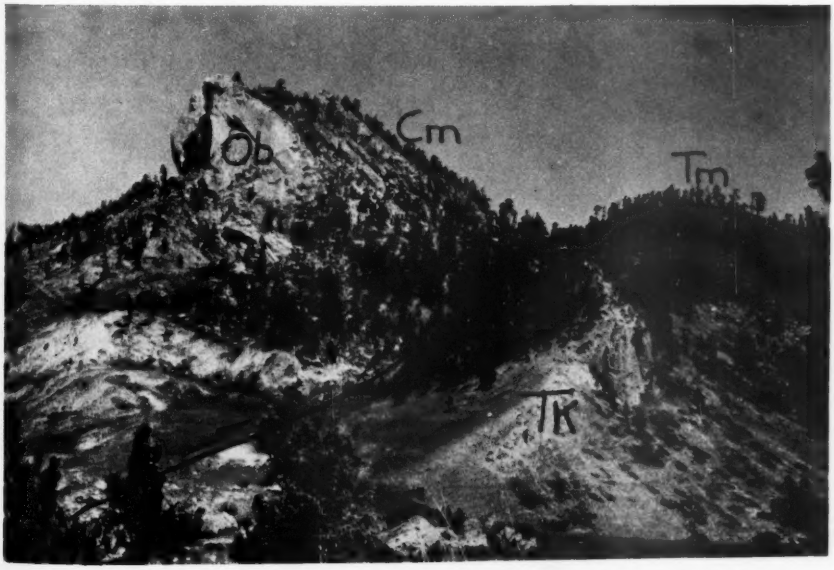

Figure 2. Johnson Creek wrench fault: view looking north across Johnson Creek. Gros Ventre-Gallatin (Cgg), Bighorn (Ob), and Madison (Cm) faulted against vertical beds of Kingsbury gravel (Tk) and gently dipping Moncrief gravels (Tm). Not shown is a thin sliver of Cretaceous clay in the saddle.

CLEAR CREEK THRUST AND JOHNSON CREEK WRENCH FAULT, WYOMING

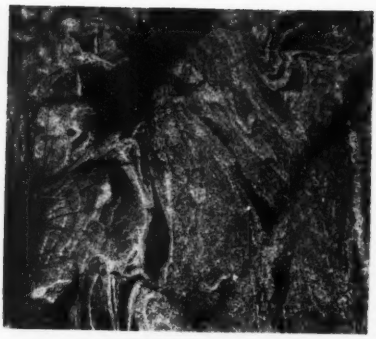

Figure 1

Figure 2

Figure 3

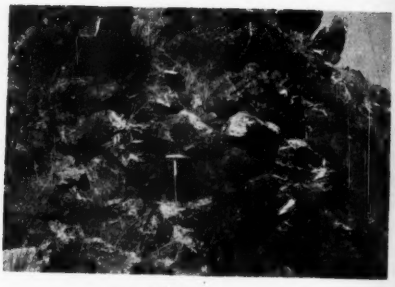

Figure 4

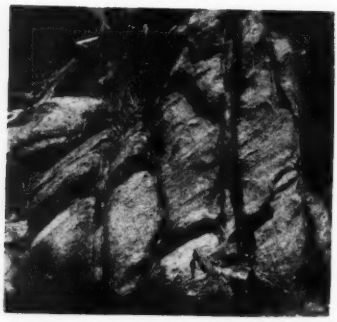

Figure 5

Figure 6

Figure 7

PRECAMBRIAN ROCKS FROM CLEAR CREEK THRUST AREA
NEAR BUFFALO, WYOMING

HOPPIN, PLATE 3
Geological Society of America Bulletin, volume 72

Where the rock had such closely spaced shears that it was foliated, the structure was designated S_2- foliation; where the surfaces were more widely spaced the structure was termed S_2- shear fracture.

Every thin section of gneiss shows evidence of granulation and recrystallization. The existence of these deformation fabrics has an important bearing on petrographic descriptions and on petrologic interpretations of the gneisses.

Lineation is nowhere a dominant feature of the rock fabric. Almost all the lineation observed was on the S_2- surfaces; this lineation is the trace of the older S_1. An excellent confirmation of this was found 3 miles west of the area in a ridge just north of the Hunter ranger station. In one exposure the gneiss has a very prominent S_2- foliation trending N. 5° E., dipping 87° E. On the foliation surfaces a lineation is expressed by a streaking of light and dark minerals which plunges 40° N. Another exposure 100 years to the west consists of gneiss with an S_1- foliation trending N. 70° E., dipping 40° N., cut by vertical, north-trending S_2- shear fractures with a spacing of 1-3 feet.

Every exposure contains several fracture sets. Fracturing is discussed under fracture analysis.

Quartzofeldspathic veinlets ranging from less than one quarter of an inch in width and from a few inches to several hundreds of feet in length are present throughout the gneisses. Some outcrops are interlaced by feldspathic veins exhibiting pinch and swell structure. At some localities, one face of an outcrop has a prominently banded appearance resulting from alternation of felsic and mafic layers, yet another face at right angles to the first reveals a crisscross pattern of the felsic layers, some of which are displaced by other felsic bands. The light bands in some places parallel the biotite foliation and in other places cut across the foliation at a high angle. In some places these veinlets have rather sharp contacts, but in many others the contacts with the gneisses are diffuse. Contorted and irregular felsic bands deformed by shear are common (Pl. 3, fig. 3); these commonly resemble ptygmatic folds (Pl. 3, fig. 2).

Microscopic Features of the Gneiss

The gneisses vary considerably in the amounts of the main minerals. However, biotite, plagioclase, and quartz (in order of increasing abundance) are invariably the essential constituents. Microcline is absent in some rocks, is a minor interstitial constituent in others, and is an essential constituent in still others.

Less abundant minerals are muscovite, epidote, hornblende, sphene, pyroxene, apatite, chlorite, zircon, allanite, and magnetite. No garnet was observed, but it is present farther north (Osterwald, 1955) and in the Horn area.

Plagioclase feldspar is mainly oligoclase-andesine (An_{20}–An_{42}). Lesser amounts of albite and sodic oligoclase (An_5–An_{15}) also occur. The oligoclase-andesine occurs entirely as relics ranging from 0.1 to 5 mm in diameter, with a few as large as 1 cm. They are augen left as a result of deformation. Many are granulated around the margins, thus exhibiting a striking development of mortar structure. Many of the feldspar grains contain tiny

---

PLATE 3. PRECAMBRIAN ROCKS FROM CLEAR CREEK THRUST AREA NEAR BUFFALO, WYOMING

Figure 1. Migmatite, North Fork Crazy Woman Creek, 12 miles south of U.S. Highway 16

Figure 2. Shear folding feldspathic bands. Same location as Figure 1

Figure 3. Shear folding of feldspathic veinlet. Shear foliation trends N. 48° E., dips 68° northwest. Center SE ¼ sec. 8, T. 50 N., R. 83 W.

Figure 4. Amphibolite. Irregular stringers and aggregates of quartz and sericitized pink oligoclase. SE ¼ sec. 16, T. 50 N., R. 83 W.

Figure 5. Vertical N. 10° E. shears cutting older shear foliation (parallel to hammer handle) which trends N. 35° E. and dips 48° northwest. SW corner NE ¼ sec. 30, T. 51 N., R. 83 W.

Figure 6. Close-spaced fractures in gneiss just above thrust (center NE ¼ sec. 14, T. 51 N., R. 83 E.). Trends range between N. 60° E. and N. 75° W; dips 30°–38° south. These fractures are found only very close to the thrust; they probably are related to the northeasterly movement of the Precambrian wedge.

Figure 7. Relict sheeting(?) in gneiss on west side of Clear Creek (sec. 10, T. 50 N., R. 83 W.). A pre-Flathead regolith is preserved on the top of a cliff on the east side of the creek (to left of photograph). The sheeting trends N. 10° W., dips 40° east.

fractures and bent twin lamellae. Some grains show an indistinct undulatory extinction. The augen very commonly show a tendency toward dimensional elongation parallel to the preferred orientation, but many grains are more equidimensional and stand conspicuously athwart the foliation (Pl. 4, fig. 5). In an extreme example (Pl. 4, fig. 6) the augen look like projectiles pushing aside the matrix.

The relationship of the albite to the more calcic feldspar is not too clear. The feldspathic bands generally contain sodic plagioclase rather than oligoclase-andesine. In a few places the gneisses contain augen of albite. In several thin sections sodic feldspar appears to cut more calcic plagioclase; in a few sections, albite was closely associated with recrystallized quartz of the matrix. These few situations suggest, inconclusively, that the sodic plagioclase is later than the oligoclase-andesine, and that it is partly predeformation and partly postdeformation. An interesting feature is that pink feldspar is not necessarily a potassium feldspar. At the south end of the area the gneisses range from gray to pink. Thin-section examination reveals that the pink feldspars are plagioclase highly altered to sericite and minor calcite. The intensity of the pink coloration is directly proportional to the degree of alteration of the plagioclase.

Hornblende occurs rarely as xenomorphic grains cut and replaced by later biotite, epidote, sphene, and quartz. It is strongly pleochroic from dark green to pale yellow. Two sections contain a few grains of pale-green diopsidic pyroxene rimmed by hornblende. The hornblende-plagioclase contacts are irregular and interlocking, which suggests that the two are contemporaneous. Locally, the gneisses grade into quartz-hornblende-plagioclase gneisses. These rocks show little sign of deformation (wavy extinction in quartz) and no foliation, although the hornblende does show a lineation. Perhaps the lack of deformation in the hornblende-rich varieties and in the amphibolites is a result of their being more competent than the other gneisses with respect to shear deformation (Ramberg, 1952, p. 128; 1956, p. 189).

Quartz occurs mainly as clear, fine-grained (0.01–0.5-mm) interstitial material. It is usually concentrated in bands or aggregates in which the grains show strong undulatory extinction. Contacts between quartz grains are serrate. The quartz, both single grains and elongate aggregates, tends to have a dimensional elongation parallel to the planes of deformation and biotite foliation (Pl. 4, fig. 4). The optic axes tend to lie parallel to these directions; sections cut parallel to deformation surfaces contain a high percentage of grains that give flash figures. In some rocks the quartz grains and aggregates bend around plagioclase augen and locally are highly contorted and swirled (Pl. 4, fig. 5). Several thin sections reveal a lamellar rather than undulatory extinction of the quartz. This lamellar structure is probably due to translation gliding on Boehm lamellae, as the bands are roughly parallel to the basal pinacoid (Turner, 1948, p. 260–261). Fractures in some plagioclase augen are filled with fine quartz. Other augen have "scalloped" margins where replaced or even embayed by quartz. The only quartz which does not have wavy extinction is that occurring as inclusions in relict plagioclase and hornblende; such quartz represents an earlier generation than the bulk of the quartz in the gneiss.

Microcline is present in widely varying amounts. In some gneisses it is absent, whereas in others it is the dominant feldspar. It ranges from interstitial granular material 0.01–0.1 mm in diameter to anhedra up to 1 cm in diameter. The microcline is usually clear and undeformed, although it may be perthitic in some samples. There are many unequivocal examples in thin sections of microcline cutting and replacing plagioclase feldspars, both oligoclase-andesine and albitic types. Myrmekite is commonly developed between plagioclase augen and replacement microcline. The fine interstitial microcline is invariably found in granulated zones with quartz and in some cases also replacing quartz. Examples were noted in thin section of microcline

PLATE 4. PHOTOMICROGRAPHS OF GNEISSES FROM CLEAR CREEK THRUST AREA NEAR BUFFALO, WYOMING

Figure 1. Plagioclase augen with stringers of muscovite, biotite, epidote, and quartz. Plain light. × 16

Figure 2. Phyllonite. Shears marked by muscovite and biotite. Matrix of quartz, albite, epidote (high relief), and allanite (dark). Plain light. × 22

Figure 3. Same as Figure 2, but different part of slide. Crossed nicols. × 30

Figure 4. Plagioclase augen (right center) cut by biotite (left corner of grain). Foliation marked by muscovite, biotite, and elongated quartz. There is intergranular microcline and epidote. Crossed nicols. × 30

Figure 5. Swirling of quartz around plagioclase augen. Augen are granulated and replaced by quartz and integranular microcline. Crossed nicols. × 30

Figure 6. Curving of quartz (note wavy extinction) around corner of large plagioclase augen. Right edge of grain is partly replaced by epidote and biotite. Sericite alteration in center of grain. Crossed nicols. × 30

Figure 1

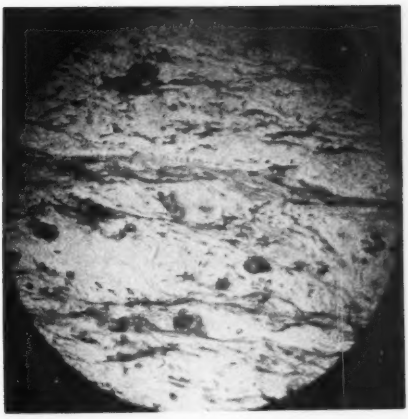

Figure 2

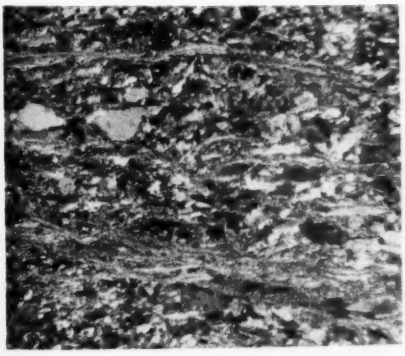

Figure 3

Figure 4

Figure 5

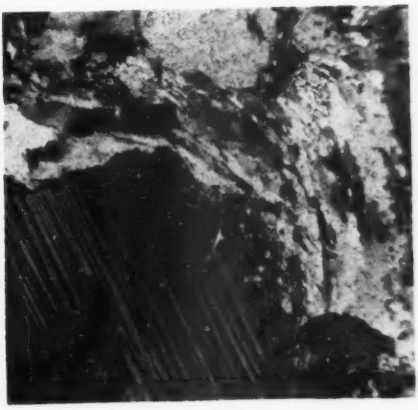

Figure 6

PHOTOMICROGRAPHS OF GNEISSES FROM CLEAR CREEK THRUST AREA NEAR BUFFALO, WYOMING

HOPPIN, PLATE 4
Geological Society of America Bulletin, volume 72

Figure 1. Shears in Madison limestone. Trend of shears is N. 55° E., dip 80° south.

Figure 2. Gashing and brecciation in massive Bighorn dolomite. Trends of fractures range from N. 55° E. to N. 85° E., dips 65°–80° south.

Figure 3. Prominent fractures (N. 40° E., dip 57° northwest) in bedded basal Bighorn as contrasted with the intensely broken massive dolomite above. Exposure is at base of Ob cliff in Figure 2 of Plate 2.

SHEARING IN SEDIMENTARY ROCKS IN RIDGE NORTH OF JOHNSON CREEK, WYOMING

HOPPIN, PLATE 5
Geological Society of America Bulletin, volume 72

replacing biotite although in many instances microcline and biotite and in all slides microcline and muscovite appear to have formed contemporaneously. The introduction of the microcline appears to have followed the main period of early Precambrian deformation. Numerous shears and granulated zones facilitated this introduction.

Biotite for the most part has recrystallized along the shear surfaces as fine-grained (0.01–0.1-mm) plates which emphasize the planar fabric of the gneiss (Pl. 4, fig. 2). Occasionally larger grains (up to 0.5 mm) are present in areas of a thin section between shear zones; some of these larger grains are bent and fractured, suggesting that they are older than the finer, undeformed biotite which recrystallized in the sheared portions of the rock. There are numerous examples (Pl. 4, fig. 6) in thin section of biotite cutting into plagioclase augen. In other instances the biotite "flows" around the augen (Pl. 4, fig. 1). The biotite recrystallized later than the quartz; the quartz is strained and is cut and replaced by plates of undeformed biotite.

Muscovite is much less abundant than biotite. It is absent in many thin sections, and at most amounts to only 2–3 per cent of the total minerals in a slide. However, the amount of muscovite appears to be a function of the intensity of shearing and granulation of the rock: the greater the deformation, the greater the amount of muscovite. Like biotite, the muscovite cuts and replaces the plagioclase augen or streams around the edges. The muscovite is fine-grained (0.01–0.1 mm). Muscovite formed later than some of the biotite, as is shown by numerous examples in thin section of cutting and replacement of biotite by muscovite.

Epidote is present in every thin section, usually amounting to 1–5 per cent of the total minerals. In highly sheared rocks, coarser grains (0.2–0.5 mm) and aggregates of finer material (0.01–0.1 mm) have been granulated and are actually augen. Some of the epidote is closely associated with the micas and probably formed at about the same time as the micas. Almost all slides contain examples of epidote surrounding euhedral cores of brown allanite.

The laft phases of mineralization are represented by chlorite replacement of biotite, sericitization of plagioclase, a late introduction of epidote along joints and fissures, one small zone (1 foot wide) of prehnite, and minor green copper stain.

Other Rock Types

Coarse feldspathic bodies and pegmatites. Only a few small, irregular bodies containing coarse-grained quartz and feldspar and minor magnetite were observed. These are of two types. In one, the feldspar is plagioclase of the same composition as the plagioclase of surrounding rocks (although slightly more sodic). These masses appear to be just coarser-grained representatives of the feldspathic bands noted heretofore. The country rock is richer in biotite in the vicinity of these bodies than is the bulk of the gneiss. The bodies are either pod-shaped bodies a foot or two in diameter or elongate lenses a few tens of feet long and a few inches to 2 feet wide. The walls are wavy and irregular; the biotite of the country rock and the relatively small amount of biotite in the feldspathic bodies have the same preferred orientation. These relationships indicate that feldspathic bodies formed by replacement during metamorphic differentiation. In the second type of irregular body, the feldspar is perthitic microcline. One such band, 1 foot wide, has very sharp, straight borders, which cut across the foliation of the gneiss at a high angle. The inner zone, 3 inches wide, contains coarse pink perthite and quartz. The outer zones are much finer-grained and contain a small amount of biotite whose orientation is parallel to the biotite of the country rock. A thin section cut across the contact zone between pegmatite and country rock reveals that the pegmatitic material has replaced the country rock; megascopically the contact is relatively sharp, but microscopically the contact is irregular and diffuse.

Amphibolite. The only body of amphibolite (Pl. 3, fig. 4) is a lens 560 feet long and 120 feet wide at the south end of the map area just 100 feet northwest of a diabase dike (SE¼ SE¼ sec. 16, T. 50 N., R. 83 W.). The rock consists mainly of dark-green coarse-grained anhedral hornblende (3 mm–1.5 cm) cut by and interlaced with veinlets and irregular aggregates of coarse quartz and greatly sericitized pink oligoclase. Many of the veinlets have concentrations up to 1 inch wide of hornblende along their borders. The hornblende appears to be randomly oriented. Thin sections show considerable pale-green pyroxene (0.1–3 mm) which is cut and replaced by the hornblende. The rock as a whole shows little effect of deformation other than slight wavy extinction of the quartz. A thin section of one light-colored band 2 inches wide in almost pure hornblende rock showed that it was a deformation band containing relict, granulated hornblende and oligoclase, granular epidote, sphene, and quartz, and late, clear microcline. Some of the quartz showed a tendency to be elongated in the plane of the layering.

Ultramafic rocks. One large ultramafic body is exposed along U. S. Highway 16. Two smaller plugs half a mile to the east-southeast (Pl. 1) and a few small, poorly exposed dikes constitute the remainder of the ultramafic occurrences.

In the large mass, the most abundant rock type consists of large (up to 5 cm) ragged crystals of bronzite which contain exsolved clinopyroxene and poikilitic inclusions of partially serpentinized olivine. Other rock types include serpentinite, pyroxenite, and a little anorthosite. The clinopyroxenes show considerable variation in optic angle from almost uniaxial pigeonite to augite. The mass has numerous slickensided, curved fracture surfaces and local thin broken and shattered gouge zones. Deformation in thin section is not nearly so noticeable as in the gneisses. In one slide bronzite had wavy extinction. In some other thin sections there were parallel fractures in the pyroxenes along which some serpentinization has taken place.

W. C. Luth (1960, M.S. thesis, State University of Iowa) has studied these ultramafic rocks in more detail.

Mafic dikes. Mafic dikes are present throughout the area. Some are very small and poorly exposed. Only the few larger dikes that could be traced any distance are shown on Plate 1. Contacts with the gneiss are rarely exposed. Only the dike in secs. 9 and 10, T. 50 N., R. 83 W. had contacts that could be closely studied. This dike is 100 feet wide. The dense contact zone is about 3 feet wide and consists of very fine-grained hornblende, and plagioclase laths 0.1–1.0 mm long. The plagioclase laths are arranged in excellent flow lineation parallel to the contact. The bulk of the dike is medium-grained diabasic gabbro consisting of labradorite and augite (pigeonitic) with minor magnetite and green hornblende. The N. 85° W. trend of this dike is parallel to a fairly consistent direction of jointing and shearing in this area.

The large dike at the south end of the area is 175 feet wide where it is completely exposed on a knob located on the line between secs. 15 and 16, T. 50 N., R. 83 W. A central zone 75 feet wide consisting of medium-grained gabbro is flanked by finer-grained zones of diabase 50 feet wide. This dike trends N. 55° E. parallel to a strong northeasterly direction of shearing.

The group of dikes in secs. 19, 20, 29, and 30, T. 51 N., R. 83 W. trend parallel to the prominent N. 10° E. direction of shearing. Some specimens are quite fresh quartz diabase, whereas others show more alteration of plagioclase to sericite and of pyroxene to hornblende and biotite, particularly in the coarser rocks.

Several other small occurrences of green dike rock showed strong alteration of the original mafic rock to pale-green amphibole, epidote, chlorite, and sericite.

Summary of Precambrian Events

No definite conclusions can be made as to whether the gneisses are paragneisses or orthogneisses, or mixtures. No undoubted metasedimentary rock such as Eckelmann and Poldervaart (1947) reported in the Beartooth Mountains could be identified in the map area. The mineral assemblages are characteristic of the staurolite-quartz subfacies of the almandine amphibolite facies (Fyfe, Turner, and Verhoogen, 1958, p. 229). The foliation in all cases is due to shear deformation; this foliation, in turn, is cut by later shearing (Pl. 3, fig. 5). As deep-seated deformation and metamorphism continued, feldspathic bands and veinlets tended to segregate, probably because of metamorphic differentiation. These veinlets have a haphazard, crisscrossing pattern. They, also, are cut by shear surfaces (Pl. 3, fig. 3). Some veins are displaced by others; both apparent normal and reverse types of displacement were noted. With the end of active deep-seated shear deformation, microcline was introduced along the deformation surfaces. It now occurs as fine-grained clear interstitial material, as larger anhedral porphyroblasts, and in replacement pegmatities.

With the relaxation of the stresses and uplift, fractures opened up along surfaces of structural weakness formed by earlier shear deformation. Mafic magma was intruded along these fractures.

The position of the ultramafic bodies in this sequence is uncertain. Current studies of these bodies are directed toward determining which of the following origins is most likely. (1) The bodies were early intrusions into a sequence of sedimentary and igneous rocks and acted as "resisters" during subsequent metamorphism and deformation. (2) The bodies represent basic fronts or residual segregations formed during feldspathization and granitization. (3) The bodies were postmetamorphic intrusions.

Following uplift the Precambrian rocks were peneplaned. Remnants of an ancient regolith are preserved. A particularly good exposure is at the top of a 50-foot cliff on the east side of Clear Creek (SE corner NW ¼, sec. 10, T. 50 N., R. 83 W.). The zone is 20 feet thick and grades upward from fresh gneiss into partly weathered rock with good secondary exfoliation and finally into gruss. The regolith is overlain by basal Flathead sandstone.

FRACTURE ANALYSIS

General Statement

The detailed discussion that follows combines data and interpretations. In most instances it is desirable to separate facts from interpretation. However, as the data gathering, field interpretation, data representation and interpretation, and thin-section study were so intimately co-ordinated in this investigation, the discussion is presented in the same manner.

Fractures are sometimes classified as shear or tension fractures. In this study the term shear fracture was used wherever there was a displacement along the fracture, however small, of foliation, borders of crosscutting feldspathic bands, and of bedding planes or stratification in the sedimentary rocks. (Although the intitial fractures in the gneiss originated by shearing, they were probably further opened by tension when the rocks were raised closer to the surface where expansion due to unloading took place

(Price, 1959). They are still designated as shear fractures in this discussion). The other primary fractures are not here classed as tension fractures unless there is strong evidence that they can be correlated with tensional stresses developed during regional deformation.

Many individual fractures are curved. Some fractures are parallel or normal to cliff faces, tend to be short and discontinuous, and end abruptly against other fractures. Another set of fractures dips at about the same angle as the nearby sedimentary rocks and is quite prominent only in the vicinity of the contact between the Precambrian and the Flathead sandstone (Pl. 3, fig. 7); these are interpreted as relict sheeting formed before the deposition of the Flathead formation. All these fractures are considered to be topographically controlled (Chapman, 1958) and along with secondary fractures are not included in the fracture diagrams.

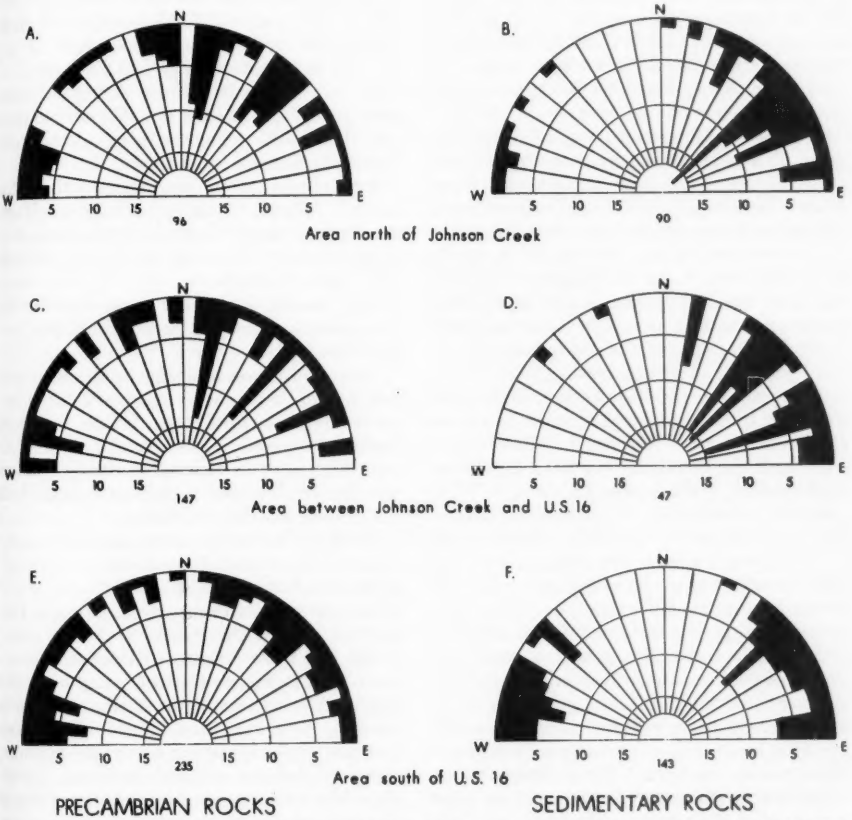

Figure 4. Fracture distribution diagrams of Clear Creek area, Wyoming. Percentage distributions of high-angle fractures in Precambrian and sedimentary rocks. Figures below the center of each diagram refer to the number of recorded observations. Each recorded observation represents an average of a number of measurements of each direction.

The fractures that are included in the tabulation are all high angle (greater than 45° dip; by far the largest number have dips greater than 65°).

In Figures 4 and 5 and in the text discussion the Precambrian and sedimentary rocks are treated separately. The main map area is

divided into three parts. As might be expected, the fracture pattern for the Precambrian rocks is more complex than that for the sedimentary rocks.

Area North of Johnson Creek

PRECAMBRIAN: Figure 4A shows two strong maxima centered about the N. 10° E. and N. 40° E. trends. Both of these fracture trends can be correlated with similar trending shear zones in the field. The N. 10° E. direction is the better developed of the two. Exposures tend to be aligned about N. 20° E. as a result of the combination of these two directions. This elongation intersects the general drainage trend at a large angle and shows up well on aerial photographs, even though the forest cover is heavy. A 10-foot vein of massive white quartz was found which strikes N. 10° E. Near the wrench fault in secs. 18 and 19, T. 51 N., R. 83 W., the N. 10° E. fractures were reactivated during the Laramide faulting. As a result of reactivation along these fractures, microcline in pegmatites and in the more granitized gneisses has been granulated. Most of the zones do not seem to have been refractured as shown by the undeformed nature of the microcline in thin section. The small diabase dike in sec. 13, T. 51 N., R. 84 W. has a right-hand displacement of 30 feet along a trend N. 5° E.

A fairly consistent system of widely spaced fractures striking N. 70°–80° W. is also present.

SEDIMENTARY ROCKS: The sedimentary rocks show a very strong concentration of fracture trends between N. 45° E. and N. 70° E. Close examination of the fracturing in outcrops reveals that it is due to shearing as shown by slight displacements of bedding planes and laminae.

Fracturing in the massive sandstones in the Flathead formation is very irregular but generally trends northeast. These fractures are seamed with white quartz and tend to stand out in relief. Fractures in the basal red sandstone are poorly developed. The northeast trends are widely spaced; locally there are N. 10° E. trends. The scattered N. 40° W. fractures are probably longitudinal tension fractures developed when the beds were arched.

The contrast between the deformation of the basal beds of the Bighorn dolomite and that in the massive part is striking. The bedded unit has closely spaced fractures, whereas the massive unit is gashed and broken by irregular fractures (Pl. 5, figs. 2,3).

The Madison limestone contains closely spaced fractures in most places (Pl. 5, fig. 1), particularly in the thin-bedded units; more massive units tend to be gashed. Many of the fractures are filled with veinlets of coarse calcite. Locally, the upper ledge of Madison contains few regular fractures but is shattered and seamed with veinlets of very fine-grained quartz. Two slickensided surfaces were noted in the Madison just east of the wrench fault, NW ¼ SE ¼ sec. 14, T. 51 N., R. 83 W. Both surfaces are vertical. One face trends N. 32° E., and the slickensides plunge 15° southwest; the other face strikes N. 55° E., and the slickensides plunge 37° southwest. These directions and degrees of plunge indicate dominantly horizontal shearing movements.

It is interesting to note that in the ridge north of Johnson Creek, fractures in the Madison directly up-dip from the Bighorn tend to strike about 20° more toward the east than do those in the Bighorn.

The Amsden is in most places considerably brecciated, especially in the basal beds. Fracturing is not well developed.

Massive sandstone units in the Tensleep have few fractures but contain irregular calcite veinlets in most places. Thinner-bedded members commonly contain close-spaced fractures. At one location, thin-bedded sandstone showed slip displacements of 1 to 2 mm along shear fractures which trend northeast.

Southeast of Sayles Creek the sedimentary rocks are overturned. Northwest-striking longitudinal fractures are locally well developed and have been rotated during overturning so that they now dip 60° northeast.

The origin of the mass of Paleozoic formations (Gros Ventre-Gallatin, Bighorn, and Madison) lying east of the mountain front is puzzling. Section B-B' of Plate 1 suggests that the mass was punched out by the Precambrian wedge to the west and slid down as a gravity slide. However, the direction of movement of the Precambrian block must have been to the northeast, as only the sedimentary units to the northeast have been overturned. The sedimentary rocks to the southeast have merely been dragged, as would be expected if the fault bounding the southeast side of the block was a right-lateral wrench fault.

Area Between Johnson Creek and Highway 16

PRECAMBRIAN: The pattern between Johnson Creek and Highway 16 is about the same as farther north. Both the N. 10° E. and the N. 40° E. maxima in Figure 4C can be correlated

with evidence of shearing in individual outcrops. An older shear foliation trends northeasterly but dips at a lower angle to the northwest than do the later northeast fractures. Figure 5 of Plate 3 shows vertical N. 10° E. fractures cutting this older shear foliation.

The Johnson Creek wrench fault could not be traced south of French Creek, although it can be found as a zone of highly fractured gneiss on the north side of the creek. A prospect pit on the fault (NE corner SW ¼ sec. 29, T. 50 N., R. 83 W.) contains highly brecciated gneiss cemented by white quartz.

Again, the widely spaced N. 75° W. fractures are present throughout.

The mafic dikes south of Johnson Creek strike north-south to N. 10° E., parallel to the prominent N. 10° E. fracture trend.

SEDIMENTARY ROCKS: The trends here are almost exclusively within two strong northeasterly maxima. The few N. 10° E. directions are mostly represented by thin (3 inches to 1 foot) breccia zones in the massive Bighorn.

Fracturing is very poorly developed in the somewhat friable Flathead sandstones.

Figure 4D suggests that the N. 70° E. and N. 45° E. trends are complementary shear fractures. However, at a given exposure there is only one prominent set of shear fractures; these are normal to the strike of the sedimentary rocks. Between Johnson Creek and French Creek, the main fracturing trends N. 65°–70° E., with only local development of strong N. 45° E. shears. These latter are best developed near a group of four small N. 45° E. right-lateral wrench faults, only the largest of which is shown on Plate 1. South of French Creek there are many shear zones (1 inch to 10 feet wide) in the Bighorn formation. These swing around to N. 70° E. at the highway.

The presence of a dominant set of fractures at right angles to the strike of the tilted sedimentary rocks would suggest that these are the tension fractures called for by theory. However, study shows that these are definitely shears. A possible answer to this seeming anomaly is suggested by some theoretical considerations of Muehlberger (1958). According to his reasoning, the dihedral angle between conjugate shears decreases with decrease in confining pressure (and, hence, depth) and could be zero. This single plane of shear failure, lying parallel to the maximum principal stress (N. 65° E. and approximately horizontal in this instance), is a tension fracture according to the normal usage. This suggests that this effect of Laramide deformation revealed in the sedimentary rocks in this area is a shallow-depth phenomenon.

Area South of Highway 16

PRECAMBRIAN: Figure 4E shows that fracture directions practically box the compass. The important groupings are N. 30°–50° E. and N. 70°–90° W. Because of the lack of any really predominant directions, outcrops do not show any tendency toward elongation as do those at the north end of the area. The N. 10° E. trend so prominent farther north is only locally developed.

The northeasterly trends again can be correlated with numerous examples of shearing. Just south of the left-lateral wrench fault crossing Clear Creek, a N. 30° E. vertical surface revealed a lineation of elongate biotite clots plunging 55° northeast. At another location a N. 43° E. vertical shear (one-half inch displacement) contains white quartz. These northeast trends also cut pegmatites and also appear in the two large dikes; this suggests that these fractures are either late Precambrian or Laramide. At the south end of the area these fractures shift to slightly more easterly trends of N. 50°–80° E. Just north of the southern wrench fault, three thin quartz veins trending N. 75° E. and dipping 73° S. all contained slickensides striking N. 50° E. and plunging 65° southwest. The large dike trends N. 55° E. This suggests that the northeasterly shears were first developed during a Precambrian deformation and were later reactivated.

The N. 70°–90° W. fractures are prominent. The wrench fault across Clear Creek has this trend. The dike three-quarters of a mile south of the fault also strikes in this direction; this dike and the one to the south both contain joints of this direction. Again, these relationships suggest that fractures having this trend may have first formed during the Precambrian but were reactivated during the Laramide.

A consistent N. 20°–45° W. group of fractures is present. These dip 55°–90° southwest. In the large dike north of Clear Creek they cut across the contact between the diabase and gneiss; no displacement of the contacts along this fracture was apparent. This group is probably a longitudinal set of tension fractures developed during Laramide uplift and arching.

Foliation is poorly developed for the most part. In the northern half of this section it strikes N. 15°–20° W. and dips 43°–55° E. At the south end there is a well-developed foliation

trending N. 45°–80° E. and dipping 70°–90° S. Locally this foliation is strongly folded and swirled.

SEDIMENTARY ROCKS: Figure 4F shows that the fractures are grouped within a range from N. 40° E. to N. 60° W. All these directions are shears. The relatively few N. 45° W. fractures are probably tension fractures. In many outcrops two sets of shears are present, intersecting at small angles; in some exposures, only one direction at right angles to the strike of the bedding could be discerned. Changes in strike of the sedimentary rocks due to drag in the vicinity of the large and small wrench faults caused some rotation of the fractures.

Fracturing in the Flathead sandstone is best developed in thin-bedded quartzitic layers where two trends are present, one N. 60°–85° W. and the other N. 40° E. In the friable sandstones, the fractures are quite irregular and are coated with very fine-grained quartz.

The Gallatin and lower Bighorn formations are cut by several small faults, two of which are shown on Plate 1. Movement on these faults, and along the two large wrench faults, was mainly horizontal with a small vertical component as indicated by the nature of the drag of the formations and by the low southwestward plunge of the few slickensides that could be found. All these faults follow one or the other of the conjugate shear directions to be expected for an east-west direction of maximum stress in this area.

The fracturing noted for the Bighorn formation and the Madison limestone to the north is also found here and will not be redescribed. There was more tendency for the two sets of conjugate shears to be present in the same outcrop than was the case north of Highway 16. The Madison, and to a lesser extent the Gallatin, have good crisscross patterns. The Bighorn, and the Madison and Amsden formations, just above the thrust, are severely fractured and broken.

In the Paleozoic and Mesozoic formations south of the thrust the fracturing is mostly N. 70° W. to N. 80° E. in trend. A few fractures are present in the Alcova limestone member of the Chugwater formation and in a ledge of silty limestone in the Gypsum Springs formation.

Sisters Hill Area

A foliation (S_1) is present in the gneiss, trending N. 75° W. (average) and dipping 35°–67° N. This foliation is cut and minutely displaced by shear fractures striking N. 30°–53° E., dipping 60°–90° northwest (Fig. 5A). On one vertical N. 53° E. fracture surface slickensides plunge 30° southwest. A few north-south to N. 10° E. shear zones are present in the gneiss.

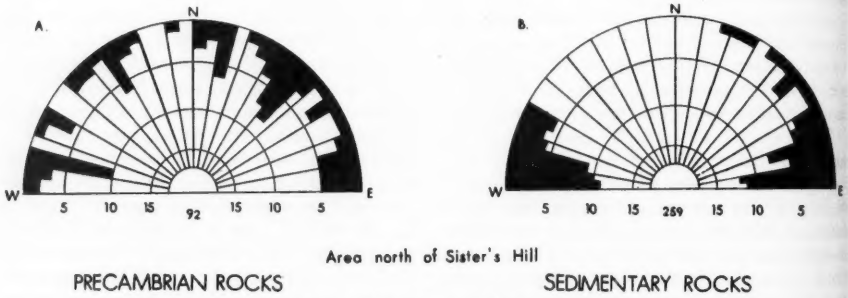

Figure 5. Fracture distribution diagrams of Sisters Hill area, Wyoming

The gneiss very commonly cleaves parallel to the foliation. However, a prominent set of fractures strikes almost parallel to the foliation (N. 75° W.–N. 80° E.), which dips at a high angle to the south. In several places the earlier foliation is slightly displaced by the later fractures. This shear-fracture set is by far the most prominent group in the sedimentary rocks (Fig. 5B) where shear displacements of bedding and small wrench faults parallel to this direction are abundant. This fracture set was, therefore, formed during Laramide deformation.

Megascopic lineation in the foliation of the

gneisses was observed at several outcrops. The lineation is marked by elongate hornblende, biotite, and quartz; it plunges parallel to the direction of dip, or very near to it, of the foliation.

The N. 30°–35° W. fractures in the gneiss, particularly at the north end of the area, are locally filled with quartz. They are usually spaced from 3 feet to a few tens of feet apart and are smooth-surfaced. These are most probably tension fractures.

The fault-wedge of Precambrian rock (Fig. 2) does not appear to have been controlled by any Precambrian structure; rather it appears to be a small thrust block formed as a result of a locally intensified east-west compressive stress. The N. 75° W.–N. 80° E. shear fractures fit this stress system.

Summary

The fracture systems in the sedimentary rocks as compared to those in the Precambrian rocks are strikingly simple. The almost complete lack of the N. 10° E. trends in the sedimentary rocks indicates that this trend is a Precambrian one. The wrench faults having this trend occur only in the northern two-thirds of the Clear Creek thrust area where similar trends of shear fractures and shear zones in the Precambrian are particularly well developed. Therefore, there is good reason to conclude that the orientation of these Laramide wrench faults was controlled by zones of weakness previously established during Precambrian deformation. The other directions of shearing (N. 45° E. and N. 75° E.–N. 75° W.) are well developed in both Precambrian and the later sedimentary formations. Other wrench faults follow either of these two directions. These two trends are probably Laramide in age, although the presence of mafic dikes in the gneisses paralleling these trends suggests that these trends may also have been reactivated along minor Precambrian directions. These two fracture sets fall within the directions of conjugate shearing expected for a mainly horizontal, N. 65° E. oriented principal compressive stress (Fig. 3).

PROBLEMS OF REGIONAL CONTROL AND THE FORCES RESPONSIBLE FOR UPLIFT

Answers to the last two problems mentioned in the Introduction must await the evaluation of data now being gathered in other parts of the range by the author and his students. However, a few remarks might be pertinent at this point.

The shear foliation and fractures along this portion of the east flank (except for a relatively few tension fractures) trend in just about every direction other than that parallel to the axis of the range. Only the N. 10° E. trend is at all close. Osterwald (1959, p. 39) states that there is a close correlation between the attitude of closely spaced primary joints and the trend of the range near Tongue River, lending strong support to the hypothesis that the present outline of the range is controlled by pre-existing primary joint planes. He bases this theory on his diagram A of Plate 3, which he believes statistically suggests that the most prominent joint set trends northwesterly. However, his diagram contains maxima that are just as pronounced for a set of northereasterly trending joints; his major conclusion does not seem justified. Osterwald remarks (1949, p. 37) that many outcrops of sheared granite occur in narrow zones, usually oriented east-northeast. It appears, therefore, that shear deformation of much the same character as in the vicinity of the Clear Creek thrust also occurs west of Sheridan. Wise (1958, p. 25) reports a strong fracture cleavage in the southern Beartooth Mountains. He does not attach any genetic connotation to this close-spaced fracturing. This is probably much the same type of fracturing reported here as occurring along surfaces of shear formation. He reports a strong concentration of fracture cleavage with a north-northeast strike. This direction may well turn out to be a key feature in these two ranges.

It does not seem reasonable at this stage of our investigations to make any categorical statement regarding regional control, as only a small part of the Precambrian rocks have been studied in detail. All we can say is that our data to date have not revealed any Precambrian structure, such as foliation, shear, or other fractures, that has exerted control on other than a local scale.

Conclusions regarding the relative role of vertical versus horizontal forces cannot be offered from this study of the Clear Creek thrust area. Although the eastward thrusting suggests horizontal compression, this is present only in a narrow marginal zone. Good down-dip exposures of the contact between the Precambrian rocks and the Flathead sandstone are needed in order that either block movement or bending be demonstrated. Unfortunately, no

such exposures are present along the east flank of the Bighorn Mountains. The contact is covered almost everywhere, and in most cases can only be traced laterally. Wilson (1934, Fig. 4) presents a cross section in the Five Springs area on the northwest flank of the range in which he shows a bending of the contact and a fan-shaped pattern of joints in the Precambrian rocks. Perhaps what we describe as arching due to horizontal compression will turn out to be only a marginal feature, a sort of mushrooming effect on the flanks of a vertically rising crystalline core (Billings, 1960, Fig. 16; Sanford, 1959, Fig. 18).

CONCLUSION

The present study has shown that a strong N. 10° E. direction of shearing prominent only in the Precambrian rocks was responsible for the trends taken by the two dextral wrench faults of Laramide age at the north end of the Clear Creek thrust. Where this set of shear fractures was less well developed, wrench faulting occurred along directions in accordance with the local stress system responsible for the Laramide movements.

The fault in the Sisters Hill area does not appear to have been influenced by any Precambrian structure.

The origins of fractures are quite varied. One must guard against trying to fit a fracture pattern into a single stress system, particularly when dealing with only the Precambrian rocks.

The depths at which the original rocks became metamorphosed to amphibolite facies range (depending on the temperature gradient and H_2O pressure) between 12 and 36 km (Fyfe, Turner, and Verhoogen, 1958, Figs. 77, 78, p. 183). At such depths, fracturing cannot occur, but the rocks will deform plastically with considerable shear deformation. Much of the folding observed is shear folding. This is non-affine deformation, or as Carey (1953) has termed it, rheid folding. The deformation surfaces are high angle, much as in diapir intrusions of salt, gypsum, and serpentine. Such shear surfaces served as avenues along which the clear replacement microcline formed. Some of the fractures in the gneiss formed after the main Precambrian orogenic deformation when the rocks were uplifted and uncovered to within a few thousand feet of the surface (Price, 1959, p. 150) in the later part of the Precambrian. The fractures tended to open up along the earlier shear surfaces; late mafic dikes, in turn, were intruded along these fractures.

The deformation during the Laramide was of a much shallower nature. The total thickness of the sedimentary cover was probably no greater than 15,000 feet. The great thickness of Paleocene and Eocene gravels, containing boulders of Paleozoic and Precambrian rocks, east of the Clear Creek thrust indicates that erosion kept pace with uplift. Therefore, shear and tension jointing could have taken place concurrently with uplift and thrusting because of the relatively shallow depth (Price, 1959, p. 162). In this situation, one can postulate a local stress system such as suggested in Figure 3. The Laramide high-angle fractures in both the gneisses and the sedimentary rocks can be fairly well related to this stress system.

REFERENCES CITED

Beckwith, R. H., 1941, Structure of the Elk Mountain district, Carbon County, Wyoming: Geol. Soc. America Bull., v. 52, p. 1445–1486

Billings, M. P., 1960, Diastrophism and mountain building: Geol. Soc. America Bull., v. 71, p. 363–398

Bucher, W. H., Chamberlin, R. T., and Thom, W. T., Jr., 1933, Results of structural research in the Beartooth-Bighorn region, Montana and Wyoming: Am. Assoc. Petroleum Geologists Bull., v. 17, p. 680–693

Bucher, W. H., Thom, W. T., Jr., and Chamberlin, R. T., 1934, Geologic problems of the Beartooth-Bighorn region: Geol. Soc. America Bull., v. 45, p. 167–188

Carey, S. W., 1953, The rheid concept in geotectonics: Jour. Geol. Soc. Australia, v. 1, p. 67–117

Chamberlin, R. T., 1945, Basement control in Rocky Mountain deformation: Am. Jour. Sci., v. 243-A, p. 98–116

Chapman, C. A., 1958, Control of jointing by topography: Jour. Geology, v. 66, p. 552–558

Cloos, E., and Cloos, H., 1934, Pre-cambrian structure of the Beartooth, the Bighorn, and the Black Hills uplifts, and its coincidence with Tertiary uplifting: Geol. Soc. America Proc. for 1933, p. 56

Darton, N. H., 1906a, Geology of the Bighorn Mountains: U. S. Geol. Survey Prof. Paper 51, 129 p.

Darton, N. H., 1906b, Description of the Cloud Peak and Fort McKinney quadrangles, Wyoming: U.S. Geol. Survey Atlas, Folio no. 141, 16 p.

Demorest, Max, 1941, Critical structures of the Bighorn Mountains, Wyoming: Geol. Soc. America Bull., v. 52, p. 161–176

Eckelmann, F. D., and Poldervaart, Arie, 1957, Geologic evolution of the Beartooth Mountains, Montana and Wyoming, Part 1: Archean history of the Quad Creek area: Geol. Soc. America Bull., v. 68, p. 1225–1262

Fyfe, W. S., Turner, F. J., and Verhoogen, J., 1958, Metamorphic reactions and metamorphic facies: Geol. Soc. America Mem. 73, 259 p.

Hose, R. K., 1954, Geology of the Crazy Woman Creek area, Johnson County, Wyoming: U. S. Geol. Survey Oil and Gas Investigations, Map OM 142

— 1955, Geology of the Crazy Woman Creek area: U. S. Geol. Survey Bull. 1027–B, 118 p.

Mapel, W. J., 1954, Geology and coal resources of the Lake De Smet area, Johnson County, Wyoming: U.S. Geol. Survey Coal Investigations, Map C 23

Muehlberger, W. R., 1958, Conjugate shear joint sets of small dihedral angle: Geol. Soc. America Bull., v. 69, p. 1618

Osterwald, F. W., 1949, Structure of the Tongue River area, Bighorn Mountains, Wyoming: Wyo. Geol. Assoc., 4th Ann. Field Conf. Guidebook, p. 37–39

— 1955, Petrology of Precambrian granite in the Northern Bighorn Mountains, Wyoming: Jour. Geology, v. 63, p. 310–327

— 1959, Structure and petrology of the northern Bighorn Mountains, Wyoming: Geol. Survey Wyo., Bull. 48, 47 p.

Price, N. J., 1959, Mechanics of jointing in rocks: Geol. Mag., v. 46, p. 149–167

Ramberg, Hans, 1952, The origin of metamorphic and metasomatic rocks: Chicago, Univ. Chicago Press, 317 p.

— 1956, Pegmatities in West Greenland: Geol. Soc. America Bull., v. 67, p. 185–214

Sanford, A. R., 1959, Analytical and experimental study of simple geologic structures: Geol. Soc. America Bull., v. 70, p. 19–52

Sharp, R. P., 1948, Early Tertiary fanglomerate, Bighorn Mountains, Wyoming: Jour. Geology, v. 56, p. 1–15

Spencer, E. W., 1959, Geologic evolution of the Beartooth Mountains, Montana and Wyoming, Part 2: Fracture patterns: Geol. Soc. America Bull., v. 70, p. 467–508

Thom, W. T., Jr., 1947, Structural features of the Bighorn Basin rim: Wyo. Geol. Assoc., 2nd Ann. Field Conf. guidebook, p. 173–177

Turner, F. J., 1948, Mineralogical and structural evolution of the metamorphic rocks: Geol. Soc. America Mem. 30, 342 p.

Wilson, C. W., Jr., 1934, A study of jointing in the Five Springs Creek area, east of Kane, Wyoming: Jour. Geology, v. 42, p. 498–522

Wise, D. U., 1958, The relationship of Precambrian and Laramide structures in the southern Beartooth Mountains, Wyoming: Billings Geol. Soc. 9th Ann. Field Conf. guidebook, p. 24–30

Manuscript Received by the Secretary of the Society, June 16, 1959
Project Grant 708–56–S57

WILLIAM T. HOLSER *California Research Corp., La Habra, Calif.*
CECIL J. SCHNEER *Dept. Geology, University of New Hampshire, Durham, N. H.*

Hydrothermal Magnetite

Abstract: The solubility of magnetite was measured in dilute aqueous solutions of HCl at high temperature and pressure. At 390° C., 440 bars, in 0.0002 M HCl, 300 ppm ferrous iron is dissolved. Solubility decreases with acid concentration; in pure water at the same conditions solubility is less than 0.02 ppm. Calculation of real-gas equilibria from thermodynamic data shows that the contribution of volatile Fe_2Cl_6 molecules is insignificant in such dilute solutions. Comparison with room-temperature data suggests that ferrous iron is brought into true solution mainly as Fe^{2+} ion, by reaction with H^+, although complexes such as $FeCl^{2+}$ and $FeOH^{2+}$ may participate.

Magnetite was synthesized by reaction of acidic iron chloride solutions with calcite at high temperature and pressure.

The amount of iron measured in solutions with HCl concentrations less than a hundredth of that of natural fluids is great enough to be geologically significant.

CONTENTS

Hydrothermal iron deposits 369
Geological environment 369
Theories of formation 370
Experimental and theoretical program 370
Acknowledgments 370
Previous experimental work 371
Experimental procedures 371
Equilibration 371
Sampling and analysis 372
Experimental results 373
Pure water 373
HCl solutions at high temperature 373
Other solutions at high temperature 374
HCl solutions at room temperature 375
Hydrothermal synthesis of magnetite 375
Summary and intercomparison of the data 376
Variations with temperature and pressure . . . 376
Variations with acid concentration 376
Relations of ferrous to ferric iron in solution . . 377
Comparison with other published data. 377
Interpretation 377
Solubility and volatility 377
Calculation of theoretical iron halide-gas equilibria at high temperature and pressure. . 378
Mechanism of solution 379
General statement 379
Relation of room-temperature measurements to hydroxide solubilities 379
Role of complex ions in iron halide solutions . 380
Solubility mechanism at high temperature and pressure 381
Geological implications 381
References cited 383

Figure
1. Solubility of magnetite in HCl solutions at room temperature and pressure 376
2. Theoretical solubility of iron hydroxides at room temperature and pressure as calculated from thermodynamic data 376

Plate
1. Photomicrographs of synthetic hydrothermal magnetite . . . . . Facing 378

Table
1. Experiments on solution of magnetite in pure water at high temperature and pressure . . 373
2. Experiments on solution of magnetite in HCl solutions at high temperature and pressure. 374
3. Equivalent molar concentrations of HCl in some natural fluids 381

HYDROTHERMAL IRON DEPOSITS

Geological Environment

A large class of iron deposits is neither sedimentary nor magmatic and has been variously designated as contact metamorphic, pneumatolytic, pyrometasomatic, or hypothermal. These deposits include both vein fillings and widespread replacements of sedimentary rocks (particularly the carbonates) and are characteristically associated with igneous activity. Evidence from structure, texture, and mineral associations has generally led to the conclusion that such deposits were formed from some kind of dilute fluid at moderate to high temperatures, and we will call them hydrothermal.

The general characteristics of the group are: (1) the associated silicates (some of which orig-

Geological Society of America Bulletin, v. 72, p. 369–386, 2 figs., 1 pl., March 1961

inated at an earlier time and a higher temperature than the magnetite) represent metamorphic equilibria in the amphibolite (in some cases pyroxene hornfels) facies; (2) magnetite is the principal iron mineral, with hematite and pyrite subordinate; (3) some of the magnetite is in the form of veins, in many cases indicating open-space filling as well as replacement of the host rock.

Theories of Formation

A complete theory must include: (1) the source of iron; (2) the state of iron during transportation; (3) the change of conditions responsible for deposition of the iron as magnetite crystals.

Iron must be concentrated from its general dispersion (5 per cent) in the earth's crust by a factor of six to make a minable deposit. The low concentration ratio allows practically any rock type to be an ultimate source of the iron. The mobilized iron might originate from a rock melt by some process of magmatic differentiation, or it may be mobilized directly from a crystalline rock: even solid granite may provide sufficient iron to form magnetite veins (Mackin, 1954).

The theories of mobilization generally fall into one of two categories. Many geologists (best summarized by Fenner, 1933) base their theories on the high "volatility" of a halide gas (Fe_2Cl_6, $FeCl_3$). Others have emphasized the importance of hydrothermal solutions in the transport of iron. They have generally been less specific in describing such a fluid, but a liquid aqueous solution involving hydration and some dissociation is implied. The conditions of temperature and pressure we are considering are above the critical point of any such fluid, and the strict distinction of gas and liquid is lost. However, even if both water and halide are present, there is still a valid question as to whether the system is acting mainly as a simple mixture of gases (including volatile compounds), or whether appreciable interactions between iron and water give it the aspect of a solution in the usual liquid sense.

The term pneumatolytic is often associated with theories that involve volatile halides. However, a pneumatolytic fluid is defined in terms of its origin as a gas in equilibrium with a denser liquid-phase solution. The term therefore concerns the origin of the mobilizing fluid and is not pertinent to considerations of any of its properties once it is on its way to deposit iron.

The principal object of this investigation is to test experimentally some of the possible modes of transport of iron and to apply theory toward an understanding of them.

Experimental and Theoretical Program

The program is essentially one of determining the manner in which the concentration of iron in a fluid phase varies with temperature, pressure, and composition of the system. We began with an attempt to measure the solubility of magnetite in pure water at high temperature and pressure. In a second phase of the measurements, we investigated the effect of HCl on the solubility. No doubt other components, such as CO_2 and HF are also important in nature.

In order to determine whether the concentration of iron in our system actually represented a solubility, rather than the formation of an iron halide gas, Holser calculated the equilibrium concentration of iron halide gas at various temperatures and pressures.

Finally, we made direct experiments of the deposition of magnetite by a change in composition of the system.

The experimental work and many of the theoretical calculations were done in the Department of Geology at Cornell University during 1951–1954. Some of the preliminary results were reported in an abstract (Holser and Schneer, 1953), and a complete report was distributed later (Holser and Schneer, 1957). The present paper summarizes some results that may be of general interest; readers wishing further details may obtain the earlier report.

ACKNOWLEDGMENTS

The experimental program was begun in 1949 with the assistance of E-an Zen. In early 1951 the Graduate School of Cornell University made a small grant for equipment. Later in 1951 The Geological Society of America generously provided funds for equipment and supplies under Research Grant 575-51. During 1952–1954 contract Nonr-40107 with the Office of Naval Research supported the purchase of additional equipment and supplies and the salary of a research assistant. The position was filled during summers by M. Blinder, H. H. Schlanger, and H. H. Vinnedge. In 1957 the Institute of Geophysics at the University of California, Los Angeles, provided facilities for writing this summary of our experimental program. We are also indebted to R. M. Garrels, G. C. Kennedy, E. F. Osborn, and H. S. Yoder for valuable suggestions concerning the experi-

mental program and to A. F. Buddington, F. C. Dickson, H. P. Eugster, G. C. Kennedy, George Tunell, and H. S. Yoder for constructive criticism of the original report. The investigation has depended heavily on all this support and assistance.

PREVIOUS EXPERIMENTAL WORK

The program outlined above is concerned with parts of the system $Fe–O_2–H_2–Cl_2$, particularly in the regions $Fe_3O_4–H_2O$ and $Fe_3O_4–H_2O–HCl$. These are not true binary and ternary systems. The data on various parts of the quarternary system are voluminous.

The system $Fe–O_2$ has been ably summarized by Darken and Gurry (1945; 1946), who included detailed studies of oxygen pressures over the various oxides. The thermodynamic relations for the system $Fe–O_2–H_2$ were summarized by Ralston (1929), with later additions in the hydrogen-rich portion by Emmett and Schultz (1933), Fricke and others (1941), and Muan (1958); and in the oxygen-rich portion by Schmahl (1941). (*See* Eugster, 1959.) In the system $Fe–O_2–H_2$, the stable phase in the presence of water was magnetite, when there is a low hydrogen pressure, and hematite when there is a very low oxygen pressure. These data were all gathered at temperatures higher than 1000° C. and low pressures, so that as far as high-pressure liquid-phase water is concerned, they tell us only what the equilibrium solid phase may be but not the extent of its reaction with water. The system $Fe–O_2–H_2$ has also been treated in studies of corrosion and electrochemistry. Most of such work was done with liquid water at room temperatures; the definitive experimental study is by Corey and Finnegan (1939). Gould and Evans (1947) investigated corrosion at 100° C., and Miller and others (In press) have done some related work at higher temperatures and pressures. Here again magnetite was found to be in equilibrium with "oxygen-free" water.

The system $Fe_2O_3–FeCl_3–H_2O–HCl$ was first investigated in detail by Stirnemann (1925a) who applied his results to geological problems (Stirnemann, 1925b). Stirnemann's thesis has been superseded by the detailed work of Schäfer (1950). More recent results by Wilson and Gregory (1958) do not differ substantially from Schäfer's work. These experiments were at low pressures and high temperatures and therefore concerned with gaseous reactions among the components. As such they are important in the theoretical interpretation of our results. Some work on these systems at low temperatures and low pressures has been done by Schimmel (1952), and there is a considerable volume of data on the solution chemistry of iron chlorides (Brosset, 1941; Rabinowitz and Stockmayer, 1942). Some experiments pertinent to our problem have been done on the corrosion of iron by HCl solutions (at room temperature); in particular Pryor and Evans (1949) studied the solution mechanism of hematite in acid solutions.

In summary, considerable information is available on gas-solid reactions at high temperatures and low pressures, some information on systems involving aqueous solutions at room temperature, but no information on the reactions of iron oxides with pure water or acid solutions at high temperatures and high pressures.

EXPERIMENTAL PROCEDURES

Equilibration

Measurements were made by cooking coarsely crystalline natural magnetite in a solution at constant temperature and pressure, quickly cooling, and analyzing the fluid for ferrous and ferric iron. The magnetite was from Mineville, New York, Cornell No. 237–73. Although this particular material was not analyzed, magnetite from the same locality has been found to have nearly the ideal composition (Newhouse and Glass, 1936). In most cases crystals were ground to pass 60 mesh and the very fine material removed by washing. A few measurements were made of the solubility of hematite, using Baker and Adamson reagent-grade Fe_2O_3.

The pressure vessels were 20 cc closed bombs generally like those described by Morey and Ingerson (1937), made from 303 stainless steel. Liners were needed to eliminate contamination of the solution with iron from the stainless steel: for pure water a shrink-fit ⅛-inch-thick cup of Haines No. 25 alloy; for acid solutions, a close-fitting liner spun from 0.010-inch platinum sheet. Discs of sheet platinum sealed the top.

A bomb was charged with a weighed amount (about 1 g) of magnetite, and the required amount of distilled water or acid solution was measured in with a calibrated pipette. In most of the experiments with acid solutions, magnetite samples were placed on a pedestal above the solution, to avoid reaction at low temperature at the beginning and end of the run.

A major problem in all such experiments is to

keep the system free of oxygen, other than the equilibrium concentration that might be generated by reaction between magnetite and solution. This could be accomplished satisfactorily by using distilled water that had been boiled under a neutral atmosphere and had been continuously flushed with an inert gas during the loading process. The gases used were Seaford-grade nitrogen and welding-grade argon (National Cylinder Gas Co.). Tanks of these gases were specified to contain not more than 0.002 and 0.001 volume per cent oxygen, respectively, and were not further purified. These concentrations in the loading atmosphere correspond to a maximum partial pressure of oxygen of the order of 10^{-5} bars at the experimental conditions. Some oxygen adsorbed on the bomb walls was not detected until late in the experimental program. It was removed by baking the bomb in an argon atmosphere before use. Extrapolation to 400° C. of the thermodynamic data of Darken and Gurry (1946) indicates that an oxygen pressure as low as 10^{-25} should be necessary to prevent the oxidation of magnetite to hematite. As pointed out by Muan (1958, p. 177), this is considerably less than the equilibrium oxygen pressure because of the dissociation of pure water at this temperature. Our oxygen (or hydrogen) pressure was not measured. The thermodynamic data suggest that in our experiments either (1) the oxygen pressure was kept at a sufficiently low value by a minute amount of reaction with metallic iron in the bomb wall, or (2) a very small amount of hematite was formed by oxidation of the magnetite. A low Fe^{3+}/Fe^{2+} was attained in most of our experiments, and $Fe(OH)_2$ was colored only pale grayish green in similar runs. This indicates that the magnetite was not oxidized as in (2). Reaction with the bomb wall as in (1) should have been detectable in the very sensitive iron analysis of the blank runs.

The bombs were heated in two alundum core furnaces of standard design, with the usual control and measurement of temperature. The over-all uncertainty of temperatures was less than 2° C.

The closed liners made it necessary to generate a calculated pressure by degree of filling with water. The resulting uncertainty of the specific volume, about 0.5 per cent, is principally due to uncertainty in the diameter of the cavity. The pressure calculation assumed that: (1) none of the water leaked during the run, and (2) the p-v-T relations of the fluid were not appreciably affected by the presence of ions in the solution. These assumptions could be verified only approximately. The level of water in the bomb was checked qualitatively at the end of the run, and if it was low the run was rejected. However, only a very few runs showed any visual lowering of the water level unless they were dry. Thus leakage was probably negligible in most of the recorded runs, so that although one or two runs may have been considerably in error this would not seriously affect the mean of the large number of runs. The only measurements of partial molal volume at high temperature and pressure are those of Benson and others (1953) for NaCl in the range 385°–395° C. and 240–300 bars. In this range 0.001 N NaCl lowers the pressure (relative to pure water) 0.2–0.5 bars, or 1.0–0.2 per cent. The low dissociation of HCl in this range (Fogo and others, 1954, p. 216; Franck, 1956) suggests that the effect of 0.001 HCl on the specific volume will also be small and well within the precision of specific volume measurement.

The effects on the calculated pressure, of uncertainties in specific volume and temperature, are of the same order of magnitude. The total uncertainty in pressure ranges from 1 to 3 per cent. The p-v-T data of Kennedy (1950a) for pure water were used in all the calculations. Errors introduced by that data (Holser and Kennedy, 1958; 1959) are less than those introduced by other factors, and the results were not recalculated.

Sampling and Analysis

Reprecipitation of iron during cooling was minimized as far as possible by quenching the bomb under water in a few seconds. The cap was unscrewed, a hole punched in the top seal, and four samples of solution extracted by pipette for immediate analysis. The samples could be easily removed without contamination by the original coarse grains of magnetite. Any iron that may have reprecipitated during the quenching undoubtedly did so as a colloidal hydroxide, and such dispersed material would be sampled and analyzed with any iron still in true (supersaturated?) solution.

Iron was determined colorimetrically using 1,10-(ortho) phenanthroline (monohydrate from G. F. Smith Chemical Co.). The general procedures have been summarized by Sandell (1950, p. 375–378) and Smith and Richter (1944, p. 59–79). Modifications of their technique and extreme care in analysis gave a sensitivity of somewhat better than 0.1 ppm (parts

per million by weight). Concentrated reagents were added by micropipette to the 1-ml samples in special long, narrow cuvettes. The analyses were carried out in a Lumetron type 402-E colorimeter, which is a null-type photoelectric instrument. For the determination of total iron, all iron was reduced to the ferrous state with hydroxylamine hydrochloride.

A comparison of 30 paired analyses (both for ferrous and for total iron) in the usable range (0 to 2 ppm) showed a standard deviation of 0.02 ppm, not particularly dependent on the concentration. Ferric iron was determined by difference, and consequently its precision is lower; how much lower depends on the relative levels of ferrous and total iron.

The concentration of dilute HCl solutions was determined at room temperature and pressure with an electronic pH indicator.

However, the concentration is recorded in the unequivocal terms of molar concentration of HCl as a component, rather than as ionic activity. Inasmuch as we are interested in the final equilibrium state, this measurement is of the concentration at the end of the run, after the solution had been removed from the bomb.

New data published since our experiments and calculations were completed allow interpretation of the molar concentrations (Tables 1, 2) in terms of hydrogen-ion activity (the pH, by definition), at the temperature and pressure of the experiment. Franck (1956, p. 200) calculates the dissociation constant of HCl at high temperature and pressure from his conductivity measurements. From his table we deduce, for example, that a 0.0002 M HCl solution at 390° C. and 440 bars has a pH of 3.8, compared with a pH of 3.9 at room temperature and pressure. The pH of "neutral" pure water is 5.3 at the high temperature and pressure (Franck, 1956, p. 203), compared with pH = 7.0 under standard conditions.

EXPERIMENTAL RESULTS

Pure Water

Experiments made in platinum liners showed that any iron dissolved from magnetite into pure water over a considerable range of temperatures and pressures was less than the limit of sensitivity of 0.02 ppm (Table 1). A blank (water and no magnetite) run at 400° C. and 485 bars gave a similarly low result.

Some earlier experiments of lower sensitivity indicated only that dissolved iron was less than 0.6 ppm for 200–300 bars at about 400° C. and less than 0.4 ppm ion in solution for 400–1300 bars at about 500° C. Times were 40–150 hours. A few experiments on the solubility of synthetic hematite were also of low sensitivity but still gave less than 0.2 ppm at 500–1100 bars and about 500° C. The length of runs was 40–100 hours.

Table 1.—Experiments on Solution of Magnetite in Pure Water at High Temperature and Pressure

Experiment no.	Temperature (°C.)	Pressure (bars)	Time (hours)	Analysis of solution, ppm Fe^{2+}	Fe^{3+}
193	494	1185	94	0.02	0.01
194	509	1260	67	0.00	0.02
195	299	1025	46	0.01	0.01
196	183	690	93	0.00	0.03

HCl Solutions at High Temperature

Fifteen runs equilibrated to 0.0002 M HCl (starting concentrations 0.001 M HCl) at about 390° C. and 440 bars. An equal number of runs was made at other temperatures, pressures, and concentrations. (See Table 2.) Several blank (acid solution without magnetite) runs under various conditions gave total iron of less than 1 ppm.

The analyses in the range 380°–400° C., 499–480 bars, for about 0.0002 M HCl, fall into two groups (with a single exception): 0–25 ppm and 250–300 ppm ferrous (and total) iron. The latter are believed to approximate the true solubility, for the following reasons. Late in the series of experiments it was discovered that some of the runs giving low values also showed a thin deposit of hematite on the magnetite. Oxygen contamination was suspected as the cause of the low values, and this was confirmed by sweeping run 284 with oxygen instead of

with an inert gas. The contamination was not observed in many of the runs, and therefore it probably did not come from the gas used for a loading atmosphere. It may have been adsorbed on the liner wall while the bomb was being cleaned in air between runs. This proposition was tested in the last two runs by baking the bomb and liner at 180° C. in an argon atmosphere just before loading in an argon atmosphere. High iron concentrations were obtained in both of these runs.

The experimental program had to be stopped at this point. Further experiments to check these conclusions would have been desirable. Removing the uncertainty of the solubility in this restricted range would have helped interpret the determinations made at other temperatures, pressures, and acid concentrations. The partial correlation between iron and acid concentration was significant (at the 5 per cent level). This is consistent with the iron concentration of 0.02 ppm previously obtained for zero acid concentration. The results of our experiments are too variable to indicate consistently any change of iron concentration with temperature or pressure in the range 200°–500° C. and up to 1100 bars. A similar lack of correlation between iron concentration and length of run indicates that the analyses represent equilibrium concentrations to at least the precision of these determinations.

Table 2.—Experiments on Solution of Magnetite in HCl Solutions at High Temperature and Pressure

Experiment no.	Loading atmosphere*	Molar concentration of HCl (final)	Temperature (°C.)	Pressure (bars)	Time (hours)	Analysis of solution, ppm Fe^{2+}	Fe^{3+}
202	N_2	0.000002	379	380	71	0.24	0.04
204	N_2	0.000005	383	400	42	0.00	0.03
205	N_2	0.000005	388	420	141	0.01	0.02
207	N_2	0.0003	388	420	119	4.7	1.1
221	N_2	0.00016	393	450	120	17.4	1.0
257	N_2	0.00009	382	360	49	14.8	2.7
259	A	0.00013	390	410	108	17.8	0.0
260	A	0.00009	389	410	163	297.	19.
262	A	0.00016	391	420	46	256.	8.
267	A	0.00015	375	320	47	265.	4.
273	A	0.00013	403	490	44	295.	2.
274	A	0.00013	391	430	44	264.	5.
275	A	0.00016	400	480	19	2.40	0.22
276	A	0.00016	391	420	17	254.	6.
277	A	0.00016	299	85†	24	165.	7.
278	A	0.00016	296	81†	24	193.	4.
279	A	0.00018	350	165	23	164.	4.
280	A	0.00017	345	155	23	87.	5.
281	A	0.00016	502	1130	19	14.9	0.6
282	A	0.00019	495	1090	19	7.4	0.6
283	A	0.00016	199	15†	18	4.6	0.5
284	O_2	0.00015	400	480	17	6.9	0.2
285	H_2	0.00014	401	480	17	26.	0.
286	H_2	0.00015	401	480	40	16.3	0.5
287	A**	0.0008	383	360	16	214.	3.
288	A**	0.00023	398	470	41	284.	0.

* All experiments were in bombs lined with platinum or tantalum sheet.
† Sample was in the denser of the two fluid phases.
** Bomb was baked out at 180° C. in A atmosphere before loading.

Eight earlier experiments were made in approximately 10^{-6} M HCl at 180°–300° C. and saturation pressure always in the vapor phase. Analyses did not exceed the sensitivity limit of 1 ppm.

Other Solutions at High Temperature

A few experiments with solutions other than HCl provide supporting data. The experi-

ments gave only a maximum value of possible iron content.

A number of experiments were run at 500° C. and 1000 bars in solutions buffered at pH = 9.0 (sodium borate) and pH = 6.1 (sodium bicarbonate). Analyses were less than the background level of 1 ppm.

Four experiments were made with 0.0008 M NaOH solution in the range 330°–550° C. at about 1000 bars. The analyses on these early runs were made by a visual method with a sensitivity of 2 ppm iron, and neither the runs with magnetite nor the blank runs showed any detectable iron.

Another eight experiments were made with magnetite in (neutral) 0.20 M NaCl solution at about 500° C. and 500 bars. Solution of silver from the liner used in these experiments interfered with the iron analyses, but in no case was the amount above this background of 5 ppm.

HCl Solutions at Room Temperature

The variations of solubility of magnetite in HCl solutions at high temperature and pressure suggested a comparison with the similar variability at room temperature and pressure. It is well known that at room conditions magnetite dissolves in concentrated HCl at a rapid rate, and that no solubility is measured in pure water. If a reasonable assumption is made concerning the mechanism of solution, a theoretical curve of equilibrium iron concentration as it varies with, say, hydrogen-ion concentration, might be derived from available thermodynamic data. However, the lack of specific measurements and some uncertainty concerning the solution mechanism made it desirable to measure solubility.

An excess of −60-mesh magnetite, doubly washed to remove fines, was placed in about 100 ml of HCl of appropriate concentration, in a Pyrex Erlenmeyer flask. The HCl solution was swept with argon before adding the magnetite and during subsequent measurements. The flasks were sealed with wax between measurements. For convenience, they were kept at laboratory temperature, which ranged between 20° and 25° C. during the experiments. Diffusion, convection, and time, rather than mechanical mixing, were depended on for attainment of equilibrium.

Seven experiments were run at initial HCl concentrations ranging from 1 M to 10^{-6} M. The solutions were sampled with a micropipette at intervals of increasing length; the total lengths of the experiments were 330–490 days. The samples were analyzed for ferrous and total iron, and also for acid concentration by the pH meter.

Results of the numerous analyses are outlined in Figure 1. Final analyses for ferrous and ferric iron are plotted against final acid concentration. Approximate equilibrium concentrations are indicated by lines, as determined by the following considerations. For HCl concentrations below 10^{-4}, analyses reached a steady value in 20 or 30 days, and this was assumed to be an equilibrium concentration. With higher concentrations of HCl, the iron concentration continued to increase with time until the end of the runs. Therefore, the solution rate was plotted against concentration to find an approximate value toward which the data were trending. This approximation became increasingly uncertain with increasing HCl concentration because the data showed no decrease of solution rate with time. The relative precision of the analytical method decreases to zero between 0.1 and 0.01 ppm, and ferric iron is determined by difference. Many of the very low values are probably overestimates.

Hydrothermal Synthesis of Magnetite

After we established that measurable amounts of iron could be mobilized in HCl solutions at high temperature and pressure, but not in neutral or alkaline solutions, it was evident that such a solution should deposit magnetite with an increase in the pH. At room temperature, the acidity of a solution of iron chlorides could be reduced by reaction with calcium carbonate. However, this change in pH is accomplished at the expense of adding another component to the system. Calcite is a likely candidate for such a reaction in view of the natural occurrence of iron oxides in limestones, and qualitative experiments were made with it. Magnetite had previously been synthesized from iron chlorides and calcite (for example, *see* Vinogradov and Dontsova, 1952), but always at low pressures.

Iron chloride solutions were made up to about 1000 ppm Fe^{3+} and 500 ppm Fe^{2+}, with a pH of about 2. A measured quantity of the solution was placed in the bottom of the bomb, and a weighed calcium carbonate sample placed on a platinum pedestal above the solution. The experiments were made using temperatures and pressures along the steam saturation line in order to minimize reaction while the bomb was being raised to temperature. In two of the experiments, finely ground calcite was pac-ed in-

side a short length of capillary Inconel tubing in order to slow down the rate of reaction. In four other experiments, a cleavage rhomb of optical grade calcite was placed in the open on the pedestal. The runs lasted 24 to 77 hours.

At a temperature of 320° C. with either arrangement, the principal product was crystalline magnetite. Under high magnification the cleavage surface of the calcite was found to be covered with minute etch pits, many of them occupied by sharp octahedra of magnetite (truncated slightly by dodecahedral faces). (*See* Plate 1.) The X-ray-powder diffraction pattern was identical with that of our standard Mineville magnetite.

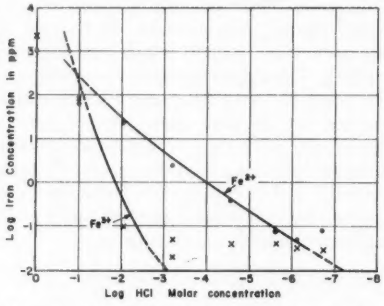

Figure 1. Solubility of magnetite in HCl solutions at room temperature and pressure. Concentrations measured at the end of 300–500 days experiments are indicated by circles for Fe^{2+} and crosses for Fe^{3+}. The equilibrium concentrations shown by the lines are inferred from this data as discussed in the text.

At temperatures of 240° and 150° C. the X-ray diffraction patterns of the products indicated approximately 70 and 90 per cent hematite, respectively, with the remainder magnetite. There are not sufficient observations to attach very much significance to this variation of reaction product with temperature.

Analyses of the solutions after the runs showed less than 200 ppm Fe^{2+} and less than 20 ppm Fe^{3+}, with pH between 5 and 6. Some of the iron probably precipitated at preparation pressure and temperature. Although these experiments did not necessarily establish equilibrium, the magnitude of the iron concentrations is consistent with the solubility measurements.

These qualitative experiments confirm the anticipated deposition of magnetite by neutralization of iron chloride solutions at geologically significant temperatures and pressures and emphasize the disproportionately greater effect on solubility of composition as compared with temperature and pressure.

SUMMARY AND INTERCOMPARISON OF THE DATA

Variations with Temperature and Pressure

The best value of iron concentration in acid solution was 300 ppm in 0.0002 M HCl at about 390° C., 440 bars, and a specific volume of 1.77.

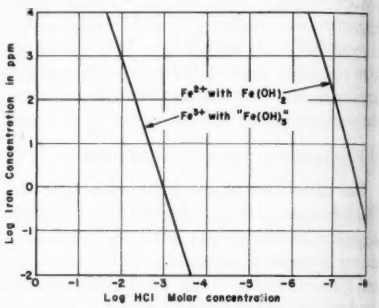

Figure 2. Theoretical solubility of iron hydroxides at room temperature and pressure as calculated from thermodynamic data (equations 7–11). This diagram may be compared with the solubility determination for magnetite, which is shown in Figure 1 at the same scale.

The data for 22° C., 1 bar, specific volume 1.00 (Fig. 1) may be interpolated to give a value of 1.3 ppm at the same HCl concentration. The measurements were too rough to show any consistent trend among the high-temperature measurements themselves.

Variations with Acid Concentration

The decrease of iron with decreasing acid concentration, as indicated roughly by analysis of Table 2, is consistent with the value of less than 0.02 ppm iron in pure water (Table 1). Note the very low iron in HCl concentrations of about 10^{-6} M (Table 2, experiments 202–205). The maximum established for iron concentration in "buffered" solutions is also consistent with this correlation of solubility with acid concentration. They furthermore suggest that the observed decrease may be continued into the range of basic solutions, and that it

may be in some measure independent of the acidic anion.

Figure 1 confirms the analogous decrease of iron with decreasing acid concentration that would be expected at room temperature and pressure.

Relations of Ferrous to Ferric Iron in Solution

The best analyses of supercritical HCl solutions showed very low concentrations of ferric iron, of the order of 1 ppm. Inasmuch as ferric iron was determined by difference, and the precisions of the ferrous and total iron determinations are about 2 per cent each, the measured values of ferric iron may only be interpreted as rough upper limits to the possible concentration. Figure 1 indicates that for a similar acid concentration at room temperature, ferric iron in solution also is at an unmeasurably low value. At room temperature the concentration of ferric iron in equilibrium with magnetite rises steeply as the HCl concentration is increased above that of 10^{-2} M. Thus the rather surprising result, that all the iron in solution at high temperatures and pressures is ferrous iron, may possibly be understood in terms of the results at room temperatures, as discussed below.

Comparison with Other Published Data

The only pertinent solubilities at high temperature were published by Morey (1957, p. 242; Morey and Hesselgesser, 1951), who measured the solubility in pure water of a number of oxides, including hematite but not magnetite. Morey found 90 ppm of Fe_2O_3 dissolved from hematite at 500° C. and 1000 bars. However, Morey found some iron oxide dissolved in all his experiments with other minerals. Presumably this came from solution of the walls of his Inconel X bomb, although no blank runs were made. Morey's method was a dynamic one, in which the solution was moved through the bomb under pressure. The conditions of the experiments indicate that each portion of water remained in the bomb in contact with mineral for only about 30–60 minutes. The short duration of these runs therefore would tend to make his values low, if anything. Therefore contamination of Morey's samples by solution from the metallic iron of the bomb may not be sufficient to explain the discrepancy between his results and ours. Although most other oxides (Morey, 1957, p. 242) had lower solubilities than hematite, the lowest solubility (0.2 ppm for uraninite) was higher than those we obtained for magnetite in pure water.

INTERPRETATION

Solubility and Volatility

We believe that the mechanism mainly responsible for the mobility of iron in our HCl–H_2O mixtures at high temperature and pressure is of the same general type that operates in similar mixtures in the liquid phase at room temperature and pressure. We wish to demonstrate the complete inadequacy of another sort of process that can operate in gaseous systems, in which iron might be mobilized as a gas in molecular combination with chlorine. This distinction is particularly important, in view of the extensive speculation on gas processes in the geological literature.

A common type of solution is that of a salt in liquid water. One may also think of a solution of a salt in steam. In both cases the solubility of the salt is a result of an interaction, "solvation," of the salt component and the water to form the solution. On the other hand, a salt may have an appreciable vapor pressure by itself—this might be called its volatility—an entirely different sort of effect. If a fluid contains a given amount of a salt component in equilibrium with the solid salt, what part of that amount is a result of a simple volatility of the salt, and what part is due to interaction of the pure fluid and the salt component? The part due to fluid-salt interaction might be thought of as a "true," or "liquid-type," solubility and will hereafter be called solubility, with due recognition of the fact that even a simple mixture of gases is a solution in strict thermodynamic nomenclature.

Solubility, as defined above, is found by subtracting from the total of mobilized component the fraction due to volatility. At low total pressure the amount due to volatility can be calculated directly from the applicable thermodynamic equilibrium constant, taking into account any compounds formed by the mobile component as it vaporizes. Then as total pressure is increased, some of the changes in concentration of the mobile component are characteristic of the molecular species already present at low pressure, not of new phenomena of interaction with the "solvent." These are: (1) the increase in vapor pressure of the solid due to change in total pressure, and (2) the departure of individual gases from their low-pressure ideality.

The following calculations show that the iron concentrations measured in the present study were not significantly affected by volatility of

iron chloride but represented solvent action. An HCl concentration of 2.7 M would be needed to volatilize as little as 1 ppm of iron as $FeCl_2$ gas under the conditions of temperature and water pressure of the experiments. This is several orders of magnitude different from the 300 ppm iron measured at 0.0002 M HCl.

Calculation of Theoretical Iron Halide-Gas Equilibria at High Temperature and Pressure

The volatility of iron chlorides is demonstrated by their vapor pressures in approximately single component systems. For example, at 500° C. ferric chloride is a liquid with a vapor pressure of 9.5 bars Fe_2Cl_6 gas (Stirnemann, 1925a, p. 353; Schäfer, 1950, p. 143) and 0.2 bars $FeCl_3$ gas (Schäfer, 1949, p. 68; 1950, p. 143). This is not strictly a single component system, inasmuch as the ferric chloride dissociates slightly to crystalline $FeCl_2$ and gaseous Cl_2. For the stated conditions the chlorine pressure is 0.1 bar (Schäfer and Oehler, 1953, p. 212). In contrast the vapor pressure of crystalline $FeCl_2$ at 500° C. must be less than 10^{-5} bar, found by extrapolating the higher-temperature liquid–vapor pressure data of Schäfer and Krehl (1952, p. 36).

At earth pressures any system involving only one of these components would be "condensed." But if an inert gas was present, the iron could be concentrated in the vapor in proportion to its vapor pressure. If we neglect the small increase of vapor pressure with increase of total pressure and assume a geological temperature of 500° C. and total pressure of 500 bars, a vapor pressure of 10^{-4} bars might be significant (see below). Evidently Fe_2Cl_6 is the only volatile species of importance. In the following calculations we shall make the generous assumptions that the volatile iron is present as Fe_2Cl_6 molecular gas, that the HCl concentration (relative to water) is as high as 0.001 M, and that the temperature and pressure are as high as 500° C. and 500 bars.

It has long been known that the simple single-component volatility of the iron halides is not even a first approximation to a natural situation. The concentration of iron halides in the vapor state is very sharply restricted by the presence of component water, because it reacts to form iron oxide. The equation

$$Fe_2O_3(c) + 6HCl(g) \rightleftharpoons Fe_2Cl_6(l) + 3H_2O(g) \quad (1)$$

(where the nature of a phase is indicated by *c*-crystal, *l*-liquid, and *g*-gas) is displaced strongly to the left. In measuring the thermodynamic equilibrium constant

$$K_1 = \frac{[Fe_2Cl_6]\,[H_2O]^3}{[HCl]^6} \quad (2)$$

at very low pressures (ideal gas), each bracketed fugacity may be replaced by a formal partial pressure, p_x, or a product of the mole fraction, n, times the total pressure, p:

$$K_1 = \frac{p_{Fe_2Cl_6} \cdot p^3_{H_2O}}{p^6_{HCl}} = \frac{n_{Fe_2Cl_6} \cdot n^3_{H_2O}}{p^2 n^6_{HCl}} \quad (3)$$

The value measured by Schäfer (1949, p. 71) for 500° C. (and pressure in bars) is $9.38 \cdot 10^{-7}$. Solving for a concentration of iron chloride would give

$$n_{Fe_2Cl_6} = K_1 p^2 \frac{n^6_{HCl}}{n^3_{H_2O}} = 9.38 \cdot 10^{-7} \cdot 500^2 \cdot \frac{(1.81 \cdot 10^{-5})^6}{1.00} = 8.9 \cdot 10^{-30}\ mole/mole, \quad (4)$$

or $5.5 \cdot 10^{-23}$ *ppm Fe*

if the gases were still ideal at that pressure. Stated in another way, a concentration of 8.9 M HCl is required to keep as little as 1 ppm iron in the gas phase. The value for the equilibrium constant, determined by Stirnemann (1925a) and used in his similar calculations, was larger than Schäfer's by a factor of 200; this led to a correspondingly larger iron concentration.

For nonideal gases, we assume that the fugacity of a gas depends only on its formal partial pressure, and not on interactions with other components. This is a precise assumption in that it defines the conditions of volatility that we are trying to calculate; otherwise "true" fugacities that take account of interactions would give results that are really a form of solubility. It is convenient to use the fugacity coefficient ν_x, which is the ratio of fugacity to the actual partial pressure. In these terms equation (2) becomes:

$$K_1 = \frac{n_{Fe_2Cl_6} \cdot n^3_{H_2O}}{p^2 \cdot n^6_{HCl}} \cdot \frac{\nu_{Fe_2Cl_6} \cdot \nu^3_{H_2O}}{\nu^6_{HCl}} \quad (5)$$

The fugacity coefficient of water was calculated for this purpose (Holser, 1953) from Kennedy's (1950a) p-v-T data. Fugacity coefficients for HCl and Fe_2Cl_6 were estimated by the principle of corresponding states (Hirschfelder, Curtiss, and Bird, 1954, p. 235–239). Using critical points measured for HCl and guessed from empirical rules for Fe_2Cl_6

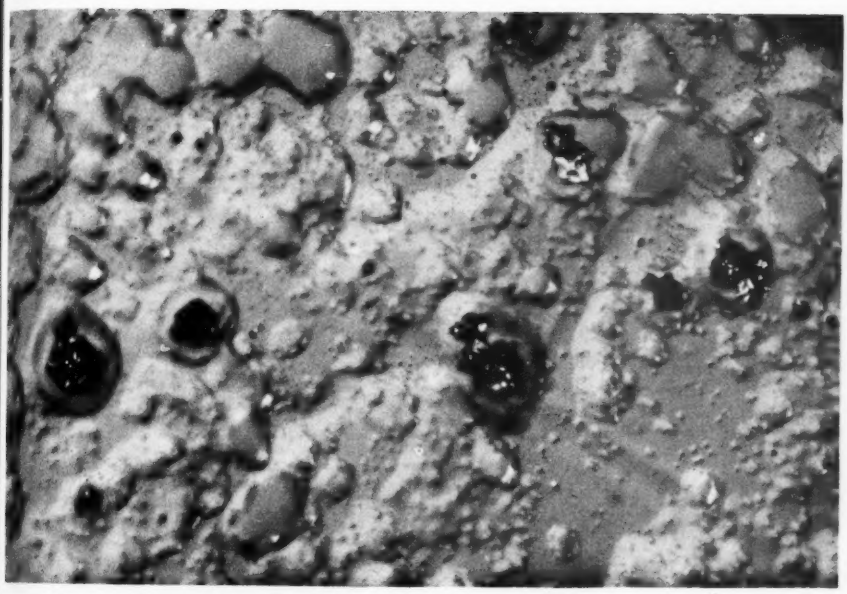

Figure 1. Magnetite crystals in etch pits on a calcite cleavage surface. Formed by reaction of iron chloride solutions with calcite in the gas phase at 320° C. ×100

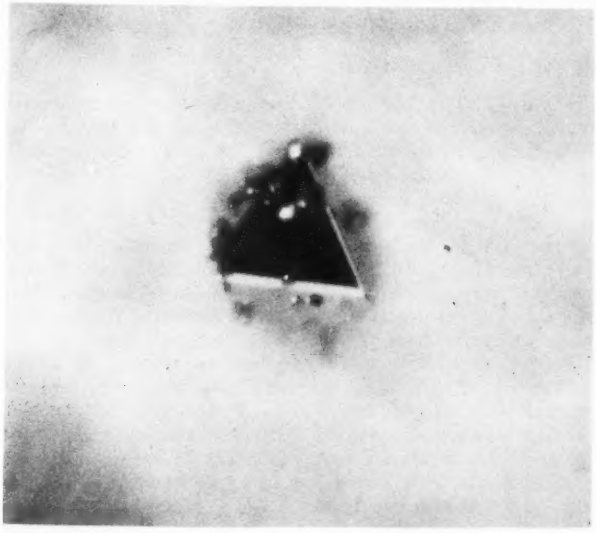

Figure 2. A single magnetite crystal in an etch pit. Same conditions as Figure 1. ×500

PHOTOMICROGRAPHS OF SYNTHETIC HYDROTHERMAL MAGNETITE

HOLSER AND SCHNEER, PLATE 1
Geological Society of America Bulletin, volume 72

(Hirschfelder, Curtiss, and Bird, 1954, p. 238, 252), we entered reduced temperatures and pressures for 500 bars and 500° C. on Newton's (1935) average graphs. Substituting these fugacity coefficients in equation (5) gives:

$$n_{Fe_2Cl_6} = K_1 p^2 \frac{n^6_{HCl}}{n^3_{H_2O}} \cdot \frac{\nu^6_{HCl}}{\nu_{Fe_2Cl_6} \cdot \nu^3_{H_2O}} \qquad (6)$$

$$= 8.9 \cdot 10^{-30} \frac{1.01^6}{0.042 \cdot 0.655^3}$$

$$= 8.0 \cdot 10^{-29} \textit{ mole/mole} \text{ or } 5.0 \cdot 10^{-22} \textit{ ppm Fe.}$$

This is 90 times as much iron as calculated for an ideal gas but is still an insignificant amount, and no reasonable variation of our approximations could make it significant. The corresponding concentration of HCl necessary to mobilize 1 ppm Fe as Fe_2Cl_6 gas is 2.7 M.

We conclude that volatility of iron halides does not account for any significant proportion of the equilibrium concentration of iron in HCl solutions equilibrated with magnetite. The measured iron concentration may be confidently assigned to some sort of interaction between fluid and solid and designated as true solubility. This conclusion seems to contradict calculations recently published by Krauskopf (1957), who finds 0.5 ppm Fe in a magmatic vapor 0.06 M in HCl at 600° C. and 1000 bars. Although Krauskopf took into account the effect of reactions with sulfides, he did not allow for the reaction of water with the iron chloride (equation 1), which is the principal deterrent to halide gas transport of iron in a natural system.

Mechanism of Solution

General statement. The nature of iron solutions has been studied previously at room temperature by a wide variety of measurements of E.M.F., conductivity, vapor pressure, and spectrophotometry. The solubility of magnetite in acid solutions at room temperature can be interpreted first in relation to these data. Then the interpretation may be tentatively extrapolated to the high-temperature measurements.

Relation of room-temperature measurements to hydroxide solubilities. The solution of ferrous hydroxide may be represented by

$$Fe(OH)_2(c) \rightleftarrows Fe^{2+}(aq) + 2(OH)^-(aq), \qquad (7)$$

where *aq* indicates an aqueous solution phase. The solubility product has been evaluated by Miller and others (In press) from new measurements made by four methods:

$$K_7 = [Fe^{2+}]\,[OH^-]^2 = 10^{-15.60} \qquad (7a)$$

including a critical evaluation of 18 earlier determinations. The hydroxyl-ion activity in equation (7a) is in turn related to the hydrogen-ion activity through the ionization constant of water

$$K_8 = [H^+]\,[OH^-] = 10^{-14.17}. \qquad (8)$$

From these two constants one can calculate how the Fe^{2+} activity increases with hydrogen-ion activity (pH), according to the equation

$$Fe(OH)_2(c) + 2H^+(aq) \rightleftarrows Fe^{2+}(aq) + 2H_2O(l)$$

$$K^9 = \frac{[Fe^{2+}]}{[H^+]^2} = \frac{K_7}{K_8^2}. \qquad (9)$$

At these great dilutions the activities may be equated to the respective ionic concentrations. The results of this calculation are graphed in Figure 2.

The analogous calculation for ferric hydroxide is not so clearly defined. The reaction is usually written

$$Fe(OH)_3(c) \rightleftarrows Fe^{3+}(aq) + 3\ OH^-(aq) \qquad (10)$$

with a solubility product as evaluated from available data by Cooper (1937):

$$K_{Fe(OH)_3} = [Fe^{3+}]\,[OH^-]^3 = 10^{-38.6}.$$

But while $Fe(OH)_2$ is a crystalline species whose unit activity is closely approached by the material measured by Miller, $Fe(OH)_3$ is an indefinite term either for a red ferric oxide sol, which insofar as it is crystalline has the hematite structure, or for a yellow ferric oxide monohydrate sol, with the geothite structure (Weiser, 1935, p. 39, 44). Most of the measurements have probably been made on the former material, but even this material is highly variable in particle size and content of adsorbed ions, both of which affect its activity and the calculated solubility product (Lamb and Jacques, 1938, p. 1224; Evans and Pryor, 1949). Hematite is unstable relative to goethite at room temperature (Smith and Kidd, 1949; Schmalz, 1959). With these reservations in mind, we calculated and plotted the total ferric iron in equilibrium with "$Fe(OH)_3$" from the above constant (Fig. 2).

The increasing solubility of magnetite with increasing acid concentrations follows a similar trend, which suggests that a reaction with

hydrogen ion is responsible for the solution of magnetite at room temperature. However, the amount of ferrous iron in equilibrium with magnetite should be substantially lower than that in equilibrium with ferrous hydroxide at the same acid concentration, because ferrous hydroxide decomposes to magnetite in oxygen-free water, according to the following equation:

$$3Fe(OH)_2(c) \rightleftharpoons FeFe_2O_4(c) + 2H_2O(l) + H_2(g). \quad (11)$$

This reaction has been studied by Hüttig and Moldner (1931), Corey and Finnegan (1939), and Fricke and Rihl (1943).

The above considerations show why the solubility of ferrous iron from magnetite should lie below the solubility curve for ferrous hydroxide, as observed. However, if the solution of magnetite were to proceed strictly by analogy with equation (9):

$$FeFe_2O_4(c) + 8H^+(aq) \rightleftharpoons Fe^{2+}(aq) + Fe^{3+}(aq) + 4H_2O(l); \quad (12)$$

then the concentration of ferric iron should always be twice that of ferrous iron. In fact (Fig. 1) ferric iron is less than ferrous iron for concentrations of HCl below 10^{-2} and is imperceptible for concentrations below 10^{-3}. This suggests that the solution of magnetite in low HCl concentrations goes according to an equation like

$$2FeFe_2O_4(c) + 12H^+(aq) \rightleftharpoons 6Fe^{2+}(aq) + 6H_2O(l) + O_2(g) \quad (13)$$

which may also be written

$$FeFe_2O_4(c) + 6H^+(aq) + H_2(g) \rightleftharpoons 3Fe^{2+}(aq) + 4H_2O(l). \quad (13a)$$

Equation (13) also accounts for the strong inhibition of solubility by presence of small amounts of oxygen. It does not account for the shallow slope of the curve (Fig. 1) for ferrous iron vs acid concentration.

Another possibility is that the ferric ions in the magnetite structure are not reduced into solution. An equation may be written as follows:

$$FeFe_2O_4(c) + 2H^+(aq) \rightleftharpoons Fe^{2+}(aq) + \text{“}Fe_2O_3\text{”} + H_2O(l). \quad (14)$$

This equation is nonspecific in that “Fe_2O_3” is a component of an unspecified solid phase. In this respect there seem to be three possibilities: (1) the ferric oxide is present as “colloidal Fe_2O_3,” (2) it is present as crystalline hematite, or (3) it is present as ferric ions in the magnetite structure. Ferric iron may remain behind either as a new precipitate, as crystalline hematite, or as a solid solution in the magnetite-maghemite series. We observed a thin irregular film of red hematite coating the magnetite charge in some of the runs.

Pryor and Evans (1949) studied the dissolution of hematite in acid solutions. Their procedure was similar to ours, although most of their experiments were for only 1 hour. Their resulting curve of ferric iron from hematite lies near our curve for ferrous iron from magnetite, down to their minimum concentration of 10^{-3} M HCl, but has even smaller slope. They also found a small amount of ferrous iron in longer runs at low acid concentrations. They interpreted this as preferential solution of non-stoichiometric ferrous ions from the hematite structure, but it may also be due to reduction of ferrous iron in dilute acid. (*See* equations 13–14.)

Role of Complex Ions in Iron Halide Solutions. The formation of complex ions can increase the total iron in solution, if other conditions are equal.

The iron complex $FeOH^{2+}$ is particularly important at high pH. The investigations of Cooper (1937), Lamb and Jacques (1938), and Brosset (1941) give association constants that indicate more iron as the complex than as free Fe^{3+} ions, at pH above 2.5. Lamb and Jacques (1938), Arden (1951), and Ito and Yui (1953) also postulate a further association to $Fe(OH)_2^+$. Therefore this complex may be important in stabilizing the small amount of ferric iron detected by us in the range of concentrations from 10^{-2} to 10^{-3} M HCl.

As the concentration of the HCl solutions increases, ferric iron associates with chlorine to form the complex ions $FeCl^{2+}$, $FeCl_2^+$ (Brosset, 1941; Rabinowitz and Stockmayer, 1942; Siddall and Vosburgh, 1951), and finally in very concentrated solutions $FeCl_4^-$ (Friedman, 1952), or Fe_2Cl_6 (Brady, 1958). The first of these is the major complex in the acidity range of our measurements on magnetite, and the measured equilibrium constants indicate that it may be important in fixing the total ferric iron in solution at concentrations of HCl greater than 10^{-2}.

The solution chemistry of ferrous iron contrasts strikingly with the above data on ferric iron. Stokes and Robinson (1948) show by detailed measurements that ferrous chloride is a

strong electrolyte, dissociating completely in aqueous solution, although a small concentration of $Fe(OH)^+$ may be present at high pH (Leussing and Kolthoff, 1953). The Fe^{2+} ion is hydrated with about 12 water molecules, as are many other simple cations (Robinson and Stokes, 1949). Even in very concentrated solutions it does not form complexes with HCl (Schimmel, 1952).

Summarizing the information for room-temperature solutions, we conclude that although not all features of the experiments have been satisfactorily explained, the principal cause of solution over most of the range of concentration is probably the reaction with hydrogen ions represented by equation (13). At HCl concentrations greater than 0.1 M, equation (12) becomes important, and ferric iron increases sharply. The solution of ferric iron in these highly acid solutions is aided by the formation of the complex ion $FeCl^{2+}$, and in the less acid solutions the small amount of ferric iron is enhanced by $FeOH^{2+}$. Ferrous iron does not form complex ions.

Solubility Mechanism at High Temperature and Pressure. At high temperature and pressure the experiments (Table 2) show an increase of iron concentration with increasing acid concentration, and a lack of ferric iron in the solution, both of which parallel the more detailed observations at room temperature. The decomposition of $Fe(OH)_2$ to magnetite (equation 13) is even faster at high temperature; it has been observed up to 290°C. (Berl and van Taack, 1928; Miller and others, in press). All this suggests that the dissolution of magnetite at high temperature and pressure also proceeds by a hydrogen-ion reaction similar to that of equation (13) above.

The importance of complex ions in the solutions at high temperature and pressure is difficult to evaluate, particularly in view of the fact (Franck, 1956; Fogo and others, 1954, p. 216) that HCl is no longer a strong electrolyte under these conditions. Rabinowitz and Stockmayer (1942, p. 340–341) observed that the stabilities of $FeOH^{2+}$ and $FeCl^{2+}$ ions increase markedly with temperature in the range 25°–45° C., and this is interpreted in terms of an endothermal process in formation of complex ions. Friedman (1952) studied the spectra of one of the complex ions, $FeCl_4^-$, in media of low dielectric constant, and found the complex still stable. The weak dissociation of NaCl and HCl, at 390° C. and critical density, suggests that the usually strong electrolyte $FeCl_2$ may also tend to be more highly associated under these conditions. Thus the formation of complex ions might be important in the solubility process at high temperature, even for ferrous iron.

TABLE 3.—EQUIVALENT MOLAR CONCENTRATION OF HCl IN SOME NATURAL FLUIDS

Source	Maximum	Minimum	Mean	Number	Reference
Kilauea volcanic gases	0.22*	0.00	0.04	24	Shepherd (1938, p. 321)
Vesuvius volcanic gases	0.09	0.00	0.03	3	Gautier (1909)
Katmai fumarolic gases	0.31	0.003	0.07	15	Allen (1922, p. 80)
White Island fumarolic gases			0.25	4	Wilson (1953)
Amygdules in Japanese lavas	0.0006	0.000	0.0001	5	Kokubu and others (1957, p. 157)
Gases from various rocks in vacuo	0.29*	0.004	0.17	20	Shepherd (1938, p. 326)
Fluid inclusions in various pegmatitic minerals	0.05	0.00	0.02	6	Wahler (1956, p. 129, 135)

*Less a single erratically high analysis.

Geological Implications

Anything less than 1 ppm iron in solution is not significant in the formation of hydrothermal iron-ore deposits. Huber and Garrels (1953, p. 354) use 3 ppm for sedimentary iron ores. Evidently pure water cannot provide even this small amount in solution.

But what HCl concentrations are available to increase solubility in natural fluids? Table 3 was calculated on the assumption that H_2 and Cl_2 are combined at equilibrium into HCl, and this is mixed with the H_2O to form an HCl solution. At 500° C. the thermodynamic equilibrium constant for the formation of HCl is $4.5 \cdot 10^{16}$ (Lewis and Randall, 1923, p. 503), and this is reduced only as far as $2.5 \cdot 10^{16}$ when the effect of real gases at 500 bars is taken into account. Effectively all the

H_2 or all the Cl_2 (in some cases Cl^- was used) will react to form HCl, depending upon which is in the least concentration.

When the diversity of the analytical methods and the sources of material are considered, it is surprising that this series of analyses is concordant in order of magnitude. Only two single analyses from Kilauea (Shepherd, 1938) and from Mihara (Iwasake, 1951) show exceptionally high values of .66 and 1.4 M HCl respectively. Possibly much of the chlorine in igneous rocks corresponds to a similar concentration of HCl in the original magma or its derivative solutions. Kuroda and Sandell (1953) found 0.022 per cent Cl in granitic rocks; if this were HCl dissolved in the usual 1 per cent water, the concentration would be 0.6 M.

These considerations place some restrictions on the chloride and possible HCl concentrations that may be expected in natural fluids. Concentrations in the range 0.01–0.1M are probably common, but concentrations higher than 0.5 M are unlikely. Similar considerations led Krauskopf (1957, p. 793) to find a concentration of 0.06 M HCl. The simple assumptions neglect many reactions that may have changed the compositions of the solutions (Fyfe, Turner, and Verhoogen, 1958, p. 144–146; Ellis, 1957, p. 423).

Our measurements show that geologically significant concentrations of iron can be mobilized at temperatures and pressures similar to those at which hydrothermal deposits were formed and in solutions two orders of magnitude more dilute in HCl than these natural fluids. Transport by HCl solutions can therefore be important in the formation of some magnetite deposits. Further high-temperature experiment is necessary to compare solubilities in HCl solutions with those in other important acids such as HF and H_2CO_3. The importance of the latter is well attested by the geological work of Behrend (1934), the low-temperature experiments of Huber and Garrels (1953, p. 355), and a few observations by Morey (Abelson, 1954, p. 123) at high temperature and pressure.

The solubility of iron compounds in all these solvents will undoubtedly decrease with decreasing acid concentration, and we can suggest no mechanism by which it will increase in basic solutions. Shand (1947) was forced to depend upon a ferrous hydroxide hydrosol for transport in an alkaline medium. However, the instability of this sol at high temperatures has already been pointed out above (Solubility Mechanism at High Temperatures), and the ineffectiveness of colloidal suspensions in the replacement process has been discussed in detail elsewhere (Holser, 1947, p. 387–388). On the other hand, it is difficult to reconcile acid transport of iron with the cogent arguments of many petrologists (Shand, 1947; Kennedy, 1955, p. 498; Ridge, 1956; Fyfe, Turner, and Verhoogen, 1958, p. 143–144) that the final derivative of many magmas is probably alkaline rather than acid. If HCl is important in the transport of iron, the common deposition of magnetite in carbonate rocks is easily explained by the reaction between the acid solution and calcium carbonate. The experiments suggest that the mechanism of solution depends principally on acidity; then the mechanism of deposition depends on neutralization.

Our limited data are insufficient to give quantitative conclusions concerning the effect of temperature and pressure changes on the deposition of dissolved material in acid solutions. But the calculated volatility at very low pressure, compared with the measured values of real solubility at high pressure, indicates that the dissolved load must be dropped during a pressure drop. This is of course a general feature of supercritical solutions (Kennedy, 1950b, p. 648–649; *see* Fyfe, Turner, and Verhoogen, 1958, p. 135–137). But much more experimental work remains to be done before we can interpret in detail the deposition with lowered pressure and analogous deposition expected with lowered temperature.

In his detailed discussion of the ore-forming fluid Graton (1940, p. 344) concluded that ". . . The venerable thesis that metals and other components for mineral formation are transferred as volatile compounds of the halogen elements is found to require a great pyramiding of favoring assumptions." But techniques as new as isotopic analysis have been called to its defense (Vinogradov and Dontsova, 1952), although the reasoning is far from clear. A comparison of our experimental data with the theoretical calculations for real-gas equilibria should make it abundantly clear that HCl solutions are capable of transporting far more iron, under conceivable earth conditions, than can possibly be accounted for by the volatility of a halide gas. If the natural occurrence of these dilute aqueous solutions of HCl is doubtful, then concentrations of HCl sufficiently anhydrous to volatilize $FeCl_2$ are certainly out of the question. These con-

clusions might be juxtaposed in the following way: calculation indicates that water prohibits iron chloride volatility, but experiment shows that the dilute acid solutions formed by this water are capable of transporting iron in true solution.

REFERENCES CITED

Abelson, P. H., 1954, Annual report of the Director of the Geophysical Laboratory: Carnegie Inst. Washington Year Book 1954, p. 95–145

Allen, E. T., 1922, Chemical aspects of volcanism with a collection of the analysis of volcanic gases: Franklin Inst. Jour., v. 193, p. 29–80

Arden, T. V., 1951, The hydrolysis of ferric iron in sulphate solution: Chem. Soc. London Jour., p. 350–363

Behrend, Fritz, 1934, Rezenter Vulkanismus und die Bildung von Eisenerzen: Zeitschr. Deutsch. Geol. Gessel., v. 66, p. 360–367

Benson, S. W., Copeland, C. S., and Pearson, David, 1953, Molal volumes and compressibilities of the system NaCl–H_2O above the critical temperature of water: Jour. Chem. Physics, v. 21, p. 2208–2212

Berl, E., and Von Taack, F., 1928, Über die Schutzwirkung von Natriumsulfat bei der Einwirkung von Laugen und Salzen auf Flusseisen unter Hochdruck: Arch. für Warmewirtschaft, v. 9, p. 165–169

Brady, G. W., 1958, Structure in ionic solutions. III.: Jour. Chem. Physics, v. 29, 1371–1375

Brosset, Cyril, 1941, The ionic equilibrium in acid ferric chloride solutions of fixed ionic strength: Svensk Kemisk Tidskrift, v. 53, p. 434–440

Cooper, L. H. N., 1937, Some conditions governing the solubility of iron: Royal Soc. London. Proc., v. 124B, p. 299–307

Corey, R. C., and Finnegan, T. J., 1939, The pH, dissolved iron concentration and solid product resulting from the reaction between iron and pure water at room temperature: Am. Soc. Testing Materials Proc., v. 39, p. 1242–1260

Darken, L. S., and Gurry, R. W., 1945, The system iron-oxygen. I. The wustite field and related equilibria: Am. Chem. Soc. Jour., v. 67, p. 1398–1412

— 1946, The system iron-oxygen. II. Equilibrium and thermodynamics of liquid oxide and other phases: Am. Chem. Soc. Jour., v. 68, p. 798–816

Ellis, A. J., 1957, Chemical equilibrium in magmatic gases: Am. Jour. Sci., v. 255, p. 416–431

Emmett, P. H., and Schultz, J. F., 1933, Equilibria in the system Fe–Fe_3O_4–H_2O–H_2 at 400, 500, and 600 C: Am. Chem. Soc. Jour., v. 55, p. 1376–1389

Eugster, H. P., 1959, Reduction and oxidation in metamorphism, p. 397–426 *in* Abelson, P. H., Researches in geochemistry: New York, John Wiley & Sons, 511 p.

Evans, U. R., and Pryor, M. J., 1949, The passivity of metals. Part IX. The solubility product of freshly precipitated $Fe(OH)_2$: Chem. Soc. London Jour., Supp., p. 157–160

Fenner, C. N., 1933, Pneumatolytic processes in the formation of minerals and ores, p. 58–106 *in* Ore deposits of the Western states (Lindgren Volume): Am. Inst. Min. and Metal. Engineers, 797 p.

Fogo, J. K., Benson, S. W., and Copeland, C. S., 1954, Electrical conductivity of supercritical solutions of sodium chloride and water: Jour. Chem. Physics, v. 22, p. 212–216

Franck, E. V., 1956, Hochverdichteter Wasserdampf III, Ionendissoziation von HCl, HOH, und H_2O in uberkritischem Wasser: Zeitschr. Physikal. Chemie, v. 8, p. 192–206

Fricke, R., and Rihl, S., 1943, Zur Beständigkeit des $Fe(OH)_2$: Naturwiss., v. 31, p. 326–327

Fricke, R., Walter, K., and Lohrer, W., 1941, Über die Beeinflussung des Gleichgewichtes Fe/Fe_3O_4 mit H_2O/H_2 durch den physikalischen Zustand der festen Reaktionsteilnehmer: Zeitschr. Elektrochem., v. 47, p. 487–500

Friedman, H. L., 1952, The visible and ultraviolet absorption spectrum of the tetrachlorferrate (III) ion in various media: Am. Chem. Soc. Jour., v. 74, p. 5–10

Fyfe, W. S., Turner, F. J., and Verhoogen, J., 1958, Metamorphic reactions and metamorphic facies: Geol. Soc. America Mem. 73, 260 p.

Gautier, Armand, 1909, Sur les gaz des fumarolles volcaniques: Acad. Sci. Paris Compte Rendu, v. 148, p. 1708–1715

Gould, A. J., and Evans, U. R., 1947, Corrosion of steel by boiling water: Iron and Steel Inst. Jour., v. 155, p. 195–200

Graton, L. C., 1940, Nature of the ore-forming fluid: Econ. Geology, v. 35, supp. 2.

Hirschfelder, J. O., Curtiss, C. F., and Bird, R. B., 1954, Molecular theory of gases and liquids: New York, John Wiley & Sons, 1219 p.

Holser, W. T., 1947, Metasomatic processes: Econ. Geology, v. 42, p. 384–395

—— 1953, The fugacity coefficient of water at high temperature and pressure: Jour. Phys. Chemistry, v. 58, p. 316–317

Holser, W. T., and Kennedy, G. C., 1958, Properties of water, Part IV. Pressure-volume-temperature relations of water in the range 100–400 C, 100–1400 bars: Am. Jour. Sci., v. 256, p. 744–754

—— 1959, Properties of water, Part V. Pressure-volume-temperature relations of water in the range 400–1000 C, 100–1400 bars: Am. Jour. Sci., v. 257, p. 71–77

Holser, W. T., and Schneer, C. J., 1953, Deposition of high-temperature nonmagmatic magnetite (Abstract): Geol. Soc. America Bull., v. 64, p. 1435

—— 1957, Hydrothermal geochemistry of iron: U.S. Office of Naval Res., Final Rept. on Project NR 081-120: U.S. Dept. Commerce, Office Tech. Services Doc. PB 147802, 61 p.

Huber, N. K., and Garrels, R. M., 1953, Relation of pH and oxidation potential to sedimentary iron mineral formation: Econ. Geology, v. 48, p. 337–357

Hüttig, G. F., and Moldner, H., 1931, Das System Eisen (II)–oxyd/Wasser und sein Ubergange zu dem System Eisen (III)–oxyd/Wasser: Zeitschr. anorg. allg. Chemie, v. 196, p. 177–187

Ito, T., and Yui, N., 1953, The hydrolysis constants of ferric iron in nitrate solution: Sendai, Japan, Tohoku Univ. Sci. Repts., v. 37, p. 19–27

Iwasaki, I., 1951, Geophysics of volcano Ooshima, Izu: Jour. Geography, Tokyo, v. 60, p. 140–143

Kennedy, G. C., 1950a, Pressure-volume-temperature relations in water at elevated temperatures and pressures: Am. Jour. Sci., v. 248, p. 540–564

—— 1950b, A portion of the system silica-water: Econ. Geology, v. 45, p. 629–653

—— 1955, Some aspects of the role of water in rock melts: Geol. Soc. America Special Paper, v. 62, p. 489–504

Kokubu, Nobuhide, Watanabe, Syosuke, and Ide, Yasusi, 1957, Liquid inclusions in the amygdaloidal cavities of olivine-basalt from Imazu, Hukuoka City, Japan: Fukuoku, Japan, Kyushu Univ. Fac. Sci. Mem., ser. C, v. 2, p. 151–160

Krauskopf, K. B., 1957, The heavy metal content of magmatic vapor at 600°C: Econ. Geology, v. 52, p. 786–807

Kuroda, P. K., and Sandell, E. B., 1953, Chlorine in igneous rocks: Geol. Soc. America Bull., v. 64, p. 879–896

Lamb, A. B., and Jacques, A. G., 1938, The slow hydrolysis of ferric chloride in dilute solution. II. The change in hydrogen ion concentration: Am. Chem. Soc. Jour., v. 60, p. 1215–1225

Leussing, D. L., and Kolthoff, I. M., 1953, The solubility product of ferrous hydroxide and the ionization of the aquoferrous ion: Am. Chem. Soc. Jour., v. 75, p. 2476–2479

Lewis, G. N., and Randall, Merle, 1923, Thermodynamics and the free energy of chemical substances: New York, McGraw-Hill Book Co., 653 p.

Mackin, J. H., 1954, Geology and iron-ore deposits of the Granite Mountain area, Iron County, Utah: U. S. Geol. Survey Mineral Invest. Field Studies maps, MF 14

Miller, P. D., and others, in press, The solubility product of ferrous hydroxide: Am. Chem. Soc. Jour.

Morey, G. W., 1957, The solubility of solids in gases: Econ. Geology, v. 52, p. 225–251

Morey, G. W., and Hesselgesser, J. M., 1951, The solubility of some minerals in superheated steam at high pressures: Econ. Geology, v. 46, p. 821–835

Morey, G. W., and Ingerson, Earl, 1937, A bomb for use in hydrothermal experimentation: Am. Mineralogist, v. 22, p. 1121–1122

Muan, Arnulf, 1958, Phase equilibria at high temperatures in oxide systems involving changes in oxidation states: Am. Jour. Sci., v. 256, p. 171–207

Newhouse, W. H., and Glass, J. P., 1936, Some physical properties of certain iron oxides: Econ. Geology, v. 31, p. 699–711

Newton, R. H., 1935, Activity coefficients of gases: Industrial and Engineering Chemistry, v. 27, p. 302–306

Pryor, M. J., and Evans, U. R., 1949, The passivity of metals. X. The mechanism of direct dissolution of ferric oxide: Chem. Soc. London Jour., p. 3330–3336

Rabinowitz, Eugene, and Stockmayer, W. H., 1942, Association of ferric ions with chloride, bromide and hydroxyl ions (a spectroscopic study): Am. Chem. Soc. Jour., v. 64, p. 335–347

Ralston, O. C., 1929, Iron oxide reduction equilibria: U. S. Bur. Mines Bull. 296, 326 p.

Ridge, J. D., 1956, Transportation and deposition of hydrothermal minerals: Intern. Geol. Cong. 20th Sess. Resumes, p. 100

Robinson, R. A., and Stokes, R. H., 1949, The role of hydration in the Debye-Hückel theory: New York Acad. Sci. Annals, v. 51, p. 593–604

Sandell, E. B., 1950, Colorimetric determination of traces of metals: 2d ed., New York, Interscience Publishers, Inc., 673 p.

Schäfer, Harald, 1949, Die Einwirkung von Chlorwasserstoff auf Eisenoxyd und die Auswertung der Reaktionsgleichgewichte: Zeitschr. anorg. allg. Chemie, v. 259, p. 53–74

— 1950, Das System Fe_2O_3–FeOCl–$FeCl_3$–H_2O–HCl zwischen etwa 100 und 1000°C: Zeitschr. anorg. allg. Chemie, v. 261, p. 142–152

Schäfer, Harald, and Krehl, Kurt, 1952, Das Reaktionsgleichgewicht $FeCl_2$ gas$+H_2=Fe+2HCl$: Zeitschr. anorg. allg. Chemie, v. 268, p. 35–46

Schäfer, Harald, and Oehler, Eberhard, 1953, Der Chlordurck über den festen Bodenkorpern $FeCl_3$ und $FeCl_2$: Zeitschr. anorg. allg. Chemie, v. 271, p. 206–216

Schimmel, F. A., 1952, The ternary systems ferrous chloride-hydrogen chloride-water, and ferric chloride-ferrous chloride-water: Am. Chem. Soc. Jour., v. 74, p. 4689–4691

Schmahl, N. G., 1941, Die Beziehungen zwischen Sauerstoffdruck, temperatur und zusammensetzung im System Fe_2O_3–Fe_3O_4: Zeitschr. Elektrochem., v. 47, p. 821–835

Schmalz, E. F., 1959, A note on the system Fe_2O_3–H_2O: Jour. Geophys. Research, v. 64, 575–579

Shand, S. J., 1947, The genesis of intrusive magnetite and ores: Econ. Geology, v. 42, p. 634–636

Shepherd, E. S., 1938, The analysis of gases obtained from volcanoes and from rocks: Jour. Geology, v. 33, p. 289–369

Siddall, T. H., and Vosburgh, W. C., 1951, A spectrophotometric study of the hydrolysis of iron (III) ion: Am. Chem. Soc. Jour., v. 73, p. 4270–4272

Smith, F. G., and Kidd, D. J., 1949, Hematite-goethite relations in neutral and alkaline solutions under pressure: Am. Mineralogist, v. 34, p. 403–412

Smith, G. F., and Richter, F. P., 1944, Phenanthroline and substituted phenanthroline indicators: Cincinnati, Ohio, G. Frederick Smith Chem. Co., 103 p.

Stirnemann, Ernst, 1925a, Das System Eisenchlorid-Wasser bei höherer Temperatur: Neues Jahrb. Min. Pet., Beil. B., v. 52A, p. 334–377

— 1925b, Ueber die Bildungsverhaltnisse der Eisenerzlagerstatten im System Eisenchlorid-Wasser: Neues Jahrb. Min. Pet., Beil. B., v. 53A, p. 59–94

Stokes, R. H., and Robinson, R. A., 1948, Thermodynamic study of bivalent metal halides in aqueous solution. XVII. Revision of data for all 2:1 and 1:2 electrolytes at 25°: Faraday Soc. Trans., v. 44, p. 295–307

Vinogradov, A. P., and Dontsova, E. I., 1952 (Isotopic composition of oxygen in minerals of a skarn origin): Akad. Nauk SSSR Doklady, n. s., v. 85, p. 1341–1343

Wahler, William, 1956, Über die in Kristallen eingeschlossenen Flussingkeiten und Gase: Geochim. et Cosmochim. Acta, v. 9, p. 105–135

Weiser, H. B., 1935, Inorganic colloid chemistry, v. II. The hydrous oxides and hydroxides: New York, John Wiley & Sons, Inc., 429 p.

Wilson, L. E., and Gregory, N. W., 1958, Vapor-solid equilibria in the iron-chlorine system: Jour. Phys. Chemistry, v. 62, p. 433–437

Wilson, S. H., 1953, Chemical investigations of the hot springs of the New Zealand thermal region: Pacific Sci. Cong., 7 Sess., v. 2, p. 449–469

Manuscript Received by the Secretary of the Society, June 19, 1959

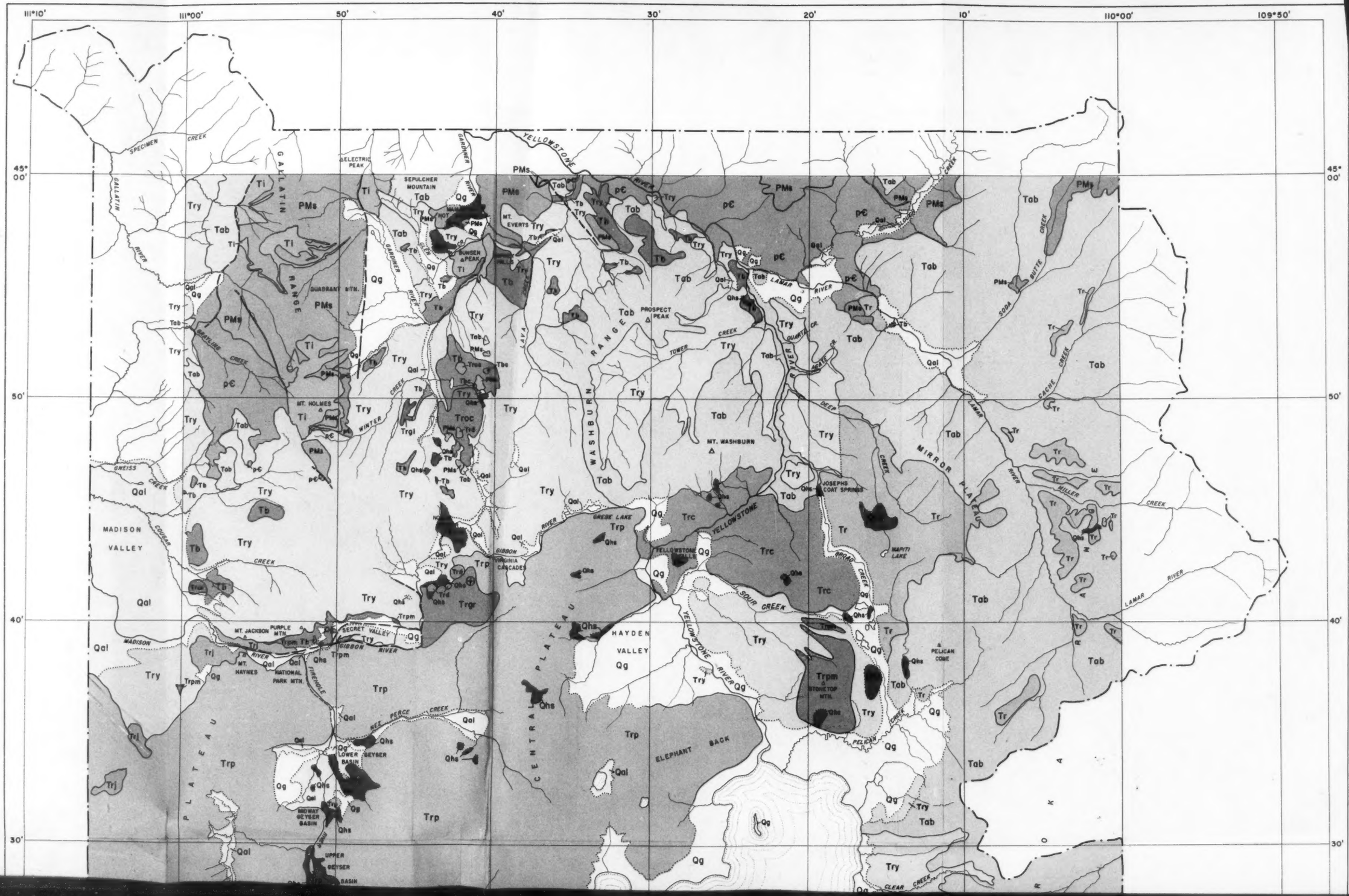
111°10'
111°00'
50'
40'
30'
20'
10'
110°00'
109°50'
45° 00'
50'
40'
30'
SPECIMEN CREEK
GALLATIN RIVER
GALLATIN RANGE
ELECTRIC PEAK
SEPULCHER MOUNTAIN
GARDNER RIVER
YELLOWSTONE RIVER
MT. EVERTS
BUNSEN PEAK
QUADRANT MTN.
GRAYLING CREEK
MT. HOLMES
WINTER CREEK
GNEISS CREEK
COUGAR CREEK
MADISON VALLEY
MT. JACKSON
PURPLE MTN.
SECRET VALLEY
GIBBON RIVER
MADISON RIVER
MT. HAYNES
NATIONAL PARK MTN.
FIREHOLE RIVER
PLATEAU
NEZ PERCE CREEK
LOWER GEYSER BASIN
MIDWAY GEYSER BASIN
UPPER GEYSER BASIN
SWAN LAKE FLAT
GIBBON VIRGINIA CASCADES
GREBE LAKE
CENTRAL PLATEAU
HAYDEN VALLEY
ELEPHANT BACK
YELLOWSTONE RIVER
PELICAN CREEK
SOUR CREEK
YELLOWSTONE LAKE
YELLOWSTONE LAKE OUTLET
LAVA CREEK
WASHBURN RANGE
MT. WASHBURN
PROSPECT PEAK
TOWER CREEK
QUARTER CR.
AGATE CR.
DEEP CREEK
LAMAR RIVER
JOSEPHS COAT SPRINGS
WAPITI LAKE
ROAD CREEK
MIRROR PLATEAU
PELICAN CONE
STONE TOP MTN.
SODA BUTTE CREEK
CACHE CREEK
MILLER CREEK
CLEAR CREEK
Ti
Try
Tab
PMs
pC
Qg
Qal
Tb
Trgr
Trgl
Troc
Trc
Trp
Trpm
Trj
Tr
Qhs

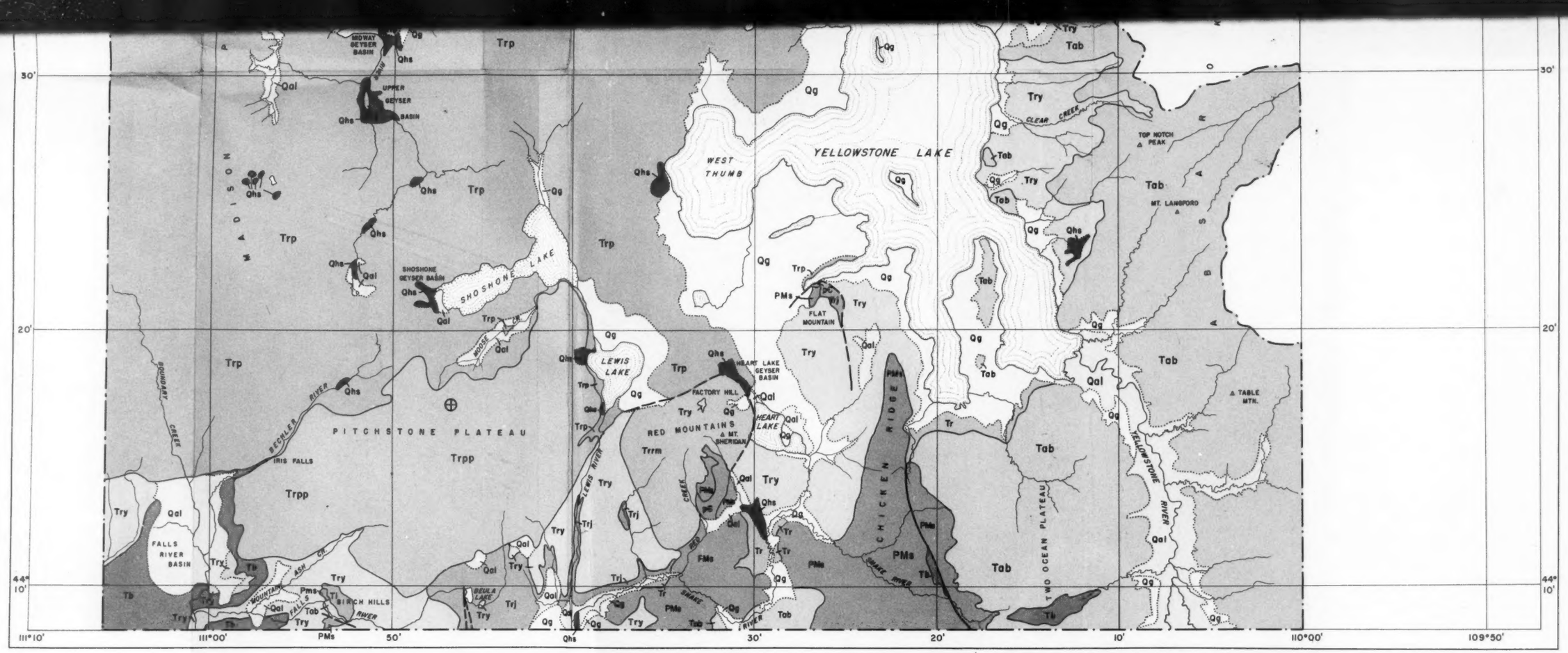

0 10 Miles

Geology of the rhyolite areas by F. R. Boyd, R. Schmalz, R. Lundin, P. Calkin

Geology exclusive of the rhyolite after U. S. G. S. Folio no 30

QUATERNARY

- Qal — Alluvium
- Hot spring deposits
- Qg — Glacial and glacial lake deposits

PLIOCENE

- Troc — Obsidian Cliff flow; rhyolite; Plateau flows
- Trcs — Crystal Springs flow; rhyolite; Plateau flows
- Trgc — Cougar Creek flow; rhyolite; Plateau flows
- Trc — Canyon flow; rhyolite; Plateau flows

PLIOCENE

- Trpp — Pitchstone Plateau flow; rhyolite; Plateau flows
- Trgr — Gibbon River flow; rhyolite; Plateau flows
- Trp — Plateau flows; undifferentiated; rhyolite
- ⊕ — Vent for Plateau flow
- Trgl — Grizzly Lake rhyolite–basalt complex
- Tbc — Basaltic cinder cone

PLIOCENE

- Tb — Basalt; both pre and post Yellowstone tuff
- Try — Yellowstone tuff; welded rhyolite tuff
- Trpm — Purple Mountain pumice breccia; rhyolite
- Trd — Rhyolite dome
- Trj — Jackson flows; undifferentiated; rhyolite
- Trrm — Red Mountains rhyolite; flows and flow breccias; undifferentiated
- Tr — Rhyolite; undifferentiated; pre Plateau flows

EARLY TERTIARY

- Tab — Andesite breccia and basalt
- Ti — Intrusive rocks

PALEOZOIC MESOZOIC

- PMs — Sedimentary rocks

PRE-CAMBRIAN

- pC — Gneiss and schist

Concealed fault

GEOLOGIC MAP OF YELLOWSTONE NATIONAL PARK, WYOMING

BOYD, PLATE 1
Geological Society of America Bulletin, volume 72

FRANCIS R. BOYD *Geophysical Laboratory, Carnegie Institute of Washington, Washington, D.C.*

Welded Tuffs and Flows in the Rhyolite Plateau of Yellowstone Park, Wyoming

Abstract: The rhyolite plateau in Yellowstone Park is made up of flows and welded tuff with subsidiary rhyolite domes, basalt, and rhyolite-basalt mix-lava. The two most important units are the Yellowstone tuff, exposed over 600 square miles within the Park, and a group of younger flows, the Plateau flows, which cover 1000 square miles in the Madison, Central, and Pitchstone plateaus.

The Plateau flows occupy a tectonic basin rimmed by Yellowstone tuff and older rocks in central and southwestern Yellowstone Park. Individual flows range up to 1000 feet in thickness and cover areas up to at least 100 square miles. Surficial features, including vent domes, are locally well preserved. Exposed portions of these flows are, for the most part, banded obsidian and perlite and breccias formed by incorporation of fragments of pumiceous crust in the moving flows.

The Yellowstone tuff is welded to obsidian at its base and grades upward through indurated, lithoidal rhyolite to loose ash at the top of an uneroded section. Probably all the Yellowstone tuff was erupted in a single rapid series of eruptions from dispersed vents.

Textural and structural evidence suggests that the Yellowstone tuff was emplaced as pyroclastic flows. A thermodynamic analysis of this type of eruption is given. Energy changes within the conduit and during emplacement are evaluated. The minimum temperature at which rhyolite glass will weld, determined experimentally, is approximately 600°C. The data of Tuttle and Bowen (1958) are used to fix the range of initial magma temperature. Welding in the Yellowstone tuff can be explained if the tuff was emplaced as pyroclastic flows and if the magma contained less than about 4 per cent H_2O at the start of the eruption.

CONTENTS

Introduction 388
Stratigraphy of the rhyolite plateau 389
General statement 389
Red Mountains rhyolite 390
Jackson flows 392
Purple Mountain pumice breccia 393
Yellowstone tuff 393
Rhyolite domes 400
Basalts 401
Rhyolite-basalt mix lavas 403
Plateau flows 403
Glacial deposits 409
Hot-spring deposits 409
Age of the rhyolite 410
Structure of the rhyolite plateau 410
General statement 410
Faults older than the Plateau flows 410
Faults younger than the Plateau flows 412
Origin of the faulting 412
Mechanism of eruption of the Yellowstone tuff . . 412
General statement 412
Field evidence 413
Pyroclastic flows or froth flows 413
Thermodynamic considerations 414
Statement of problem 414
Magma temperature 414
Experimental determination of welding temperature 414
Permissible cooling 416
Heat losses during emplacement 417
Energy changes within the conduit 418
Total cooling during eruption 421
Problem of the welded ash 422
Lack of welding in historic pyroclastic flows . . 423
Mobility of pyroclastic flows 424
References cited 424

Figure

1. Geologic section of the base of the Yellowstone tuff on Mt. Everts, Yellowstone Park, Wyoming 395
2. Diagrammatic section of a vent on Mt. Everts, Yellowstone Park, Wyoming 397
3. Compositions of sanidine phenocrysts 399
4. X-ray diffractometer patterns of 201 reflections of sanidines from the section of Yellowstone tuff in the Gardiner Canyon, Yellowstone Park, Wyoming 400
5. Geologic section of the Gardiner Canyon 0.3 mile north of Osprey Falls, Yellowstone Park, Wyoming 402
6. Front of one of the Plateau flows, Reas Pass, Montana 404
7. Analyses of Yellowstone rhyolites on a diagram of the system $KAlSi_3O_8$-$NaAlSi_3O_8$-SiO_2. 407
8. Temperature of the minimum in the system Ab-Or-SiO_2-H_2O as a function of H_2O dissolved in the melt 414

Geological Society of America Bulletin, v. 72, p. 387–426, 11 figs., 6 pls., March 1961

Figure

9. Cooling of a rhyolitic magma by reversible, adiabatic expansion 421
10. Heat of evaporation of H_2O from an albite melt 421
11. Maximum total cooling of a rhyolitic welded tuff during eruption 422

Plate — Facing

1. Geologic map of Yellowstone National Park, Wyoming 387

Following

2. Rhyolite flows and welded tuffs 402
3. Flow fronts and fault scarps 402
4. Photomicrographs of rhyolite flows and flow breccias 402
5. Photomicrographs of welded rhyolite tuffs . . 402

Facing

6. Geologic map of the Madison Canyon, Norris Geyser Basin, and Obsidian Cliff areas, Yellowstone National Park, Wyoming . . 426

Table

1. Stratigraphy of the Yellowstone rhyolite plateau, Yellowstone Park, Wyoming . . . 39
2. Mode of obsidian from the base of the Yellowstone tuff, Mt. Everts, Yellowstone National Park 39
3. Chemical analyses and norms of Yellowstone basalts 40
4. Modes of Plateau flows 40
5. Modern analyses of Yellowstone rhyolites . . 40
6. Normative mineralogy of the Yellowstone rhyolites 40
7. Loss of weight on ignition at 1200°C. of welded-tuff glasses from Yellowstone Park and vicinity 41
8. Dehydration of welded-tuff glass from Mt. Everts, Yellowstone Park (specimen YP-51-68) 41
9. Welding runs on Mt. Everts ash 41
10. Phenocryst contents of some welded tuffs and historic pyroclastic flows 42

INTRODUCTION

GENERAL STATEMENT: Formation of the rhyolite plateau of Yellowstone National Park was one of the major volcanic events in the development of the Rocky Mountains. The volume of rhyolite erupted to form the plateau is estimated to have exceeded 400 cubic miles. The plateau contains many different types of rhyolite extrusive rocks, and volcanic surficial features are well preserved. Only the Taupo-Rotorua district in New Zealand and the Lake Toba area in Sumatra compare with Yellowstone in volume of salic volcanic rocks.

The present study of the Yellowstone plateau has been stimulated by the growing interest in the importance of welded tuffs in rhyolitic volcanism and in their origin. Marshall (1935), Gilbert (1938), and others have shown that many rhyolites are not true lava flows but are compacted and welded tuffs. Since no observed volcanic eruption has produced a welded tuff, knowledge of their mechanism of eruption must come primarily through study of eroded volcanic areas. Welded tuffs are well exposed in Yellowstone, and it has proved to be an ideal area in which to evaluate the importance of welded tuffs relative to flows and in which to seek data on their mode of eruption.

ACKNOWLEDGMENTS: The author is indebted to Harvard University, the Carnegie Institution of Washington, and the National Park Service for support of this investigation. Harvard University provided field expenses for the summers of 1951 and 1952 and funds for the purchase of aerial photographs. The Geophysical Laboratory of the Carnegie Institution of Washington has generously financed field expenses for the summers of 1953 and 1954 and all other expenses subsequent to 1953. The National Park Service permitted the author to carry out field work in Yellowstone National Park, and personnel of the Park Service have aided in many ways in the execution of the field work.

Robert Schmalz, Richard Lundin, and Parker Calkin assisted the author in the field. Their help is greatly appreciated.

The author is particularly grateful to George C. Kennedy, who first interested him in Yellowstone and in the problem of welded tuffs. Many of the interpretations developed herein have grown out of stimulating discussions with Kennedy. The suggestions of Francis Birch with regard to the thermodynamic analysis of the eruption of a welded tuff have been especially valuable. James B. Thompson, Jr., and Marland P. Billings read the dissertation on which this paper is based, offered in partial fulfillment of the requirements for the degree of Doctor of Philosophy at Harvard University. Their criticism has been of great assistance.

MAPPING: Aerial photographs (scale, 1:36,000) purchased from the Aero Service Corporation were used for the geologic mapping. Subsequently, the U. S. Geological Survey released advance proofs of the Gallatin 1, Gallatin 4, Mt. Holmes, and Madison Junction quadrangles (scale, 1:48,000). Copies of these proofs were obtained from the Survey through the courtesy of Donald E. White. The detailed geologic mapping is presented on a base taken from portions of these four sheets (Pl. 6). The reconnaissance mapping (Pl. 1) is presented on a base taken from the topographic map of the Yellowstone National Park (scale, 1:125,000), partially revised in 1921.

GEOGRAPHY OF THE YELLOWSTONE PLATEAU: The rhyolite plateau in Yellowstone Park covers 2000 square miles and has an average altitude of 8000 feet. It is surrounded on the northwest, north, east, and south by mountains ranging up to about 14,000 feet in elevation. To the southwest, close to the Park boundary, the plateau drops off abruptly to the Snake River Plains. The plateau is cut by numerous canyons, with local relief up to 2000 feet. Excellent exposures are found in the canyons, but outcrops are sparse on the plateau surface between canyons. The rhyolite area is covered with tall stands of lodgepole pine, and it is difficult to gain much perspective in the field. For this reason, aerial photographs proved indispensable in carrying out the field work. The road network in Yellowstone Park is limited, but access to many areas is furthered by a system of trails, some maintained by the National Park Service and some by Yellowstone's large herds of elk and buffalo.

PREVIOUS GEOLOGIC INVESTIGATIONS IN YELLOWSTONE: The first geologic investigations of the Yellowstone area were reconnaissance studies concerned primarily with geography and with the hot springs and geysers (Hayden, 1872; 1873). A subsequent report (Hayden, 1883) contains more data on the bedrock geology.

A more thorough geologic and topographic study was undertaken in 1883 (Hague, 1896; Hague *et al.*, 1899). Hague (1896) has shown the boundaries of the rhyolite, and J. P. Iddings (*in* Hague *et al.*, 1899, p. 356–432) has described it. No attempts were made by these investigators to map units within the rhyolite. The boundaries between the rhyolite and other rocks shown in Plate 1 of this report are, for the most part, as shown by Hague (1896).

Allen and Day (1935) carried out a detailed investigation of the hot springs of Yellowstone Park. Fenner studied the alteration of the rhyolite by hot-spring waters (Fenner, 1934; 1936) and the petrology of the Gardiner River complex (Fenner, 1938; 1944). Wilcox (1944) has subsequently mapped this complex.

Howard (1937) described the geomorphic history of the Grand Canyon of the Yellowstone and made many observations on the rhyolite and other volcanic rocks.

PRE-RHYOLITE VOLCANISM: Volcanic outbursts occurred intermittently in and near Yellowstone Park throughout the Tertiary, beginning in the early Eocene (Dorf, 1939). The oldest volcanic rocks range from andesite to dacite; they are predominantly breccias and agglomerates having the appearance of mudflows (Rouse, 1937, p. 1281). Emplacement of the breccias was followed by eruption of basaltic lava flows. After an interval of erosion a series of andesitic breccias and basalts was again erupted. The age of this second series is not well known (Rouse, 1937, p. 1272). Its eruption may have extended into the Miocene (Howard, 1937, p. 78).

The andesitic breccias and associated basalts have accumulated to a maximum thickness of 6500 feet in the Absaroka Range along the eastern border of the Park (Rouse, 1937, p. 1262). The breccias also crop out in the Gallatin Range in the northwest corner of the Park, in the Washburn Range north of Yellowstone Lake, and at a number of localities in the foothills of the Wind River and Teton ranges along the southern boundary of the Park (Pl. 1). The breccias may underlie the rhyolite over a large area.

The location of the centers of eruption of the breccias has been disputed. A group of intrusive rocks similar to the breccias in compositional range crops out in the Gallatin Range. J. P. Iddings (*in* Hague *et al.*, 1899, p. 141) has interpreted an andesitic stock in this range, at Electric Peak, as the core of a volcano and the source of the breccias in that area. He has identified (*in* Hague *et al.*, 1899, p. 215–268) Hurricane mesa, in the Absaroka Range, as the core of another major volcano. Rouse (1937, p. 1275) doubts that Hurricane mesa is a remnant of a large volcano. He believes (p. 1295) that the breccias were erupted "through hundreds of small vents and a few volcanos of moderate size" scattered throughout the area.

The pre-rhyolite volcanic sequence includes, in addition to the breccia series, a few exposures of trachyrhyolite in the northern part of the Park. Howard (1937, p. 22) named this the Lost Creek trachyte. The trachyte is younger than the oldest sequence of breccias, but its age relative to the youngest sequence is uncertain (Howard, 1937, p. 78). The outcrop area of the trachyte is small and is not shown on Plate 1.

The eruption of the breccias was followed by an interval of erosion. The rhyolite now covering two-thirds of the Park and a large area to the west and southwest has been erupted on this erosion surface.

STRATIGRAPHY OF THE RHYOLITE PLATEAU

General Statement

The rhyolite plateau consists mainly of rhyolite flows and welded tuff interbedded with

small basalt flows. Rhyolite domes, basaltic cinder cones, and several small bodies of mixed rhyolite and basalt have also been found. The plateau was partially veneered by glacial deposits subsequent to the eruption of the volcanic rocks.

The rhyolite has been erupted in four principal stages. The oldest rhyolites exposed, altered flows and breccias, crop out in the Red Mountains, a fault-block range in the southern part of the Park. A second series of flows, the Jackson flows, spread over a wider area, and

Hot springs have been active on the plateau both during and since the volcanic eruptions. The hot springs have altered the rhyolite extensively at a number of localities, as in the walls of the Yellowstone Canyon in the vicinity of Yellowstone Falls.

crops out principally in the Madison and Lewis canyons. The flows are named after Mt. Jackson on the rim of the Madison Canyon. After an interval of erosion, during which hot springs were active, pyroclastic flows[1] covered a large portion of the Park and adjacent areas to the west and southwest. These pyroclastic flows have been welded in part and form a widespread unit named the Yellowstone tuff. A period of faulting followed the eruption of the Yellowstone tuff. The broken surface of these earlier rhyolites was then inundated by rhyolite flows. These flows make up the Central, Madison, and Pitchstone plateaus. They are grouped as the Plateau flows. Together, the Plateau flows and the Yellowstone tuff form about 95 per cent of the exposed rhyolite in Yellowstone Park.

Two tuff-filled vents on Mt. Everts are the only certain intrusive rhyolites found in Yellowstone. Rhyolite volcanoes have not been found.

Table 1 shows the relative ages of the units. Each of these units is described hereafter.

[1] The term "pyroclastic flow" is used herein to describe eruptions in which fragmented lava buoyed by escaping gas is emplaced at high temperature in avalanches. The products of some pyroclastic flows can be classified into types exemplified by historic eruptions, such as *nuées ardentes* and pumice flows. For a recent discussion of the classification of pyroclastic flows, *see* Aramaki (1957, p. 21). "Welded tuff" is used to refer to that portion of the Yellowstone tuff or other tuff in which the shards and fragments of pumice have been deformed and welded at high temperature so that the rock is indurated. The degree of welding varies with depth in the Yellowstone tuff, and some portions have partially or wholly crystallized after welding.

Red Mountains Rhyolite

The rhyolite which crops out in the Red Mountains is believed to be the oldest exposed in Yellowstone Park. The Red Mountains rise 1500 to 2000 feet above the level of the plateau in the southern part of the Park (Pl. 1) and measure about 10 miles north to south and about 6 miles east to west. The range has steep northern and eastern faces but drops off gradually to the level of the plateau on the west and south. The mountains have been deeply scalloped by mountain glaciers, and their flanks are mantled by till.

The Red Mountains are composed of rhyolite, with subordinate pre-Tertiary sediments. The sediments crop out principally in the southern end of the range. The rhyolite is an altered mass of flows and breccias. These have been grouped as the Red Mountains rhyolite and have not been found elsewhere in Yellowstone Park.

The Red Mountains rhyolite is unconformably overlain by the Yellowstone tuff. Several patches of Yellowstone tuff lie high on the crest of the range, the largest patch lying between Mt. Sheridan and Factory Hill (Pl. 1). The age of the Red Mountains rhyolite relative to the Jackson flows, which are also pre-Yellowstone tuff, is not certain. These age relationships are discussed hereafter.

The commonest type of rhyolite in the Red Mountains is a dense, flinty, gray to pink rock. This rhyolite is usually streaked with light seams of tridymite and alkali feldspar. Some specimens are massive; well-developed flow banding is rare. The phenocrysts are quartz, sanidine, and oligoclase. The two feldspars show considerable variation in proportion: either may be dominant. No ferromagnesian phenocrysts remain, but considerable iron oxide appears to be pseudomorphous after pyroxene.

Next in abundance to this type of rhyolite is a group of lavas whose textures resemble those of the collapsed pumice breccias in the younger Plateau flows. These breccias have formed by vesiculation of the surface of a rhyolite flow to pumice and incorporation of the pumice in the moving flow. Collapsed pumice breccias in the unaltered Plateau flows are generally glassy; the similar breccias in the Red Mountains have been devitrified in most places. The breccias in the Red Mountains are indurated and black or red. Some show no hint of a breccia structure on a freshly broken surface. On a weathered surface, however, the breccias appear lighter in color

with elongate, dark patches whose ends feather out into the surrounding material. These dark patches probably originated as fragments of pumice, although in thin section no trace of a pumiceous texture remains.

The author suspected that these rhyolites were welded tuffs when he first saw them in the field. Their megascopic resemblance to certain varieties of welded tuff is pronounced in some outcrops. Nevertheless, flow-banded rhyolite crops out sparsely in almost all parts of the Red Mountains. Moreover, microtextures typical of welded tuffs have not been seen. The evidence favors the interpretation that these rocks are altered flows and flow breccias.

J. P. Iddings (*in* Hague *et al.*, 1899, p. 381) found exposures on Mt. Sheridan which he believed to be dikes. The present author did not find any contacts in the Red Mountains which appeared to be intrusive. The large quantities of collapsed pumice breccia seem to preclude the possibility that an appreciable amount of the Red Mountains rhyolite is intrusive.

Optical and X-ray investigations of the

TABLE 1. STRATIGRAPHY OF THE YELLOWSTONE RHYOLITE PLATEAU, YELLOWSTONE PARK, WYOMING

	Deposit		Description
PLEISTOCENE-RECENT		Alluvium	
		Hot-spring deposits	Includes some preglacial deposits
		Glacial and glacial-lake deposits	
		—Faulting and Erosion—	
PLIOCENE	Plateau flows	Plateau flows; undifferentiated	Rhyolite; phenocryst assemblages include either one or two feldspars; individual flows 200–1000 feet thick; aggregate thickness probably more than 1000 feet in central part of outcrop area
		Pitchstone Plateau flow	Rhyolite
		Gibbon River flow	Rhyolite
		Cougar Creek flow	Rhyolite
		Canyon flow	Rhyolite
		Obsidian Cliff flow	Rhyolite; no phenocrysts
		Crystal Springs flow	Rhyolite; no phenocrysts
		Basalt	Labradorite-olivine basalt; aggregate thickness up to 200 feet; small, scattered flows; cinder cones in Obsidian Cliff area; includes a few flows that are pre-Yellowstone tuff
		Rhyolite-basalt mix-lavas	Small masses; limited to Obsidian Cliff area
		—Faulting and Erosion—	
		Yellowstone tuff	Two-feldspar welded rhyolite tuff; eroded sections up to 1000 feet; crops out throughout Park and adjacent areas to west and southwest
		Purple Mountain pumice breccia	Two-feldspar rhyolite; up to 1000 feet thick; stratified; in part welded; limited to Madison Canyon and to Stonetop Mountain areas
		Rhyolite domes	Four in all; two-feldspar rhyolite; limited to Norris-Obsidian Cliff area; pre-Plateau flows, but age relative to Yellowstone tuff not known
		—Erosion—	
		Jackson flows	One- and two-feldspar rhyolite; prominent exposures in Madison and Lewis Canyons; up to 1500 feet thick; base not exposed
		Red Mountains rhyolite	Altered flows and breccias; pre-Yellowstone tuff; age relative to Jackson flows not certain; limited to Red Mountains
		Rhyolite; undifferentiated	Predominantly Yellowstone tuff but includes some Jackson flows; areas shown as undifferentiated rhyolite in Plate 1 either have too poor outcrop to permit mapping or are areas not visited by the author

groundmass of the Red Mountains rhyolite show a high proportion of quartz relative to tridymite. The quartz forms poikilitic patches, in some cases in optical continuity with quartz phenocrysts. The dominant silica mineral in the groundmass of unaltered rhyolites is tridymite, and hence the quartz patches are probably recrystallized tridymite. The recrystallized groundmass gives this rhyolite its distinctive appearance.

Along the steep eastern face of the Red Mountains some of the rhyolite is greatly altered; the rocks megascopically resemble those altered by hot springs, but evidence suggests that the alteration had a more deep-seated origin. The altered rhyolite is dense, white material in which the only recognizable phenocrysts are quartz. The feldspars have been replaced by sericite or, in many cases, have been leached out. X-ray study of the cherty, white groundmass showed, in one specimen, that it was largely quartz with minor feldspar: there has evidently been a considerable enrichment of silica. Another specimen has a groundmass composed of quartz and muscovite. Dark rhyolite that has been brecciared and veined with granular, white quartz was found at one locality halfway up the east face of Mt. Sheridan. Some of the quartz veins in this rock are an inch in width.

The granular quartz and the muscovite suggest a deep-seated alteration. The characteristic secondary minerals in rhyolites altered by hot springs in Yellowstone are clays, zeolites, and opaline silica or chalcedony (White, 1955). In the Red Mountains, the most intense alteration is localized along the fault scarp bounding the range on the east. The alteration of the rhyolites in the interior of the range consists only of a recrystallization of the groundmass and oxidation of the ferromagnesian phenocrysts.

The low-grade metamorphism of the Red Mountains rhyolite seems to have preceded the eruption of younger rhyolites. Neither the patches of Yellowstone tuff capping the range nor the Jackson flows which envelop the range on the west and south have been affected.

Jackson Flows

The Jackson flows probably once covered a large part of Yellowstone Park, although their area of exposure is now small. They are exposed in fault scarps, in canyons which have cut through the overlying volcanic rocks, or where the flows form mountains of sufficient height to have escaped burial by the products of later eruptions. The two patches of Jackson flows 7–10 miles southwest of Mt. Haynes are examples of this last case (Pl. 1). Correlation of the scattered exposures of the Jackson flows is based on similar and distinctive lithology and, where possible, on stratigraphic position relative to the Yellowstone tuff.

The Jackson flows are best exposed in the canyons of the Madison, Lewis, and Snake rivers. Fifteen hundred feet of Jackson flows is present in the north wall of the Madison Canyon at Mt. Jackson (Pl. 6). The sections in the canyons of the Lewis and Snake rivers attain a maximum thickness of about 400 feet. The base of this unit is nowhere exposed.

The Jackson flows have been mapped to within a quarter of a mile of exposures of the Red Mountains rhyolite near the junction of Red Creek and the Snake River (Pl. 1). Here as elsewhere, however, the contact between the two units is masked by the Yellowstone tuff which is younger than either. Hence, the relative ages of the two units cannot be clearly established. Nevertheless, the Red Mountains rhyolite has been recrystallized, whereas the lavas of the Jackson are relatively fresh. The Red Mountains rhyolite is, therefore, probably the older.

The most abundant type of rhyolite in the Jackson flows is a gray, lithoidal rock with prominent, white tablets of sanidine and oligoclase and with rounded grains of quartz. A poorly defined, coarse flow banding is common. Gas cavities and lithophysae are locally developed; commonly these cavities are lined with quartz crystals, and the quartz crystals are stained red by hematite. The hematite stain may permeate the entire rock. Little glassy rhyolite is found in exposures of the Jackson flows, in contrast to the younger Plateau flows.

The proportion of oligoclase to sanidine in the Jackson flows ranges from about 1:1 to 1:10. In exposures of the Jackson flows centering around the Madison Canyon (Pl. 6), the oligoclase is sparsely developed; in the exposures of this unit in the southern part of Yellowstone Park (Pl. 1), the plagioclase is much more prominent. The opacity of the feldspars is due to inclusions of cryptocrystalline groundmass materials.

Biotite is present as phenocrysts in flakes up to half a millimeter in diameter. Where fresh, it is pleochroic in light and dark brown; it is commonly altered to a reddish brown, however, and is completely replaced by magnetite

in some specimens. The biotite nowhere forms more than a fraction of 1 per cent of the rock. Biotite has been found in one of the rare glassy specimens from the Jackson flows, and, hence, is primary. The biotite phenocrysts offer a means of distinguishing the Jackson flows from the younger Plateau flows. The latter do not carry biotite.

The typical groundmass texture of the Jackson flows is a regular mosaic of tiny spherulites, each spherulite being 0.1–0.2 mm in diameter. This pattern is relieved in places by a coarser patch of tridymite, or quartz and tablets of alkali feldspar.

Purple Mountain Pumice Breccia

Eruption of a welded, rhyolitic pumice breccia locally preceded the eruption of the Yellowstone tuff in Yellowstone Park. This breccia has been named the Purple Mountain pumice breccia, after a peak on the north rim of the Madison Canyon. The breccia did not spread over so wide an area as the Yellowstone tuff. The two principal outcrop areas of the pumice breccia are in the north wall of the Madison Canyon (Pls. 1, 6) and at Stonetop Mountain, north of Yellowstone Lake (Pl. 1). A third, small area is in an unnamed canyon 4 miles southwest of Mt. Haynes. In the first and third areas mentioned the breccia can be seen to underlie the Yellowstone tuff. At Stonetop Mountain the breccia is in contact with the Yellowstone tuff, but the exposures are inadequate to show the relative ages. The breccia at Stonetop Mountain is hence correlated with the exposures in the Madison Canyon area on the basis of similar lithology.

The pumice breccia and the overlying Yellowstone tuff both appear to be the products of pyroclastic flows. The pumice breccia is in part welded. The chief difference between it and the Yellowstone tuff is that the pumice breccia is filled with angular fragments of pumice, whereas the Yellowstone tuff contains only a small proportion of pumice.

The pumice breccia ranges from soft, coherent tuff to densely indurated rock. Soft and indurated zones alternate. The pumice breccia evidently was erupted in a number of stages which probably were not separated by considerable intervals of time. No trace of an erosion interval has been found within the pumice breccia. The maximum observed thickness of 1000 feet is in the Madison Canyon.

The commonest type of breccia is an indurated, white, buff, or pink rhyolite studded with angular fragments of pumice. The pumice fragments are flattened and welded in the indurated breccias; they are commonly leached out in the less indurated varieties. Most range up to 2 inches in their largest dimension; however, pumice fragments up to a foot in diameter have been found. Fragments of rhyolite flows are present but are much less common than pumice. The breccia in the Stonetop Mountain area carries up to 2 per cent of fragments from the early Tertiary andesitic rocks.

The proportion of fragments to matrix and the size of the fragments vary considerably. Such variation appears as a crude banding in a large exposure about 1 mile east-northeast of Madison Junction (Pl. 6). Banding of this sort can be produced by laminar flow in a pumice avalanche (Kuno, 1941, p. 147).

The phenocrysts in the Purple Mountain pumice breccia are quartz, sanidine, and oligoclase. The sanidine shows well-developed iridescence. Any original ferromagnesian phenocrysts have been altered to iron oxide.

In most places the matrix of the pumice breccia is partly or wholly cryptocrystalline. The matrix is likely to be more thoroughly crystallized in the soft breccia than in the welded varieties. Evidently gases rising through the pumice flows after emplacement have promoted crystallization. The soft, porous types were the most severely affected. These gases probably came from the pumice flows themselves. Secondary fumaroles on the surfaces of pumice flows have been noted in historic eruptions (Kozu, 1934, p. 138).

Yellowstone Tuff

AREAL EXTENT: The Yellowstone tuff is exposed over an area of 600 square miles in Yellowstone Park. It crops out principally as a brown or purple, friable, lithoidal rock in highlands cut by numerous deep canyons. Areas underlain by the Yellowstone tuff have a striking difference in appearance to the Madison, Central, and Pitchstone plateaus, which are built of younger and less eroded, glassy flows. Since the tuff surrounds the outcrop area of the younger Plateau flows on all sides it probably underlies the flows over an additional area of 1000 square miles. The thickness of the tuff varies owing to erosion subsequent to its eruption and to irregularities of the surface on which it was erupted. Eroded sections range up to about 1000 feet in thickness. A single complete section is 475 feet thick. The average original thickness was probably on the order of 500 feet

and, hence, the original volume of the tuff within the borders of the Park is estimated to have been in the range of 150 to 200 cubic miles.

Welded rhyolite tuff similar in texture and mineralogy to the Yellowstone tuff crops out over large areas west of the Park in Montana and Idaho. Much of this tuff was probably emplaced in the same series of eruptions as the Yellowstone tuff. Mansfield and Ross (1935, p. 311) state that

> ". . . the area in eastern Idaho covered by rocks of this type is at least approximately 3000 square miles. If to this the areas mentioned in Montana are added, the figure might be raised to as much as 5000 square miles or more."

The total amount of tuff erupted may therefore have been two to three times as large as that estimated to have been present within Yellowstone Park.

STRUCTURE: The commonest lithologic type in the Yellowstone tuff is an indurated lithoidal rock varying through shades of brown, gray, and purple. It is characteristically fractured on a minute scale so that it crumbles easily, weathers in spheroidal masses, and forms talus that has the consistency of fine gravel. In addition to an irregular fracturing, the welded tuff typically has a pronounced foliation. This is produced by flattened pumice fragments and by flattened, tridymite-filled vesicles. Figure 1 of Plate 2 shows a typical outcrop of Yellowstone tuff.

In large outcrops the Yellowstone tuff shows a crude columnar jointing (Pl. 2, fig. 1). Some of the columns are 100 feet or more high, and most are about 5 feet thick.

This lithologic type is the variety most commonly encountered both because it forms the thickest part of any section of Yellowstone tuff and because its induration makes it resistant to weathering. There are, however, a number of other facies of the tuff. These facies form a regular sequence in any section, and this sequence is repeated with little variation throughout the outcrop area of the tuff.

In most places where the base of the Yellowstone tuff is exposed, it is underlain by up to 10 feet of finely laminated, rhyolitic ash. The ash is composed of crystals identical to the phenocrysts in the tuff (quartz, sanidine, plagioclase (An_{10}), ferroaugite, and fayalite), small fragments of pumice, glass shards, and dust. The ash is well sorted into coarse and fine layers and locally shows cross-bedding.

The contact between the banded ash and the base of the overlying tuff is sharp in some places and transitional over a few inches to a foot in others. The uppermost few inches of the ash below the base of the tuff are welded in most places. The ash is the product of an initial, more explosive phase of the same eruptions that produced the Yellowstone tuff.

The base of the Yellowstone tuff is characteristically a layer of dense, black obsidian 1–15 feet thick. Commonly the glass has a few spherulites in its upper part, close to where it grades into the lithoidal main mass of the tuff.

The contact between the glass of the base and the lithoidal tuff is gradational over a few inches in degree and coarseness of crystallinity. The black glass passes upward into a rock which is black, but with a stony luster, and that passes into a dark brown or purplish lithoidal material, and finally into a rock of a lighter brown, purple, or gray. In thin section, the glass is light brown and translucent; the black, stony phase is almost opaque. Above this layer, the birefringence increases in thin section with the lightening in color of the hand specimen.

The lithoidal welded tuff commonly has a layer of vesicles, a foot or two thick, a few feet above the top of the glassy base. The concentration of vesicles ranges from one every foot or so along a layer to one every inch or two. Some of these vesicles have septae, like lithophysae. The vesicles may have been produced by gas pressed out of the collapsed and welded base.

The Yellowstone tuff shows little variation in texture or induration for several hundred feet above the vesiculated zone. Soft, coherent tuff is present in the upper portion of the section is complete. As the section is traced upward the tuff becomes sufficiently soft to be easily broken apart. Pumice fragments, which are flattened in the more indurated tuff below, are scarcely deformed in the soft tuff. The uppermost 20–30 feet of a complete section is loose ash. The upper ash is not banded as is the layer of ash at the base of the unit. Exposures of the soft, upper part of the Yellowstone tuff are rare.

This type of section represents a single welded tuff emplaced as a unit. However, breaks in sections of the Yellowstone tuff suggest that in some places the products of more than one pyroclastic flow are present. These breaks are commonly marked by layers of dense, flinty rhyolite with sparse, small phenocrysts and no pumice fragments or collapsed vesicles. Such layers are generally a few feet thick. In thin section, the flinty rhyolite is seen to be cryptocrystalline, with a groundmass composed of

shards that are little deformed. Layers of this sort are exposed in the road cut at the Virginia Cascades (Pl. 1) and at the "Golden Gate," where Glen Creek drops into the valley of the Gardiner River, near Mammoth Hot Springs (Pl. 1). The layering in the Golden Gate exposure is more pronounced than that elsewhere in the Park.

The fine-grained layers are believed to represent accumulations of fine ash that settled on freshly erupted pyroclastic flows. While the flows were still hot, further eruptions buried these ash layers and indurated them.

Many of the features observed in exposures of the Yellowstone tuff can be more adequately described with reference to particular sections.

The section of Yellowstone tuff in the east wall of the canyon of the Gardiner River, near Osprey Falls (Fig. 5), is the only complete section found in Yellowstone Park. The overlying basalt has protected the upper surface of the tuff from erosion. The section of tuff is entirely exposed in a cliff forming the canyon wall.

This section appears to be the product of a single pyroclastic flow. It is 475 feet thick, and there is an uninterrupted gradation from a glassy base, through lithoidal welded tuff, to soft tuff, and finally to loose ash in the top 50 feet. The dense, glassy base is underlain by a layer of fine ash. An anomalous feature is that there are three vesiculated zones above the vitrophyric base, rather than the usual single zone. The welded tuff near the base has inclusions of dacite similar to that which crops out on Bunsen Peak across the canyon. The ash at the top is reddened for a few inches below the basalt; there is no intervening soil zone.

One of the best exposures of the base of the Yellowstone tuff is on Mt. Everts (Fig. 1; Pl. 2, fig. 2), above the junction of the Gardiner River with Lava Creek. The Yellowstone tuff on Mt. Everts unconformably overlies Cretaceous shales and sandstones. The tuff with a layer of underlying ash rests on about 10 feet of boulder gravel, evidently a stream deposit derived from early Tertiary, andesitic breccias. A few inches of soil, barren of organic remains, overlies the gravel. The rhyolitic ash is finely laminated, and some layers are cross-bedded. It is separated from the welded tuff by a sharp contact, but the upper part of the ash is welded to a black, resinous glass.

About 100 feet of Yellowstone tuff is exposed in a vertical cliff above the base. The lithoidal welded tuff in this cliff has a crude columnar jointing, which is apparent from the road below. The lithoidal welded tuff which makes up the bulk of the section has the streaky foliation typical of welded tuff throughout the Park. Within a few feet of the top of the cliff, this tuff passes into a fine-grained, indurated layer with sparse phenocrysts and no foliation. At one point along the top of the cliff, the fine-grained layer is overlain by streaky welded tuff similar to that in the lower part of the cliff. At the contact between the fine-grained tuff and the welded tuff below is a 6-inch zone of scoria. Apparently the lower unit was still cooling and giving off gas when fine ash settled on its surface and a second pyroclastic flow was erupted over it, and the gas was trapped along the contact.

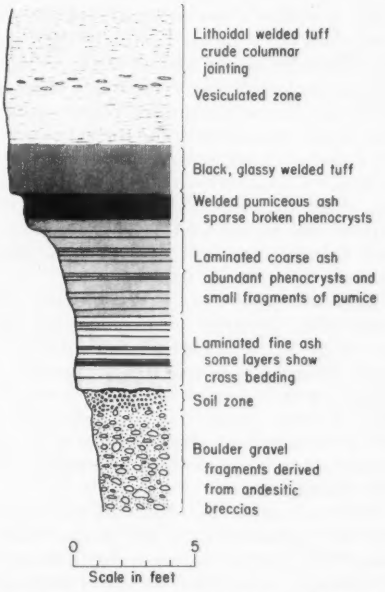

Figure 1. Geologic section of the base of the Yellowstone tuff on Mt. Everts, Yellowstone Park, Wyoming. Photograph of section shown in Figure 2 of Plate 2.

A number of excellent exposures of the Yellowstone tuff are present in the walls of the Yellowstone Canyon between the junctions of the Yellowstone River with Quartz Creek and with Broad Creek. The Yellowstone tuff overlies early Tertiary andesitic breccia and basalt in this area (Pl. 1). The nature of the contact

between the tuff and the underlying rocks indicates that the Yellowstone tuff has buried an erosion surface similar to the present topography.

The canyon of the Yellowstone in this area is joined on its eastern side by four tributary canyons, but there are no tributaries on the western side. On the eastern wall, the contact between the Yellowstone tuff and underlying breccia rises high on the canyon wall between the points of entry of the tributary canyons but drops to within a few hundred feet of river level where the tributaries enter the main canyon. The relief on the contact surface is about 600 feet and, with minor variations, seems to mirror the present topography. On the western wall of the main canyon, the contact between the Yellowstone tuff and the underlying breccia maintains a relatively even level of about 500 feet above the river. Evidently the tuff was erupted into an ancestral Yellowstone canyon with tributary canyons in roughly the same positions that they are today.

Exhumation of the pre-Yellowstone tuff topography is probably due to differential compaction of the tuff. When the tuff, initially inflated by gas, collapsed and compacted, it settled a greater amount where the section was thickest. After compaction the surface of the tuff was marked by depressions over buried canyons, and these depressions localized the new drainage.

Both walls of the Yellowstone Canyon show excellent exposures of the base of the Yellowstone tuff. These are similar to the exposure on Mt. Everts, except that in the Yellowstone Canyon the contact between the welded tuff and the underlying ash is gradational over a few inches. The gradation shows up in the size of phenocrysts. As at the Mt. Everts locality, the uppermost few inches of the basal, laminated ash are welded.

The north wall of the Madison Canyon is made up of a section of Yellowstone tuff and Purple Mountain pumice breccia overlying Jackson flows (Pl. 6). An erosion surface had been cut on the Jackson flows at the time of the eruption of the Yellowstone tuff and the pumice breccia. The local relief on the erosion surface is about 1200 feet. The form of the erosion surface, as seen in the present canyon wall, is a relatively flat plain at Madison Junction which rises to a mountain at the site of Mt. Jackson and drops off to the west into Madison Valley.

The eruption of Purple Mountain pumice breccia was of insufficient volume to completely bury the eroded surface of the Jackson. The Yellowstone tuff, which was erupted after the pumice breccia, buried the remaining exposures of the Jackson flows, so that the Yellowstone tuff now rests partly on pummice breccia and partly on Jackson flows.

The Yellowstone tuff has a chilled, glassy base where it overlies the eroded surface of the Jackson flows. The contact between the glassy base of the welded tuff and the Jackson flows is exposed in the canyon wall a few hundred feet above the road 1¼ miles southeast of the bridge at the mouth of the Madison Canyon (Pl. 6). East of this point the Yellowstone tuff overlies the pumice breccia, and the contact appears to be a plane surface. This contact is exposed in a small notch in the canyon wall 1½ miles northeast of Madison Junction (Pl. 6). There is no trace of a soil zone, and both the Yellowstone tuff and the pumice breccia are indurated and lithoidal at the contact. The base of the Yellowstone tuff was not chilled where it came to rest on the pumice breccia. Evidently the pumice breccia was still hot when the Yellowstone tuff was erupted.

The basal sections of Yellowstone tuff in the Madison Canyon differ in another way from others in the Park. At the base of the tuff where it overlies the Jackson is a layer of breccia a few feet thick, composed of angular fragments of rhyolite from the Jackson set in a matrix that is largely phenocrysts of quartz and sanidine. This breccia replaces the stratified ash normally found at the base of the tuff.

The Yellowstone tuff in the southern part of Yellowstone Park has been deeply eroded, so that, for the most part, it now discontinuously veneers older rhyolites. There are, however, good exposures of the tuff in the Lewis Canyon near the south entrance.

The best of these exposures is in the west wall of the Lewis Canyon above the cascades of the Lewis River, about 5 miles south of Lewis Lake (Pl. 1). The Yellowstone tuff overlies the Jackson flows in this exposure. A soil zone is present at the base of the tuff. The soil zone is overlain by a thin layer of fine ash which is welded. This section is strikingly similar to the sections in the Yellowstone Canyon 50 miles to the northeast and to the sections in the vicinity of Mammoth, 60 miles to the north.

VENTS: The sites of the eruptions which produced the hundreds of cubic miles of Yellowstone tuff now spread over Yellowstone Park and adjacent areas are, with two minor exceptions, unknown. No structures within the area

resemble rhyolitic volcanoes. Although such volcanoes may have existed once and been buried by more recent eruptions, it seems more probable that the Yellowstone tuff was erupted from a number of dispersed fissures.

Two features which appear to be tuff-filled vents are exposed at the crest of the steep, southwest face af Mt. Everts. One of these is shown in cross section in Figure 2; it is about 1 mile east of the bridge over the Gardiner River. The vent, which has the form of a funnel exposed in section, is filled with indurated rhyolitic tuff and cuts both the Cretaceous sediments which make up the bulk of the mountain and the thin capping of Yellowstone tuff. The tuff within the vent is lithoidal. In thin section its groundmass appears evenly cryptocrystalline; the outlines of the shards are preserved and show little deformation. This tuff is densely indurated in the interior of the vent but is soft along the edges. It is similar to the material in the fine-grained indurated layers in many sections of Yellowstone tuff.

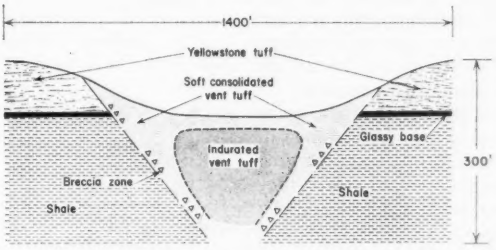

Figure 2. Diagrammatic section of a vent on Mt. Everts, Yellowstone Park, Wyoming

The walls of the vent dip in at an angle of 30°. Along the crest of the mountain the vent measures about 1000 feet in diameter. At least several hundred vertical feet has been eroded, and the original width of the vent at the surface must have been correspondingly greater.

Breccia lenses in the soft tuff along the edges of the vent have the same attitude as the walls of the vent. The lenses are up to 20 feet in length and contain angular fragments of Yellowstone tuff up to 2 feet in diameter. No fragments of Cretaceous sediments were found in the breccia lenses, even though the vent is cut largely in such sediments. The fragments of Yellowstone tuff in the breccia lenses can be found at elevations as much as 100 feet below the base of the Yellowstone tuff, and the lenses have evidently formed by slumping of the Yellowstone tuff in the ash which filled the vent at the cessation of the eruption.

The Yellowstone tuff is reddened for a few feet away from the contact with the vent. From the evidence afforded by the inclusions, the Yellowstone tuff had been emplaced and had sufficient time to weld before the tuff now filling the vent was erupted. The time interval may, however, have been on the order of days or weeks.

Another vent on Mt. Everts 0.5 mile southeast of the one described is similar but not so well exposed.

These vents are small, and it seems improbable that they can have supplied a considerable fraction of the Yellowstone tuff now found in the area. A number of vents for rhyolite flows and domes have been discovered elsewhere in Yellowstone Park, but no evidence indicates that these have also acted as vents for the Yellowstone tuff. The Washburn Range and Mt. Sheridan in the Red Mountains have been interpreted (Hague, 1896, p. 3) as volcanoes and centers of eruption of rhyolite. The Washburn Range has an outline suggestive of a caldera (Pl. 1), and the amphitheater in the center of the Range is filled with Yellowstone tuff. Nevertheless, the tuff may have flowed in the open eastern side rather than erupted within the amphitheater. The Red Mountains owe their elevation above the level of the plateau to faulting. They do not seem to have the structure of a volcano, and the Yellowstone tuff overlies the eroded surface of the Red Mountains rhyolite.

EVIDENCE FOR SIMULTANEOUS ERUPTION OF YELLOWSTONE TUFF OVER THE ENTIRE AREA: The structure of the Yellowstone tuff in Yellowstone Park and surrounding areas suggests that it has been emplaced in a single, rapid series of eruptions. Over the entire area the tuff has a constant lithology except for minor

differences in inclusions and textural differences which are a function of vertical position in a section rather than areal position. Although many sections appear to contain two or more beds of tuff, none of the units in such sections are separated by a soil zone or erosion surface. Moreover, in such sections there is only one glassy base and usually only one soft, unwelded top. Where one welded tuff overlies another, the upper unit does not have a chilled base, and the lower unit is commonly welded at its top. Evidently, the lower units were still hot when the overlying ones were emplaced.

PETROGRAPHY: Thin sections show that the welded tuff in Yellowstone, like that in other areas, is composed mainly of fragmented, glass shards. These shards have been compacted and welded into dense rhyolite. The outlines of the shards are preserved in densely welded tuff by the inclusion of dust along their contacts.

This texture is best preserved in the black obsidian from the base of the Yellowstone tuff (Pl. 5, figs. 1, 2). The deformation of the glass shards is particularly pronounced where they have been folded around or pinched between phenocrysts (Pl. 5, fig. 2). Fragments of pumice, collapsed and welded, are common.

Crystallization of the Yellowstone tuff has partially destroyed its primary texture. In few specimens, nevertheless, is the primary texture completely eradicated. The coarseness of the crystallization in the groundmass of a typical specimen of lithoidal welded tuff changes greatly from point to point. Flattened vesicles, filled with coarse tridymite, are common. The crystallization in the groundmass next to these vesicles is generally coarse enough to have obliterated the outlines of the shards. Similarly, there may be eyelike streaks of coarse crystallization adjacent to phenocrysts. These represent low-pressure areas where gases collected during compaction and have fluxed the crystallization of the adjacent tuff. In areas between phenocrysts and flattened vesicles in lithoidal tuff, the crystallization is typically on a submicroscopic scale, and the shard outlines are still preserved (Pl. 5, fig. 3).

Pumice fragments are readily identifiable in glassy welded tuff but can be recognized only by their outlines in lithoidal tuff. These fragments have been crystallized to relatively coarse tridymite and alkali feldspar.

Thin sections from the layers of fine-grained tuff indurated by inclusion between two beds of welded tuff reveal that these layers are made up largely of shards. The shards in the fine-grained tuff, however, do not show as much deformation as those in the adjacent welded tuff. Moreover, the fine-grained layers do not contain the flattened, tridymite-filled vesicles and collapsed, altered, pumice fragments which are typical of the welded tuff. Probably the induration of the thin, fine-grained layers is due more to crystallization than to welding.

The shards show little deformation in thin sections of soft tuff from the upper parts of the Yellowstone tuff. Shards with elliptical central cavities undeformed and filled with crystals of tridymite can be found in such rocks.

TABLE 2. MODE OF OBSIDIAN FROM THE BASE OF THE YELLOWSTONE TUFF, MT. EVERTS, YELLOWSTONE NATIONAL PARK

YP-54-A2. Table 5, analysis no. 1

	Volume Per Cent
Glass	88.8
Quartz	2.7
Sanidine	4.5
Plagioclase (An_{10})	3.9
Ferroaugite	<0.1
Fayalite	..
Opaque minerals	0.1
	100.0

The kind and composition of the phenocrysts in the Yellowstone tuff show little variation. Quartz, sanidine, and plagioclase (An_{10}) are invariably present. The sanidine is more abundant than the plagioclase. Ferroaugite and fayalite are commonly found in sections cut from specimens of the glassy base of the tuff. The ferromagnesian minerals are generally altered to iron oxide in the course of crystallization of the groundmass. Biotite and hornblende are extremely rare. The principal accessory minerals are magnetite and zircon. Table 2 indicates the proportions of these phenocrysts to each other and to the groundmass.

The compositions of sanidines from the Yellowstone tuff have been studied by measurement of their $\bar{2}01$ spacings. The sanidines were homogenized by heating at 1000°C., and the curve established by Bowen and Tuttle (1950) was used to relate spacing to composition. The compositions of 21 specimens are plotted in Figure 3A. The total range in composition is from 48 to 54 per cent Or, with a mean of 52.3 per cent Or. The variation about this mean is little more than the measurement error.

These sanidines are cryptoperthitic. The degree of unmixing is related to distance from a cooling surface in a section of tuff. Figure 4 shows tracings of the $\bar{2}01$ reflections of a suite of sanidines from the Gardiner Canyon tuff section. Crystals from the glassy base (E) and the sanidine from the naturally quenched base.

The compositions of 10 plagioclases from specimens of Yellowstone tuff have been determined by measurement of their gamma indices. The gamma indices showed a variation of 1.539 to 1.543 (about a mean of 1.542), indicating a composition of An_{10} (Chayes, 1952b).

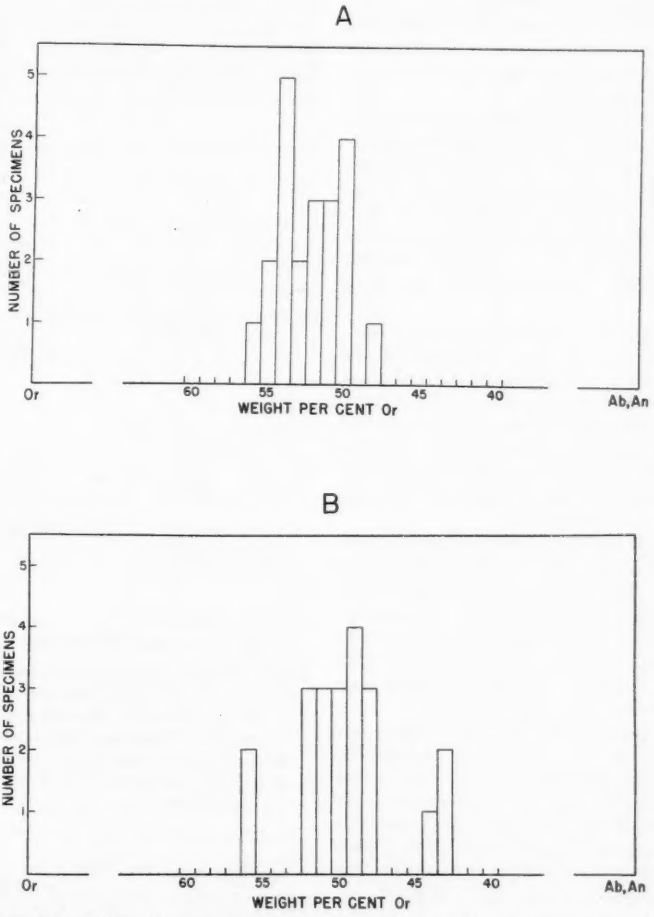

Figure 3. Compositions of sanidine phenocrysts. A. Twenty-one specimens from the Yellowstone tuff, associated with plagioclase (An_{10}). B. Twenty-one specimens from single feldspar plateau flows.

from the loose ash at the top of the section (A) show little or no unmixing. Sanidines from the interior of the tuff (B, C, D) are unmixed to two phases. These may be homogenized by heating, as has been done with (C). The resulting single phase has the same composition as

The ferroaugite has a pale pleochroism in shades of yellowish green. The optic angles of a dozen specimens from the Plateau flows and the Yellowstone tuff were measured on a universal stage. The angles ranged from 42° to

66°, with a mean of 55°. The indices of one specimen from the ash beneath the Yellowstone tuff on Mt. Everts are $N_x = 1.730$ and $N_z = 1.755$. The composition of these pyroxenes therefore ranges around $Wo_{36}En_{11}Fs_{53}$.

The fayalite occurs as honey-yellow rounded grains. Indices measured on a specimen from the ash beneath the Yellowstone tuff on Mt. Everts were $N_x = 1.807$ and $N_z = 1.859$. The composition is, therefore, close to Fe_2SiO_4 but with small amounts of magnesium or manganese or both in solution.

The Yellowstone tuff commonly contains inclusions and, in this respect, differs markedly from the rhyolite flows, which have very few inclusions. The commonest inclusions in the tuff (excluding pumice) are rhyolite of indeterminate origin and altered fragments derived from the early Tertiary andesitic volcanic rocks. Quartzite inclusions have also been found.

The Yellowstone tuff in the vicinity of Bunsen Peak carries abundant inclusions of the dacite exposed in that mountain. One of these inclusions was embayed by unvesiculated rhyolite. Hence, the inclusion was probably picked up prior to eruption of the tuff. Inasmuch as the dacite has a limited outcrop area, the vent for this portion of the Yellowstone tuff was probably near Bunsen Peak.

The welded tuff on the west side of the narrow ridge between Mt. Sheridan and Factory Hill, in the Red Mountains, contains carbonaceous inclusions up to an inch in diameter. These appeared to be carbonized wood, but an ignition check showed a loss in weight of only 4 per cent. They are, therefore, probably fragments of shale rich in organic materials.

The inclusions in the tuff range from a few tenths of an inch to, rarely, 4–5 inches. The proportion of inclusions in the tuff varies widely but seldom exceeds 1 per cent.

CHEMISTRY: Four analyses of the Yellowstone tuff are plotted in Figure 7, and Table 5 gives two modern analyses. These analyses show no significant differences from those of the flows.

Analysis No. 2 in Table 5 is of a sample from the drill core taken in the Norris Geyser Basin, which Fenner (1936, p. 303) has described as altered welded tuff. Fenner was misled by the streaks of tridymite and feldspar in the groundmass, which are actually primary. The present author has examined the Norris core material and believes that the samples taken below the uppermost few feet have not been appreciably attacked by hot-spring waters.

Rhyolite Domes

Four rhyolite domes have been found in Yellowstone Park. Three are south of the Norris Geyser Basin, along the southeastern margin of Gibbon Meadows (Pl. 6); the fourth protrudes through the Obsidian Cliff flow about a half a mile northeast of Lake of the Woods (Pl. 6). Three of the domes are of sufficient size to have been given topographic names. These are the Landmark, Gibbon Hill and Paintpot Hill.

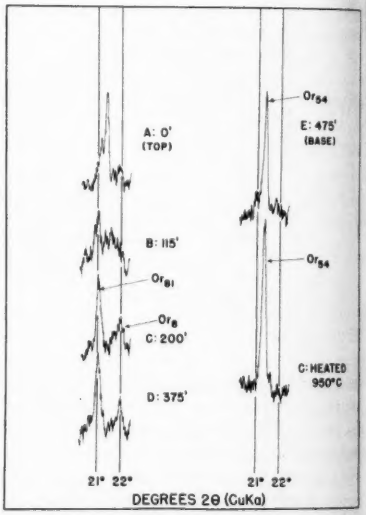

Figure 4. X-ray diffractometer patterns of 201 reflections of sanidines from the section of Yellowstone tuff in the Gardiner Canyon, Yellowstone Park, Wyoming. Distances of specimens below the top of the section are indicated. Note progressive unmixing from A to D; E is from the chilled base.

Gibbon Hill, the largest of the domes, is nearly a mile in diameter at its base and rises about 800 feet above the Yellowstone tuff on its northwest flank. The Paintpot Hill dome rises about 600 feet above the meadows at its base. The other two domes are considerably smaller.

All four domes are in contact with the Plateau flows, and the Gibbon Hill dome is also in contact with the Yellowstone tuff. It is clear from the manner in which the Plateau flows envelope the domes that the domes are older

than the Plateau flows. The contact between the Gibbon Hill dome and the Yellowstone tuff is not exposed. Hence, the age of the domes relative to the tuff has not been established.

The domes are identified by topography, lithology, and structure. All the domes are circular or elliptical in plan, with smooth, steep flanks. Most of the rhyolite in them is lithoidal and flow-banded. The upper portions of three of the domes are littered with pumice. The flow banding in exposures on Gibbon Hill strikes tangentially to the flanks and dips in toward the center of the dome at angles ranging from 25° to 50°. Plate 6 shows the structure obtained on this dome. Outcrops on the other domes are too poor to permit structural study.

Sanidine is the dominant feldspar in the dome rhyolites. Oligoclase is present both as individual phenocrysts and as small grains embedded in the sanidine and in optical continuity with the sanidine. Ferromagnesian phenocrysts are scarce in these rocks. Biotite has been found in one specimen from Gibbon Hill. Other specimens contain only magnetite.

Basalts

Basalt has been erupted along with the rhyolite in a number of areas in Yellowstone Park. The basalts are most abundant in the northern part of the rhyolite plateau, but they have also been found along the western and southwestern margins of the plateau. These basalts merge to the southwest with the basalts of the Snake River Plains.

The basalts were erupted as small flows from a number of vents. Although the basalt flows are numerous, the volume of the basalt is not more than a small fraction of 1 per cent of the volume of the associated rhyolite.

J. P. Iddings (*in* Hague *et al.*, 1899, p. 433–439) has described the basalts. He distinguished them from older basalts associated with the andesitic breccias. Howard (1937, p. 15–79) made a detailed field study of the basalts in the area around the Yellowstone Canyon and differentiated six groups. He proved that basalt flows both overlie and underlie the Yellowstone tuff in this area (Howard, 1937, p. 68–69, 76).

Typically, the basalts are holocrystalline, light to dark gray, and sparsely porphyritic. Phenocrysts or microphenocrysts of labradorite (An_{60-68}) and olivine (Fo_{75-85}) are set in a groundmass of plagioclase laths with interspersed granules of pyroxene and magnetite. The labradorite and olivine are found in glomeroporphyritic aggregates up to an inch in diameter. The basalts show little variation in mineralogy and texture. Alteration of the olivine to iddingsite and bowlingite is uncommon. Amygdular fillings are similarly rare and where present are zeolite or carbonate.

TABLE 3. CHEMICAL ANALYSES AND NORMS OF YELLOWSTONE BASALTS

		(1)	(2)	(3)	(4)
SiO_2		48.49	49.90	50.50	52.09
TiO_2		2.19	1.80	1.68	0.39
Al_2O_3		18.35	15.26	15.89	17.84
Fe_2O_3		7.63	1.76	2.20	4.27
FeO		1.21	8.87	8.20	4.56
MnO		none	0.13	0.15	0.14
MgO		6.72	7.59	7.28	5.33
CaO		10.40	11.07	10.30	8.03
Na_2O		3.02	2.49	2.71	3.39
K_2O		0.57	0.44	0.51	1.98
P_2O_5		0.20	0.37	0.25	0.27
SO_3		0.52	n.d.	n.d.	n.d.
Li_2O		0.02	n.d.	n.d.	n.d.
H_2O		0.67	0.57	0.43	1.77
CO_2		n.d.	n.d.	0.00	n.d.
		99.99	100.25	100.10	100.06
		CIPW Norms			
Q		0.6	..	..	0.7
Ab		26.1	21.2	23.1	29.2
Or		3.3	2.2	2.8	11.7
An		34.9	30.0	29.8	28.8
Py	Wo	5.5	9.5	8.5	4.1
	En	16.9	18.3	18.1	13.5
	Fs	..	11.5	10.6	4.2
Ol	Fo	..	0.7	..	..
	Fa	..	0.4	..	..
Il		2.6	3.5	3.2	0.8
Mt		..	1.7	3.2	6.3
Ap		0.3	1.0	0.7	0.7
Tn		2.2	..	..	..
Hm		7.6	..	..	..

(1) Basalt; north base of Prospect Peak (Iddings specimen no. 634, in Hague *et al.*, 1899, p. 438)

(2) Basalt; Sheepeaters' Cliffs, Gardiner River (Fenner specimen no. YP1024, 1938, p. 1450)

(3) Basalt; second cataract, Gardiner River (Fenner specimen no. YP969, 1938, p. 1450)

(4) Basalt; north side of Timber Creek, Crandall Basin (Iddings specimen no. 1252 *in* Hague *et al.*, 1899, p. 260)

Quartz xenocrysts have been found in specimens collected from the Gardiner Canyon downstream from Osprey Falls (Pl. 1), from the basalt area northwest of Mt. Jackson (Pl. 6), and from basalts in the vicinity of Obsidian Cliff (Pl. 6).

Pyroxene is not present as phenocrysts in the

basalts associated with the rhyolite. In this respect, the basalts associated with the rhyolite differ from the basalts associated with the early Tertiary, andesitic breccias. The latter basalts commonly have augite phenocrysts (Hague *et al.*, 1899, p. 266, 276). The pyroxene in the groundmass of the basalts associated with the rhyolite is ordinarily too fine-grained to permit estimate of its composition. In a few instances the pyroxene was found to be a clinopyroxene with a large optic angle, on the order of 50°. On one specimen, from the Cave Falls Road, at the southwest corner of the Park, the optic angle was measured on the universal stage and found to be 45°; N_x is 1.690. According to the determinative charts compiled by Hess (1949, p. 634, p. 638), the composition of this pyroxene is about $Wo_{38}En_{41}Fs_{21}$.

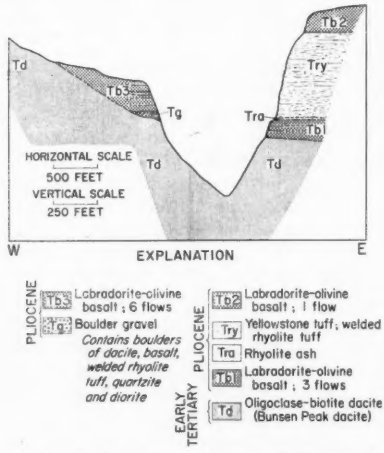

Figure 5. Geologic cross section of the Gardiner Canyon 0.3 mile north of Osprey Falls, Yellowstone Park, Wyoming

Analyses of three of the basalts associated with the rhyolite, together with their norms, are given in Table 3, along with an analysis of a basalt from Crandall Basin (east of Yellowstone Park), which is associated with the andesitic breccias. The three analyses of basalts associated with the rhyolite (Nos. 1, 2, and 3) are similar; the Prospect Peak basalt differs from the two Gardiner River basalts in oxidation of the iron and in being a little richer in alumina. The older basalt from the andesitic breccias (No. 4) is much richer in alkalis and a little richer in silica.

The basalt has been erupted both before and after the Yellowstone tuff. The youngest rhyolites in Yellowstone, the Plateau flows, are definitely younger than a part of the basalt. In the Bechler Canyon the Plateau flows overlie basalt which, in turn, overlies Yellowstone tuff. None of the basalt in Yellowstone has definitely been observed to overlie Plateau flows. Two of the outlying Plateau flows, the Obsidian Cliff flow and the Cougar Creek flow, have surfaces littered with considerable quantities of basalt float. Persistent search, however, failed to reveal any outcrops of basalt on these flows. The float seems best interpreted as glacial in origin and derived from the extensive basalt areas which surround these flows. No basalt has been found in the main outcrop area of the Plateau flows. The basalt is, hence, believed to be older than the Plateau flows.

One of the best exposures of basalt in Yellowstone is in the Gardiner Canyon 0.3 mile north of Osprey Falls. This section contains all the types of basalt found in association with the rhyolite and illustrates the age relationships with the Yellowstone tuff. Figure 5 shows a cross-section of the canyon at this point.

The first eruptions produced the three lower basalts on the east side of the canyon. These basalts overlie the eroded flank of the dacite plug which forms Bunsen Peak, a mile to the west of the canyon. Following their eruption, the Yellowstone tuff and the basalt which directly overlies the tuff were emplaced. The contact between the Yellowstone tuff and the overlying basalt is well exposed and shows no sign of an erosion interval. The upper portion of the Yellowstone tuff, which is unconsolidated, has been preserved, and the eruption of the tuff was evidently followed immediately by the eruption of the basalt. A canyon was then cut, in approximately the same position as the present canyon, to a depth indicated by the base of the gravel horizon on the west wall of the present canyon. Diorite and quartzite boulders occur in the gravel and indicate that the river which cut this ancestral Gardiner Canyon had its headwaters, as does the Gardiner River today, in the Gallatin Range. The ancestral canyon was then filled by a sequence of six basalt flows, exposed on the west wall of the present canyon, and the canyon was re-excavated to its present depth.

Basalt has been erupted on the eroded surface of the Yellowstone tuff in the Obsidian Cliff area (Pl. 6). Two basaltic cinder cones have been found near the northeast corner of

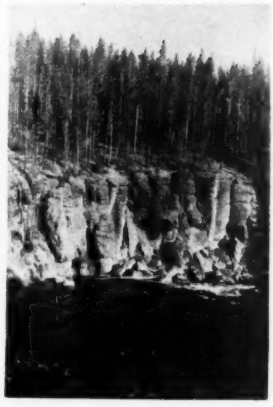

Figure 1. Typical exposure of the Yellowstone tuff, Lewis Canyon, Yellowstone Park, Wyoming.

Figure 2. Base of the Yellowstone tuff on Mt. Everts, Yellowstone Park, Wyoming. *See* Figure 1 for a geologic section of this outcrop.

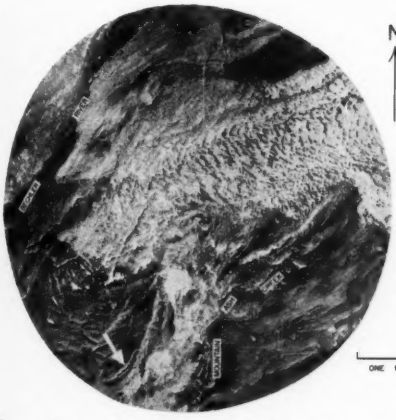

Figure 3. Aerial photograph of the western portion of the Pitchstone Plateau, Yellowstone Park, Wyoming. Arrow indicates a crack in the chilled surface of the flow. Aero Service Corporation photograph WY-18A-213.

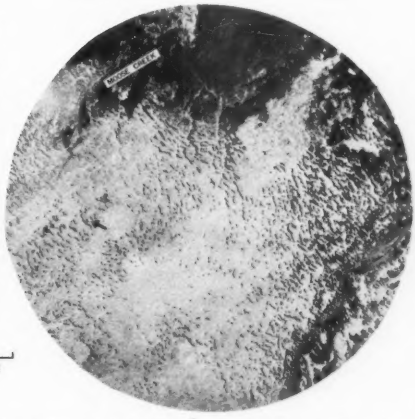

Figure 4. Aerial photograph of the central portion of the Pitchstone Plateau, Yellowstone Park, Wyoming. Arrow indicates position of vent. Aero Service Corporation photograph WY-18A-17.

RHYOLITE FLOWS AND WELDED TUFFS

Figure 1. Aerial photograph of the area west of the Shoshone Geyser Basin, Yellowstone Park, Wyoming. Scarps marked by arrows are believed to be flow fronts; others are faults. Aero Service Corporation photograph WY-18A-162.

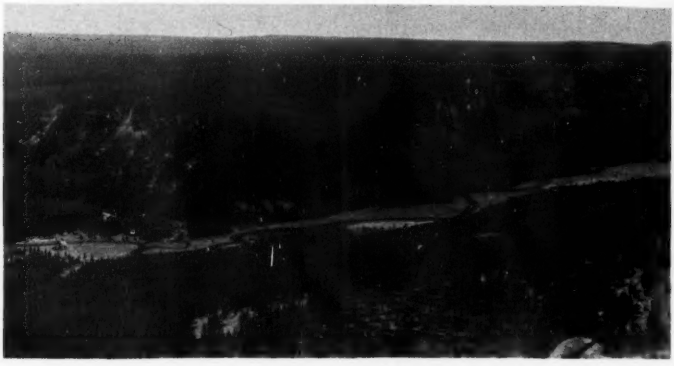

Figure 2. Madison Plateau seen from the north wall of the Madison Canyon, Yellowstone Park, Wyoming. Cliffs are the eroded front of a single rhyolite flow.

FLOW FRONTS AND FAULT SCARPS

BOYD, PLATE 3
Geological Society of America Bulletin, volume 72

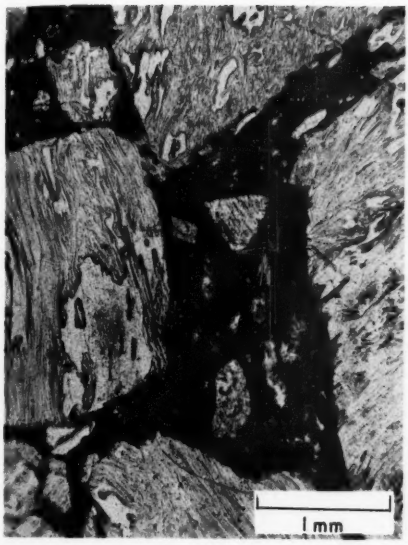

Figure 1. Collapsed pumice breccia, Obsidian Cliff, Yellowstone Park, Wyoming.

Figure 2. Collapsed pumice breccia, road cut 1.4 miles north of Lake Junction, Yellowstone Park, Wyoming. Q = quartz, F = ferroaugite.

Figure 3. Deformed collapsed pumice, Canyon flow, Ponuntpa Springs, Yellowstone Park, Wyoming. Q = quartz.

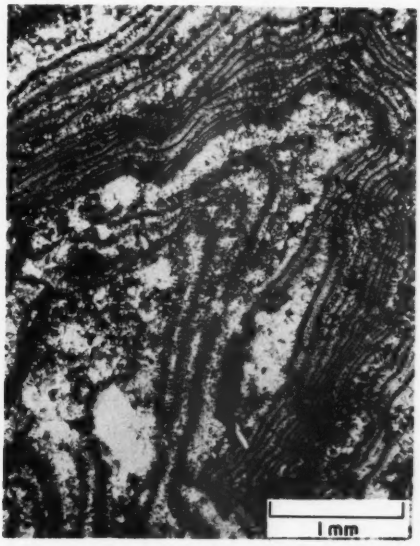

Figure 4. Coarse quartz at apex of a fold in flow banding, Madison Canyon, Yellowstone Park, Wyoming.

PHOTOMICROGRAPHS OF RHYOLITE FLOWS AND FLOW BRECCIAS

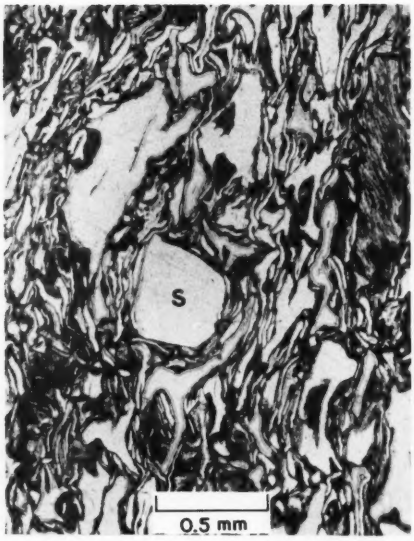

Figure 1. Glassy welded tuff, Yellowstone Canyon, Yellowstone Park, Wyoming. S=sanidine; fragment of collapsed pumice at upper right.

Figure 2. Glassy welded tuff, Yellowstone Canyon, Yellowstone Park, Wyoming. Q=quartz.

Figure 3. Cryptocrystalline welded tuff, Gardiner Canyon, near Osprey Falls, Yellowstone Park, Wyoming. Q=quartz.

Figure 4. Mt. Everts ash welded artificially at 750°C., 52 bars, for 72 hours. The glass fragments were dusted with "platinum black" before welding so that the borders of the shards would show in the photograph. Run is all glass with opaque, aggregated patches of platinum.

PHOTOMICROGRAPHS OF WELDED RHYOLITE TUFFS

BOYD, PLATE 5
Geological Society of America Bulletin, volume 72

this map area. These cones are now covered by timber, and few or no traces of craters remain. However, basaltic tuff, consisting of basaltic lapilli and scoriaceous bombs embedded in a matrix of ash, crops out on both cones. The smooth flanks of the cones are littered with basaltic scoria.

A somewhat similar, although less well preserved, basaltic vent has been found in the basalt area northwest of Mt. Jackson (Pl. 6).

Rhyolite-Basalt Mix-Lavas

Rhyolite-basalt mix-lavas have been found at four localities in Yellowstone Park. Their volumes are small, and all are within a few miles of Obsidian Cliff (Pl. 6). The largest, the Grizzly Lake rhyolite-basalt complex, is apparently a flow three-fourths of a square mile in area and 100–200 feet thick. All four of the mix-lava masses appear to be younger than the Yellowstone tuff.

The character of these mix-lavas indicates that they have been produced by processes ranging from the mingling of liquid basalt and rhyolite to the inclusion of quantities of cold basalt in rhyolite. Basalt and rhyolite have been erupted alternately and at close intervals in this part of the Park, and it is surprising that the mix-lavas are of such restricted occurrence.

J. P. Iddings (*in* Hague *et al.*, 1899, p. 430–432) was the first to describe rhyolite-basalt mix-lavas on the Gardiner River. The complex in which these lavas occur has attracted the attention of a number of petrologists (Fenner, 1938; 1944; Wilcox, 1944; Hawkes, 1945). The descriptions of this complex in the literature are detailed, and further discussion is beyond the scope of this paper.

The largest rhyolite-basalt mix-lava is an irregularly shaped mass whose center lies 1.5 miles due west of Obsidian Cliff (Pl. 6). The best exposures are on the edge of the steep bluff overlooking the northern end of Grizzly Lake. The complex has the appearance of a flow of intimately mixed rhyolite and basalt.

The Grizzly Lake mix-lava is petrographically similar to the Gardiner River material except that it shows conclusive evidence of the simultaneous fluidity and mingling of rhyolite and basalt. Contaminated basalt includes isolated blebs of dominantly rhyolitic material and vice versa. The contact between contaminated rhyolite and contaminated basalt may appear sharp in hand specimen but is commonly vague when seen under the microscope. Thin seams of rhyolitic glass have been observed with interlaminated basalt. The feldspar microlites in the basalt are oriented with their long axes parallel to the rhyolite seams.

The character of this lava suggests mixing of rhyolite and basalt at depth and extrusion as a single flow.

A small rhyolite flow, the Crystal Springs flow, crops out about half a mile northeast of Obsidian Lake (Pl. 6). This flow is glassy, nonporphyritic, and filled with small angular fragments of basalt. The basalt locally forms several per cent of the flow. The basalt xenoliths have not been affected by inclusion in molten rhyolite except for a slight reddening around the edges.

The Crystal Springs flow appears to be an example of a rhyolite flow which picked up fragments of cold basalt. The quantity of basalt is surprising inasmuch as inclusions are very rare in other rhyolite flows in the Park.

A small exposure of rhyolite contaminated by basalt has been found on the eastern edge of the Obsidian Cliff flow about three-fourths of a mile due east of the Landmark. The exposures are not adequate to permit the relationship between this outcrop of mix-lava and the Obsidian Cliff flow itself to be established with certainty. The outcrop is high on the front of the flow, however, and there is nothing in the field relationships to indicate that it is not a part of the flow.

Plateau Flows

AREAL EXTENT: Most of the Plateau flows occupy a single outcrop area of 1000 square miles in central and southwestern Yellowstone Park (Pl. 1) and adjacent parts of Montana and Idaho. Exposures of the flows are largely their surficial parts. Only the Madison and Yellowstone rivers have cut deep canyons into them. The Bechler River, which drains the southwestern part of the Park, occupies a depression between the fronts of two adjacent flows. The aggregate thickness of the flows in the central part of their outcrop area is unknown. Many individual flows are 500–1000 feet thick. Assuming an average total thickness of 1000 feet, the volume of the flows would be about 200 cubic miles.

The Pitchstone Plateau in the southwestern corner of the Park appears to be one flow. The front along the southwestern margin of the plateau is 1000 feet high; along the eastern and southern margins, the front ranges between 300 and 500 feet in height. The area covered by the Pitchstone Plateau flow is close to 100 square

miles. If the average thickness is taken to be 500 feet, then 10 cubic miles of rhyolite has been erupted to form this single flow. Larger flows are probably present in the Madison and Central plateaus.

FIELD RELATIONSHIPS: The most abundant rhyolite exposed in the outcrop area of the Plateau flows is a black, perlitic, flow-banded glass. The flow banding consists of alternate bands of lithoidal rhyolite and glass, or layers of spherulites and lithophysae in glass; the bands range from a fraction of an inch to many tens of feet in thickness. The banding is commonly contorted, and its attitude may change in a haphazard manner from one outcrop to another.

of shards and broken phenocrysts. The base of the flow itself is a spherulitic perlite. The perlite becomes richer in spherulites with increasing distance above the base until, about 30 feet above the breccia, it passes into a lithoidal flow-banded rhyolite.

The breccia probably formed from pumice and ash which rolled down the front of the advancing flow. As the flow moved over this deposit, the hot pumice fragments were collapsed and welded to dense obsidian.

SURFICIAL FEATURES: The surface of a flow typically consists of a series of ridges 25–50 feet high. Steeply dipping obsidian crops out in these ridges. In aerial photographs the ridges

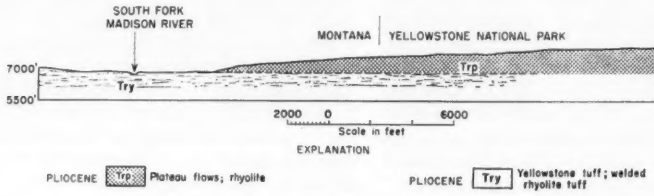

Figure 6. Front of one of the plateau flows, Reas Pass, Montana

Holocrystalline specimens have banding consisting of fine and more coarsely crystalline layers. Some lithoidal varieties have a mottled texture or are even-grained. Distinguishing hand specimens of the latter type from welded tuff can be difficult. In outcrop, however, pockets filled with rubble or irregular vugs are found in the flows, but not in welded tuff.

The interior of one of the Plateau flows can be seen in the south wall of the Madison Canyon (Pl. 3, fig. 2). Scoriaceous glass forms the top of the plateau along the southern edge of the canyon. One hundred feet below the rim, glassy rhyolite gives way to finely flow-banded, lithoidal rhyolite which shows no further change as the section is traced down. The thickness of the exposed section of this flow ranges from 400 to 1000 feet along the canyon wall; the base is buried in talus.

The base of one of the Plateau flows, exposed at Iris Falls on the Bechler River, in the southwestern corner of Yellowstone Park, rests on a breccia which overlies basalt. The breccia consists of angular fragments of spherulitic obsidian in a soft, coherent matrix. Microscopic examination of the fragments shows them to be collapsed and welded pumice; the matrix consists

are resolved into a pattern similar to the surface of a glacier. Figure 3 of Plate 2 shows a lobe of the Pitchstone Plateau flow. The trees on the Pitchstone Plateau grow only on the ridges and emphasize the pattern of corrugations and pressure ridges on the surface of the flow. Cracks in the surface of this flow, produced by movement of liquid lava beneath a chilled crust, are up to half a mile long and 75 feet deep (Pl. 2, fig. 3).

Fronts of the Plateau flows range from a few tens of feet to 1000 feet in height. The slope of a front is ordinarily between 20° and 30°. The profile of a typical flow front is shown with no vertical exaggeration in Figure 6. Large-scale flow banding tends to be parallel to the front and to dip back into the flow. In many outcrops, however, small-scale flow banding strikes at an angle to the front.

VENTS: Vents for two of the Plateau flows have been located by study of the flow patterns on their surfaces. The vent for the Pitchstone Plateau flow is shown in Figure 4 of Plate 2. The corrugations on the surface are roughly concentric around the vent. This vent is inconspicuous on the ground. It is a low dome about 300 feet in diameter and 30 feet high. The rhy-

olite in the dome is lithoidal and scoriaceous in contrast to the surrounding glassy surface of the flow. Flow banding in the vent dome strikes tangentially and dips outward at an average angle of 30°.

A second vent on the northwest margin of the Central Plateau, 1 mile southeast of Gibbon Hill (Pl. 6), is marked by a broad dome about 150 feet high. The dome is covered by timber and littered with pumice.

COLLAPSED PUMICE BRECCIA: Irregularly shaped masses of breccia have been found at many localities in the outcrop area of the Plateau flows. Most of the fragments in the breccias are, or were, pumice. The matrix varies greatly in proportion and degree of induration.

The least indurated varieties consist of fragments of finely vesiculated pumice with or without a matrix of ash. More commonly, the pumice fragments have been collapsed and welded. The collapsed fragments are not recognizable as pumice in hand specimen, but in thin section their primary pumiceous texture is evident. In many cases, the pumice fragments and matrix are both welded to dense glass, and the rock has been plastically deformed so that the pumice fragments are drawn into streaks. J. P. Iddings (*in* Hague *et al.*, 1899, p. 403–406) has graphically described these temperatures and correctly interpreted them.

Such breccias can usually be recognized by their color. The pumice commonly oxidizes during inflation, and a breccia formed of collapsed and welded fragments of pumice is mottled with variegated yellow, brown, or red patches. Figures 1–3 of Plate 4 show microtextures characteristic of collapsed pumice breccias.

The pockets of collapsed pumice breccia are formed from masses of pumice and ash dragged from the surfaces of moving flows into the liquid lava beneath. The larger fragments of pumice retain their initial heat better than the fine ash. Hence, breccias with collapsed and welded pumice fragments in a soft, coherent matrix are formed in some places.

OUTLYING FLOWS: Three small flows lie north of the main outcrop area of the Plateau flows. The largest, the Obsidian Cliff flow, has an area of 4.5 square miles.

The Obsidian Cliff flow (Pl. 6) was erupted from the plateau of welded tuff and basalt east of Obsidian Cliff (J. P. Iddings *in* Hague *et al.*, 1899, p. 360). It spilled into a canyon, and the stream occupying the canyon re-established its course by cutting down between the flow and the welded tuff in the west wall of the canyon. The section of the flow exposed in this way is Obsidian Cliff.

Obsidian Cliff is about 200 feet high. The rhyolite in the cliff is glassy except for the development of spherulites and lithophysae. A section of obsidian 200 feet thick is unusual and probably results from the particularly rapid cooling of a flow emplaced in a steep-walled canyon. The rhyolite in Obsidian Cliff has well-developed columnar jointing. Such jointing is rare in rhyolite flows, although common in welded tuff. The development of columnar jointing in volcanic rocks seems to be related to a massive structure. Rhyolite flows are typically well banded, and in such lavas the reduction in volume which accompanies cooling and crystallization can be accommodated by parting of the flow laminae. That part of the rhyolite in Obsidian Cliff which has well-developed columnar jointing has poorly developed flow banding; that which is filled with lithophysae, or in which the flow banding is well developed, has no columnar jointing.

The rhyolite in the Obsidian Cliff flow, unlike the bulk of the Plateau flows, is nonporphyritic. However, its composition is within the range established by analyses of other Yellowstone rhyolites. Figure 7 shows plots of four analyses of the obsidian from Obsidian Cliff.

A second small outlying flow, the Crystal Springs flow, crops out on the plateau of welded tuff and basalt half a mile north of the northern boundary of the Obsidian Cliff flow (Pl. 6). The Crystal Springs flow is nonporphyritic and contains a large number of inclusions of basalt.

The smallest of the Plateau flows crops out at the eastern edge of the Madison Valley, northwest of Mt. Jackson (Pl. 6). The Cougar Creek flow carries sparse, small phenocrysts of quartz, sanidine, oligoclase, and accessory ferroaugite and magnetite. The flow is roughly circular in outline and about a mile in diameter.

CANYON FLOW: The Canyon flow crops out at the head of the Yellowstone Canyon and east of the canyon in the area bounded approximately by Sour and Broad creeks (Pl. 1). This flow has textures and structures which suggest that it may have been emplaced in a type of eruption transitional between a lava flow and a pyroclastic flow.

In restricted areas the Canyon flow has well-developed, steeply dipping flow banding on

both a coarse and a fine scale. Such banding can be seen in the altered rhyolite at the Lower Falls of the Yellowstone River. Hot-spring solutions have there selectively altered and silicified bands in the rhyolite, and the falls are held up by a particularly resistant layer. Banding on a major scale can also be seen in the east wall of the Yellowstone Canyon about 7 miles downstream from Yellowstone Falls. Outcrops of flow-banded rhyolite have been found east of the falls. The surface of the Canyon flow is glassy and, in many areas, perlitic. The interior of the flow is exposed in the Yellowstone Canyon and is predominantly lithoidal. Near the head of the Yellowstone Canyon, the Canyon flow is more than 1000 feet thick.

Despite many outcrops of well-banded rhyolite, the Canyon flow, on the whole, has poorly developed flow banding. The lithoidal portions of the flow are brown and friable and look much like welded tuff. The similarity to welded tuff is pronounced in an exposure of the base of the flow in the west wall of the Yellowstone Canyon above Seven-Mile Hole (a point about 7 miles below Yellowstone Falls). At the base of the flow at this locality is about 10 feet of poorly banded ash containing fragments of pumice, scoria, and phenocrysts. The ash is similar to the banded ash which underlies the Yellowstone tuff in this area, and the glassy base of the flow in this outcrop has a texture very similar to a welded tuff. Most of the major structures in the Canyon flow indicate that was emplaced as a lava flow and not as a pyroclastic flow. However, all the thin sections of the Canyon flow show textures which suggest that the rhyolite has vesiculated and then collapsed. The flow was possibly emplaced as a froth which was not thoroughly ruptured into fragments but which collapsed and continued to move as a lava.

This is a mechanism of eruption suggested by Kennedy (1954, p. 495) for the welded tuff in Yellowstone. The present author believes that the texture of the welded tuff indicates formation from avalanches rather than froths, for reasons which will be discussed in the section of this report dealing with the mode of eruption of the Yellowstone tuff. However, the Canyon flow is worthy of detailed study as a possible example of a froth flow.

PETROGRAPHY: The phenocrysts in the Plateau flows show little variation in kind and composition except in the variable development of plagioclase. The usual phenocrysts are: quartz, sanidine with or without sodic oligoclase, ferroaugite, fayalite, and magnetite. There are generally trace amounts of zircon and rutile. Other assemblages are rare. Two of the outlying flows, the Obsidian Cliff flow and the Crystal Springs flow, have no phenocrysts. The rhyolite in the Upper Geyser Basin (Pl. 1) has plagioclase (An_{28}) and ferroaugite as the only phenocrysts. Assemblages including quartz without sanidine, or vice versa, have not been observed.

Sanidine is the only feldspar present as phenocrysts in slightly more than half of 60 thin sections of the Plateau flows. These specimens are believed to represent a good sampling of the flows. In most of the specimens found to contain plagioclase, plagioclase is subordinate to sanidine.

Practically all the plagioclase-bearing specimens come from the Central Plateau (Pl. 1). Specimens from the flows making up the Madison and Pitchstone plateaus, with only one exception, had sanidine as the only feldspar. Not all the Central Plateau lavas, however, have two feldspars.

X-ray determinations have been made of the compositions of sanidines from single-feldspar flows. The sanidines were first homogenized by heating at 1000° C. Compositions were then obtained by measurement of the $\bar{2}01$ spacings. Quartz was used as an internal standard. The compositions were obtained from the curve of Bowen and Tuttle (1950).

The compositions of 21 samples of wide geographic distribution are plotted in Figure 3B. The range in composition is from 43 to 56 per cent Or. This range is about twice that obtained for a group of sanidines from two-feldspar welded tuffs (Fig. 3A).

Refractive indices of the plagioclases in the Plateau flows show that their average composition is about An_{20}. In flows which carry abundant plagioclase, the plagioclase composition ranges up to about An_{30}.

Ferroaugite and fayalite occur as microphenocrysts and typically constitute only a few tenths of a per cent of the rock. In some specimens with a lithoidal groundmass the ferromagnesian silicates are altered to iron oxide. Biotite or hornblende has nowhere been observed in the Plateau lavas as phenocrysts. Rarely they line vugs or vesicles.

The proportion of phenocrysts to groundmass in the Plateau flows ranges from zero to about 15 per cent. Table 4 gives modes of two specimens of Plateau flows.

Inclusions are extremely rare in the Plateau

flows. One outlying flow, the Crystal Springs flow, has picked up abundant fragments of basalt, but only three or four inclusions have been found in all the other flows. These inclusions are basalt and siltstone.

TABLE 4. MODES OF PLATEAU FLOWS
Volume per cent

	(1)	(2)
Glass	95.4	90.6
Quartz	2.0	2.2
Sanidine	2.5	4.9
Plagioclase	..	1.8
Ferroaugite	0.1	0.2
Fayalite	..	0.1
Opaque minerals	<0.1	0.1
	100.0	99.9

(1) Mode of obsidian, Reas Pass, Montana Plateau flows. YP-54-A1. Table 5, analysis no. 3

(2) Mode of perlite, Midway Geyser Basin, Yellowstone National Park. Plateau flows. YP-54-A3. Table 5, analysis no. 5

The minerals in the groundmass of the Plateau flows are tridymite, quartz, and feldspar. The tridymite and feldspar commonly form cryptocrystalline growths. The composition of the feldspars in these growths has not been determined owing to the interference on their X-ray patterns of tridymite lines. Relatively coarse quartz is found in places in vuggy patches in the groundmass of the flows (Pl. 4, fig. 4).

CHEMISTRY: Twelve analyses of flows from the Yellowstone area are plotted in Figure 7. Four of these are modern analyses, two of them new with this report (Table 5). The remaining eight have been taken from Hague *et al.* (1899, p. 426). The identifications of the older analyses as flows have been made by the present author on the basis of J. P. Iddings' (*in* Hague *et al.*, 1899) lithologic descriptions and his descriptions of their localities.

The boundary in Figure 7 dividing the fields of primary crystallization of quartz and feldspar, and the position of the minimum on this boundary, are taken from the data of Tuttle and Bowen (1958). The positions of this boundary and of the minimum have been found by Tuttle and Bowen to shift slightly in the composition plane with change in water pressure. With increase in water pressure the minimum moves toward $NaAlSi_3O_8$. The positions of the boundary and the minimum shown in Figure 7 are for 500 kg/cm² (H_2O).

All the analyses group close to the minimum in the system $NaAlSi_3O_8-KAlSi_3O_8-SiO_2$. Such a relationship has been noted before for rhyolites (Bowen, 1937, p. 18) and for granites (Chayes, 1952a, p. 242). As Bowen and Chayes have stressed, the coincidence between the

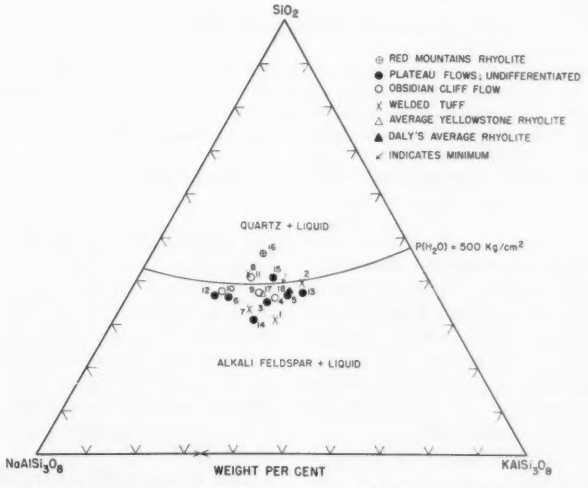

Figure 7. Analyses of Yellowstone rhyolites on a diagram of the system $KAlSi_3O_8$-$NaAlSi_3O_8$-SiO_2. Phase-equilibrium data after Tuttle and Bowen (1958)

minimum on the liquidus and the compositions of rhyolites and granites is a powerful argument for the dominant influence of crystal-fractionation processes in the genesis of these rocks.

The plots of the analyses in Figure 7 have a considerable spread along the SiO_2 axis and overlap the boundary dividing the fields of

Assemblages (3) and (4) are found in only an infinitesimal fraction of the rhyolite. Assemblages (1) and (2) are divided almost equally in the bulk of the rhyolite.

The constant appearance of quartz and sanidine together as phenocrysts is the more surprising in view of the fact that the total volume

Table 5. Modern Analyses of Yellowstone Rhyolites

	(1)	(2)	(3)	(4)	(5)	(6)
SiO_2	73.15	76.95	76.77	76.78	73.91	67.09
TiO_2	0.14	0.13	0.15	0.08	0.26	0.47
Al_2O_3	12.13	12.18	11.71	12.09	11.83	13.08
Fe_2O_3	1.12	1.07	0.64	0.56	0.92	1.60
FeO	0.66	0.26	1.05	0.81	0.66	1.94
MnO	0.04	0.01	0.05	0.02	0.04	0.05
MgO	0.13	0.12	0.33	0.10	0.11	0.53
CaO	0.71	0.28	0.49	0.57	0.68	1.89
BaO	0.08	0.08	0.02	0.00	0.10	0.09
Na_2O	4.01	2.98	4.01	3.79	3.34	3.97
K_2O	5.27	5.50	5.10	4.93	5.14	2.75
P_2O_5	0.00	0.07	0.00	0.09	0.00	0.08
ZrO_2	0.04	0.03	0.04	0.01	0.04	0.02
H_2O+	1.91	0.24	0.10	0.12	2.76	4.23
H_2O-	0.21	0.06	0.16	0.08	0.29	2.08
Cl	0.06	..	0.06	0.05	0.09	0.05
F	..	0.00	..	0.15	..	..
CO_2	0.00	0.04	0.00	..	0.00	0.01
S	..	0.41	..	0.06	..	..
SO_3	0.00*	..	0.03*	..	0.14*	0.15
less O for	99.66	100.41	100.71	100.29	100.31	100.08
F, Cl, S−	0.01	0.15	0.01	0.10	0.02	
	99.65	100.26	100.70	100.19	100.29	

*Total sulfur as SO_3

(1) Glassy welded tuff; base of Yellowstone tuff, Mt. Everts, Yellowstone National Park; analyst H. B. Wiik (new analysis; specimen no. YP-54-A2)

(2) Lithoidal welded tuff; Norris Geyser Basin core; no. YP750; analyst C. N. Fenner (Fenner, 1936, p. 309)

(3) Obsidian scoria (flow); Reas Pass, Montana, analyst H. B. Wiik (new analysis; specimen no. YP-54-A1)

(4) Obsidian (flow); Obsidian Cliff, Yellowstone National Park; analyst E. S. Shepherd (*in* Bowen, 1935, p. 493)

(5) Perlite (flow); road cut by Midway Geyser Basin, Yellowstone National Park; analyst H. V. Wiik (new analysis; specimen no. YP-54-A3)

(6) Perlite (flow); Upper Geyser Basin core; no. YP279; analyst C. N. Fenner (Fenner, 1936, p. 264)

primary crystallization of quartz and alkali feldspar. This relationship suggests that quartz and alkali feldspar should each be the first to crystallize in some of the rhyolite and that, in places, each of these minerals would be the only phenocrysts. This is not the case. The phenocryst assemblages that have been observed (excluding trace amounts of ferromagnesian phases) are, in order of abundance:

(1) quartz+sanidine+plagioclase (An_{20})
(2) quartz+sanidine
(3) no phenocrysts
(4) plagioclase (An_{29})

per cent of phenocrysts in all the rhyolites ranges from 0 to about 30 per cent. The explanation may, in part, be found in the fact that the liquidus on the feldspar side of the boundary has a very gentle slope. Crystallizing melts whose compositions correspond to any of the points in Figure 7 below the quartz-feldspar boundary would shift to the boundary with a drop in temperature of no more than about 40° C.

Half of the analyses of Yellowstone rhyolites are slightly peraluminous (*See* Table 6, column 8). In the average of these analyses (Table 6,

No. 17) the sum of the alkalis and lime is almost exactly equal to the alumina. The appearance of corundum in the norms of eight of the analyses is probably due to slight alteration or to analytical error. Almost all the fresh specimens of rhyolite examined by the author contained small amounts of clinopyroxene. Such a pyroxene would probably not be stable in a peraluminous environment with an excess of silica.

Table 6. Normative Mineralogy of the Yellowstone Rhyolites

All values given in weight per cent. Analyses 7–16 are from J. P. Iddings (*in* Hague, *et al.*, 1899, p. 426). Numbers in parentheses are Iddings' specimen numbers.

Analysis	Or+Ab+Q	Or+Ab+Q=100			Or+Ab+An=100			C	Ac
		Or	Ab	Q	Or	Ab	An		
1	96.1	33.0	36.0	31.0	47.8	52.2	0.0	..	..
2	95.3	34.4	26.4	39.2	55.3	42.3	2.4	0.8	..
3	95.3	29.2	35.7	35.1	43.5	56.5	0.0	..	1.9
4	95.4	30.3	33.5	36.2	46.2	51.1	2.7	..	..
5	94.6	32.8	30.5	36.7	49.8	46.2	4.0	..	..
6	82.9	20.8	43.0	36.2	27.4	56.7	15.9	0.2	..
7 (2121)	86.0	26.5	40.2	33.3	35.9	54.5	9.6	..	..
8 (1862)	91.0	22.0	36.3	41.7	35.3	58.3	6.4	2.5	..
9 (2187)	92.6	26.4	36.2	37.4	39.5	54.2	6.3	1.4	..
10 (2256)	92.3	18.7	43.7	37.6	27.8	65.0	7.2	0.7	..
11 (2220)	91.5	23.1	36.1	40.8	36.4	56.9	6.7	2.4	..
12 (2164)	84.8	17.7	45.7	36.6	24.1	62.1	13.8	..	..
13*	92.2	35.6	27.3	37.1	51.9	39.8	8.3	..	..
14 (1924)	89.6	28.6	40.4	31.0	38.6	54.6	6.8	..	..
15 (2066)	89.7	27.9	31.5	40.6	42.4	48.1	9.5	0.6	..
16 (1980)	90.3	22.8	30.8	46.4	39.4	53.2	7.4	1.8	..
17†	91.3	27.4	35.6	37.0	39.8	51.8	8.4	0.1	..
18**	89.2	29.9	32.3	37.8	43.5	47.0	9.5	1.0	..

*Midway Basin. No number listed by Iddings. Probably same locality as 5
†Average Yellowstone rhyolite
**Daly's (1933, p. 9) average rhyolite

Glacial Deposits

Glacial gravels have been deposited in varying amount on the rhyolite plateau subsequent to the volcanic eruptions. The original surface of the Pitchstone flow (Pl. 2, figs. 3, 4) in the southwestern corner of the Park is well preserved, but the surfaces of the Central Plateau and the Mirror Plateau are covered by glacial debris over much of their extent.

The glacial deposits predominantly form a veneer rather than moraines. At least two glacial advances can be recognized. In the lower Geyser Basin glaciofluvial sands and boulder gravels, indurated by hot springs, are overlain by younger, unconsolidated outwash. The older deposits form the Twin Buttes and several other prominent hills in the Geyser Basin (Pl. 1). The younger outwash has spread into the Geyser Basin at its western margin in the form of a large delta.

Small glaciers formed along the fronts of the large rhyolite flows. These have scalloped the edges of the flows with small cirques and have left terminal moraines a few hundred yards or less in advance of the flow fronts.

Detailed studies of the glacial geology of areas in the Park have been made by Howard (1937) and N. A. Miner (1937, Ph.D. thesis, State Univ. of Iowa). Glacial deposits are shown on Plates 1 and 6 only where they completely mask the bedrock.

Hot-Spring Deposits

Hot springs have been active on the rhyolite plateau both during and since the eruption of the rhyolite. Evidence for inter-rhyolite hot-spring activity is preserved in the north wall of the Madison Canyon. The oldest unit, a rhyolite flow belonging to the Jackson flows, has been altered by hot springs. The Yellowstone tuff, which overlies the eroded surface of this flow, has not been affected. This relationship is well exposed in cliffs about a mile upstream

from the bridge in the Madison Canyon (Pl. 6). The contact between the Yellowstone tuff and the hot-spring-altered, underlying flow is visible from the road.

Evidence for post-Yellowstone tuff but preglacial hot-spring activity is exposed on Terrace Mountain, near Mammoth Hot Springs, at the northern border of Yellowstone Park (Pl. 1). The Yellowstone tuff in Terrace Mountain is overlain by travertine. Glacial drift, with boulders derived from the Gallatin Range to the west, litters the surface of the travertine (Hague, 1911, p. 108–109). The travertine itself has been incorporated in drift found to the east of Terrace Mountain (N. A. Miner, 1937, Ph.D. thesis, State Univ. of Iowa, p. 12).

Since the Pleistocene, hot springs have been active in many areas on the rhyolite plateau. Allen and Day (1935) give a wealth of descriptive data relating to these hot springs and discuss their origin.

Hot-spring deposits are shown on Plates 1 and 6 where there are deposits of sinter or travertine or where alteration has obliterated the texture of the bedrock.

Age of the Rhyolite

No fossils were found in the present investigation, and there are few gravels or soil zones interbedded with the rhyolite in Yellowstone Park in which fossils might be preserved. Love (1956a, p. 91) found rhyolite welded tuff and flows intertongued with the Teewinot formation south of Yellowstone Park. The Teewinot contains middle Pliocene vertebrate fossils. The welded tuff in the Teewinot is probably correlative with the Yellowstone tuff within the Park, and the flows possibly belong to the Jackson group. More work is necessary to establish a sound correlation between the Tertiary stratigraphy worked out by Love for the Jackson Hole area and the rhyolite sequence in Yellowstone, but it can be tentatively assumed that the Yellowstone tuff, and possibly the Jackson flows, are middle Pliocene.

The Plateau flows unconformably overlie the Yellowstone tuff. In most areas these flows are covered by glacial debris, but locally the original surfaces of the flows have been preserved, and these have evidently not been glaciated. Nevertheless, no exposures were found in which flows of the Plateau group could be seen to overlie glacial deposits, and accordingly their age was believed to be Pliocene.

However, Love (1956b, p. 150), noting the unglaciated surface of the Pitchstone Plateau flow, has suggested that the flow was erupted at the close of the Pinedale glacial stage. Recently Gerald M. Richmond and Warren Hamilton (Personal communication) have found evidence that the flow making up the northwest corner of the Madison Plateau "... overlies moraines of the Bull Lake stage of glaciation southwest of West Yellowstone, but was scoured by a valley glacier of the Pinedale stage in Madison Canyon." Work now in progress may therefore show that the Plateau flows are all or in part Pleistocene rather than Pliocene, as has been assumed in this report.

STRUCTURE OF THE RHYOLITE PLATEAU

General Statement

Block faulting which took place in two periods during and subsequent to the eruption of the rhyolite in Yellowstone Park has not notably deformed the rhyolite. Fault blocks have bounding scarps up to 3000 feet high, but the rhyolite in the blocks has not been tilted more than 10°–15° in most places.

Although the rhyolite plateau is made up of a number of stratigraphic units, most of these are too thick to be of aid in working out the structure. However, foliation in the welded sections of the Yellowstone tuff, consisting of flattened pumice fragments and vesicles, develops horizontally and can be measured to ±5°. The banding in the rhyolite flows is useless as an indicator of secondary deformation, inasmuch as it may have any primary orientation. In a few places, hot springs have obviously been localized by faults, but there is little sign of hot-spring activity along many of the large faults.

Faults are shown in Plate 1 only where there is both stratigraphic and physiographic evidence for their existence. Some of the minor faults shown in Plate 6 are expressed only as scarps.

Faults Older Than the Plateau Flows

The largest faults cut the Yellowstone tuff but are older than the Plateau flows. These faults depressed the central part of the plateau; the depression has been in large part filled by the Plateau flows. It is open to the west and southwest and is bordered along the rest of its circumference by isolated blocks and highlands capped with Yellowstone tuff. These highlands generally present abrupt but irregular scarps to the fronts of the Plateau flows.

The largest scarps are on the northern and eastern faces of the Red Mountains (Pl. 1). The Red Mountains form a roughly rectangular block tilted southwest. Small erosion remnants of Yellowstone tuff lie on the crest of the range, 2000 feet above the tuff at its base.

Flat Mountain, 2 miles northeast of the Red Mountains, is also tilted to the southwest. Jackson flows form the core of Flat Mountain and are exposed at its northern end. Yellowstone tuff mantles the Jackson flows and dips southwest beneath a tongue of Plateau flows which has flowed south between the Red Mountains and Flat Mountain.

Along the eastern side of Yellowstone Lake, the rhyolite plateau is bordered by spurs of the Absaroka Range. These spurs are made up in the main of early Tertiary, andesitic volcanic rocks. Erosion remnants of Yellowstone tuff crop out along the eastern side of the lake. The Plateau flows, which form the high tableland west of the lake, are not found along its eastern side. The Lake has formed in a depression between the front of the Plateau flows on the west and the Absaroka Range on the east.

Northeast of the lake, a block comprising Stonetop Mountain and a series of long ridges trending northwest extends out into the basin and has been enveloped on three sides by the Plateau flows. This block has been broken into a series of cuestas which dip to the southwest. The block is predominantly Yellowstone tuff, but Stonetop Mountain itself is pumice breccia.

The Canyon flow, a member of the Plateau flows, has flowed around the northern flank of this block as far as Broad Creek. At Broad Creek, the Canyon flow abuts against a scarp which forms the border of the Mirror Plateau. A thick mantle of glacial debris on the Mirror Plateau has prevented working out the nature and structure of the rhyolite; outcrops of Yellowstone tuff and of Jackson flows are present on the plateau. This area is shown as undifferentiated rhyolite in Plate 1. The scarp bordering the Mirror Plateau is met by a spur of the Washburn Range at Josephs Coat Springs. The Yellowstone River has cut through this spur. From Josephs Coat Springs west to Grebe Lake, the Plateau flows abut against andesitic volcanic rocks in the southern flank of the Washburn Range.

From Grebe Lake west to the Norris Geyser Basin, and thence south and west along the Gibbon and Madison rivers, the Plateau flows are in contact with the Yellowstone tuff and Jackson flows. This contact has been mapped in detail between the mouth of the Madison Canyon and the Norris Geyser Basin (Pl. 6).

The Yellowstone tuff and Jackson flows crop out along this contact in a fault scarp. Subsidiary faults have scalloped the main scarp east of Madison Junction (Pl. 6). At Madison Junction, the main scarp, forming the north wall of the Madison Canyon, rises 1700 feet above the level of the river. The Madison and Gibbon rivers have eroded the depression between the scarp and the fronts of several Plateau flows which have flowed against it. The southeast corner of the fault block bounded by this scarp has been dropped relative to the main block along a subsidiary fault in Secret Valley. Both the displacement of the contact between the Purple Mountain pumice breccia and the Yellowstone tuff and the height of the fault scarp suggest that the throw along the Secret Valley fault is in the range of 600 to 800 feet. The block dropped along the Secret Valley fault is itself scalloped by a small fault (Pl. 6). The Yellowstone tuff in the north wall of the Madison Canyon, and in the scarp rising above Secret Valley, dips 10° to 15° north. Near the Secret Valley fault line, local dips are as high as 75°. Outcrops of Yellowstone tuff northeast of Gibbons Falls are slickensided where the Secret Valley fault intersects the main scarp.

The contact between the Plateau flows and older rhyolites follows the Madison River west as far as Mt. Haynes. At Mt. Haynes this contact swings south and then west to Reas Pass, a few miles west of the Yellowstone Park boundary. At Reas Pass the advance of the flows has been checked by an eastern spur of the Henry Mountains.

The position of the western margin of the Plateau flows has been located by reconnaissance. The front winds southward, nowhere more than about 8 miles west of the Yellowstone Park boundary, to a point east of Gerrit, Idaho, where it swings east into Yellowstone Park, along the north side of the Falls River basin.

From Reas Pass to Gerrit, the Plateau flows have come to rest in open country consisting of alluvial flats or low ridges of Yellowstone tuff. Their front can be seen from the main highway south of Henry's Lake and can be reached by a number of secondary and logging roads between Big Springs and Gerrit.

The front of the Plateau flows trends east from the Falls River basin. Here the flows have been emplaced on an erosion surface cut in Yellowstone tuff and Jackson flows. From

Beula Lake the flow margins swing north to the western flank of the Red Mountains.

In summary, that portion of Yellowstone Park now covered by the Plateau flows was a basin prior to the eruption of these lavas. This basin was bordered by highlands of Yellowstone tuff and older volcanic rocks along its northern, eastern, and southeastern margins. It was open to the west and southwest. The basin is bounded by fault scarps along a portion of its circumference.

Faults Younger Than the Plateau Flows

A second period of block faulting took place after the eruption of the Plateau flows. Few of the fault scarps which cut the Plateau flows are more than a few hundred feet high, and few can be traced for more than a couple of miles. No regularity in trend of these faults was found.

The surface of the Plateau flows is broken by innumerable scarps of many sizes and orientations. Distinguishing those of fault origin from those marking the fronts of flows is difficult. No criteria which could be applied in the field were found to be of consistent value. Study of aerial photographs of the Plateau flows permits a distinction to be made in a few cases. Scarps of serpentine outline which are parallel to the major banding in a flow clearly mark the fronts of flows. Scarps which crosscut the major banding, or groups of markedly linear and parallel scarps, are probably faults. Figure 1 of Plate 3 shows faults which cut the Plateau flows west of Shoshone Lake. The group of small fault scarps (Pl. 3, fig. 1) at the west end of Shoshone Lake strikes directly into the Shoshone Lake Geyser Basin. The larger scarp which crosses this photograph from north to south is probably a flow front.

Origin of the Faulting

Large volcanic areas are characterized by calderas or volcano-tectonic depressions (Williams, 1941). Most of these are probably caused by collapse of the roofs of magma chambers after the eruption of large bodies of lava. Two rhyolite areas comparable to Yellowstone in size possess such depressions. These are the Taupo-Rotorua area in New Zealand (Williams, 1941, p. 315) and the Lake Toba area in Sumatra (Van Bemmelen, 1949, p. 690). Van Bemmelen has emphasized the genetic relationship between the formation of the Lake Toba "cauldron" and the eruption of an enormous volume of welded rhyolite tuff.

The tectonic basin in south-central and southwestern Yellowstone Park doubtless has a similar origin. It is not certain, however, whether the formation of the basin is related to the eruption of the Yellowstone tuff which crops out around the periphery of the basin or to the eruption of the Plateau flows which now fill the basin. It is reasonable to suppose that the collapse of the basin followed the eruption of the Yellowstone tuff. It is, nevertheless, conceivable that the formation of the basin proceeded simultaneously with the eruption of the Plateau flows, that is, that flows collapsed the roofs of their magma chamber(s) as they moved out from centrally located vents.

If the basin's formation is related to the eruption of the Yellowstone tuff, as seems most probable, then the eruption of the Plateau flows has produced no comparable local subsidence. The surfaces of the Plateau flows are broken by fault scarps, but these are of minor dimensions. Possibly the magma chambers which supplied the Plateau flows were located deep in the crust, and the collapse of their roofs has produced a regional subsidence rather than a well-delineated, tectonic basin.

MECHANISM OF ERUPTION OF THE YELLOWSTONE TUFF

General Statement

Three eruptive mechanisms have been proposed for welded tuffs. These are the tuff-flow or pyroclastic-flow mechanism, the froth flow, and an ash fall with the heat to produce welding assumed to come from a source other than the initial heat of the magma.

The pyroclastic-flow mechanism is a concept developed primarily from observations of *nuées ardentes* and from reconstruction of the tuff eruption in the Valley of Ten Thousand Smokes (Fenner, 1923). Proponents (Marshall, 1935, p. 14; Gilbert, 1938, p. 1851) believe that a welded tuff is emplaced as an avalanche of fine particles of viscous melt which are at high temperature and exsolve gas. The avalanche is believed to move dominantly under the influence of gravity. Such an avalanche, inflated by gas, would be fluid, and its emplacement would be rapid. On coming to rest, the avalanche deposit would compact; it is supposed that the finely comminuted fragments of melt would retain sufficient heat to deform and weld.

Incandescent pyroclastic flows of various types have been observed in Martinique (Per-

ret, 1937), Japan (Kozu, 1934), and Java (Van Bemmelen, 1949, p. 199–200). The existence of this type of eruption is well established. Nevertheless, the deposits of historic pyroclastic flows are not welded.

Kennedy (1954, p. 495; Personal communications) has proposed that the welded tuff in Yellowstone has formed from "collapsed froth flows" rather than from pyroclastic flows ("*nuées ardentes*"). Kennedy pictured the erupting magma moving as an expanded lava froth rather than as an avalanche.

Mansfield and Ross (1935, p. 309) have concluded that the welded tuffs in southeastern Idaho were "sprayed or Ducoed" over an erosion surface with a relief of 3000 feet. They found that the thickness of the tuff was uniform and independent of the underlying topography. These relationships seemed to them to be inconsistent with the pyroclastic-flow mechanism. They have argued that the eruptions of the Idaho tuffs were more explosive, *i.e.*, that the constituents of the tuff were blown into the air and settled out in a manner similar to the emplacement of the classic variety of tuff. Volcanic ash could not, in such circumstances, land at a high enough temperature to weld. Hence, Mansfield and Ross (1935, p. 312) have suggested that the heat was supplied by exothermic gas reactions.

Field Evidence

The texture and structure of the Yellowstone tuff support the interpretation that it was emplaced in a sequence of pyroclastic flows. Air- or water-borne tuffs characteristically show lamination, except in the immediate vicinity of their vents; textures of pyroclastic flows are either completely chaotic or show a crude lamination in the form of lenticular patches of coarse fragments produced by locally laminar flow in the avalanches during emplacement (Kuno, 1941, p. 147; Fenner, 1923, p. 35). In the Yellowstone tuff the size of the fragments ranges from a few tenths of a millimeter for the glass shards to about 10 cm for the larger inclusions. Yet over an area of thousands of square miles and in sections up to 1000 feet thick there is typically no localization of phenocrysts or inclusions in layers. Rare exceptions to this generalization are crude bands similar to those in historic pyroclastic flows.

If a welded tuff has been emplaced as an avalanche its thickness should depend on the topography on which it was erupted. The primary surface of the tuff should be approximately a plane, and the tuff should thin, or pinch out, over ridges and hills on the underlying topography.

In Yellowstone the welded tuff has been extensively eroded and faulted, and it is rarely possible to demonstrate a dependence of thickness on underlying topography. Exposed sections of the tuff range from a few tens of feet to a thousand feet thick. The present surface is in many places a plateau, and in some areas there is a large amount of local relief on the underlying surface. However, the present surface is in most places an erosion surface developed on the indurated central portion of the tuff. Probably several hundred feet of soft tuff and unconsolidated ash have been removed by erosion over most of the outcrop area.

In the north wall of the Madison Canyon the flat, primary surface of a welded pumice breccia has been preserved (Pl. 6). The welded pumice breccia was deposited on an erosion surface with a local relief of 1200 feet. The pumice breccia is 1000 feet thick in the vicinity of Madison Junction but pinches out against the flank of a mountain which it partially buried. The Madison Canyon exposure has been described in more detail in the section on the structure of the Yellowstone tuff. It is the only exposure found in Yellowstone where the relationship between the thickness of a welded tuff or pumice breccia and the underlying topography can be seen clearly.

The wide variation in thickness of sections of the Yellowstone tuff is not in accord with the field relationships of the similar tuff in southeastern Idaho reported by Mansfield and Ross (1935). It is noteworthy that the 20-foot section from the Ammon quadrangle described by them is similar to the base of the tuff in many exposures in Yellowstone Park. Possibly the welded tuff in Idaho has been extensively eroded and only the densely welded base has been preserved. Faulting subsequent to emplacement might account for some of the range in elevation of outcrops of the tuff in Idaho.

Pyroclastic Flows or Froth Flows

There is possibly a gradational eruptive sequence from lava flows, with little exsolving gas, through froth flows (Kennedy, 1954, p. 495), to pyroclastic flows in which the gas pressure is sufficient to rupture the magma.

Evidence in Yellowstone indicates that this sequence is real. The present author has sug-

gested that the Canyon flow, which has characteristics of both a flow and a welded tuff, may have been emplaced as a froth flow. Nevertheless, the magma was fragmented in the course of eruption of the Yellowstone tuff. This is evident in the upper part of a section where the tuff is soft or unconsolidated. Thin sections of densely welded tuff also show textures which suggest rupture prior to welding (Pl. 5, fig. 1). It therefore appears probable that the Yellowstone tuff is the product of avalanches rather than froth flows.

Thermodynamic Considerations

Statement of problem. Field evidence supports the pyroclastic-flow mechanism of eruption for the Yellowstone tuff. Inasmuch as incandescent pyroclastic flows have been observed in historic eruptions, the major assumption involved in extrapolating this mechanism to welded tuffs is the assumption that such flows can have temperatures of emplacement high enough to permit them to weld. A combination of experiment and thermodynamic argument shows that this assumption is reasonable.

It is first necessary to estimate the permissible cooling. The permissible cooling is defined as the difference between the initial magma temperature and the minimum temperature at which welding will take place.

Magma temperature. Recent work by Tuttle and Bowen (1958) on the system $NaAlSi_3O_8$-$KAlSi_3O_8$-SiO_2-H_2O has provided information about the temperatures of rhyolitic magmas. Figure 8 shows the temperature of the minimum in this system as a function of H_2O in solution in the melt.

The compositions of most rhyolites group closely around the composition of this minimum. In Figure 7 all the analyses of Yellowstone rhyolites are plotted on a diagram of this system. The welded tuffs show small deviations from the minimum. But, inasmuch as these welded tuffs invariably contain phenocrysts of quartz together with two feldspars, the composition of the melt fraction of the Yellowstone tuff magma must have corresponded closely to the composition of the minimum.

Thus the curve in Figure 8 gives to a good approximation the temperature at the time of eruption of the Yellowstone tuff magma as a function of the H_2O in solution in the melt.

Experimental determination of welding temperature. The minimum temperature at which fragments of rhyolite glass will weld has been determined by experiment. This temperature is a function of pressure, time, and the H_2O content of the glass.

The pressure under natural conditions will be that exerted by the mass of the overlying tuff. Pressure promotes welding by deforming the shards and increasing the area of contact between them. The time during which the materials of a tuff are maintained at high temperature will be a factor, since the welding of hot glass fragments is a diffusive process. The viscosity of the glass is reduced by H_2O so that it deforms more easily.

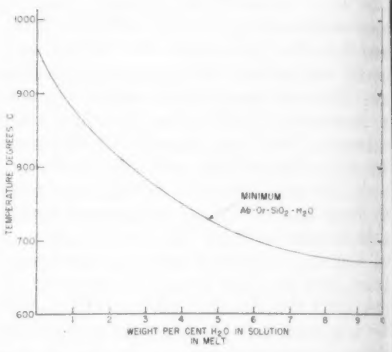

Figure 8. Temperature of the minimum in the system Ab-Or-SiO_2-H_2O as a function of H_2O dissolved in the melt. Data from Tuttle and Bowen (1958)

The pressure present during the welding of a tuff under natural conditions and the H_2O content of the tuff can easily be duplicated in the laboratory. The time available under natural conditions will be longer than the convenient length of laboratory runs (2 weeks). Nevertheless, only a small reduction in minimum welding temperature was observed when runs were lengthened from 3½ days to 2 weeks. It is unlikely that a further increase in the length of runs would produce a large decrease in the observed minimum welding temperature.

The H_2O content of the samples of tuff used in the experiments described hereafter requires explanation. The H_2O contents of a number of welded-tuff glasses have been determined by ignition (Table 7). These glasses fall into two groups. One, samples of which are by a large factor the most abundant in Yellowstone, has from 2 to 3 per cent loss of weight on ignition

at 1200° C.; the other, examples of which are rare, has a loss of weight on ignition of only a few tenths of 1 per cent. The samples falling into the group with 2–3 per cent H_2O are all either relatively porous, welded ash from beneath the Yellowstone tuff or samples of the black, glassy base of the tuff which have a perlitic texture. The perlitic cracking is on a minute scale, and the glasses are quite friable. The three specimens which showed a weight loss of only 0.1–0.2 per cent, on the other hand, are all dense obsidians with no perlitic cracking.

Most of the H_2O is believed to be of meteoric origin in the specimens which contain 2–3 per cent H_2O. The evidence for this belief lies in the rate at which H_2O will diffuse out of such glasses and in the fact that they will absorb H_2O at relatively low temperatures and vapor pressures. Ross and Smith (1955) and Ross, Friedman, and Smith (1955) have reached this same conclusion with respect to H_2O-rich perlite glasses from different evidence.

The rate at which H_2O can be driven off from glasses containing 2–3 per cent H_2O is fast at high temperature. Table 8 presents dehydration data for a specimen of welded-tuff glass from Mt. Everts. When heated at 1200°C. for several hours this glass lost 2.26 per cent of its weight. However, the glass lost most of its H_2O in a few hours at 325° C. and all of it in a few minutes at 800° C. (Table 8).

If a welded tuff erupts as a tuff avalanche in the temperature range of 600° to 900° C., most of the H_2O remaining in the fine particles of glass after vesiculation will diffuse out in a few minutes. Water will remain in the glass only in response to the pressure exerted by water vapor trapped in the moving tuff flow. The pressure of trapped water vapor can be no more than a value on the order of 30 bars (pressure at the base of a bed of tuff 500 feet thick with a mean specific gravity of 2.0). Extrapolation from the data of Goranson (1938, p. 77) indicates this pressure would be in equilibrium with a water concentration in the glass of about 0.4 per cent.

The dense welded-tuff glasses have H_2O contents on the order of 0.4 per cent (Table 7). Meteoric water has not had access to these glasses because of their lack of cracks or primary pores. For the welding experiments described hereafter in which H_2O was present in the glass, H_2O contents of about 0.4 per cent were used.

Table 7. Loss of Weight on Ignition at 1200° C. of Welded-tuff Glasses from Yellowstone Park and Vicinity

Sample	Description	Locality	Per Cent Loss Weight
Yp-51-238	Welded ash*	Gardiner Canyon	3.05
YP-51-136	Welded ash*	Yellowstone Canyon	2.80
YP-51-67	Welded ash*	Mt. Everts	2.77
YP-52-104	Welded ash*	Lewis Canyon	2.55
YP-51-237	Welded tuff	Gardiner Canyon	3.20
YP-51-150	Welded tuff	Antelope Creek	2.50
YP-51-68	Welded tuff	Mt. Everts	2.26
YP-51-334	Welded tuff	Grassy Lake	0.10
YP-53-124	Welded tuff	Henry's Lake Mts.	0.20
YP-53-110	Welded tuff	Centennial Range	0.07

*Collected from the zone a few inches below the base of the Yellowstone tuff

Loose rhyolite ash from beneath the Yellowstone tuff on Mt. Everts was chosen for starting material in the welding runs. This ash contains the same phenocrysts as the Yellowstone tuff, together with glass shards and fragments of pumice. The ash was sieved and a 100–200 mesh fraction saved. This fraction was rich in phenocrysts, most of which were removed with bromoform; the final fraction contained more than 95 per cent glass.

On ignition at 1200° C. this fraction was found to contain 2.72 per cent H_2O. One portion was completely dehydrated, and other portions dehydrated until about 0.4 per cent H_2O remained in the glass. These portions were used as starting materials.

The technique used in making welding-temperature runs was similar to that employed in hydrothermal investigations. Small samples (0.2 gm) of the ash were sealed in platinum capsules. The capsules were made from short lengths of seamless tubing with ends crimped and sealed by electric welding. The capsules

containing ash, in some cases with dissolved H_2O in the glass, were then placed in cold-seal bombs. Argon, at the desired pressure, was introduced into the bombs through steel capillary tubing. During the run a platinum capsule acts as a bellows transmitting the pressure exerted by the argon outside the capsule to the sample on the inside. The bombs were heated by electrical resistance furnaces. Temperature was controlled by variacs on a regulated AC line and measured by chromel-alumel thermocouples placed in wells in the bases of the bombs.

Table 8. Dehydration of Welded-tuff Glass from Mt. Everts, Yellowstone Park
Specimen YP-51-68

Temperature (°C.)*	Time (Hours)	Per Cent Loss Weight
110	24	0.21
325	1.25	1.56
325	16	1.93
325	68	2.08
800	0.2	2.32
1200	1	2.26

*A fresh sample was used at each temperature.

Table 9 gives the data obtained in these runs. Those runs listed as densely welded were reduced to a slug of obsidian similar to the black glass of the base of the Yellowstone tuff. Runs made a few tens of degrees above the minimum welding temperature were not so densely welded. These runs were brown, rather than black, and were more porous. They greatly resembled the glass from the welded ash beneath the Yellowstone tuff.

Thin sections cut from artificially welded glass reveal textures similar in many ways to those found in natural welded tuff. The borders of the individual shards in the runs listed in Table 9 are, however, not well delineated and proved impossible to photograph. This is also true of some natural welded tuffs in Yellowstone, although others have a coating of opaque dust on the surfaces of the shards and their outlines are easily seen (Pl. 5, figs. 1, 2). To better show the texture obtained in artificially welded glass, a run was made in which the ash used as starting material was dusted with "platinum black". The finely divided platinum coated the surfaces of the fragments of glass and made their outlines clearly discernible after welding (Pl. 5, fig. 4). There are several differences from natural welded tuffs. Cusp-shaped fragments are sparse in the run owing to the nature of the ash used as starting material. Although cusp-shaped shards are present in the Mt. Everts ash, their grain size is generally coarser than the sieved fraction used in these runs. Also the individual fragments in the artificially welded glass do not show as much distortion as shards in natural welded tuff. This is because the pressure on the run was hydrostatic, whereas natural welded tuffs form under a gravitational load.

For runs of about 80 hours, 52 bars pressure, and 0.45 per cent H_2O in the glass, the minimum welding temperature lies between 590°C. and 620°C. Increasing the time to more than 2 weeks reduces the welding temperature to between 550°C. and 590°C. For the dehydrated ash the welding temperature is somewhat higher. A run at 48 bars and 72 hours showed slight welding at 690°C.; a run at 655°C. showed no welding. Reducing the pressure from 52 bars to 28 bars increases the welding temperature of glass with 0.45 per cent H_2O to about 650°C.

These data suggest that the minimum temperature at which welded tuffs can form is on the order of 600°C.[2]

Table 9. Welding Runs on Mt. Everts Ash

Temperature (°C.)	Time (Hours)	Pressure (Bars)	H_2O Content (Weight Per Cent)	Results
755	72	52	0.35	Densely welded
685	72	52	0.35	Densely welded
640	72	52	0.45	Welded
620	85	52	0.45	Welded
590	84	52	0.45	Not welded
590	430	52	0.45	Welded
550	360	52	0.45	Not welded
675	74	28	0.45	Welded
640	70	28	0.45	Slight welding
740	70	48	0.00	Welded
690	72	48	0.00	Slight welding
655	74	48	0.00	Not welded

Permissible cooling. The data described

[2] Previous data (Boyd and Kennedy, 1951) obtained for crushed pumice with a piston and cylinder apparatus indicated a minimum welding temperature for dry rhyolite glass of about 800°C. This figure is 100° higher than that indicated by the runs on dry glass in Table 9. The discrepancy is believed due to oxidation of the piston and retaining ring so that a large friction developed and the load on the piston was not fully communicated to the sample.

heretofore indicate that the difference between the initial magma temperature (Fig. 8) and the minimum welding temperature will be in the range 50°–350°C., depending on the initial H_2O content of the magma. For an eruptive model to be reasonable, the total cooling must lie within the range set for its initial H_2O content.

Heat losses during emplacement. There are three principal sources of heat loss during the emplacement of pyroclastic flow: (1) radiation, (2) conduction to the ground, (3) conduction and convection to the atmosphere. The amount of heat dissipated in these ways will depend on a number of factors, of which the most important are the degree of turbulence in the moving flow, the time elapsed during emplacement, and the thickness of the flow.

The time involved in the emplacement of a pyroclastic flow can be estimated from the data available on *nuées ardentes*. During the 1929 eruption of Mt. Pelée, the largest *nuée ardente* erupted had an average velocity approaching 80 m. p. h. (Perret, 1937, p. 96). Smaller *nuées ardentes* commonly had velocities of 20–40 m. p. h. Since gravity is the dominant force behind a pyroclastic flow, the speed a flow attains will be a function of the slope down which it moves. The Yellowstone tuff is probably the product of fissure eruptions. The slopes on which the pyroclastic flows were emplaced and, hence, their velocities must have been less than those recorded for *nuées ardentes*. A velocity on the order of 10 m. p. h. is assumed for the pyroclastic flows in Yellowstone; the time elapsed during emplacement is taken to be in the range of 1 to 10 hours.

The thickness of many sections of Yellowstone tuff ranges from 100 to 1000 feet. In most places the upper surface of these sections is eroded, and the original thicknesses must have been greater. A few sections show evidence of being composed of several units. The heat lost during emplacement of a pyroclastic flow is inversely proportional to its thickness. To maximize the calculated cooling it is assumed that the individual pyroclastic flows were 100 feet (30 m.) thick.

Under static conditions the amount of heat that could be conducted or radiated from the surfaces of a mass of inflated ash 100–1000 feet thick in 1–10 hours would have a negligible effect on the temperature of the interior portion. Only the material within a few feet of the upper and lower surfaces would cool significantly. If the flow was laminar, then the loss of heat would still be insignificant. If, however, there was turbulence within a moving flow, then the heat lost in any interval of time would be greater, since hot material would be constantly supplied to the surfaces.

The unsorted texture of the Yellowstone tuff suggests that the flows which deposited it moved principally by turbulent flow. In the analysis which follows, it will be assumed that turbulence during emplacement was so effective that the temperature at any point in a moving flow was a function only of the time elapsed since extrusion and not of vertical position in the flow, *i. e.*, that, at any instant during emplacement, any vertical section of a flow was at a constant temperature from top to bottom. The assumption is only a rough approximation, but it will ensure a maximum estimate of the heat loss.

RADIATION: The heat lost by radiation from the upper surface of the moving pyroclastic flow may be approximately evaluated by use of the familiar Stefan-Boltzmann equation for black-body radiation,

$$Q/t = \sigma T^4$$

where Q = total energy radiated per cm^2; T = absolute temperature; t = time; and σ = a constant having the value 5.67×10^{-5} ergs $sec^{-1}cm^{-2}\ deg^{-4}$.

If the average temperature of the flow is taken as 850° C., Q is found to be 7750 cal per hour per cm^2 of surface. If the average specific gravity is taken as 2.0 for the collapsed tuff, a vertical column 1 cm^2 in cross section through a welded tuff 30 m thick would contain 6×10^3 gms of tuff. Hence, the heat lost per gram of tuff is 1.3 calories per hour. This is sufficient to cool the tuff by about 4° C. per hour.

HEAT CONDUCTED TO THE GROUND: The model set up corresponds to a semi-infinite solid (*i. e.*, the ground) with one plane bounding face held at an approximately constant high temperature. An expression for the heat conducted across such a boundary is given by Ingersoll, Zobel, and Ingersoll (1948, p. 91) as:

$$Q = \frac{2K(T_s - T_o)}{\sqrt{\pi\alpha}} \sqrt{t}$$

where Q = total heat flow across the boundary per unit area, in time t; K = conductivity; α = diffusivity; Ts = temperature of surface; and To = initial temperature of the ground.

Inasmuch as the Yellowstone tuff has been emplaced in most places on 5–10 feet of rhyo-

lite ash, values of conductivity and diffusivity appropriate to such material are chosen.

Let:

$K = 2 \times 10^{-3}$ cal sec^{-1}cm^{-1} deg^{-1}
$\alpha = 5 \times 10^{-3}$ cm^2 sec^{-1}
$T_s = 850°$ C.
$T_o = 0°$ C.
$t = 3.6 \times 10^3$ sec.

Hence, $K = 1600$ cal per cm^2 for the first hour, or 0.27 cal per gm of tuff, an amount sufficient to cool the tuff about 1°. Inasmuch as the heat conducted to the underlying ash is proportional to the square root of the time, the heat loss for 10 hours would be only a little more than three times this value.

CONDUCTION AND CONVECTION TO THE ATMOSPHERE: Analogy with *nuées ardentes* indicates that the upper surface of a moving pyroclastic flow would be mantled by a hot cloud of escaping gas and dust. Such a cloud would act to prevent the upper surface of the flow from coming into contact with air.

There may, nevertheless, be some cooling by contact with the air. To evaluate this effect, it will be assumed that the cloud is absent and that the upper surface of the moving flow is in contact with a stream of cold air.

The mechanism of heat transfer under these circumstances is a combination of conduction across a relatively thin film of fluid at the hot surface and convection in the outlying fluid. The general equation covering the transfer of heat in this manner is (Zemansky, 1951, p. 93):

$$dQ/dt = hA\Delta T$$

where dQ/dt = rate of heat transfer; A = area of the surface; ΔT = difference in temperature between the surface and the circulating fluid; and h = convection coefficient.

The convection coefficient, h, must be evaluated for the particular conditions of the model.

It is assumed in the present case that the flow of air near the surface is turbulent. For the turbulent movement of air across a plane surface, the convection coefficient is (Jakob and Dow, 1946, p. 123):

$$\frac{hL}{K} = 0.025\frac{(VL)^{0.8}}{(\gamma)}$$

where h = convection coefficient; L = distance from the leading edge of the hot surface; K = conductivity of the fluid; V = velocity of the fluid; and γ = kinematic viscosity of the fluid.

Let:

$K_{air} = 6 \times 10^{-5}$ cal sec^{-1} cm^{-1} deg^{-1}
$\gamma_{air} = 0.15$ cm^2 sec^{-1} (10 m. p. h.)
L = a value ranging up to 10 km.

The dependence of h on L is not great, and variation of L from 1 m to 10 km yields a range of values for h of 3.6×10^{-4} to $5.7 \times 10^{-}$ cal sec^{-1} deg^{-1}.

If a value of 1×10^{-4} cal sec^{-1} deg^{-1} is substituted for h in the general convection equation and ΔT is taken as 850°, dQ/dt is found to be 0.08 cal sec^{-1} cm^{-2}, or 0.05 cal per gm of tuff per hour, a negligible quantity.

TOTAL HEAT LOSS DURING EMPLACEMENT: If the various heat losses described are summed, the total heat loss is 1.6 cal per gm for 1 hour and 14.4 cal per gm for 10 hours. The cooling of the tuff (specific heat = 0.3 cal deg^{-1} would then be approximately 5° per hour. It is apparent that the pyroclastic flow is a thermally efficient mechanism of emplacement. The calculated cooling is not dependent on the initial H_2O content of the magma but is within the permissible range for any initial H_2O concentration up to about 10 per cent.

Energy changes within the conduit. In a magma erupting to the surface, energy changes take place as a result of:

(1) Conduction of heat to the conduit walls. The magnitude of the heat lost in this way will depend on the shape and dimensions of the conduit and the length of time of the eruption. No data are available on the principal conduits through which the Yellowstone tuff was erupted. If these were fissures, as seems probable, the heat lost by conduction to their walls would have been of the same order of magnitude as the heat conducted to the ground during emplacement of the tuff. Since this quantity has been shown to be very small, the eruption within the conduit will be assumed to have been adiabatic in the calculations which follow.

(2) Work done by the magma on its surroundings. This will include work done in opening the conduit and the work of breaking off and carrying up fragments of country rock. If the eruption is initiated by an explosion, energy will be communicated to the surroundings in the form of shock waves.

(3) Work done on the magma. Work is done when the magma moves from the depth at which the eruption starts to the surface. This work may be supplied by the magma by expansion of the gas phase.

Part or all of the gravitational work can, however, be supplied by collapse of the roof of the magma chamber. If the density of the magma is less than that of the country rock, then all the work of eruption can be provided in such fashion. Work may also be done on the magma by orogenic forces. All the work of eruption of a dry lava flow must be supplied in these ways, and they may also play an important part in the eruption of a volatile-rich magma.

(4) Heat of exsolution of the gas phase. The exsolution of H_2O from a silicate melt is endothermic. The energy involved is not large at high H_2O pressures but may become important at low H_2O pressures.

(5) Energy of vesiculation. The surface area of a magma is greatly increased by vesiculation. Nevertheless, because of the small surface energy of a silicate melt, the cooling of the magma due to the formation of this surface is negligible.

(6) Heat of crystallization. If a portion of the magma crystallizes during eruption, account must be taken of the heat of crystallization. Crystallization might be induced by loss of volatile components, and it would be expected to produce overgrowths on existing phenocrysts or new crystals of groundmass dimensions. The chilled base of the Yellowstone tuff shows that the groundmass did not crystallize during eruption, and overgrowths are not present on phenocrysts in the glassy tuffs. This term is, therefore, not important in the case of the eruption of the Yellowstone tuff.

(7) Heat of oxidation of the gas and melt. These effects have been discussed by Graton (1945) and Kennedy (1948). Graton (1945, p. 184–202) has shown that combustion of the gases given off at Halemaumau could not significantly heat the remaining lava. Kennedy (1948, p. 539) has contrasted the heat of oxidation of the ferrous iron in a basaltic lava with the rate of radiant heat loss and concluded that the lava cannot be effectively heated in this manner. In the case of a rhyolite with 0.5 to 1.0 per cent FeO, heating by oxidation of the iron must be a negligible factor at any stage of the eruption.

EVALUATION OF WORK TERMS: Graton (1945, p. 135–259) was the first to analyze a volcanic eruption by thermodynamic methods. He evaluated the energy changes in a granitic magma containing 9.4 per cent H_2O at an initial temperature of 1200° C., erupting from a depth of 40 km. He used the equation for the reversible, adiabatic expansion of a perfect gas in the calculation. He assumed that the gas phase expanded adiabatically, cooled, and then equilibrated with the melt. Graton found that the magma would cool 314° by expansion of the gas. He also evaluated a "kinetic cooling" of 98°; this is the amount the magma would cool if heat were transformed into the kinetic energy the magma would have emerging from the vent with a velocity of 500 m per second.

Verhoogen (1946, p. 748) has used a hydrodynamic approach to compute the kinetic energy developed by water vapor expanding in a volcanic conduit. Verhoogen found that the magma would cool 31° as a result of expansion of the gas. Verhoogen's analysis is not equivalent to the calculation made by Graton inasmuch as Verhoogen did not consider the kinetic energy of the melt. If the vesiculated melt and gas are erupted as a unit, the melt will have more than 90 per cent of the total kinetic energy of the system. Graton was, nevertheless, incorrect in considering a kinetic term as well as the cooling produced by the reversible expansion of the magma. If the magma expands reversibly, the maximum possible work will be done, and the maximum cooling produced. If the expansion is irreversible, so that some kinetic energy is developed by the magma, the cooling must be less than in the reversible case.

There is generally insufficient information to directly evaluate the work done in a volcanic eruption. It is difficult to assign meaningful estimates to quantities such as the energy dissipated in shock waves or the amount of work the magma does in opening the conduit. Useful limits on the work done and consequent cooling can, nevertheless, be set by analyzing an idealized eruption which is assumed to be adiabatic and reversible. The idealized eruption is not a good approximation to an actual eruption, but it can provide an estimate of the maximum possible cooling.

The reversible expansion of a system under adiabatic conditions can be described by the relationship:

$$dT = \frac{TV\beta}{C}\,dP$$

where β is the thermal expansion and C is the heat capacity at constant pressure. It is assumed that the expanding magma is composed of water vapor and melt and that during the expansion these phases are in equilibrium at the same temperature and pressure. If X_1 is the

fraction of melt and X_2 is the fraction of gas, the equation can be written:

$$\frac{dT}{T}=\frac{X_1V_1\beta_1+X_2V_2\beta_2}{X_1C_1+X_2C_2}\,dP.$$

Since the heat capacities of the gas and melt are of similar magnitude, and since the term $X_1V_1\beta_1$ can be neglected in proportion to $X_2V_2\beta_2$, the equation can be simplified to:

$$\frac{dT}{T}=\frac{X_2V_2\beta_2}{C_1}\,dP,$$

$$\beta_2=\frac{1}{V_2}\left(\frac{\partial V_2}{\partial T}\right)_P \text{ and for a perfect gas } \left(\frac{\partial V_2}{\partial T}\right)_P = R/P.$$

so that:

$$\frac{dT}{T}=\frac{X_2R}{C_1}\frac{dP}{P}.$$

The fraction of gas, X_2, will vary during the expansion, since gas exsolves from the melt as the pressure is lessened. The relationship between the amount of water in solution in a melt of rhyolite composition and the vapor pressure can be expressed by an equation (Goranson, 1931, p. 493) of the form:

$$y=\frac{P}{a+bP}$$

where y is the weight fraction of water in solution at pressure P, and a and b are constants. These constants are dependent on temperature, but for the purposes of this calculation their temperature dependence can be ignored. At any pressure during the expansion of the magma, the weight fraction of the gas phase can then be expressed as:

$$X_2=Z-\frac{P}{a+bP}$$

where Z is the weight fraction of H_2O in solution in the magma when the expansion starts. At the start of the expansion, $X_2=0$; when the system has expanded to atmospheric pressure, $X_2\approx Z$.

Therefore:

$$\int_T^{T_o}\frac{dT}{T}=\frac{ZR}{C_1}\int_P^{P_0}\frac{dP}{P}-\frac{R}{C_1}\int_P^{P_o}\frac{dP}{a+bP}$$

and

$$\log\frac{T_o}{T}=\frac{ZR}{C_1}\log\frac{P_o}{P}-\frac{R}{C_1b}\log\frac{a+bP_o}{a+bP}.$$

The cooling of a rhyolitic magma by reversible, adiabatic expansion has been evaluated using this equation, and the results are plotted in Figure 9 as a function of the initial H_2O concentration in the melt. It has been assumed that for any initial H_2O concentration, the expansion starts at the particular T_o and P_o of the liquidus for that concentration. In other words, the magma is assumed to be in equilibrium with both vapor and crystals at the start of the expansion. The dependence of liquidus temperature on H_2O concentration and vapor pressure is known from the work of Tuttle and Bowen (1958, p. 58). Some of their data have been reproduced in Figure 8. The heat capacity, C_1, has been taken to be 0.3 cal gm^{-1} deg^{-1}; $a=6.5\times10^3$, and $b=8.0$. The values for a and b have been extrapolated from the data of Goranson (1938, p. 77).

The curve in Figure 9 gives the maximum possible cooling of the magma due to expansion. The cooling is nearly linear with initial H_2O concentration; the average cooling is about 20° C. per per cent H_2O. The condition of reversibility may be approached in relatively quiescent eruptions of water-poor magma. The cooling is probably much less than the calculated amount in violent eruptions of water-rich magma.

EVALUATION OF HEAT OF EVAPORATION OF VAPOR PHASE: Goranson (1931, p. 500) has estimated that the heat of evaporation of water from a melt of granitic composition at 900° and 980 bars is –90 calories per gram H_2O. Goranson did not have sufficient data on granite-H_2O to examine the variation of the heat of evaporation with temperature, pressure, and concentration.

More data were, however, obtained for albite - H_2O. Goranson (1938, p. 81) found a mean value of —170 calories for the heat of evaporation of H_2O from an albite melt over the temperature-pressure range investigated. The present author has recalculated a series of $\Delta H_{vap.}$ values (Fig. 10) using Goranson's data together with more recent P-V-T data on water (Kennedy, 1950). The $\Delta H_{vap.}$ values are for points along the melting curve and are not at constant temperature and pressure. The solubility relations of H_2O in a rhyolitic melt and in an albite melt are very similar, and the results can probably be extrapolated to a rhyolitic magma without serious error.

The heat of evaporation of H_2O from an albite melt was found to range between 100 and 200 calories per gm H_2O in the concentra-

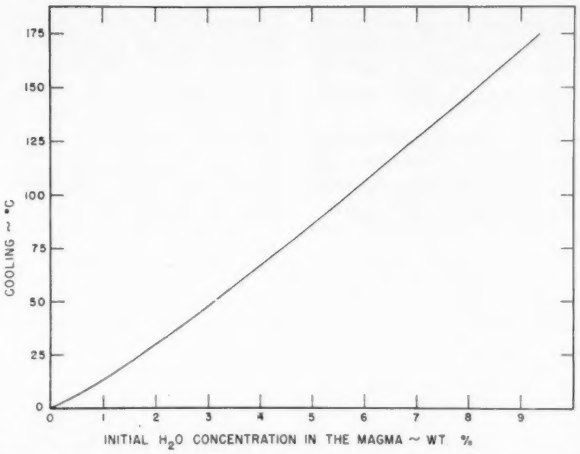

Figure 9. Cooling of a rhyolitic magma by reversible, adiabatic expansion

tion range of 3 to 9 per cent H_2O, in agreement with Goranson's result. However, $\Delta H_{vap.}$ appears to increase rapidly with decrease in H_2O concentration in the concentration range below 3 per cent. Goranson's data must be extrapolated into this concentration range, so that the increase is not of certain existence.

The reversible evaporation of the *last* 3 *per cent* of H_2O from such a melt would cool the melt by about 45° C. if the melt and gas remained in thermal equilibrium and if the apparent increase in $\Delta H_{vap.}$ is real. This cooling would be of the same order as that produced by the expansion of the evaporated H_2O and is, hence, possibly a major effect.

Total cooling during eruption. The three principal cooling effects are: (1) radiation and conduction during emplacement of the pyroclastic flow, (2) cooling by evaporation of the gas, and (3) cooling by expansion of the gas. The first will have a maximum value of about 45° C. for the analyzed model; the magnitudes

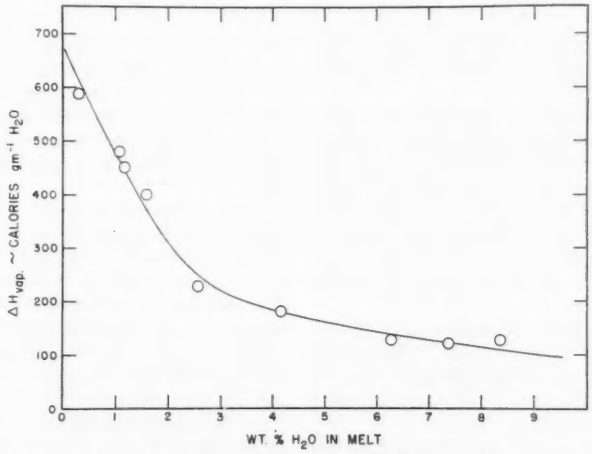

Figure 10. Heat of evaporation of H_2O from an albite melt. Calculated from data of Goranson (1938) for Ab-H_2O compositions along the liquidus

of the other two depend on the initial concentration of H_2O in the magma. The difference between the liquidus temperature and the welding temperature also depends on the concentration of H_2O.

Figure 11 shows the total possible cooling together with the difference between the liquidus temperature and the welding temperature as a function of the initial H_2O content.

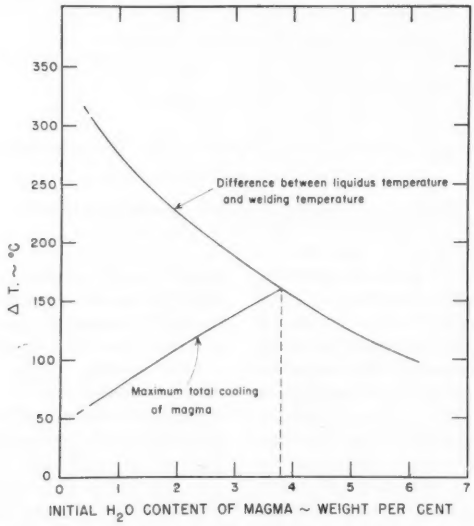

Figure 11. Maximum total cooling of a rhyolitic welded tuff during eruption

In this figure the cooling during emplacement of the tuff is assumed to have the maximum value of 45°.

The curves intersect at approximately 4 per cent H_2O. If the initial concentration of H_2O in the melt is less than about 4 per cent, the maximum possible cooling expressed in degrees will be small enough to permit the tuff to weld. This limitation on the initial H_2O content should not be taken too literally. The calculated cooling is a maximum value; the actual cooling may be less.

Nevertheless, field evidence also suggests a low initial H_2O concentration. Welded tuff magmas appear to have spilled from vents as avalanches; they evidently were not exploded in violent, pyroclastic eruptions.

Problem of the welded ash. Accounting for welding in the laminated ash which underlies the Yellowstone tuff (Fig. 1) is a problem. Commonly the upper part of the bed of ash beneath the tuff is welded to a depth of a few inches to a foot. The welded ash is more fine-grained than the tuff, and the contact is relatively sharp in most places. At a few localities laminations were found in the welded part of the ash. More commonly, the welded layer is massive but grades down into laminated ash. Since the bulk of the ash is laminated, it seems most reasonable to assume that it formed by settling from clouds of volcanic ash and that it was relatively cool at the time the pyroclastic flows that formed the Yellowstone tuff covered it. For welding to take place the temperature of the ash must have been raised to a value above 600°.

Heat conducted to the ash from the Yellowstone tuff after emplacement of the tuff cannot by itself explain the welding of the ash. If heat is conducted from a stationary pyroclastic flow to a bed of cold ash, the maximum temperature reached in the upper part of the ash would be only half the temperature of the flow, or 400°–450° C. Heat conducted to the ash *during* emplacement of the tuff, can, however, account for at least a part of the welding of the ash.

If it is assumed that the temperature of the surface of the ash (T_s) is maintained at the

same temperature as the tuff by turbulent flow in the tuff during emplacement, then the depth of welding in the ash (x) as a function of time (t) can be found from the relationship (Ingersoll, Zobel, and Ingersoll, 1948, p. 89):

$$\frac{T - T_s}{T_o - T_s} = \Phi\left(\frac{x}{2\sqrt{\alpha t}}\right)$$

where T is the welding temperature, and T_o is the initial temperature of the ash. If the following numerical quantities are chosen:

$T_s = 850°$
$T = 600°$
$T_0 = 0°$
$\alpha = 5 \times 10^{-3}$ cm^2 sec^{-1}
$t = 10$ hours,

the depth of welding (x) is found to be 8 cm (~3 inches). However, if the depth of welding is taken to be 30 cm (~1 foot), t would have to be on the order of 150 hours.

One hundred fifty hours seems definitely too long, and either the mode of eruption of the ash has not been correctly interpreted and its initial temperature was high, or a more effective method of heating the ash than conduction must have operated. Possibly the bulk of the ash section was deposited by ash falls but there were locally small eruptions of pyroclastic flows that left deposits of hot ash a few inches to a foot in thickness immediately preceding the principal eruption of Yellowstone tuff. The thin deposits of such pyroclastic flows could not by themselves weld, but under the load of the overlying tuff and with an added increment of heat conducted from the tuff, welding might be induced. It is also possible that the ash was heated by hot gas from the tuff. The ash is relatively porous, and appreciable heat might have been transported by hot gas flowing from the tuff to the ash as the tuff compacted and welded.

Lack of Welding in Historic Pyroclastic Flows

Recent studies of the products of historic pyroclastic flows make it possible to better contrast them with welded tuffs. Hay (1959) has described the deposits of the eruption of the Soufriére of St. Vincent in 1902, and Aramaki (1957) has studied the products of the 1783 eruption of Asama. The absence of welding in historic pyroclastic flows is evidently due to a number of factors. Two important factors are the small size of historic pyroclastic flows and their high degree of crystallinity. Aramaki has compiled data on the volumes of such flows and found the range for those erupted in historic times to be 0.001–10 km^3. The volumes of many welded tuffs are 10–100 times as large. The drop in temperature of a pyroclastic flow during emplacement is related to its thickness; a small flow will lose a greater proportion of its heat by radiation and conduction to the ground than a large one. Size is hence a factor of significance in determining whether welding will take place, and welded tuffs with volumes in the range shown by historic pyroclastic flows are rare.

The proportion of phenocrysts to glass is also important. A high proportion of phenocrysts will reduce the contact between glass shards and hinder welding. Values for the proportion of phenocrysts in a variety of welded tuffs and historic pyroclastic flows are collected in Table 10. The welded tuffs studied have up to 40 per cent phenocrysts, but most have 10 to 20 per cent. The three historic pyroclastic flows have more than 50 per cent phenocrysts.

Exceptions can be found. Williams (1942)

Table 10. Phenocryst Contents of Some Welded Tuffs and Historic Pyroclastic Flows

Rock	Volume Per Cent Phenocrysts
Cognate block, Kambara *Nuée Ardente*, Asama (Aramaki, 1957, p. 14)	65
Komagataké pumice flow* (Kozu and Seto, 1932, p. 384)	51
Nuée Ardente, Rabaka River Valley, St. Vincent† (Hay, 1959, p. 552)	70
Welded tuff, Yellowstone National Park, range	0.1–30
Welded tuff, New Zealand, range 3 specimens	6–40
Welded tuff, Bishop, California, range 3 specimens	12–16

*55.1 weight per cent
†73 weight per cent

has described welded tuffs at Crater Lake whose volumes are small and evidently comparable to the range of historic pyroclastic flows. On the other hand deposits of pyroclastic flows of large volume which are not welded mantle the western flank of the Peruvian Andes. Jenks and Goldich (1956, p. 165) give a mode for one of these tuffs which shows 6 per cent phenocrysts. Hence, other factors such as initial temperature and distance from the vent may be critical in determining whether welding takes place.

Mobility of Pyroclastic Flows

Subsequent to completion of this manuscript, McTaggart (1960) published an interesting discussion of the mobility of *nuées ardentes*. Calculations and field evidence lead McTaggart to doubt that the materials in a *nuée ardente* of the type erupted from Mt. Pelée could have supported themselves in transit by exsolution of gas. Experiments with the flow of dried, andesite sand down an inclined trough show that sand heated to 750° C. is considerably more mobile than cold sand. McTaggart believes that the avalanching sand entraps air; if heated, the trapped air expands and the particles of sand are carried along in an inflated, turbulently flowing mass. In applying the idea to *nuées ardentes*, McTaggart states (p. 381) that ". . . the front part of the mass is constantly fluidized by fresh supplies of air . . ." and that ". . . the rear part, less effectively fluidized, deposits a layer of hot clastic material along the track of the nuée." The large contents of primary crystalline materials in many *nuée ardente* deposits support McTaggart's view that the gas involved was principally trapped air rather than exsolved volatiles.

It seems unlikely that the process advocated by McTaggart for *nuées ardentes* of the Pelée type would be as effective in the eruption of much larger pyroclastic flows, of the sort that have formed the Yellowstone tuff. These flows are believed to have been on the order of hundreds of feet thick and to have extended as continuously flowing masses for tens of miles. Air entrapped at the front of a pyroclastic flow of this size could not effectively fluidize the bulk of the flow. The source of the gas in the large pyroclastic flows does not seem to be a problem, inasmuch as most of them consisted of 80–90 per cent liquid magma at the time of eruption. Entrapment of cold air need not, however, appreciably cool the solid particles in an avalanche. The heating of initially cold air trapped in a flow at 850° C. would cool the flow by approximately 10° per weight per cent of air. Further experiments would be necessary to determine the amount of air that could be trapped by flowing sand, but it seems unlikely that it would exceed a few per cent of the weight of the flow.

REFERENCES CITED

Allen, E. T., and Day, A. L., 1935, Hot springs of the Yellowstone National Park: Carnegie Inst. Wash. Pub. no. 466, 525 p.

Aramaki, S., 1957, The 1783 activity of Asama Volcano. Part II: Japanese Jour. Geol. and Geog., v. 28, p. 11–33

Bowen, N. L., 1935, "Ferrosilite" as a natural mineral: Am. Jour. Sci., v. 30, p. 481–494

—— 1937, Recent high-temperature research on silicates and its significance in igneous geology: Am. Jour. Sci., v. 33, p. 1–21

Bowen, N. L., and Tuttle, O. F., 1950, The system $NaAlSi_3O_8$-$KAlSi_3O_8$-H_2O: Jour. Geology, v. 58, p. 489–511

Boyd, F. R., and Kennedy, G. C., 1951, Some experiments and calculations relating to the origin of welded tuffs (Abstract): Am. Geophys. Union Trans., v. 32, p. 327

Chayes, F., 1952a, The finer-grained calcalkaline granites of New England: Jour. Geology, v. 60, p. 207–254

—— 1952b, Relations between composition and indices of refraction in natural plagioclase: Am. Jour. Sci., Bowen Volume, p. 85–105

Daly, R. A., 1933, Igneous rocks and the depths of the earth: New York, McGraw-Hill Book Co., Inc., 598 p.

Dorf, E., 1939, Middle Eocene flora from the volcanic rocks of the Absaroka Range, Park County, Wyoming (Abstract): Geol. Soc. America Bull., v. 50, p. 1906

Fenner, C. N., 1923, The origin and mode of emplacement of the great tuff deposit of the Valley of Ten Thousand Smokes: Nat. Geog. Soc. Contributed Technical Papers. Katmai series, no. 2, 74 p.

Fenner, C. N., 1934, Hydrothermal metamorphism in the geyser basins of Yellowstone Park, as shown by deep drilling: Am. Geophys. Union Trans., 15th Ann. Mtg., p. 240–243

— 1936, Bore-hole investigations in Yellowstone Park: Jour. Geology, v. 44, p. 225–315

— 1937, Tuffs and other volcanic deposits of Katmai and Yellowstone Park: Am. Geophys. Union Trans., 18th Ann. Mtg., p. 236–239

— 1938, Contact relations between rhyolite and basalt on the Gardiner River, Yellowstone Park: Geol. Soc. America Bull., v. 49, p. 1441–1484

— 1944, Rhyolite-basalt complex. A discussion: Geol. Soc. America Bull., v. 55, p. 1081–1096

— 1948, Incandescent tuff flows in southern Peru: Geol. Soc. America Bull., v. 59, p. 879–893

Gilbert, C. M., 1938, Welded tuff in eastern California: Geol. Soc. America Bull., v. 49, p. 1829–1861

Goranson, R. W., 1931, The solubility of water in granitic magmas: Am. Jour. Sci., v. 22, p. 481–502

— 1938, Phase equilibria in the $NaAlSi_3O_8$-H_2O and $KAlSi_3O_8$-H_2O systems at high temperatures and pressures: Am. Jour. Sci., v. 35-A, p. 71–91

Graton, L. C., 1945, Conjectures regarding volcanic heat: Am. Jour. Sci., v. 243-A, p. 135–259

Hague, A., 1896, Yellowstone National Park Folio, Wyoming: U. S. Geol. Survey, Geol. Atlas Folio (no. 30)

— 1911, Origin of the thermal waters in the Yellowstone National Park: Geol. Soc. America Bull., v. 22, p. 103–122

Hague, A., *et al.*, 1899, Geology of Yellowstone National Park: U. S. Geol. Survey Mon. 32, pt. 2, 789 p.

Hawkes, L., 1945, The Gardiner River rhyolite-basalt complex: Geol. Mag., v. 82, p. 182–184

Hay, R. L., 1959, Glowing avalanche deposits of St. Vincent, B. W. I.: Jour. Geology, v. 67, p. 540–562

Hayden, F. V., 1872, Fifth annual report of the U. S. Geological and Geographical Survey of the Territories for 1871, p. 11–165

— 1873, Sixth annual report of the U. S. Geological and Geographical Survey of the Territories for 1872, p. 12–250

— 1883, Twelfth annual report of the U. S. Geological and Geographical Survey of the Territories for 1878, pt. II, p. 1–488

Hess, H. H., 1949, Chemical composition and optical properties of the common clinopyroxenes, Part 1: Am. Mineralogist, v. 34, p. 621–666

Howard, A. D., 1937, History of the Grand Canyon of the Yellowstone: Geol. Soc. America Special Paper 6, 159 p.

Ingersoll, L. R., Zobel, O. J., and Ingersoll, A. C., 1948, Heat conduction: New York, McGraw-Hill Book Co., Inc., 278 p.

Jakob, M., and Dow, W. M., 1946, Heat transfer from a cylindrical surface to air in parallel flow: Am. Soc. Mech. Engineers Trans., v. 68, p. 123

Jenks, W. F., and Goldich, S. S., 1956, Rhyolite tuff flows in southern Peru: Jour. Geology, v. 64, p. 156–172

Kennedy, G. C., 1948, Equilibrium between volatiles and iron oxides in igneous rocks: Am. Jour. Sci., v. 246, p. 529–549

— 1950, Pressure-volume-temperature relations in water at elevated temperatures and pressures: Am. Jour. Sci., v. 248, p. 540–564

— 1954, Some aspects of the role of water in rock melts, p. 489–503 *in* Poldervaart, Arie, *Editor*, Crust of the earth: Geol. Soc. America Special Paper 62, 762 p.

Kozu, S., 1934, The great activity of Komagataké in 1929: Tscher. Min. Pet. Mitt., v. 45, p. 133–174

Kozu, S., and Seto, K., 1932, Petrological properties of the Komagataké magma: Proc. Imperial Academy (Japan), v. 8, no. 8, p. 383–386

Kuno, H., 1941, Characteristics of deposits formed by pumice flows and those by ejected pumice: Earthquake Research Inst. Bull., v. 19, pt. 1, p. 144–149

Love, J. D., 1956a, Cretaceous and Tertiary stratigraphy of the Jackson Hole area, northwestern Wyoming: Wyo. Geol. Assoc., Eleventh Ann. Field Conf., Jackson Hole Guidebook, p. 76–94

— 1956b, Summary of geologic history of Teton County, Wyoming, during Late Cretaceous, Tertiary and Quaternary times: Wyo. Geol. Assoc. Eleventh Ann. Field Conf., Jackson Hole Guidebook, p. 140–150

Mansfield, G. R., and Ross, C. S., 1935, Welded rhyolite tuffs in southeastern Idaho: Am. Geophys. Union Trans., pt. 1, p. 308–321

Marshall, P., 1935, Acid rocks of the Taupo-Rotorua volcanic district: Royal Soc. New Zealand Trans., v. 64, p. 1–44

McTaggart, K. C., 1960, The mobility of *nuées ardentes:* Am. Jour. Sci., v. 258, p. 269–382

Perret, F. A., 1937, The eruption of Mt. Pelée 1929–1932: Carnegie Inst. Wash. Pub. no. 458, 126 p.

Ross, C. S., and Smith, R. L., 1955, Water and other volatiles in volcanic glasses: Am. Mineralogist, v. 40, p. 1071–1089

Ross, C. S., Friedman, I., and Smith, R. L., 1955, The origins of water in glassy rocks as determined from the isotopic composition (Abstract): Am. Geophys. Union Trans., v. 36, p. 526

Rouse, J. R., 1937, Genesis and structural relationships of the Absaroka volcanic rocks: Geol. Soc. America Bull., v. 48, p. 1257–1296

Tuttle, O. F., and Bowen, N. L., 1958, The origin of granite in the light of experimental studies in the system $NaAlSi_3O_8$-$KAlSi_3O_8$-SiO_2-H_2O: Geol. Soc. America Mem. 74, 153 p.

Van Bemmelen, R. W., 1949, Geology of Indonesia, v. 1a. General Geology of Indonesia and adjacent archipelagoe: Govt. Printing Off., 732 p.

Verhoogen, J., 1946, Volcanic heat: Am. Jour. Sci., v. 244, p. 745–771

White, D. E., 1955, Thermal springs and epithermal ore deposits: Econ. Geology, 50th Anniv. Vol., p. 99–154

Wilcox, R. E., 1944, Rhyolite-basalt complex on the Gardiner River, Yellowstone Park, Wyoming: Geol. Soc. America Bull., v. 55, p. 1047–1080

Williams, H., 1941, Calderas and their origin: Univ. Calif. Pub. Dept. Geol. Sci. Bull., v. 25, p. 239–346

—— 1942, Geology of Crater Lake National Park, Oregon: Carnegie Inst. Washington Pub. no. 540, 162 p.

Zemansky, M. W., 1951, Heat and thermodynamics: New York, McGraw-Hill Book Co., Inc., 375 p.

Manuscript Received by the Secretary of the Society, November 17, 1958

ans,

p.
gist,
from
erica
the
cent

., p.
Geol.
-346
540,
p.

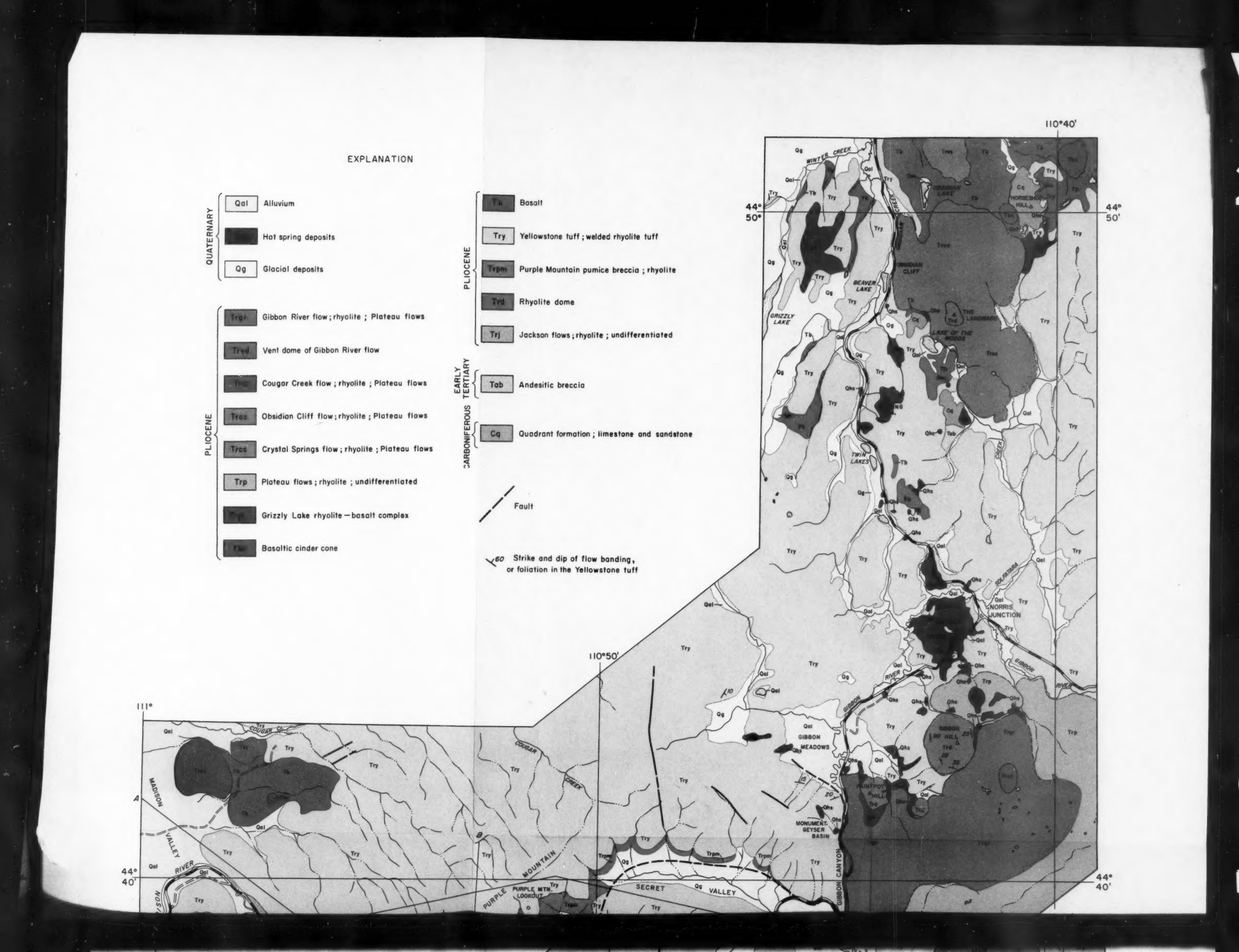
EXPLANATION
QUATERNARY
Qal Alluvium
Hot spring deposits
Qg Glacial deposits
PLIOCENE
Trgr Gibbon River flow; rhyolite ; Plateau flows
Trgd Vent dome of Gibbon River flow
Trc Cougar Creek flow ; rhyolite ; Plateau flows
Trob Obsidian Cliff flow; rhyolite ; Plateau flows
Trcs Crystal Springs flow ; rhyolite ; Plateau flows
Trp Plateau flows ; rhyolite ; undifferentiated
Trgl Grizzly Lake rhyolite—basalt complex
Basaltic cinder cone
PLIOCENE
Tb Basalt
Try Yellowstone tuff ; welded rhyolite tuff
Trpm Purple Mountain pumice breccia ; rhyolite
Trd Rhyolite dome
Trj Jackson flows ; rhyolite ; undifferentiated
EARLY TERTIARY
Tab Andesitic breccia
CARBONIFEROUS
Cq Quadrant formation ; limestone and sandstone
Fault
60 Strike and dip of flow banding, or foliation in the Yellowstone tuff
110°40'
44° 50'
110°50'
111°
44° 40'
WINTER CREEK
OBSIDIAN LAKE
OBSIDIAN CLIFF
BEAVER LAKE
GRIZZLY LAKE
THE LANDMARK
LAKE OF THE WOODS
TWIN LAKES
SOLFATARA
NORRIS JUNCTION
GIBBON RIVER
GIBBON MEADOWS
MONUMENT GEYSER BASIN
GIBBON CANYON
COUGAR CREEK
MADISON VALLEY
MADISON RIVER
PURPLE MOUNTAIN
PURPLE MTN. LOOKOUT
SECRET VALLEY
HORSESHOE HILL
A
B

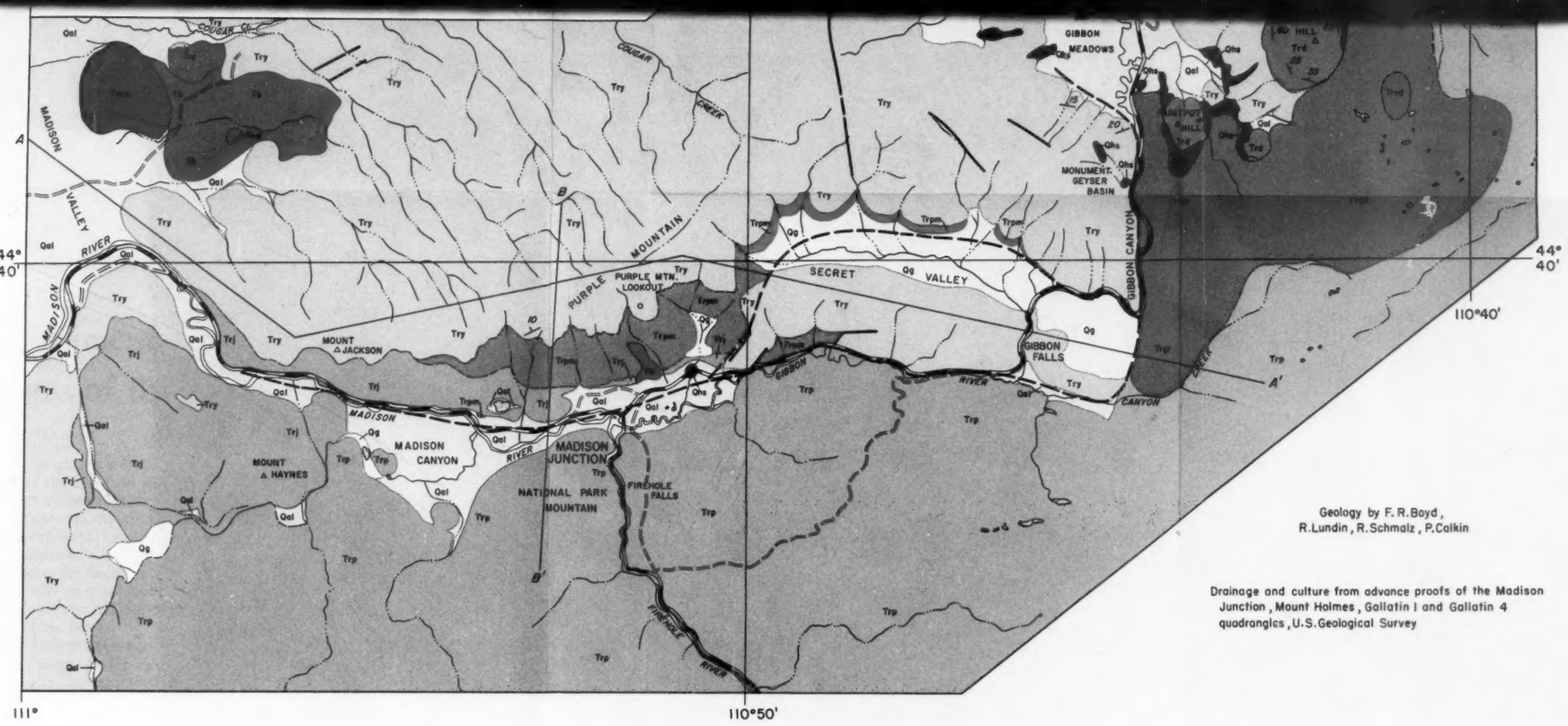

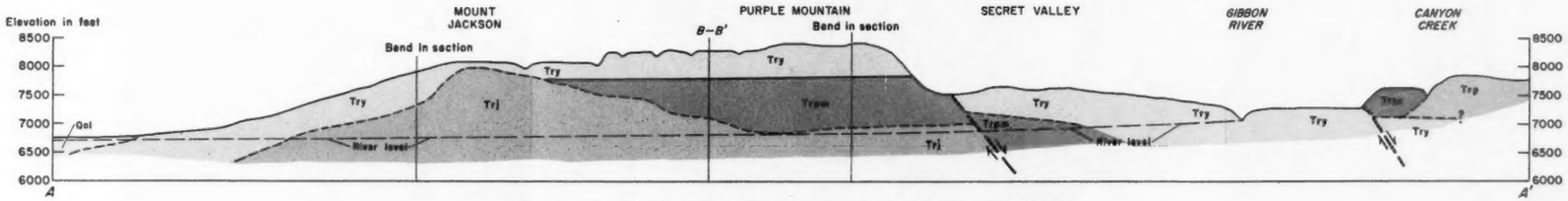

GEOLOGIC SECTION ALONG THE NORTH WALL OF THE MADISON CANYON

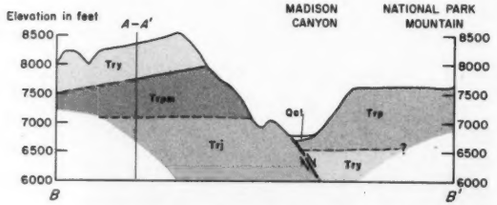

GEOLOGIC CROSS SECTION OF THE MADISON CANYON

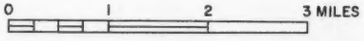

SCALE FOR MAP AND HORIZONTAL SCALE FOR SECTIONS

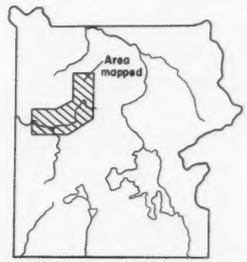

YELLOWSTONE NATIONAL PARK

GEOLOGIC MAP OF THE MADISON CANYON, NORRIS GEYSER BASIN, AND OBSIDIAN CLIFF AREAS, YELLOWSTONE NATIONAL PARK, WYOMING

BOYD, PLATE 6
Geological Society of America Bulletin, volume 72

ROBE

Lin

Mic

Abstra
lake fo
1905, i
of Cali
come a
tense
the flo
years,
cessive
and ev
Eva
sible t
compo
amoun
Measu
salinit
curren
San
from
water
textur
sedim
suspen
miner
ments
metho

Introd
Limno
Bott

Met
Phy
T
C
Che
C
C
R
Wat
Hei
Salt
Hyd
Cur
Sedim
Ger
Wa

Geolo

ROBERT E. ARNAL *Dept. Physical Science, San Jose State College, San Jose, Calif.*

Limnology, Sedimentation, and Microorganisms of the Salton Sea, California

Abstract: The Salton Sea, originally a fresh-water lake formed by the flood of the Colorado River in 1905, is located in the center of the Colorado Desert of California. By 1929, the water of the lake had become almost as saline as ocean water because of intense evaporation and solution of salts present on the floor of the basin before the flood. In recent years, in spite of the high rate of evaporation, excessive runoff from irrigation water has maintained and even raised the level of the lake.

Evaluation of the water budget has made it possible to anticipate future changes in the chemical composition of the water—*i.e.*, an increase in the amount of sulfates is predicted for the future. Measurements with a current cross and studies of salinity distribution indicate a counter-clockwise current pattern in the Salton Sea.

Sands, silts, and clays are deposited in that order from the shore line to the center of the lake. The water content, amount of calcium carbonate, and textural characteristics indicate that most of the sediments of the Salton Sea were derived from the suspended load of the Colorado River, whereas the mineralogical study suggests that some of the sediments have a local origin. Two entirely different methods of computing the rate of sedimentation and of calculating the amount of calcium carbonate in the sediments give results of the same order of magnitude. The large amount of calcium carbonate is partly due to precipitation and partly to transportation by Colorado River water.

Foraminifera are the most abundant microorganisms in the lake. Several ecological factors influence their distribution; among these factors, chlorinity and temperature are not important, depth may be important by its effect on other factors, but the variation in the pH of the sediments is significant. The living foraminiferal assemblage is due to accidental introduction, but the natural effect of environmental conditions has resulted in the creation of a dwarf fauna and many malformed individuals. In contrast to conditions in the ocean, abundance of species decreases offshore; however, as in the ocean, the number of living Foraminifera increases greatly after a bloom of phytoplankton. The average productivity of the Salton Sea is greater than that of the oceans.

Conclusions derived from this study were applied to sediments deposited in the same basin during the past and made it possible to suggest a late Pliocene or early Pleistocene age for the Borrego formation and a Pleistocene age for the Brawley formation.

CONTENTS

Introduction and acknowledgments 428
Limnology 430
Bottom topography and elevation of the Salton Sea 430
Meteorology 431
Physical characteristics of Salton Sea water . . . 431
Temperature 431
Color and turbidity of the sea 432
Chemical characteristics of Salton Sea water . . 433
Chemical composition 433
Chlorinity 433
Relationship between chlorinity and salinity . 437
Water budget 438
Height of stabilization of the sea 438
Salt budget 439
Hydrogen-ion concentration 442
Currents of the Salton Sea 442
Sedimentation 445
General considerations 445
Water content 445
The pH of the sediments 447
Organic matter in the sediments 448
Texture of the sediments 448
Insoluble residues and amount of calcium carbonate 450
Heavy minerals 452
Mineralogy of the sediments 453
Rate of sedimentation 454
Microorganisms 456
General considerations 456
Previous work 456
Foraminifera 456
General features 456
Percentage distribution of the main species . . 457
Distribution of the hyaline, porcellaneous, and arenaceous groups 457
Examples of typical distribution along profiles 458
Relationships between ecologic factors and distribution of species 459
Foraminiferal biofacies 462

Geological Society of America Bulletin, v. 72, p. 427–478, 27 figs., March 1961

Abnormal Foraminifera 465
Foraminiferal productivity of bottom sediments 467
Origin of the living foraminiferal fauna . . . 469
Other microscopic animal life 470
Phytoplankton 471
Geologic history 471
Summary 474
Bibliography 476
Appendix. Water-budget data 478

Figure

1. Location map showing Salton Sea area studied 428
2. Location of stations and topographic markers . 429
3. Bottom topography 430
4. Distribution of winds in the Salton Sea region. 432
5. Transparency of the water as measured with a Secchi Disc 434
6. Distribution of surface chlorinities. 436
7. Corresponding changes in lake level and chlorinity 437
8. Variation of surface, volume, and annual volume evaporated against lake level 439
9. Left: differences between bottom and surface chlorinities (grams per liter). Right: distribution of currents 443
10. Location of stations outside the Salton Sea . . 444
11. Left: water content of the sediments expressed in percentage of wet weight. Right: pH of bottom sediments 445
12. Percentage of organic matter in the sediments. 446
13. Grain size of the sediments 447
14. Texture data for fine sands, silts, clays, Salton Sea average, and Colorado River suspended load 450
15. Percentage of insoluble residues in the sediments 451
16. Percentage of heavy minerals in the sediments. 453
17. Distribution of the main species of Foraminifera 458
18. Distribution of *Bolivina striatula*. Distribution of the hyaline, porcellaneous, and arenaceous groups. 460
19. Distribution of the different categories of Foraminifera 462
20. Frequency distribution along profiles P4–P'4 and P9–P'9 463
21. Relationships between ecologic factors and distribution of species 464
22. Histogram distribution of species and foraminiferal number plotted against depth . . 465
23. Number of abnormal Foraminifera per 60-gram sample 467
24. Foraminiferal productivity of bottom sediments. 468
25. Phytoplankton bloom during early spring . . 470
26. Columnar section in the Salton Basin. 472
27. Number of specimens per sample reworked from the Borrego formation 473

Table

1. Wind distribution, Salton Basin 433
2. Air temperature in °F., Salton Basin 433
3. Percentage of ions in Salton Sea water and normal sea water 434
4. Average values for chlorinity and correcting constant, Salton Sea 435
5. Evolution of the chemical composition of Salton Sea water from 1907 to 1955 . . . 435
6. Salton Sea volume data, 1907–1955 438
7. Salt budget data, Salton Sea, 1905–1955 . . . 440
8. Variation in per cent of sodium chloride and sulfates, Salton Sea, 1907–1955 441
9. Per cent water content of sediments, Salton Sea 446
10. Mineralogical composition of sediments, Salton Sea 454
11. Foraminiferal facies in the Salton Sea 466

INTRODUCTION AND ACKNOWLEDGMENTS

In the fall of 1953, at the suggestion of O. L. Bandy, I began the study of the Salton Sea, California, which forms the basis of this report in order to (1) determine the action of limnological factors on inland brackish waters and on sediments deposited in these waters, (2) investigate the influence of ecological factors on microorganisms which have only recently been introduced in the lake, and (3) find out whether or not the present conditions would give a clue to the depositional environment of older sediments and their provenance.

Field work was accomplished from November 1953 to January 1955, and laboratory analyses were made during the following 2 years. All the field equipment used—water sampler, snapper sampler, Secchi disc, lead line, and current cross—was homemade but worked efficiently. The position of the collecting sta-

Figure 1. Location map showing Salton Sea area studied

tions was obtained by dead reckoning; care was taken to use a constant speed between consecutive stations along each profile. Occasionally, the position of the boat was checked by measuring with a Brunton compass the direction of several topographic markers. Travertine Rock, Mullet Island, Pumice Buttes, the old buildings of the Imperial Salt Company, and the buildings of the A.E.C. Sandia Corporation (Fig. 2) were especially useful markers. The area studied in the present report (Fig. 1) covers approximately 600 square miles of the Colorado Desert of California.

I am indebted to O. L. Bandy and K. O. Emery of the University of Southern California, L. V. Wilcox of the U. S. Salinity Laboratory in Riverside, California, and C. L. Hubbs of the Scripps Institution of Oceanography for valuable help and advice throughout the different phases of this study. Library and

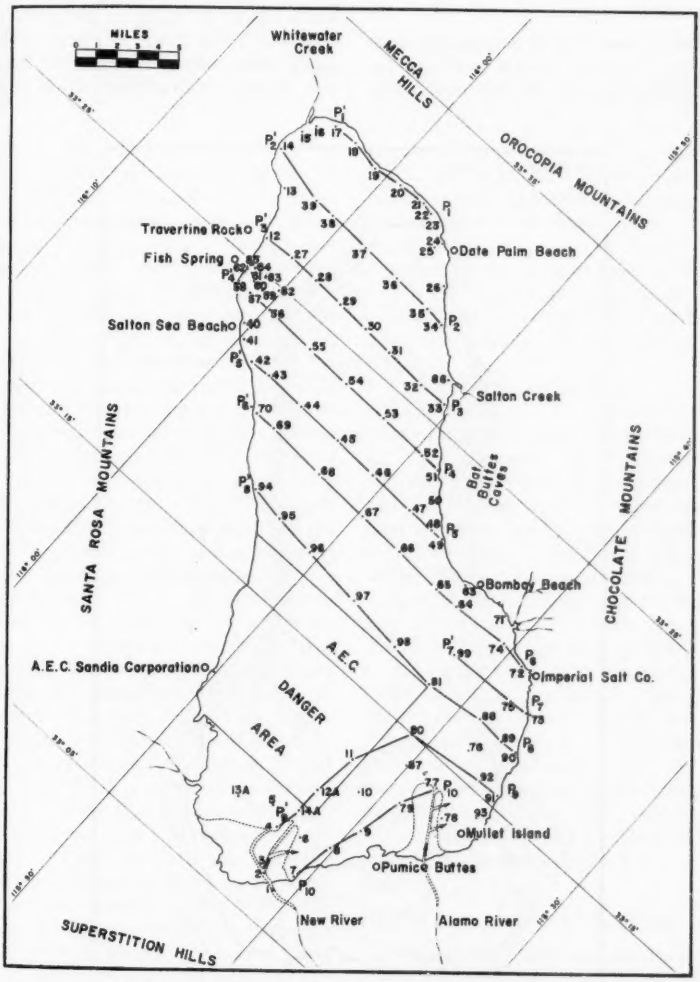

Figure 2. Location of stations and topographic markers

laboratory facilities were provided by the Allan Hancock Foundation, University of Southern California.

LIMNOLOGY

Bottom Topography and Elevation of the Salton Sea

The depth of water was determined by lead-line soundings, and the results served as the basis for constructing the bottom topography of the lake (Fig. 3). Soundings were taken over a 15-month period (November 5, 1953 to January 24, 1955). Because of intense evaporation or inflow of fresh water during that period of time, variations of the water level had to be accounted for in computing the elevation of the bottom of the lake at each station. This was achieved by using an invariable reference level which was chosen as mean sea level as on topographic maps. To obtain the exact elevation of the bottom of each station, the value of

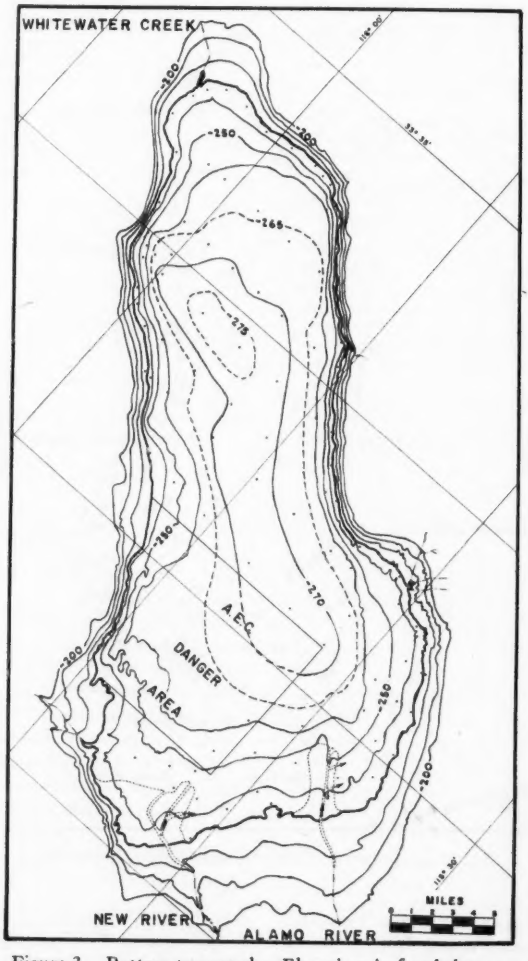

Figure 3. Bottom topography. Elevations in feet below sea level

the depth of each sounding was added to the level of the water at the time the sounding was taken. Accurate elevation of the water level of the lake was obtained for each 2-week period from November 1953 to January 1955 by using readings from the gauging station maintained at the dock of the Sandia Corporation by the Coachella Valley water district.

In measuring water depths, the velocity of the currents is never great enough to introduce appreciable error; if any, the error was certainly less than 1 per cent of the depth measured.

In Figure 3, the heavy contour line is the −230 contour, and it approximates within 2–3 feet the actual (1959) elevation of the shore line; the contour interval is 10 feet for all solid-line contours. Two intermediate contour lines represented by dashed lines have been added: one, the −265 contour, is interpolated between the −260 and the −270 contours; the other, the −275 contour, is the deepest. The lowest elevation, 276.7 feet below sea level, has been recorded at two stations within the −275 contour. All contour lines from the −200 to the −260 were obtained from the topographic map of the U. S. Geological Survey (1928) from a survey made in 1925, when the approximate level of the Salton Sea was −250. The deeper contours were added from data obtained in the course of the present study, and some other contours were corrected for better accuracy.

The lake occupies a basin, elongated northwest, in which the greatest depth is not in the geographic center of the lake, as might have been expected, but toward the north, where the lake is narrow. Roughly 277 feet below sea level, the maximum depth is only 4 feet higher than the lowest point of the United States, at Badwater, in Death Valley, California. In that part of the basin which is below the −200 contour, the slope of the floor is very gentle. The minimum declivity, 6 feet to the mile or approximately a 4-minute angle, occurs along the axis of the basin, especially to the north where Whitewater Creek enters the lake, and to the south where the Alamo and New rivers debouch into the lake. Much steeper slopes occur along the western and eastern shores; however, the angle of the slope never exceeds 2° 30′ for the portion of the basin below the −200 contour.

Examination of the subaqueous topography provides conclusions regarding the sedimentation in the basin. At the deltas of the New and Alamo rivers (Fig. 2) the contour lines established in 1925 have a position different from that of equivalent contours today. They are not parallel to the present shore line which is represented in Figure 3 by a dotted line. The contours established in 1925 were retained because they show the displacement of the −230 contour (approximate 1959 shore line) caused by accumulation of sediments since the map was surveyed.

Meteorology

In the Coachella and Imperial valleys (Fig. 4), the mountain ranges bordering the basin trend northwest and channel the wind in that direction. Prevailing winds there blow mostly to the southeast; farther south, however, the basin becomes wider, and the influence of topography on the wind direction is much less important.

Although meteorological observations in the Salton Basin are only sporadic, some statistics are available. Data in Table 1 were obtained from the Central Weather Bureau in Los Angeles.

Table 1 indicates that (1) the component wind direction at the northern end of the Salton Basin is roughly west to northwest, and (2) the component wind direction at the southern end is west to southwest (Fig. 4). These prevailing wind directions, apparently, are adequate to start a counterclockwise series of water currents in the Salton Sea.

The Weather Bureau quoted an average of 3.20 inches of rainfall per year at the Indio station over a period of 73 years and an average of 3.23 inches per year over a period of 14 years at the El Centro station. An average of 3.20 inches of annual precipitation was chosen as the best over-all value for the Salton Sea region.

Rates of evaporation in the Salton Basin were studied by Blaney (1955). He obtained from direct measurements and from computations an average figure of 72 inches per year.

Air-temperature data are given in Table 2, for several localities (Fig. 4) in the Salton Basin.

Physical Characteristics of Salton Sea Water

Temperature. The temperature of the water of the Salton Sea varies not only seasonally but diurnally. Extreme readings observed were: 12° C. (54° F.) and 34.5° C. (94° F.); however, a dual recording thermometer installed on the dock of the Sandia Corporation (Carpelan, 1955, unpublished report) recorded a surface low of 11.3° C. (52.5° F.), and a minimum of 10° C. (50° F.) at a depth of 3 m was recorded

in January 1955; the highest surface temperature recorded was 35.3° C. (95.5° F.), in August 1954.

Only a slight variation in temperature occurs from the surface to the bottom, where it is usually lower. For example, at the deepest location, 5–6 miles east of Fish Spring where the depth of the water was 13.2 m, the difference in temperature between surface and bottom was 3° C. (5.5° F.) on July 10, 1954, when the surface temperature reached 32° C. (88° F.). On November 3, 1954, in the same region, the temperature was 21.8° C. (71.5° F.) at the bottom, while at the surface it was 22.4° C. (72.5° F.), a difference of only 0.6° C. (1° F.).

At times the water is warmer at the bottom than at the surface. This occurs principally in the fall (single overturn of tropical lakes) when there is a general cooling of the body of water. At such periods the water is cooler at the surface at night, at dawn, and during the early morning. When strong winds create an intense and rapid evaporation, the temperature of surface water decreases markedly (Carpelan, 1955, unpublished report).

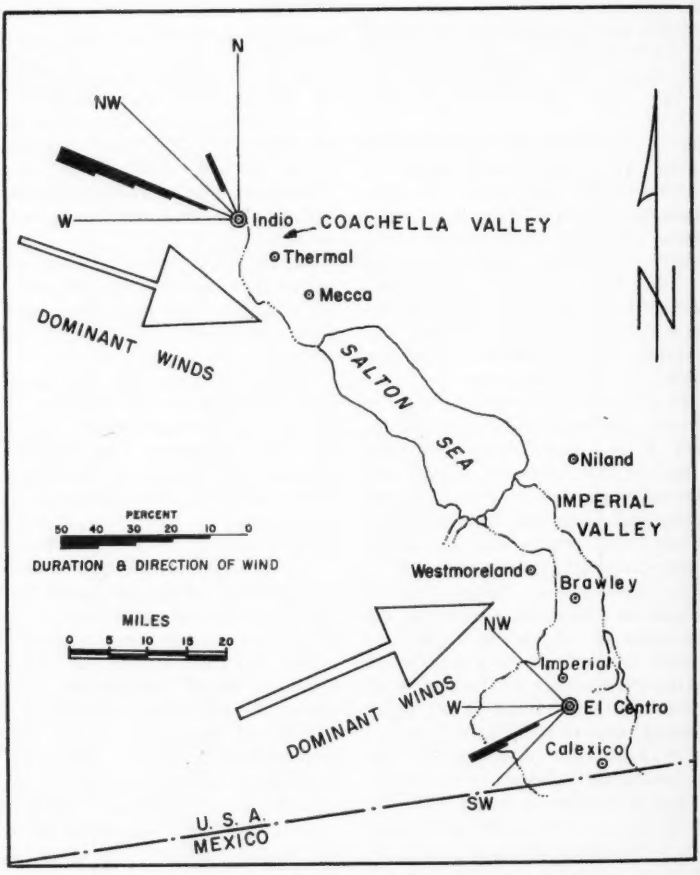

Figure 4. Distribution of winds in the Salton Sea region

Color and turbidity of the sea. To an observer on board a boat, the water of the Salton Sea always appears gray to grayish beige, because of the particles of sediment in suspension in the water. The concentration of the particles makes

the water more or less turbid and gives it a distinct color. To an observer ashore, the color of the Salton Sea ranges from a deep blue to a dark gray. Occasionally it may be beige to reddish brown in the southern part.

Table 1. Wind Distribution, Salton Basin, California

Area	Duration	Wind velocity	Remarks
Indio*	21% days	<3 knots	Wind direction is 32% from northwest (west to northwest) and 50% from the north to west quadrant
	69% days	4–15 knots	
	10% days	16–31 knots	
	Occasional	>31 knots	
El Centro†	42% days	<3 knots	Wind direction is from southwest to northwest, westerly dominant
	58% days	4–31 knots	
	Occasional	>31 knots	

*Data based on a period of 14 consecutive months of observations
†Data based on a period of 4 consecutive years of observations

Turbidity is an important factor, for it regulates the extinction coefficient of the water and indicates at what depth darkness is reached and, therefore, the depth below which plants cannot exist. The average depth at which the Secchi disc disappeared was about 7 feet, or roughly 2 m. About 85 per cent of the visible radiations disappears in the first meter of water, 85 per cent of the remainder in the second meter, and so forth.

Measurements with the Secchi disc ranged in value from 0.10 to 3.05 m. A minimum of 10 cm was observed in very shallow water, in a region flooded only recently, and during a fairly strong wind period. Maximum transparency occurred, as should be expected, in the center of the lake. The disappearance of the Secchi disc at a maximum depth of 3 m is a good indication that in the central part no light reaches the bottom of the lake; consequently almost no plant life exists there.

The turbidity measurements were made as a part of the routine work for most of the stations. Isopleths of turbidity are traced in Figure 5. The curves follow the shore-line pattern rather closely and indicate the origin of the turbid elements from the coast. However, examination of the map shows that there is also a relationship between the isopleths of turbidity and the bathymetric curves. Both are more closely spaced along the eastern and western shores than they are along the northern and southern boundaries of the Salton Sea. This suggests supply of sediments by the two rivers (to the south) and action of the currents, explained below.

Table 2. Air Temperatures in °F., Salton Basin

Locality	January average	July average	Maximum	Minimum
Brawley	52.7	91.1	121	19
Calexico	53.2	89.8	117	21
Imperial	53.6	91.9	124	16
Indio	54.2	92.5	125	13

Chemical Characteristics of Salton Sea Water

Chemical composition. One of the first complete analyses of Salton Sea water was made by Professor Forbes in July 1907 (MacDougal, 1907, p. 714). The different ions present in the water and their amount and percentage are given in Table 3. The main ions present in normal sea water (Sverdrup, Johnson, and Fleming, 1942, p. 666) are also listed for comparison. Important differences appear at once: the ratio of chlorine to total salts, which is 1.805 for normal sea water, was 2.15 for Salton Sea water in 1907; the percentage of sodium is approximately the same, but the amount of sulfates is much larger in Salton Sea water. Some calcium and magnesium are present as carbonates, and an excess of sulfates is combined as Na_2SO_4. Since the first analysis by Professor Forbes, other analyses have been made which show the evolution with the years of the salts present in the water (Table 5).

Chlorinity. Chlorinity was determined by titration of halides with silver nitrate; all halides were considered as chloride. The accuracy of chlorinity measurements is less than it would be for standard sea-water titrations, because of the necessity of using a solution suitable for a wider range of variations than is common in sea water. The degree of accuracy of the titration is ± 0.02 o/oo.

CHLORINITY OF THE SURFACE WATER: The chlorinity of the surface water in the Salton Sea fluctuates seasonally. It increases during the

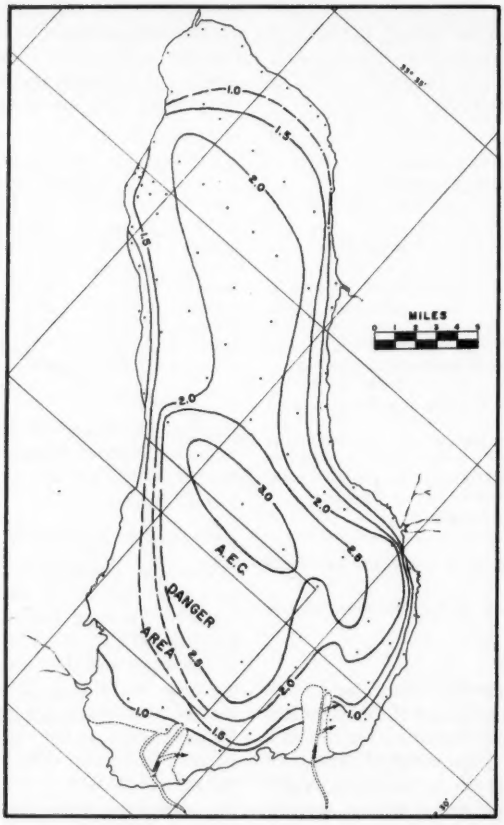

Figure 5. Transparency of the water as measured with a Secchi disc. Depth expressed in meters

TABLE 3. PERCENTAGE OF IONS IN SALTON SEA WATER AND NORMAL SEA WATER

	1907 Salton Sea water		Normal sea water	
	Parts per million	Per cent	Parts per million	Per cent
Total salts	3648		34,482	
Chlorine	1697	46.52	18,980	55.04
Sulfate	476	13.05	2649	7.68
Carbonate	66	1.81	140	0.41
Silicate	12	0.33		
Phosphate	Trace			
Sodium	1111	30.46	10,556	30.61
Calcium	99	2.71	400	1.16
Magnesium	64	1.75	1272	3.69
Potassium	23	0.63	380	1.10
Aluminum	Trace			
Iron	Trace			

summer months, approximately from April to October, when the evaporation exceeds the inflow of fresh water. When these conditions are reversed during the winter months, the chlorinity decreases.

Table 4. Average Values for Chlorinity and Correcting Constant, Salton Sea

	Average values for chlorinity in o/oo	Correcting constant in o/oo
December 1953	13.90	0.00
January 1954	13.80	+0.10
March 1954	13.60	+0.30
June 1954	13.70	+0.20
July 1954	13.90	0.00
October 1954	14.00	−0.10
November 1954	13.90	0.00
December 1954	13.85	+0.05
January 1955	13.80	+0.10
February 1955	13.70	+0.20

The average values of chlorinity for surface water during the period from December 1953 to February 1955 are given in Table 4. In order to obtain results that could be compared over the entire surface of the lake, the chlorinity values were expressed as for December 1953, when the average was 13.90 o/oo. They were changed accordingly by the addition of a correcting constant which represents the difference between the average value for any one month and the average value for December 1953. This was necessary because the samples were collected over a 15-month period during which the salinity of the water varied according to the seasons. The correcting constant for each month is given in Table 4.

Corrected values were plotted in Figure 6 to show their distribution. The maximum range is from 3.6 o/oo to 14.3 o/oo. Isopleths of chlorinity were drawn to detect regional variations. Nearly homogeneous conditions exist over most of the lake where a chlorinity of 13.80 o/oo to 14.20 o/oo generally occurs. To the northwest, the inflow of fresh water from Whitewater Creek and from a drainage canal shows as a tongue of slightly lower chlorinity. An important difference from the average chlorinity exists in the southern and southeastern regions, where the inflow of fresh water from New River and Alamo River markedly decreases the chlorinity values. The lowermost values exist on the eastern side of the New River and Alamo River deltas, where values of 5.2 o/oo and 12.2 o/oo have been recorded.

In New River the water has a chlorinity of 0.80 o/oo. In December 1954, 2 miles east of the river in the Salton Sea, the chlorinity was 5.2 o/oo, 4 miles east it was 13.2 o/oo, and 6 miles due north the chlorinity was 13.95 o/oo, which is approximately the same as the main body of water. It appears that the fresh water of New River becomes mixed with Salton Sea water within 6–8 miles after it enters the lake. The Alamo River water, added to that of drainage canals which are numerous in the southeastern region, shows as a tongue of water of lower chlorinity for a longer distance because, in December of 1954, a value of 13.2 o/oo was present offshore from the old salt works of the Imperial Salt Company located (Fig. 2) about 10 miles from the mouth of the river. In addition to regional variations, an offshore chlorinity gradient was noted by Carpelan (1955, unpublished report), who recorded the following values on November 3, 1954, from the North Shore (near outlets of North Shore drainage canals) to Fish Spring.

	Distance	*Chlorinity in o/oo*
North Shore	0 miles	13.6
	2 miles	13.91
	4 miles	13.97
Fish Spring	6 miles	13.91

Table 5. Evolution of the Chemical Composition of Salton Sea Water from 1907 to 1955

(In per cent)

	1907*	1913†	1929**	1955††
Chloride	46.52	47.85	50.84	43.33
Sulfate	13.05	12.59	10.92	20.45
Carbonate	1.81	2.72	0.78	0.54
Sodium	30.46	32.62	31.19	29.86
Calcium	2.71	1.99	1.56	2.29
Magnesium	1.75	1.64	4.68	2.86
Potassium	0.63	0.35	Included with sodium	0.67
Salinity in o/oo	3.65	9.90	32.06	33.68
Conversion factor	2.15	2.08	1.97	2.34
Lake level in feet	−198	−221	−248	−235

*Analyst, Professor Forbes (MacDougal, 1907)
†Analyst, W. H. Ross (MacDougal and others, 1914)
**Analyst, P. A. Shaw (Coleman, 1929)
††Analyst, L. V. Wilcox, U. S. Salinity Laboratory, Riverside, California

Good parallelism exists between the variations of chlorinity of the water and the level of the Salton Sea; this indicates a direct relationship between the two variables (Fig. 7).

CHLORINITY OF THE BOTTOM WATER: With a few exceptions the lowest values of chlorinity for bottom water were found in coastal regions, whereas the values were higher in the central region. The range is from 13.4 o/oo to 14.2 o/oo.

To the southeast, the lowest chlorinity recorded for bottom water is 13.4 o/oo and undoubtedly marks the point where the surface fresh water of the Alamo River, mixed with the normal Salton Sea water, reaches the bottom of the sea. The water of the Salton Sea is not deep enough to show stratification. At the deepest stations, about 6 miles east of Fish Spring in a depth of 41 feet (the greatest depth in 1954), the surface chlorinity was 14.10 o/oo and the bottom chlorinity was 14.05 o/oo; this indicates a higher surface chlorinity than at bottom. At the same time the temperature of the surface water was 89° F., whereas it was only 83° F. at the bottom. The only part of the sea where a variation of chlorinity with depth is noticeable is in the southern portion, but this variation is due to the surface flow of less saline water with further mixing and is not due to stratification of water of increasing salinity.

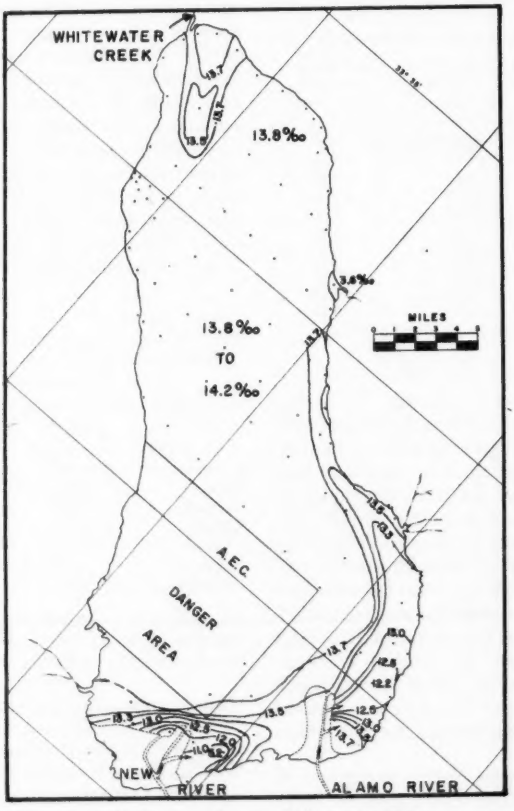

Figure 6. Distribution of surface chlorinities. Values corrected as for December 1953

Relationship between chlorinity and salinity. The salinity of ocean water is obtained by multiplying the chlorinity value by 1.805 (Sverdrup, Johnson, and Fleming, 1942, p. 51). This factor is applicable except where great dilution or great evaporation takes place, as in certain coastal waters. The equivalent factor in the Salton Sea has been variable through the recent history of the lake.

Analyses given in Table 5 show the percentages of the different ions present in Salton Sea water and the variation with time of the conversion factor.

Comparison of the four analyses indicates that the percentage of sulfate decreased from 1907 to 1929 but increased thereafter. From 1907 to 1929 the chemical composition of Salton Sea water was influenced mostly by evaporation and solution of the salts that were present in the salina of the Salton Sink before the flood. (*See* details under Salt Budget.) After 1929, irrigation development began on a large scale, and most of the drainage water flowing into the Salton Sea was derived from Colorado River water and therefore had similar chemical characteristics. The level of the sea, which was at a low of −250 feet in 1925, has risen irregularly since. Today, inflow of water exceeds evaporation. Inasmuch as most of the irrigation water is Colorado River water, the chemical composition of the water of the Salton Sea is now tending toward that of the Colorado River, especially with regard to the proportion of sulfate. This is supported by an analysis of the outflowing water at Lake Mead in 1946 (U. S. Bureau of Reclamation, 1947), reproduced below. This analysis shows 305 parts of sulfate and only 71 parts of chlorine in 776 parts per million of total salts in the water.

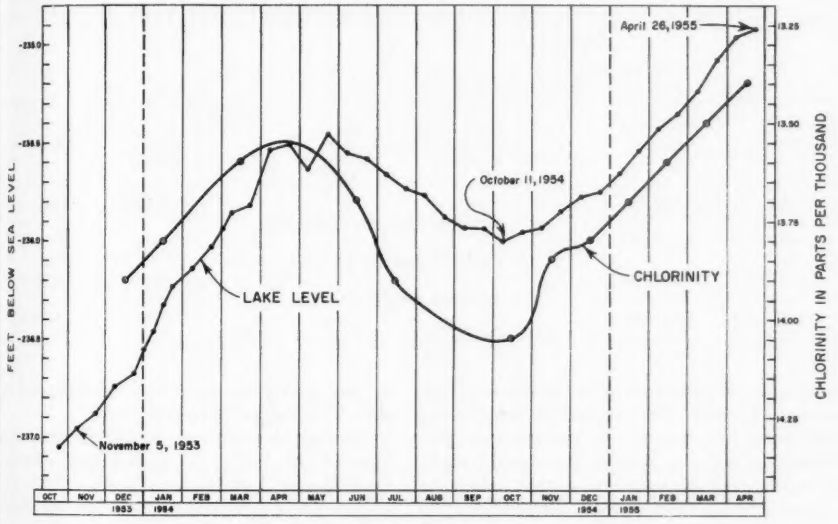

Figure 7. Corresponding changes in lake level and chlorinity

Analysis of Outflowing Water at Lake Mead
(*Parts per million*)

Silica	Calcium	Magnesium
SiO_2	Ca	Mg
14	92	28
Sodium	Potassium	Bicarbonate
Na	K	HCO_3
90	6	166
Sulfate	Chloride	Nitrate
SO_4	Cl	NO_3
305	71	4

Total salts 776

This high proportion of sulfate undoubtedly was the most important cause for the variation in the conversion factor in salinity-chlorinity relationship. If, as is expected for several years to come, the level of the Salton Sea continues to rise because of the excess inflow of irrigation water of Colorado River origin, then the value

of the conversion factor for Salton Sea water salinity and the amount of sulfate in the water probably will also increase in the future.

Water Budget

The Salton Sink, an enclosed basin, is a closed system as far as the water budget is concerned. As it has no outlet to the ocean, the difference between the amount of runoff plus precipitation and the amount of evaporation is reflected only by variations in lake level. An excess of evaporation over runoff and precipitation results in lowering of the lake level and vice versa. Stabilization of Salton Sea level will occur only when the amount of evaporation will equal the amount of precipitation plus runoff. In order to balance the water budget, it is therefore necessary to obtain values for annual precipitation, annual evaporation, and annual runoff.

Precipitation (3.20 inches per year) and evaporation (72 inches per year) have been discussed in preceding pages. Runoff varies each year according to the amount of water used for irrigation purposes. Nevertheless, it can be computed for any year by using the following formula: $R = Vp - Vo + E - P$, where R represents runoff, Vp is the volume of water in the lake during the preceding year, Vo is the volume of water in the lake during the year of computation, E is the amount of evaporation, and P is the amount of precipitation.

The surface area of the sea was computed by measuring with a planimeter the area included within each of the bathymetric contour lines shown in Figure 3. From the values obtained, a curve showing the variation of the surface area of the lake was plotted against depth of water (Fig. 8). If the depth of water is known, the coresponding surface area of the lake is obtained by direct reading on the curve.

Similarly, the volume of the sea was computed by measuring the volume of the different "slices" delineated by the successive bathymetric contours. The volume of any given slice was obtained by averaging the areas included within the upper and lower surface boundaries of the slice and by multiplying by the contour interval. The cumulative volume of the Salton Sea was calculated by adding the volumes of successive slices. In the same manner as for the surface area, a curve showing the variation of the volume of the lake was plotted against depth of water (Fig. 8). The volume of the lake at any given elevation can be obtained by direct reading on the curve.

Table 6. Salton Sea Volume Data, 1907–1955

Year	Volume in acre-feet	Balance (loss or gain) and period for which it is given	Lake level Blaney (1955)	Lake level Computed
1907	15,326,500		−198	none
		7,216,000 (loss) 1907–1913		
1913	8,110,000		−224	−224.2
		4,647,500 (loss) 1913–1929		
1929	3,463,000		−245	−244.8
		2,158,000 (gain) 1929–1955		
1955	5,621,000		−235	−234.5

Average elevations of the lake level for each year of the 1907–1955 period were obtained from Figure 2 of Blaney's paper (1955). The surface areas corresponding to these elevations were obtained by direct reading in Figure 8. Thus the annual volumes of precipitation and evaporation were calculated for each year of the 1907–1955 period by multiplying the surface area of that year by 0.266 (3.20 inches = 0.266 foot) and 6 (72 inches = 6 feet) respectively. All volumes are expressed in acre-feet. Values for precipitation, evaporation, and runoff volumes, and also the balance in gain or loss, are given for each year from 1908 to 1955 in the Appendix.

The results are summarized in Table 6.

Note the good agreement between the computed lake levels and those given by Blaney (1955). Blaney also cited total inflow values for the period 1945 to 1953, which are in good agreement with corresponding computed values given in the Appendix.

Height of Stabilization of the Sea

In 1953, the total inflow of runoff from irrigation water in the Salton Sea was ap

proximately 1,550,000 acre-feet. At the rate of 72 inches per year, this volume would be evaporated in 1 year for a surface area of 260,000 acres. This surface area would be reached at an elevation of −224 feet (Fig.8), which is therefore the height of stabilization for the volume of runoff in 1953. However, the lake would stabilize at this level only if the amount of irrigation water used in the Salton Sea basin were not increased over the amount used in 1953. The 1,550,000 acre-feet of water flowing in the Salton Sea that year represented the runoff of the water applied to about 700,000 acres of irrigated land, or about 2.2 acre-feet of runoff per acre.

Dowd (1952, unpublished paper) anticipated that under full development about 100,000 acres will be irrigated in Coachella Valley alone; this is about 70,000 acres more than in 1953. This additional acreage will require irrigation water which will result in an increase of about 160,000 acre-feet over the 1953 runoff, thus making the total return inflow 1,710,000 acre-feet. For such a return flow, the height of stabilization will be about −214 feet (Fig. 8). However, as a result of the increase in efficiency of the drainage system which is actually developed, the return flow probably will be even greater, and under full development the height of stabilization of the Salton Sea will be close to the −200-foot level. In this event, irrigation water districts of the Salton Basin would have to add 16,000 to 58,000 acres of land to the Public Water Reserve for a stabilization level of −214 to −200 feet respectively.

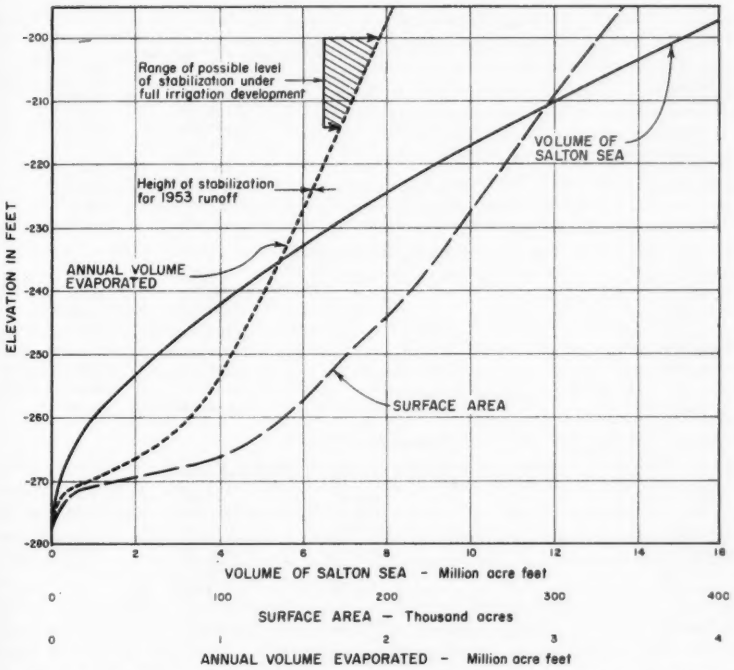

Figure 8. Variation of surface, volume, and annual volume evaporated against lake level

Salt Budget

Some of the salts present in the Salton Sea water did not originate from the Colorado River. Professor Forbes' comment (MacDougal, 1907, p. 711) is especially significant:

"If you will compare Salton water with the January 1900 sample (of Colorado River water) you

TABLE 7. SALT BUDGET DATA, SALTON SEA, 1905–1955

Analysis of salts present in Salton Sea in 1929 (computed from an analysis by P. A. Shaw; lake level, −235 feet; volume, 3,462,700 acre-feet) is not very accurate, and the grouping of sodium and potassium in the presentation of the results does not permit the determination of the different salts present in solution. Only the total dissolved solids, 32,060 parts per million, was used. This gives a total of 150,946,700 tons of salts in Salton Sea water in 1929.

Salts	Parts per million	Weight of salts in tons	Per cent of salts
*Salts brought to Salton Sea by Colorado River during flood period 1905–1907**			
(Lake level, −198 feet; volume of water, 15,322,600 acre-feet)			
KCl	28.33	590,300	4.03
NaCl	206.36	4,299,400	29.36
Na_2SO_4	173.31	3,801,900	24.66
$MgSO_4$	102.32	2,131,800	14.55
$MgCO_3$	3.80	79,000	0.54
$CaCO_3$	146.62	3,054,600	20.85
$CaSiO_3$	42.26	880,400	6.01
Total	703.00	14,837,400	100.00
Salts present in 1907†			
KCl	43.99	916,500	1.24
NaCl	2789.13	58,108,800	78.88
Na_2SO_4	73.87	1,539,000	2.09
$MgSO_4$	316.60	6,596,000	8.95
$MgCO_3$	245.73	5,119,600	6.94
$CaCO_3$	66.55	1,386,600	1.90
Total	3535.87	73,666,500	100.00
*Salts present in 1913***			
(Lake level, −224 feet; volume, 8,109,800 acre-feet)			
KCl	65.61	723,600	0.66
NaCl	7761.15	85,581,400	79.26
Na_2SO_4	546.93	6,031,000	5.58
$MgSO_4$	802.33	8,847,200	8.19
$CaSO_4$	334.90	3,693,000	3.42
$CaCO_3$	282.98	3,120,400	2.89
Total	9793.90	107,996,600	100.00
Salts present in 1955††			
(Lake level, −235 feet; volume, 5,620,500 acre-feet)			
KCl	426.48	3,259,300	1.27
NaCl	23,441.29	179,143,000	70.72
Na_2SO_4	2,210.45	16,892,700	7.08
$MgSO_4$	4,706.26	35,966,200	14.14
$CaSO_4$	2,211.59	16,901,500	6.65
$CaCO_3$	246.26	1,882,000	0.74
Total	33,242.33	254,044,700	100.00

	Salts present in Salton Sea (in tons)		Colorado River contribution (in tons)	Re-solution of salts from salina (in tons)
1907	73,666,500	1905–1907	14,837,400	58,829,100
1913	107,996,600	1907–1913	6,779,900	27,550,200
1929	150,946,700	1913–1929	33,151,000	9,799,100
1955	254,044,700	1929–1955	85,438,400	17,659,600
		Total	140,206,700	113,838,000

*Chemical analysis is average of several analyses of Colorado River water by Professor Forbes in 1900

†Computed from Forbes' analysis

**Computed from analysis by W. H. Ross

††Computed from analysis by L. V. Wilcox

will notice that the proportion of chlorine to soluble solids is 1 to 4.5 in Colorado River water, while, in Salton water, the proportion of chlorine to soluble solids is 1 to 2, which means that the proportion of salt (sodium chloride) is more than twice as great in Salton water. Comparing the same samples with reference to SO_4 the proportion is 1 to 3.5 in river water while it is 1 to 8 in Salton water. This makes it appear as if the soluble matters of the Salton Sea are not exclusively derived from the Colorado River. Either the surrounding mountains have contributed their modifying materials to the sink in times past, or certain separation changes have taken place in the salts which may have been at various times, more or less remote, laid down by the river."

Table 8. Variation in Per Cent of Sodium Chloride and Sulfates, Salton Sea, 1907–1955

	Per cent sodium chloride	Per cent of all sulfates
1907 from Colorado River water	29.35	39.20
1907 in Salton Sea water	78.88	17.98
1913 in Salton Sea water	79.26	17.19
1955 in Salton Sea water	70.72	27.87

Thus, the problem is to discover how much salt was contributed by the Colorado River and what amount comes from other sources. The most important additional source of salts is undoubtedly the salina which existed in the lowest part of the Salton Sink before the 1905 flood of the Colorado River. Salts existed there in amounts sufficient to warrant commercial exploitation by the New Liverpool Company. Some of the salts were dissolved by the incoming water and therefore contributed some of the material present in solution in the Salton Sea water. What amount was contributed and how fast was the process of re-solution?

In order to compute the salt budget of the Salton Sea and to know the evolution of the salts present, it was necessary to obtain the volume of the sea at different periods and also to obtain chemical analyses of the water for the same times. Analyses available for the years 1907, 1913, 1929, and 1955 were chosen for the successive steps of the computation of the budget. By calculating the weight of the salts contributed by the Colorado River at the same periods, the amount of salts derived from the re-solution of the bottom material was obtained by subtracting the weight of salts contributed by the Colorado River from the total amount of salts present in solution in the water at the time the analysis was made. The amount of salt contributed by the Colorado River was computed by multiplying the volume of runoff water which had flowed into the sea at the time of analysis by the salinity of runoff water. Runoff water is essentially of Colorado River origin. The salinity of the runoff water was obtained from various measurements of the salinity of Alamo River and New River water. These two rivers are the main drainage channels entering the Salton Sea basin and carry water having an average salinity of 2.270 o/oo.

Hypothetical combinations of the anions and cations indicated by the analyses for 1907, 1913, 1929, and 1955 are given in Table 7.

From 1907 to 1913, 2,709,500 acre-feet of runoff water of Colorado River origin (*see* Appendix) was added to the Salton Sea, carrying 6,779,900 tons of salts. From 1913 to 1929, 13,248,500 acre-feet of runoff water brought 33,151,000 tons of salts; and from 1929 to 1955, 34,144,700 acre-feet of water brought 85,438,400 tons of salts to the lake.

The difference between the total amount of salts present in Salton Sea water and the amount contributed from the Colorado River water by runoff represents the amount of salts dissolved from the former salina on the bottom of the basin. Thus, during the 2 years of the flood, 1905 to 1907, 58,829,100 tons was dissolved. The total contribution of Colorado River plus that from the salina represents the amount of salt in solution in the Salton Sea in 1955.

On an annual basis the rate of solution was 29.41 million tons for the period 1905 to 1907, 4.59 million tons for the period 1907 to 1913, 0.61 million tons for the period 1913 to 1929, and 0.67 million tons for the period 1929 to 1955. This indicates a very rapid solution in the early periods and a much slower rate in the last years. Such a change should be anticipated, since the most soluble salts are the first to go into solution. By 1913, most of the readily soluble salts were already dissolved, and after that year only the less soluble salts passed into solution. Therefore a soluble salt such as sodium chloride should increase in percentage from the amount in Colorado River water to the amount in Salton Sea up to 1913 and then decrease between 1913 and 1955. Conversely, the percentage of all sulfate salts should decrease from the amount in Colorado River water to the amount in the Salton Sea up to 1913 and then increase between 1913 and 1955. This happens, as shown in Table 8.

An additional factor undoubtedly influenced

the rate of re-solution of salts from the bottom of the basin, namely the actual deposition of clay sediment. By 1957 (*see* Rate of Sedimentation) about 1½ inches of clay-size material had been deposited on top of the salina. This created a barrier which eventually stopped water circulation between the Salton Sea and the salina below causing the less soluble salts (such as gypsum) to remain as a deposit in the salina. Deposition of the more soluble salts (such as sodium chloride), which are now in solution in the water, will not occur until total evaporation of the Salton Sea takes place in the future, thus completing the separation process.

In the evaporite series of the West Texas Permian Basins, this type of separation repeated many times may have been effective in separating some predominantly sulfatic salts (anhydrite and gypsum) from the predominantly sodium chloride mixture. The position of the anhydrite or gypsum beds, which usually underlie the salt (sodium chloride) beds, supports this idea.

SUMMARY OF THE SALT BUDGET: Of the 254,044,700 tons of salts present in 1955 in the Salton Sea, 140,206,700 tons was contributed by Colorado River water and concentrated by evaporation. The remainder, 113,838,000 tons, was derived from re-solution of salts of the former salina of the Salton Sink. It is anticipated that in the future there will be a decrease of the percentage of sodium chloride as compared to the total amount of salts in Salton Sea water and an increase in the total percentage of the sulfates present in the water. These conclusions may have important application with respect to the future transplantation of fish, such as has already been undertaken at the Salton Sea. Only the species that have a high tolerance to the presence of sulfates in the water will be able to live in the Salton Sea.

Hydrogen-Ion Concentration

The complete range of hydrogen-ion concentration or pH of the water in the Salton Sea is from a minimum of 7.34 in bottom water to a maximum of 8.93 in surface water. These are extreme values well above or below the usual range of pH for surface or bottom water in the lake. In the central part of the sea where the water is in equilibrium with the CO_2 in the atmosphere, the pH of surface water remains between 8.1 and 8.4. In surface coastal waters the highest values are found where the photosynthetic activity of plants has reduced the CO_2 content of the water. The highest values measured for Salton Sea water (two above 8.60; one above 8.90) are from stations around the New River delta, where plant life is the most abundant. Photosynthetic activity of plants also creates a variation of pH at any one place according to the time of day. This was noticed on several profiles in which the pH of offshore waters was lower for stations made in the morning compared with those of the early afternoon. A difference of 0.20 has been noted locally.

In subsurface waters, exchange of CO_2 with the atmosphere is impossible, and the pH varies in inverse proportion to the CO_2 content of the water. Down to a depth of 3–4 m, which is about the thickness of the euphotic zone in the Salton Sea, the pH varies but probably remains higher than 8.0, partially because of photosynthesis. Below this depth, very little or no light is present, and the only organic activity remaining is the respiration of the life present in those waters. A pH value of about 8.0 may be maintained in regions where there is a good mixing of the water by currents (southeastern parts of the lake) or at the time of overturn. With the exclusion of those factors, the pH decreases to 7.5, which is the minimum value to be attained by increase in CO_2 content. A few of the localities, however, have pH values lower than 7.5. This is doubtless due to stirring of the underlying sediments at the time of collection. Some of the sediments have a very low pH (Fig. 11), probably because of carbon dioxide formation, caused by decay of organic matter, within the sediments.

Currents of the Salton Sea

The current pattern is basically a counterclockwise gyral around the sea. The highest velocities are found where inflow of fresh water adds its effect to the general pattern of the currents. The best continuity of direction and also the highest velocity occur along those coasts that show the steepest bottom slopes (eastern and western coasts). This is especially true in the region of Bombay Beach, where the water piles up against the coast because of the configuration of the shore line, change in slope of the bottom topography, and additional inflow of fresh water from the rivers. Similar conditions exist in the region of Fish Spring.

The current pattern results from the wind distribution (Fig. 4). In the northern part of the basin the general wind direction is toward the southeast, with a resulting flow of water in that direction (Fig. 9). As Coriolis force de-

flects the water toward the right—*i.e.*, toward the coast—the southward flow of water is restricted to the west shore. When the water reaches the southwestern part of the sea, it is acted upon by predominantly eastward winds, water remains channeled by the configuration of the coast and is forced to flow toward the east, then northeast, then north. Meanwhile, the water of New River and Alamo River is added to the water accumulated by the wind, and this causes currents of higher velocity in with consequent eastward transportation of water along the southern shore. There the the southeastern region. When the water arrives at Salton Creek it may, in the absence of wind, continue flowing along the coast or be diverted by the wind to the west, thus closing a counterclockwise gyral around the Salton Sea.

Both surface and bottom chlorinities are changed locally by dilution of fresh water entering the sea from different streams and rivers. As surface and bottom chlorinity are the same in most places, the exceptions are especially significant. In order to emphasize these exceptions, a chart showing the differences was established (Fig. 9). There are two main areas of dilution:

(1) A small area to the north reflects the dilution by Whitewater Creek and a large

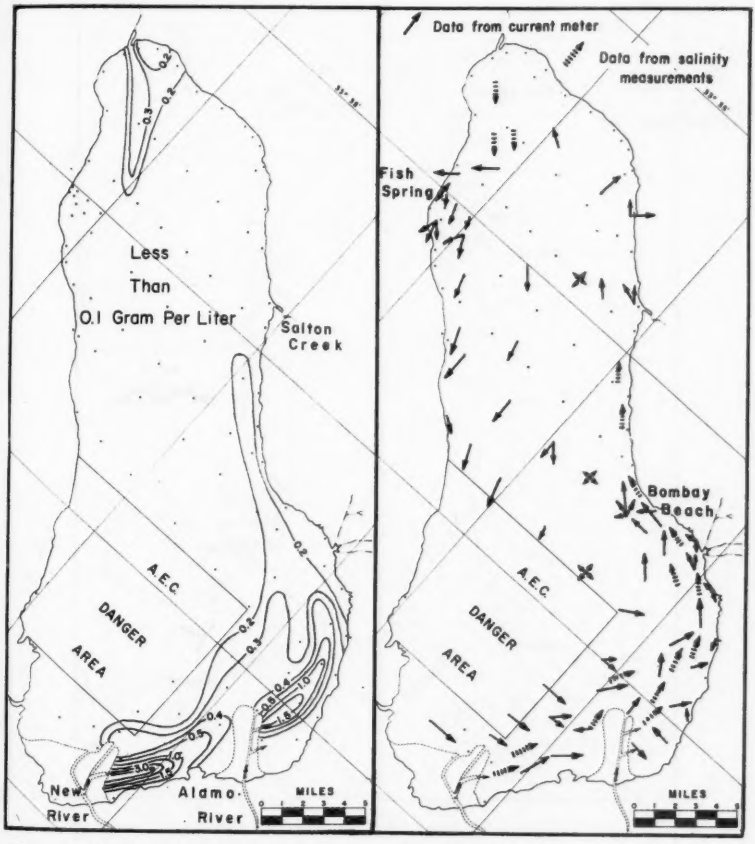

Figure 9. Left. Differences between bottom and surface chlorinities (in grams per liter). Right. Distribution of currents

irrigation canal. An indication of a southward-moving current is apparent there. The fresh water becomes mixed with normal Salton Sea water 6–7 miles from where it enters the sea.

(2) The other area of dilution is in the southeastern region. Fresh water from both the New and Alamo rivers extends to the northeast as separate tongues, with salinity lower than that of the main body of water, until the tongues become confluent along the eastern shore. This less saline water then loses its identity by mixing in the main body of water about 25 miles from where it enters the lake.

Additional evidence regarding the current pattern was obtained from direct measurements made at most of the stations with a current cross. The velocity and direction of the current at each station were also determined. At many stations two or more measurements were made at different periods of the year and are plotted in Figure 9. Each arrow represents a different measurement, its direction marks the current direction, and the length of the arrow is proportional to the velocity of the current. The general direction of the arrows shows the counterclockwise current pattern in the lake.

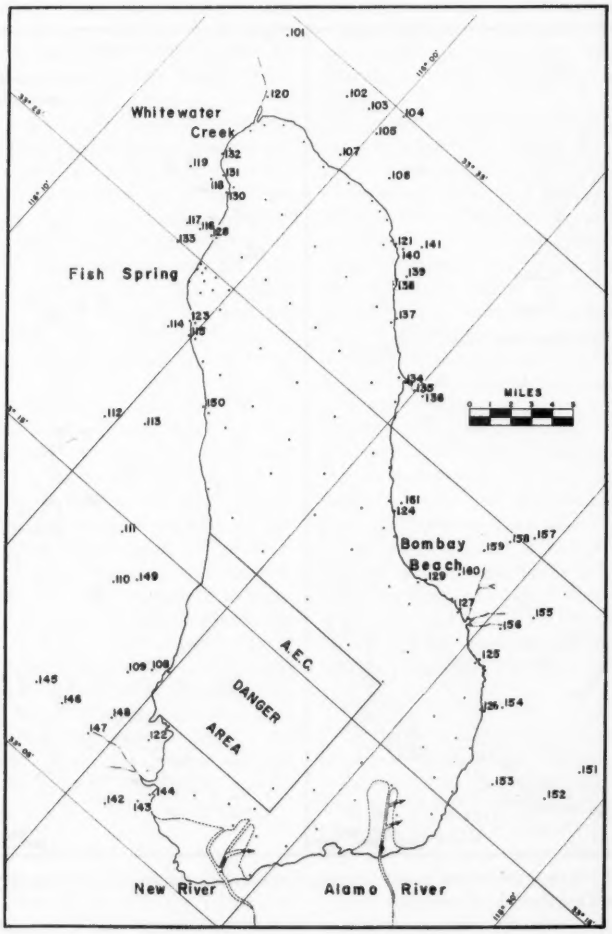

Figure 10. Location of stations outside the Salton Sea

SEDIMENTATION

General Considerations

The Salton Basin is enclosed below an elevation of 47 feet; above, it opens to the south into the Gulf of Baja California. Inasmuch as the Salton Sea lies within the enclosed part of the basin, the sediments that accumulated in the lake are derived, at least in part, from the surrounding rocks exposed at higher elevations on the borders of the basin. Similarly, the conditions of sedimentation are regulated mostly by the local factors examined above under Limnology.

Samples collected from the bottom of the lake were used in the study of the sedimentary characteristics; samples collected at 62 additional stations situated between the shores of the lake and the foot of the surrounding mountains provided information regarding the source of the sediments (Fig. 10).

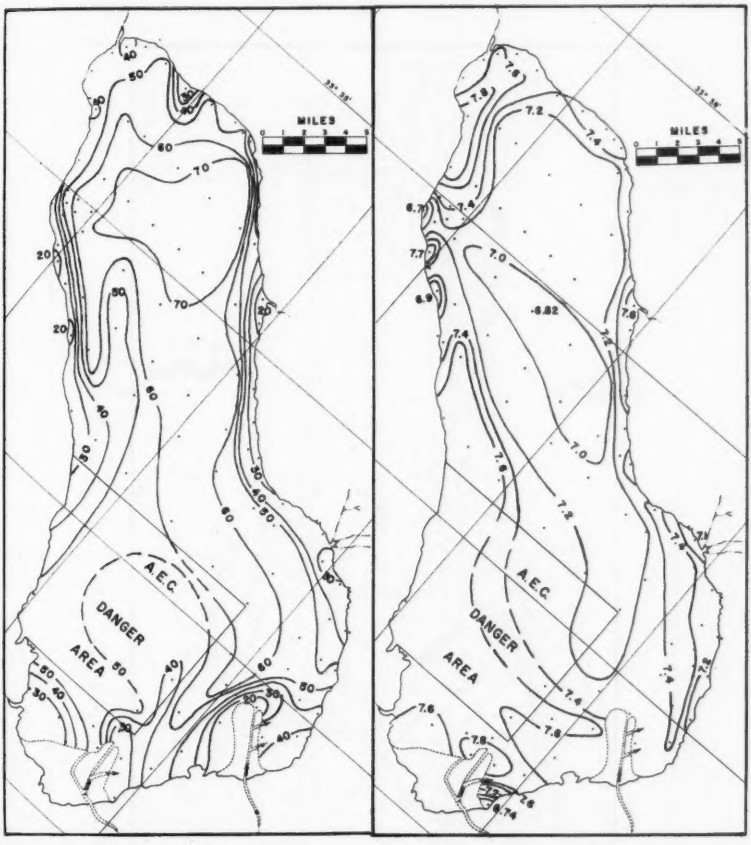

Figure 11. Left. Water content of the sediments expressed in percentage of wet weight. Right. pH of bottom sediments

Water Content

The water content of the sediment is, at least in part, related to the grain size of the material (Emery and Rittenberg, 1952); consequently, a similarity between the distribution of water content and that of the grain size is to be expected (Figs. 11 left, 13). The highest water content is found in the deepest lake sediments in which the grain size is less than 4 microns (clay size). In the part of the southern

region where the grain size lies also within the range of clay particles, the water content is only 50–60 per cent; this is due to a thin layer of "soupy" material representing recent deposition underlain by residual clay. The clay of the northern region within the 4- to 6-inch layer sampled is entirely of recent deposition; the residual clay of the southern part, which is more compacted, has a lower water content. Along the coast where the sediments are mostly fine sands, the water content is low. A tongue of low value, located southeast of Fish Spring,

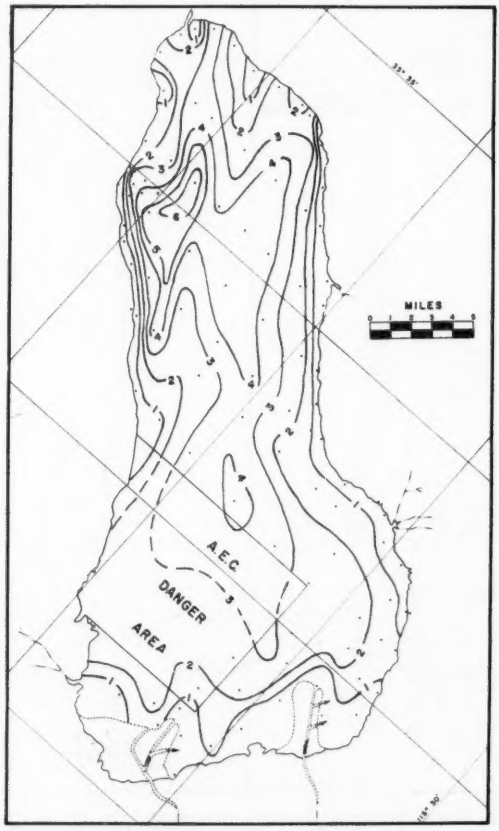

Figure 12. Percentage of organic matter in the sediments

Table 9. Per Cent Water Content of Sediments, Salton Sea

Station	Upper 2 inches	4–6 inches deep	Difference
80	59.90	59.60	0.30
81	62.70	60.60	2.10
82	67.60	64.50	3.10
83	64.80	60.70	3.10

is definitely related to a grain-size difference, which is also apparent on the map of the size distribution of the sediments.

The water content of the sediments diminishes rapidly with depth of burial; this is noticeable even in sediments within 6 inches from the surface. At a few stations where short cores were taken, the water content of the upper 2 inches of the core shows an appreciable

increase as compared to that of sediment 4–6 inches deep in the core. Table 9 summarizes some of the results.

At stations 80 to 81, to the south (Figs. 2, 11), the sediments show a smaller difference in water content than at stations 82 and 83 to the north, because of a different degree of compaction.

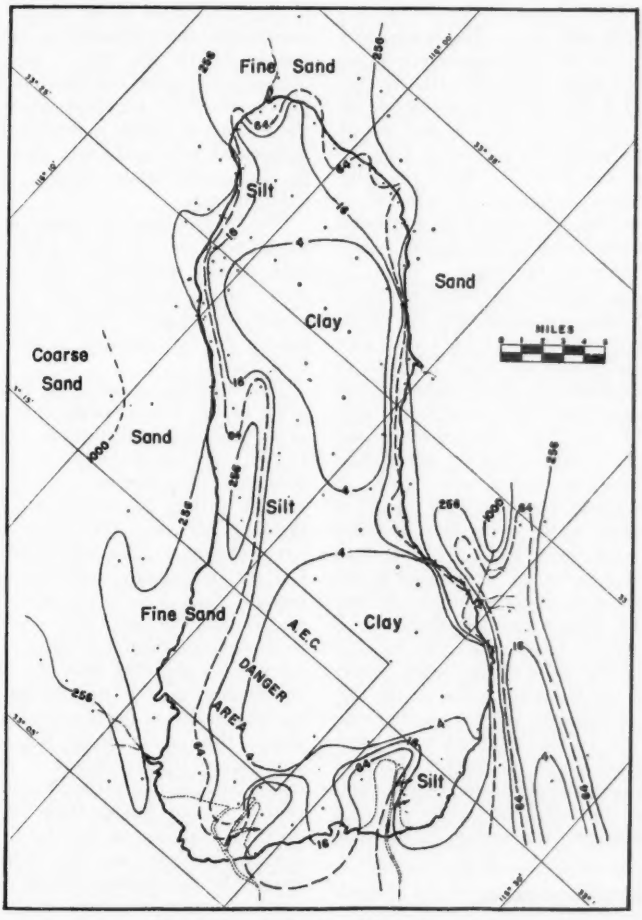

Figure 13. Grain size of the sediments

The pH of the Sediments

The pH of the sediments is regulated roughly by the content of carbon dioxide, although some other processes, such as chemical reactions between the different elements of the sediments and production of organic acids by decomposition of plant and animal organic matter, are involved. However, in most places the higher the CO_2 concentration the lower the pH. Inasmuch as carbon dioxide is produced during the decomposition of organic matter, there should be, therefore, a relationship between the amount of organic matter (Fig. 12) being decomposed and the pH (Fig. 11) of the sediment. This may be observed by comparing the distri-

bution of organic matter and that of the pH. In effect, most of the lower pH values are found in localities where the amount of organic matter is the highest in the sediments.

In sea water, at a pH below 7.6, the calcium carbonate of rocks is dissolved (Stevenson, 1954, Ph.D. thesis, Univ. Southern California). A similar phenomenon occurs at the surface of bottom sediments in the Salton Sea, but it takes place below a pH value of 7.2. This is witnessed by the etching on tests of Foraminifera within the sediments (Arnal, 1958, Pl. III, fig. 16; Pl. IV, fig. 17). Little etching is noticeable for pH values between 7.2 and 7.0, and strong etching occurs when the pH range falls between 7.0 and 6.8 (Fig. 21). Since the solubility of calcium carbonate is increased at lower temperatures, the period of maximum etching must occur during the winter, when the temperature is at a minimum.

At all stations, the pH of the overlying water is higher than that of the sediments. The difference ranges between 0.5 and 1.0 pH unit. This is in contradistinction to what happens in bottom marine sediments of the offshore basins of the California coast (Emery and Rittenberg, 1952, p. 771). To check the values of my observations, measurements of the pH of clear undisturbed bottom water were made in several instances and compared with the pH of muddy, disturbed water at the same stations. The muddy water always had a pH lower than that of the clear water. In the instance of the Salton Sea the problem is different from the one of the offshore marine basins in that there is apparently sufficient bacterial activity, in addition to the production of organic acids, always to counteract the buffering action of the carbonate and bicarbonate present in the sediments. Since the bottom water has a pH lower than the surface water but higher than the bottom sediments, the pH of the bottom water is apparently controlled largely by diffusion of acidic water from the surface of the sediments.

Organic Matter in the Sediments

Determination of the organic content of the sediments is usually obtained indirectly by measuring the weight percentage of an element present in quantity directly proportional to the total organic matter and multiplying by a conversion factor. The element measured in the present study was carbon (Allison, 1935), and the total amount of organic matter was derived by multiplying by 1.7, as recommended by Trask (1932, p. 89).

The original source of organic matter in the sediments is plant life, which in the Salton Sea is restricted to microscopic forms. As any animal life feeds more or less directly on plant life, the ultimate source of organic matter in the sediments is the phytoplankton. The organic content of the sediments depends, therefore, on the phytoplankton productivity of the waters of the Salton Sea. Carpelan (1955, unpublished report) found that the lowest productivity in the lake was 1.7 times that of the oceans during upwelling, which indicates a very high productivity for Salton Sea water. Hence, the amount of organic matter in the sediments is expected to be well above the average found in the oceans under similar conditions of sedimentation.

The distribution of organic matter in the Salton Sea (Fig. 12) shows a low organic content, usually less than 1 per cent along the shore; higher values, 4–6 per cent, are found in the central part, and a maximum of more than 6 per cent about 3 miles offshore near Fish Spring.

Two main factors influence the distribution of the organic content of the sediments: texture of the sediments and currents. The main cause for the influence of the texture on the organic content is the common effect of the currents on the settling of organic matter and sedimentary particles. Where the currents are strong enough to allow only the settling of sand and silt, few organic particles are deposited because they have a density only slightly greater than the water. The resulting action is to concentrate organic detritus in quiet places where clay particles only are deposited. A comparison of the distribution of organic matter and that of the currents (Fig. 9) demonstrates this point. Along the southern and southeastern coasts, where a wide zone of strong currents exists, the zone of little organic content extends farther from the coast than it does, for example, to the east where the currents are restricted to a narrow band along the shore. The zone of high organic content in the northern region is limited to the central part of the northern gyral in which the waters are very quiet. Comparison of the distribution of the organic content and the grain size of the sediments (Fig. 13) shows also a good correlation for the reasons previously stated.

Texture of the Sediments

Textural features of the sediments were determined by the use of settling methods after separating the samples, if necessary, in

fractions greater and smaller than 0.062 mm. Fractions greater than 62 microns were analyzed by means of Emery's Settling Tube (Emery, 1938); fractions smaller than 62 microns were analyzed by the standard pipette method. These two methods were used in preference to sieving and pipetting, because they were based on the same theoretical concepts and give more coherent results for samples containing a mixture of sand, silt, and clay.

The sediments are principally of a single type of deposition, and there exists a gradual basinward decrease in grain size (Fig. 13). The zones of the different sediment types are narrow along relatively steep bottom slopes, as along the eastern shore, and considerably wider along more gentle slopes, as in the northernmost and southernmost parts of the Salton Sea.

The first of three exceptions to the general trend in gradual decrease of particle size offshore is located along the western shore, just a little north of the A. E. C. danger area. The grain size of the sediment, which is in the medium sand range, is much larger than the grain size of the sediments at the same offshore distance farther north. This area is interpreted as the remnant of a submerged dune which was present before the flood of the Colorado River in 1905. Several lines of evidence support this idea: (1) there are many dunes in this region just a few miles to the west; (2) the direction of the wind in the surrounding region (Fig. 4) is such that the dunes would move eastward in the direction of the present Salton Sea; (3) the grain size is the same as that of the dunes farther west; (4) the sorting coefficient (2.4) is good; and (5) most of the quartz grains are frosted and well rounded.

The second area showing an anomaly in the decrease of grain size is the clay area in the southern half of the sea; it extends to the shore line, where sand should be expected. Clays are present because they are residual; they represent an older cycle of sedimentation before the existence of the present Salton Sea, as indicated by: (1) the lower water content and lower organic content, as discussed in the preceding chapters; (2) the presence close to the shore line of a small thickness of sand representing the present deposition; (3) the existence of strong currents which would prevent the actual deposition of clay except in the central part of this area (there is some deposition of clay there); and (4) the reddish chocolate color of the clay, which indicates long aerial oxidation and points to the nearby Chocolate Mountains as a rock source for the clays. These clays represent the continuation of the sediments at the foot of the Chocolate Mountains.

A third area showing a discrepant grain-size trend is located around station 159 (Fig. 10). The median diameter is more than 1.0 mm in the zone outside the lake in the eastern part of the map. The median diameter at station 159 is 2.7 mm; at station 158, to the east, it is 66 microns; at station 160, to the west, it is 38 microns. The slope is fairly gentle and regular toward the Salton Sea. The anomalous grain size at station 159 is attributed to the presence of an old shore-line deposit of receding Lake LeConte—*i.e.*, the large lake that occupied the present site of the Salton Sea in late Pleistocene or Recent time.

Field observations show that the sediments have a steep slope, about 30°, toward the west (*i.e.*, toward the lake) and a much more gentle slope, almost horizontal, eastward. The maximum thickness of the front of the old beach material is approximately 4 feet. The gravel part contains subangular fragments up to 1.5 inches long, and their long axes, although arranged in a somewhat disorderly fashion, remain parallel to the shore line; the median diameter, as already indicated, is large. Many gastropods of the fresh-water Lake LeConte are included in the sediments and were either living there or are reworked from lake deposits at the time the lake level was higher. Reworked Foraminifera typical of the Borrego formation, of late Pliocene or early Pleistocene age, are also included and were found as deep as 3 feet in the material.The rock fragments are of typical intrusive rocks, granite, granodiorite, diorite, and pegmatite, which are known to crop out in the Chocolate Mountains (Dibblee, 1954). Additional evidence of beach deposition is given by the presence, there and in the immediate surroundings, of rounded pebbles of pumice which were eroded from the Pumice Buttes, located at the south end of the present sea. The elevation of Pumice Buttes is about −125 feet, and the elevation of the old beach deposits of the recessional shore line is about −150 feet. The buttes, therefore, were protruding at least 25 feet out of the water at the time the recessional shore-line material was deposited. The pumice fragments, which are light enough to float, were transported by longshore currents and pushed ashore by wave action. They are most abundant in the southeastern part of the Salton Basin at an approximate elevation of −150 feet. Their abundance in the southeastern region suggests a current pattern for Lake LeConte similar

to the current pattern of the Salton Sea (counterclockwise).

Average median diameters were computed from the values obtained for each station. The average median diameter of sands is 170 microns, of silts 26 microns, and of clays 2.3 microns (Fig. 14). The average median diameter of the sediments of the Salton Sea is 92 microns. This value is slightly greater than that of the suspended load of the Colorado River (66 microns) computed from Sykes' analysis (1937). The latter, in turn, is coarser than the average median diameter of the sediments deposited in Lake Mead (42 microns) (Gould, 1954, p. 232).

The slight difference in median diameter between the suspended load of the Colorado River and the sediments of the Salton Sea suggests that the origin of the latter is mostly material transported by the Colorado River with a certain increment of sands and silts contributed by the Salton Basin. Yet, the sedimentary contribution of tributary streams in the Salton Sink has been relatively small, as it has affected the average median diameter of the sediments only by a few microns.

Insoluble Residues and Amount of Calcium Carbonate

From the foothills of the surrounding mountains toward the shore line, the amount of insoluble residues ranges from 98 per cent to 90 per cent (Fig. 15); the sands are nearly all quartz and feldspars. One exception along the southeastern shore occurs where the clay sediments derived from the erosion of the Chocolate Mountains extend across the shore line into the Salton Sea. The amount of insoluble residues in this area decreases to 70 per cent, because of the presence of abundant gastropod shells from Lake LeConte deposits and foraminiferal tests from the Borrego formation.

Two tongues of high percentages of insoluble residues extend northward from the mouths of the New and Alamo rivers; they are significant, as they indicate high clastic deposition from the rivers and also show the possible path of the river beds when the level of the lake was lower (as in 1925). Similar important clastic deposition, although to a smaller extent, is noticeable off the mouth of Whitewater Creek in the northern part of the Salton Sea.

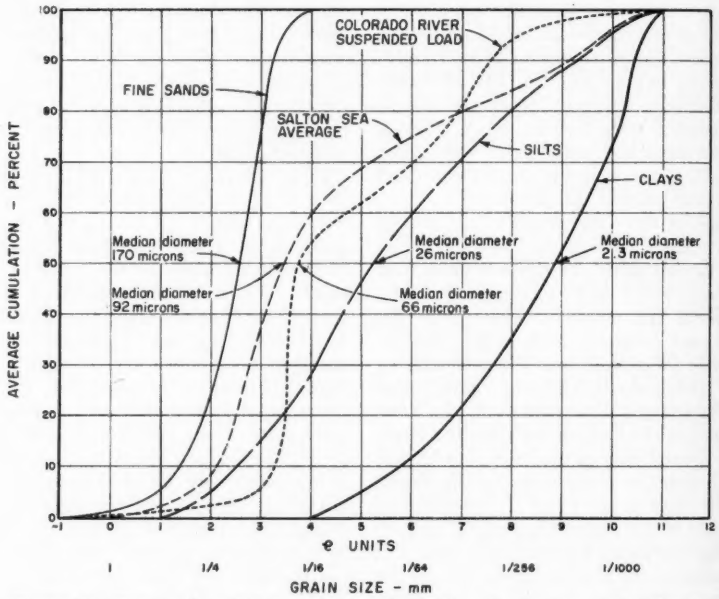

Figure 14. Texture data for fine sands, silts, clays, Salton Sea average, and Colorado River suspended load

Two zones of low percentages of insoluble residues (40 per cent and 60 per cent) occur along the western shore, and one of very low percentage (40 per cent) occurs along the northeastern shore. These are due to the presence of a great number of shells of *Balanus amphitrite saltonensis*, the subspecies of barnacle now thriving in the lake (Rogers, 1949).

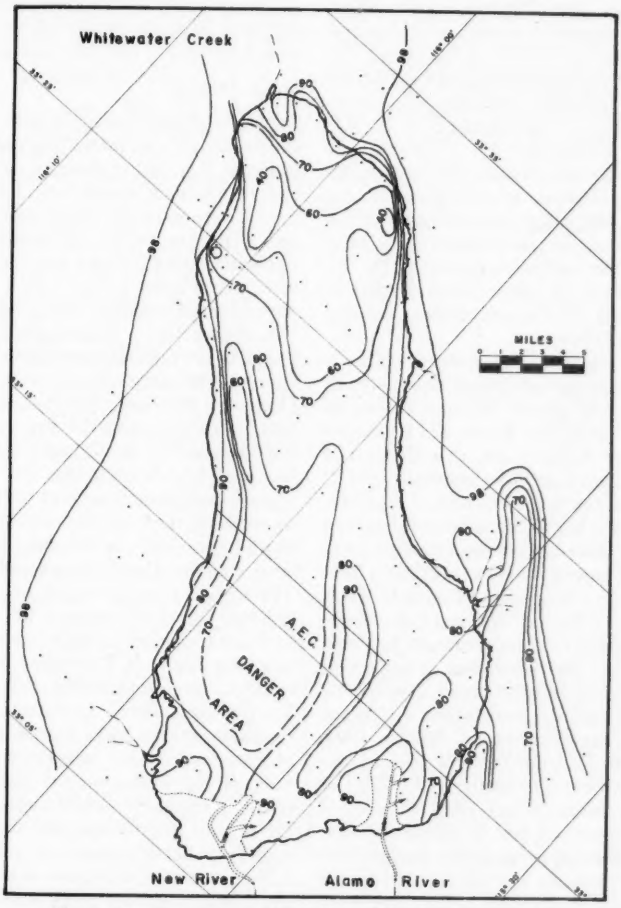

Figure 15. Percentage of insoluble residues in the sediments

The amount of insoluble residues generally decreases offshore—*i.e.*, the amount of calcium carbonate increases. This is doubtless due to a decrease in the rate of sedimentation of inorganic particles, and it explains the high percentage of calcium carbonate in the region of clay deposition in the northern part of the Salton Sea. In this area the rate of deposition of clastic particles is so slow that the shells or fragments of shells falling to the bottom, or the shells of organisms living there, are mixed only with a small amount of clastic material. The result is a high percentage of calcium carbonate in the sediments.

From the values of percentage of calcium carbonate measured at each station, average percentages for sands, silts, and clays were computed. The results indicate a weight of

calcium carbonate of 10.29 per cent for sands, 31.36 per cent for silts, and 29.52 per cent for clays. The 190,000 acre-feet of sediments deposited in the Salton Sea during the past 50 years (*see* Rate of Sedimentation) is composed of 60.32 per cent sands, 24.04 per cent silts, and 15.64 per cent clays (Fig. 14). Using these values and the respective percentage of calcium carbonate in each category, I calculated the average weight percentage of calcium carbonate in Salton Sea sediments and obtained a value of 18.60 per cent. Using Gould (1954, p. 301) estimates on specific gravity, I obtained an average of 1.65 for Salton Sea sediments. Knowing the volume, specific gravity, and weight percentage of calcium carbonate in the sediments permits the computation of the total weight of calcium carbonate present in the deposits laid down in the Salton Sea in the past 50 years. The results of the computation indicate a total of 71,430,000 tons.

Another approach to the problem makes it possible to check the validity of this result, or at least to learn if it is of the proper order of magnitude. Most of the Salton Sea sediments are of Colorado River origin. (*See* Texture of the Sediments and Rate of Sedimentation.) The contribution of the suspended load of the Colorado River to the Salton Sea sediments has been estimated (*see* Rate of Sedimentation) at 140,000 acre-feet. An analysis by Sykes (1937) indicated that 10 per cent of the Colorado River suspended load is calcium carbonate; *i.e.*, about 30,860,000 tons of calcium carbonate has been transported into the Salton Sea as suspended load in the water. In 1955 about 150,000,000 acre-feet of water had flowed into the Salton Sea since the beginning of the flood in 1905, carrying about 29,210,000 tons of calcium carbonate in solution. The analysis of 1955 (*see* Salt Budget) indicates that 1,874,000 tons of calcium carbonate was still in solution at that time. The difference between the amount carried and the amount still in solution equals 27,336,000 tons which must either have been precipitated or withdrawn from the water by barnacles and Foraminifera and finally deposited in the sediments at the death of these organisms. The total contribution of calcium carbonate from suspension and solution in Colorado River water reaches, therefore, a total of 58,196,000 tons. To this amount must be added the calcium carbonate content of the 50,000 acre-feet of sediments contributed by the Salton Basin. The weight of these sediments represents 112,215,000 tons. Assuming a percentage of calcium carbonate equal to the average of the Salton Sea sands (10.29 per cent), the weight of calcium carbonate in these sediments is 11,547,000 tons. The grand total of calcium carbonate obtained by this second method is 69,743,000 tons. It is only 2 per cent lower than the value obtained by the first method. The remarkable similarity between the two estimates computed from two entirely different methods is striking.

Heavy Minerals

The weight percentage of heavy minerals in the sediments is an interesting characteristic to study, as it furnishes some important information on the rock source from which the sediments were derived. Heavy-mineral percentages were obtained by the standard procedure but without preliminary treatment with a dilute acid in order to avoid the destruction of such minerals as calcite and apatite.

In Figure 16, no isopleth curves of distribution of heavy minerals were drawn, as the values appear to be scattered somewhat haphazardly. However, they were grouped in six different areas, as there seems to be a regional pattern of distribution. The longitudinal axis of the basin was used as a dividing line, and the different regions were given numbers I to III, from north to south on the west side, and IV to VI, from south to north on the east side. Average values were computed and characterize each region. The high percentage found in region I is attributed to the proximity of the metasedimentary rocks (mica schists and gneisses) which crop out north of Travertine Rock, as indicated on the geological map of the Imperial Valley (Dibblee, 1954). Upon weathering, these metasedimentary rocks furnish large amounts of micas and opaque minerals which form the bulk of the heavy-mineral fraction. Farther south, in regions II and III, only sands and clay are present in outcrops, and the average percentage of heavy minerals decreases sharply to 2.5–3 per cent. On the east side, in region IV, the granitic intrusive rocks of the fairly distant Chocolate Mountains furnish a relatively low percentage of heavy minerals, about 4 per cent. In region V, the source rocks are even more distant, and the percentage of heavy minerals decreases to 2.5 per cent. In region VI, the Orocopia schists contain a large amount of mica and yield a greater amount of heavy minerals, whose percentage increases to 6.5 per cent.

Within each region along the lines of maximum slope, which are distributed in a radial pattern around the lake, the percentage of

heavy minerals is small on the foothills, increases to a maximum, then decreases again close to the shore of the Salton Sea. Within the Salton Sea proper a concentration of micas (mostly biotite) occurs where the absence of currents permits the mica flakes to settle to the bottom. A good example is found along the northernmost part of the lake, where the highest percentages of heavy minerals were found.

Mineralogy of the Sediments

In all sediments, quartz and plagioclases are the dominant minerals. Micas, mostly biotite and lepidomelane, are important, as are green hornblende, chlorite, calcite, magnetite, hematite, ilmenite, and muscovite in respective order. Rare constituents are represented by apatite, garnet, zircon, titanite, kyanite, and in one sample some orthoclase.

The different regions defined in the study of heavy minerals are also characterized by different mineral suites. The minerals present in the six regions are listed in Table 10.

In zones I and III the ratio of quartz to plagioclase is less than one, whereas, in the other zones, it is well above one. This probably indi-

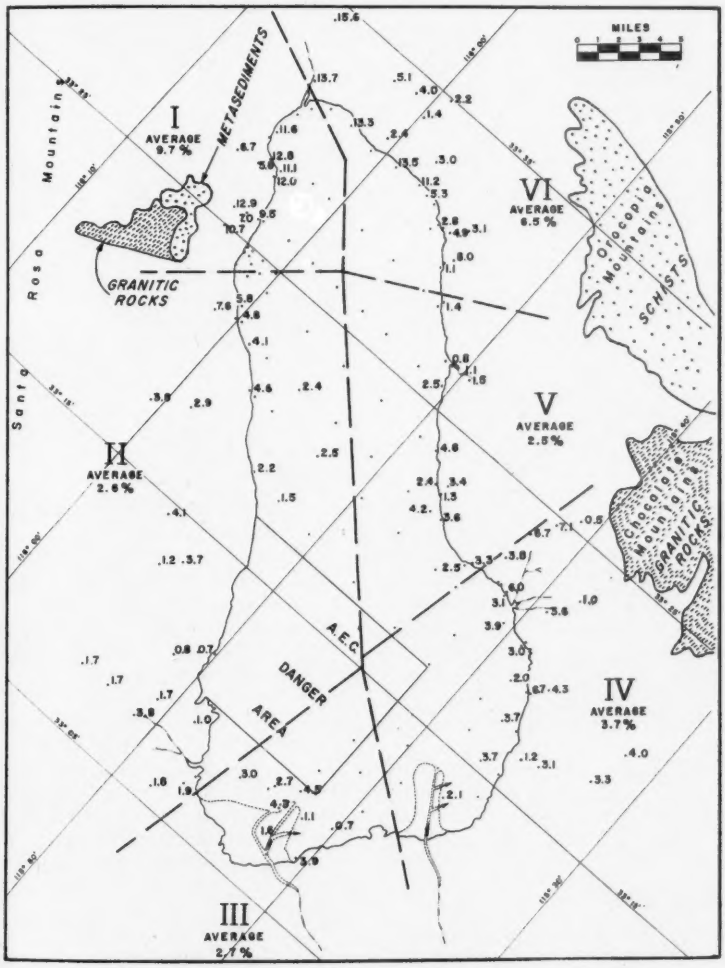

Figure 16. Percentage of heavy minerals in the sediments

cates that the intrusive source rocks on the west side are more basic than those on the east side of the Salton Sea. The greater concentration of quartz in zone II may be due to the disintegration of plagioclases during transportation, with a subsequent increase in percentage of quartz. Orthoclase present in zone IV doubtless has its origin in some pegmatitic vein or acid intrusive rock of the Chocolate Mountains (Fig. 16). Zircon in the same zone is unusually abundant, although it represents only a very small percentage. Its presence also suggests that the composition of the intrusive rocks of the Chocolate Mountains is more acidic than that of the rocks of the western side of the Salton Sea. Kyanite is present in the sediments of zone V; this points to a source in the metamorphic rocks (mica schists) of the Orocopia Mountains. Farther north, in zone VI, the same mica schists have furnished abundant muscovite flakes in the sediments.

Table 10. Mineralogical Composition of Sediments, Salton Sea
imp.—important constituent; pres.—present; rel. ab.—relatively abundant

Minerals	Regions					
	I	II	III	IV	V	VI
Quartz plagioclase ratio	31/61	81/19	35/65	75/25	77/23	77/23
Orthoclase				pres.		
Per cent of heavy minerals	9.7	2.6	2.7	3.7	2.5	6.5
Biotite	imp.	imp.	imp.	imp.	imp.	imp.
Lepidomelane	imp.	imp.	imp.	imp.	imp.	imp.
Calcite	imp.	imp.	imp.	imp.	imp.	imp.
Muscovite		imp.				imp.
Chlorite	imp.	imp.			imp.	
Vermiculite	imp.					
Green hornblende	imp.	imp.	imp.	imp.	imp.	mp.
Apatite	pres.	pres.	pres.	pres.	pres.	pres.
Titanite			pres.			
Garnet	pres.	pres.		pres.	pres.	
Zircon		pres.	pres.	rel.ab.	pres.	pres.
Kyanite					pres.	
Opaque in per cent of total (magnetite, hematite, ilmenite)	2.1	0.7	0.8	1.66	1.10	2.0

The mineralogy of the sediments in the Salton Sea and vicinity is in agreement with the geology of the surrounding region and indicates that some of the lake sediments have a local origin.

Rate of Sedimentation

Comparison of the topographic contour lines of the U. S. Geological Survey (1928) reconnaissance map and that of the present contours gives an idea of the rate of sedimentation within the deltas of the New and Alamo rivers (Fig. 3). The shore line in that region (approximate elevation is −235 feet) is represented in Figure 3 by a dashed line and crosses the old −240 contour in several places. At least 5 feet of sediments, and possibly more, must have been deposited in the area during the past 30 years to produce these changes in the position of the topographic contours; this equals a rate of sedimentation of approximately 2 inches per year at the mouths of the rivers.

Further information was gained by examination of short cores from the bottom of the lake. A core 15 inches long was recovered from the eastern side of the New River delta; the upper 9 inches of the core was dark-gray silty clay and the lower part a much lighter-gray silty clay; the change of color occurs within 2–3 mm. The lower part of the core probably represents deposition before the flood of the Colorado River in 1905, because the lighter color is probably due to oxidation when the sediments were exposed to the air. Sedimentation of the upper 9 inches must have occurred during the past 50 years; this would represent a rate of sedimentation of approximately a sixth of an inch per year.

Other small cores were taken in the central part of the sea, but there was no change which would suggest a break in the deposition of the

sediments. However, at several stations inside the −275 contour, the sediments within 1–1½ inches of the surface contained fragments of a crust of gypsum which undoubtedly represents remains of the salina that existed in the lowest part of the Salton Sink before the 1905 flood. Sediments deposited atop the crust of gypsum represent the deposition of the past 50 years in this area; there, the rate of sedimentation must have averaged 2–3 hundredths of an inch per year.

Additional information about the rate of sedimentation may be obtained by considering the ratio of living to total Foraminifera (Myers, 1942; Walton, 1955, p. 998). In places of rapid sedimentation, the Foraminifera as they die are buried in the sediments, and most or all of the Foraminifera present at the surface of the sediments are living. In places of low rate of deposition, the Foraminifera as they die are not buried, and most or all of the Foraminifera present at the surface of the sediments are dead. If the living individuals are stained with an organic dye at the time of collection, the ratio of living to total Foraminifera may be computed, and an index of the relative rates of sedimentation is obtained.

To check this method, the ratio of living to total Foraminifera was computed for a short profile, stations 55 and 60–62 (Fig. 2). Samples from these stations were collected on the same day, so that seasonal variation in productivity would not affect the different percentages. The percentage of living to total Foraminifera at station 55 is 1.6 per cent, at station 60, 6.1 per cent, at station 61, 19 per cent, and at station 62, 43 per cent. According to these different percentages, about 25 times more sediment is deposited close to shore than in the greater depths of the lake. This index is not an exact representation of the different rates of sedimentation in the lake, but it does give their order of magnitude. It is in good agreement with the rates of sedimentation mentioned above: station 61 (silt) had a rate of sedimentation 10–12 times as great as station 55 (clay), according to the foraminiferal estimate, and 7–10 times as much, according to measured estimates outlined in the preceding paragraphs. Assuming, then, that the relative rates of sedimentation based on foraminiferal estimates are of the correct order of magnitude, the rate of sedimentation for sand along the shore line should be 25 times that of clay, or 0.6 inch per year.

Another approach to this problem is to compute first the amount of sediments that were deposited in the Salton Sea during the past 50 years, using the above-mentioned rates of sedimentation, and then compare this amount with that of the sediments transported by the Colorado River water during the same time. The values obtained should be of the same order of magnitude, but that of the Salton Sea should be greater in order to account for sediments contributed by the surrounding mountains in the Salton Basin.

From planimeter measurements in Figure 13, the area of sand was found to be 46,600 acres; that of silt, 97,500 acres; and that of clay, 99,200 acres. Using the annual rates of sedimentation mentioned in preceding paragraphs, I determined that 2290 acre-feet of sand, 913 acre-feet of silt, and 594 acre-feet of clay are deposited annually, or a total of 3800 acre-feet per year for the whole Salton Sea.

The contribution of Colorado River water during the same period is based on estimates given by Thomas, Gould, and Langbein (1954) for the period 1897–1948, which most closely approximates the period of existence of the Salton Sea. They cited the following average values: average annual flow of the Colorado River, 14,700,000 acre-feet; average annual suspended load, 210,000,000 tons at the Grand Canyon station. However, they stated that the load of the River at Yuma, Arizona, is only 38–76 per cent, or an average of 60 per cent of the amount passing at the Grand Canyon station. This yields an average load of approximately 130,000,000 tons at Yuma, which is the closest station to the intake of the All American Canal.

From the beginning of the Colorado River flood in the Salton Sea in 1905, to 1934, the amount of runoff water of Colorado River origin that flowed into the lake was 35,500,000 acre-feet. This quantity of water must have carried 280,000,000 tons of sediments into the Salton Sea. The volume of these sediments having a specific gravity of 1.63 is 140,000 acre-feet. Since 1934, practically all the suspended load of the Colorado River has been retained in the Lake Mead reservoir because of the presence of Hoover Dam, and the load of the Colorado River downstream from Lake Mead is thereafter considered negligible.

A total of 140,000 acre-feet of sediments has, therefore, been contributed by the Colorado River to the Salton Sea during the period 1905–1955. This makes an average of 2800 acre-feet per year, which is about 26 per cent lower than the 3800 acre-feet annual average for the Salton

Sea. Thus, about three-fourths of the Salton Sea sediments have been contributed by the Colorado River, and one-fourth represents the sediments contributed to the lake from the Salton Basin. The contribution of the Salton Basin during the past 50 years must have been approximately 50,000 acre-feet. The over-all rate of sedimentation for the Salton Sea can be calculated from the preceding estimates at 0.20 inch per year, of which 0.15 inch was contributed by the Colorado River.

MICROORGANISMS

General Considerations

Comparison of the frequency distribution of species with certain physical factors permits the evaluation of the influence of these factors upon the composition of the populations. Emphasis is placed on the study of the Foraminifera, as they are the microscopic forms of most interest to the geologist. Conclusions as to the influence of ecologic factors on living Foraminifera may be applied to fossil faunas. This is especially interesting in view of the fact that the Salton Sea is an inland body of water, and also because records of Foraminifera living in inland waters are very rare. The only notable exception is the report of Gautier-Lievre (1935), who described several arenaceous and calcareous species living in brackish waters of the Sahara Desert. These waters also are slightly below sea level (almost 60 feet) and range from almost fresh to highly saline waters at localities where the salts are concentrated through intense evaporation. The fauna comprises some arenaceous species, several Miliolidae, and the genera *Nonion*, *Anomalina*, and *Cibicides*, represented by one or several species. The fauna of the Salton Sea is similar in many respects.

Previous Work

Cockerell (1945, p. 55) first reported the presence of Foraminifera in the Salton Sea. Subsequently, Hubbs and Miller (1948) also mentioned their presence. Rogers (1949) described a new subspecies of barnacle from the Salton Sea and gave a list of Foraminifera found in a dredge sample from the west end of the sea. He added the following comments:

> "The large number of specimens and the diversity of the species indicate that the Foraminifera were living and propagating in the sea itself rather than having been introduced into the lake sediments from adjacent marine beds. . . . As might be expected, the most abundant species are of genera known to possess a wide range of tolerance in temperature and salinity, such as *Rotalia*, *Elphidium*, and *Quinqueloculina*. . . . Definite indications of physical abnormalities resulting from the restricted environment are suggested in the many malformed tests, the variation in size and the stunted appearance in general."

In 1954 I presented a preliminary report on the sediments and Foraminifera of the lake and discussed some physical characteristics of the water as well as information on the living foraminiferal fauna. More recently a taxonomic paper was published (Arnal, 1958) describing the method of study of the foraminiferal fauna and the different species encountered; in the same paper a tabulation of the percentage distribution of the Foraminifera at the different stations (same stations as shown in Figure 2 in this paper) was presented. Finally, scientists at the University of California Salton Sea Laboratory are completing a study of the phytoplankton and other faunal elements of the lake (Carpelan, 1954, unpublished report; 1955, unpublished report).

Foraminifera

General features. In cross section, the bottom of the Salton Sea slopes smoothly from the shore toward the central part. The depth increases rapidly at first and then becomes more constant; the bottom is almost horizontal near the center. As a result of this type of bottom profile, rapid variations in the fauna can be anticipated close to shore, whereas faunal homogeneity should occur in the central region. Three main environments were therefore detected. A coastal environment occurred from the shore of the main body of water to 2–4 miles offshore. A central environment was recognized in the central part of the sea. Finally, a deltaic marsh environment was found near the southerly end of the lake in the marshes of the New and Alamo river deltas. Each environment is characterized by a distinct fauna, yet some species are found at all stations.

In the frequency counts (Arnal, 1958, p. 36) it was apparent at once that the number of species in each sample would never be large. The maximum number found was 13 species. In most places 3–5 species, and in some places only 2 species, represent 80 per cent of the total population. It is also immediately obvious that the fauna is restricted in number of species, because the species present must have a considerable tolerance toward highly variable ecologic conditions. This is supported by the following

(1) the bottom temperature may range during the year from 12° C. to 31° C., a range of almost 20° C.; (2) the pH of bottom water ranges between 7.34 and 8.41; (3) the range of pH for bottom sediment is 6.74 to 7.96; (4) the chlorinity of bottom water ranges from 13.4 o/oo to 14.2 o/oo; and (5) there is a large variation in the grain size of the sediments. The pH of the sediments appears to be the most important factor influencing the distribution of the fauna of the Salton Sea.

Percentage distribution of the main species. The distribution of *Streblus tepidus* (Fig. 17) shows four zones of abundance. The zone of less than 25 per cent is restricted along certain parts of the coast, mostly in places where less saline waters reach the bottom of the lake. Perhaps this species is sensitive to rapid variation of salinity and prefers the homogeneous conditions found in the central region where it makes up more than 75 per cent of the fauna. Another reasonable explanation is that *Streblus tepidus* is an extremely poor competitor with other species and thrives only in places where lack of competition enables it to do so.

Elphidium tumidum, the second most important species is most abundant along the shore (Fig. 17); this suggests that the species is a littoral form, a characteristic common to all the species of that genus. The zone of high percentage in the central northern portion of the lake is puzzling. It may be explained, perhaps, by displacement during storms, especially since no living Foraminifera were found in most of this area.

The next most important species, *Quinqueloculina bellatula*, also appears to be a littoral form (Fig. 17). The greatest densities are located close to the shore and also, perhaps, in areas where less saline waters reach the bottom. The less saline water brings a greater amount of nutrients and of phytoplankton, on which this species may live.

Similarly, and in an even more striking manner, the distribution of *Buliminella elegantissima* (Fig. 17) illustrates the dependency of that species on food related to an abundance of nutrients. This is well indicated by the positions of areas of great abundance of *Buliminella elegantissima* which coincide with the localities where less saline water of New River, Alamo River, and perhaps a combination of both, reaches the bottom of the sea by mixing due to current action.

Bolivina striatula (Fig. 18) is the last of the five important species which form most of the fauna of the Salton Sea. This species has its peak abundance at intermediate depth. It characterizes the deeper zone of the coastal facies and permits a subdivision of this environment. *Bolivina striatula* does not seem to be influenced by the zones of large quantities of nutrients coming from the different streams, as there is no special abundance of that species in these regions.

Distribution of the hyaline, porcellaneous, and arenaceous groups. The distribution of the hyaline benthonic species (Fig. 18) is regulated by the distribution of *Streblus tepidus*, which is the most important species of that group. In the central region, the group represents more than 90 per cent of the fauna, and there is a general decrease toward the coast where most values are less than 70 per cent. The spacing of the isobath curves (Fig. 3) is very similar to the distribution pattern of the hyaline group, and a correlation between depth and amount of hyaline Foraminifera should be made. This does not mean, however, that depth is the only factor influencing the distribution of that group of Foraminifera, as depth regulates also several other physical factors. Currents, too, may affect the distribution of this group, for the bulge of less saline water shown in Figure 6 closely duplicates the band of low percentage values of hyaline species found a little offshore of the southeastern coast. There the currents are important, since they bring a greater amount of plant food. This might be a confirmation of the suggestion that *Streblus tepidus* is a poor competitor with other species.

The distribution of porcellaneous Foraminifera (Fig. 18) contrasts markedly with that of the preceding group. None is found in the central region. Their percentage increases gradually toward the shore, and patches of high values (30 per cent and more) are found in regions where there is an inflow of fresh water. Whether they are more tolerant to a wide range of salinity, or are strongly dependent on phytoplankton, remains to be discovered. However, the latter is more probable, as the range in salinity is narrowed to small variations on the bottom of the sea where porcellaneous Foraminifera are living. The band of low percentages of hyaline Foraminifera in the southeastern part of the Salton Sea is replaced by a zone of high values of porcellaneous Foraminifera, perhaps successful competitors with *Streblus tepidus* and allied species.

The distribution of arenaceous Foraminifera (Fig. 18) is restricted to areas where they are

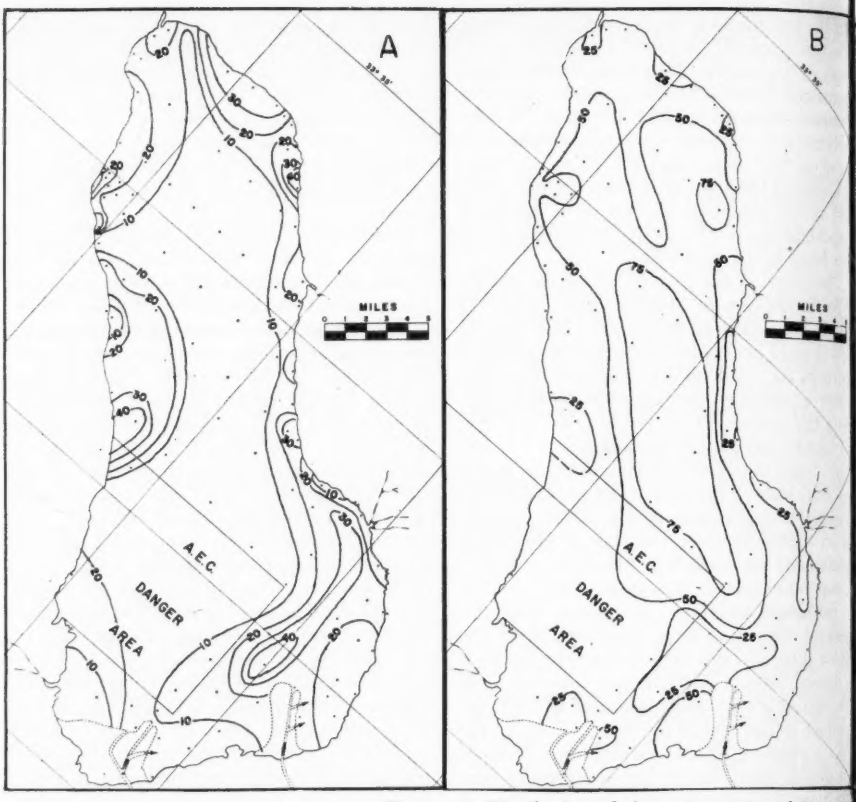

Figure 17. Distribution of the main species of Foramini fauna for *Quinqueloculina bellatula* (A), *Streblus tepidus*

able to obtain the material necessary to build their tests. They do not appear to be influenced by low salinity. Their highest percentage was recorded at two stations located on New River. They are absent where the bottom sediments are composed predominantly of clay-sized particles. Here again, the size of the sediment should not be taken as a preponderant factor, for the group is well known for its ability to gather widely spaced particles of clastic material for use in building its tests. However, there is a definite range in the size of the particles used; and if the preferred size is not present in the sediments, the test will, nevertheless, be built with a different size of particles (Salma, 1954). In the present instance, the pH of the sediments, which is generally higher where arenaceous species are present, may be of greater importance.

Figure 18 shows maps of each separate group; however, a better general perspective of the interrelationships of the different groups may be observed on a tridimensional presentation of the results (Fig. 19). The general distribution of the different categories can be readily ascertained. All the profiles show a maximum abundance of hyaline species in the central part and a decrease toward the shore. The reverse condition is observed for the porcellaneous group, which has its maximum percentage along the shore, whereas none exists in the center. Arenaceous species always represent a small percentage in the rare localities where they occur, mostly close to the coast.

Examples of typical distribution along profiles. Profile P4–P'4 typical of the general conditions over the main body of water shows that: (1) species decrease in abundance and number in an

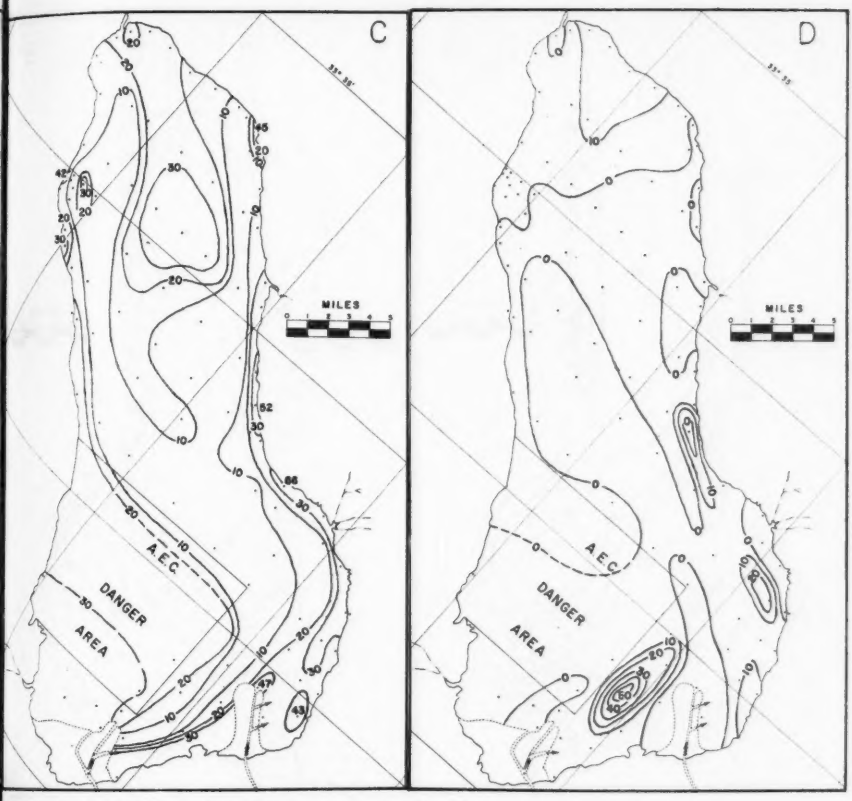

bers on the isopleth lines show the percentage of the total
idium tumidum (C), and *Buliminella elegantissima* (D)

offshore direction; (2) *Bolivina striatula* is not present close to shore, becomes abundant in depths of about 30 feet, and disappears at greater depths in the center of the lake; and (3) *Streblus tepidus* is present all along the profile, has its maximum abundance in the center, and seems to decrease in abundance more rapidly along steep bottom slopes, as on the east side of the profile (Fig. 20).

Profile P9–P'9 is representative of conditions existing around the deltas of New River and Alamo River. The western part of the profile, at station 4, illustrates conditions occurring in the delta and in surrounding marshes. Arenaceous Foraminifera show a great abundance, especially *Ammobaculites salsus*. The profile differs from the preceding one by having about equal percentages of *Streblus tepidus* (usually less than 40 per cent) and *Elphidium tumidum* (20–50 per cent). Typical species existing around river mouths are *Quinqueloculina bellatula* and *Buliminella elegantissima*, which make up approximately the same percentage along the entire profile, for they find optimum conditions within the depth range encountered along this traverse. *Bolivina striatula* begins to constitute an appreciable percentage of the fauna at a depth of approximately 10 feet, but its optimum depth is 30 feet. *Quinqueloculina rhodiensis*, *Quinqueloculina rhodiensis* var. *incondita*, and *Quinqueloculina subdecorata* are present only at intermediate depth, approximately 10–20 feet (Fig. 20).

Relationships between ecologic factors and distribution of species. In frequency graphs such as the ones just presented, the results are shown in succession as they occur in the field. To emphasize trends that may be hidden by the

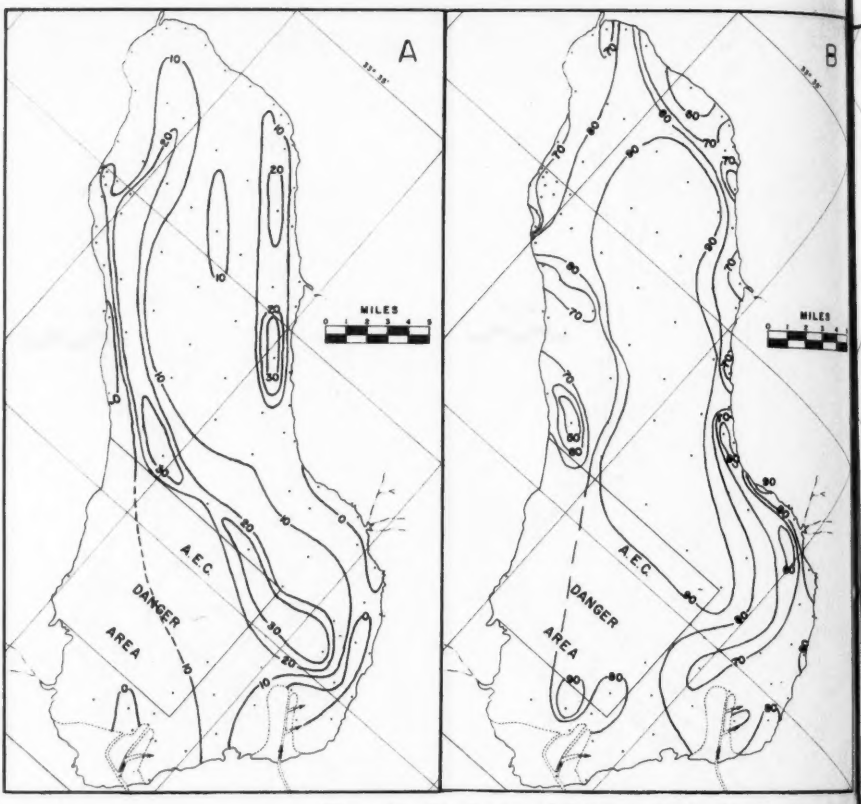

Figure 18. Distribution of *Bolivina striatula*. Distribution of the lines show the percentage of the total for *Bolivina striatula* (A).

irregularities of some factors, it is interesting to plot "a composite picture of the frequency distribution in the absence of complicating factors associated with slope reversal etc. . . ." (Bandy, 1954, p. 126). Such a composite picture is presented in Figure 21, where frequency distribution was plotted against regularly increasing depth, regardless of station location in the lake. Ecologic factors such as chlorinity of bottom water, temperature of bottom water, pH of the sediments, and grain size of the sediments were plotted in the same figure to show other possible trends. The foraminiferal number and the number of species were also added for comparison. In the composite picture, 27 stations were arranged in order of increasing depth from 1½ feet to 41 feet (maximum depth of the lake). Although some irregularities occur in the distribution of the percentages, the figure shows a continuous variation from the shallower to the deeper part. Most species decrease in abundance as the depth increases, except *Streblus tepidus*, *Elphidium tumidum*, and *Bolivina striatula* which follow the distribution pattern explained in preceding paragraphs.

Some factors follow the trend shown for depth, whereas others are erratic. The chlorinity of the bottom water ranges from 13.50 o/oo to 14.00 o/oo but does not increase with depth. The temperature of bottom water is generally greater at the deep stations, but this is due to seasonal variation and is not related to depth. The grain size decreases regularly with deeper water, as is the case when sediments are of a single type of deposition. The pH of the sediments also decreases in a fairly regular manner with increasing depth. This factor is probably very important by reason of its effects on both living

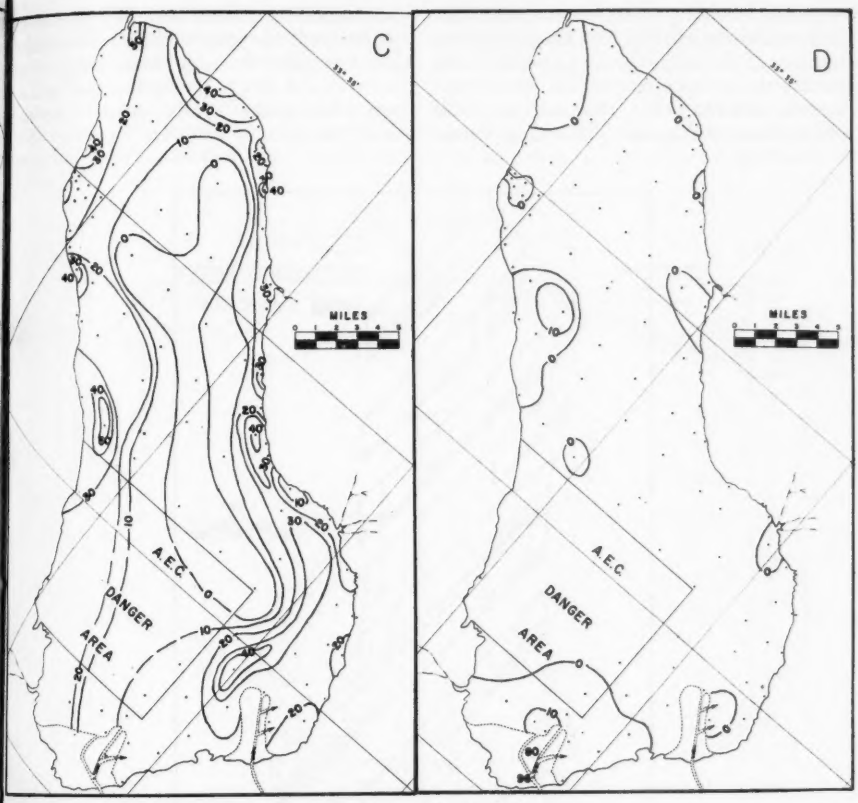

e, porcellaneous, and arenaceous groups. Numbers on the isopleth
e group (B), porcellaneous group (C), and arenaceous group (D)

and dead populations. On the living population it might be an intolerable factor, as very few Foraminifera are living in areas where the pH of the sediment is very low. On the dead population it is also very important, as this factor is responsible for the diagenetic disappearance of foraminiferal tests in certain sediments in which they had been deposited. This may be the reason why Foraminifera are not found in sediments in which all other conditions (besides pH) would lead one to expect their presence. This question of the disappearance of Foraminifera in sediments of low pH is supported by evidence observed on their tests. In the present study, Foraminifera in surface sediments collected in a depth of water greater than 20 feet show etching in variable degree. From 20 to approximately 30 feet of water depth, etching of the tests in surface sediments is not very pronounced and does not occur on all tests. Below a depth of about 30 feet of water, etching is very pronounced and is present on most of the tests found in surface sediments. In some specimens, especially of *Streblus tepidus* (Arnal, 1958, Pl. 4, fig. 17), the only part of the last whorl remaining after dissolution is the sutural zone where the test is thicker. Undoubtedly as a result of diagenetic dissolution of the tests, and also because fewer Foraminifera are present, the foraminiferal number shows a marked decrease at stations where the pH of the sediments is low. This decrease is especially pronounced for a pH below 7.20. The number of species also shows a more or less progressive decrease with increasing depth, in contrast to what usually happens in shallow water along the ocean coast.

For individual species, trends in percentage

variations according to depth are better visualized on a histogram (Fig. 22). The average percentages of the species present at most of the stations have been plotted for each 5-foot interval from 0 to 45 feet. The trends are readily observed on the diagrams. The average foraminiferal number for the same depth intervals was added to the figure to give an idea of the variation of population density with increasing depth. The marked break at a depth of about 20 feet, discussed in preceding paragraphs, shows on the diagram in spectacular fashion.

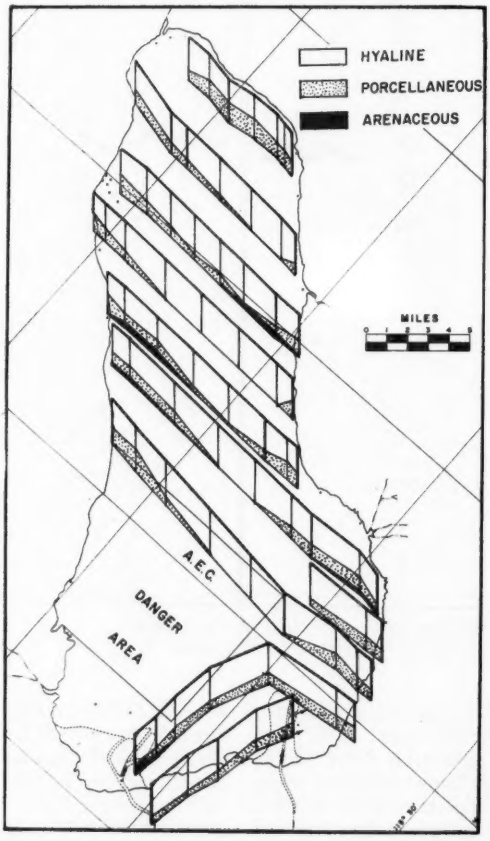

Figure 19. Distribution of the different categories of Foraminifera

Foraminiferal biofacies. No planktonic Foraminifera have been found in the Salton Sea. The following discussion refers, therefore, to benthonic Foraminifera only. Several facies are represented; the coastal facies are separated into two parts, the inner coastal facies and the outer coastal facies. The species and percentages characteristic of the different environments are listed in Table 11.

INNER COASTAL FACIES: This facies extends from the coast to an offshore distance of 1–2 miles, in water 0 to about 20 feet deep.

OUTER COASTAL FACIES: This environment usually occurs from 1 or 2 miles to about 4 miles offshore, in a depth of 20–30 feet of water. Several of the minor representative species of the preceding facies are still present but with a different percentage of abundance. This facies is

characterized by the appearance of *Calcituba simplex* and a few *Textularia earlandi*, but the much higher percentage of *Bolivina striatula* is especially characteristic.

CENTRAL FACIES: The foraminiferal assemblage characteristic of this facies occurs only in water depth greater than 30 feet; the number of species is very restricted, and the abundance of specimens is markedly less than that of the coastal facies.

DELTAIC FACIES: Arenaceous species are abundant especially in the river beds and surrounding marshes. Among the other species, *Streblus tepidus* occurs with an abundance of

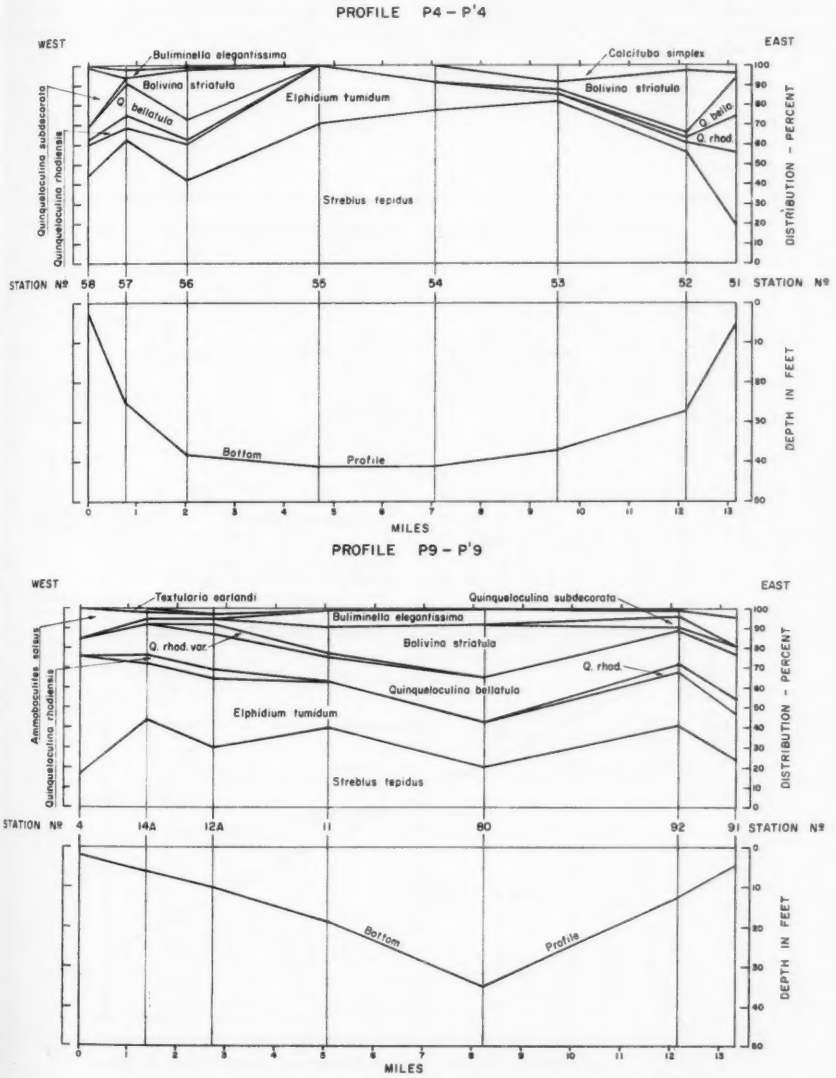

Figure 20. Frequency distribution along profile P4–P'4 and P9–P'9

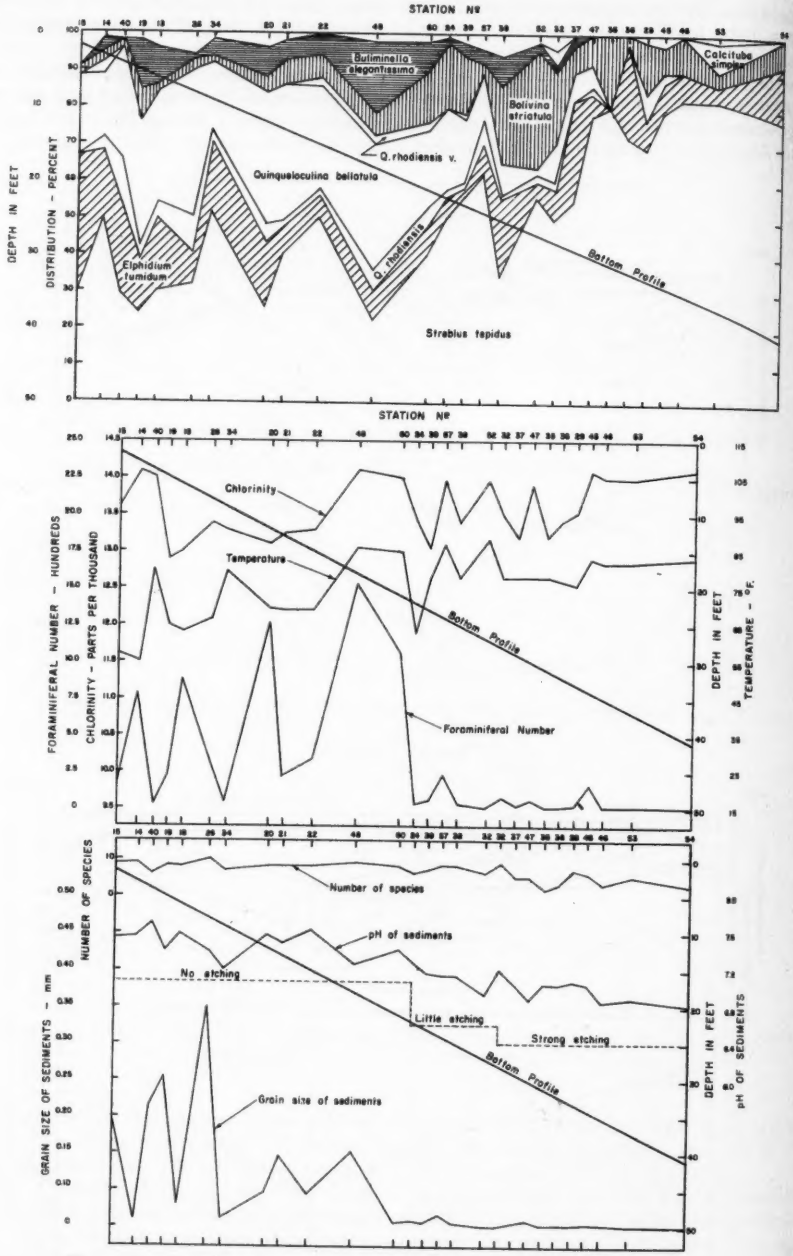

Figure 21. Relationships between ecologic factors and distribution of species

less than 40 per cent; other species have about the same percentages as in the inner coastal facies.

Abnormal Foraminifera. Several writers have attributed significance to physical abnormalities among Foraminifera. Le Calvez and Le Calvez (1951) mentioned a high degree of irregularity in the arrangement of the chambers of species of *Quinqueloculina* found in littoral ponds along the Mediterranean Coast of France. Abnormal specimens in that area are related to confined waters only sporadically in communication with sea water. Rogers (1949) noticed physical abnormalities and malformed tests in Salton Sea Foraminifera which he attributed to the restricted environment. Easom (1954, unpublished report), in a study of the Playa del Rey Lagoon in Southern California, noted the presence of abnormal Foraminifera which composed as much as 2 per cent of the fauna. The water of the lagoon is confined and in a stagnant state most of the year. These conditions lead to

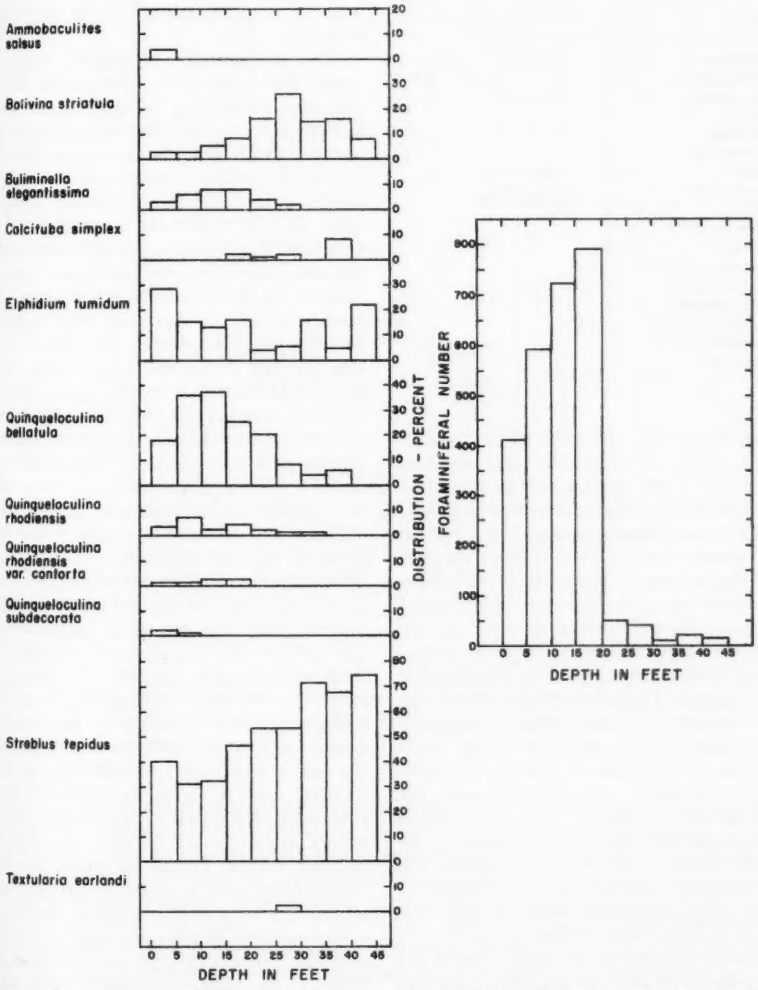

Figure 22. Histogram distribution of species and foraminiferal number plotted against depth

important changes in oxygen content and available food and also bring about salinity variations especially important in summertime (Arnal, 1954; 1955). In summary, when the environment varies somewhat from the standard oceanic environment, Foraminifera show increasing abnormalities.

TABLE 11. FORAMINIFERAL FACIES IN THE SALTON SEA
(In per cent; x = 0–2 per cent)

Species	Inner coastal	Outer coastal	Central	Deltaic
Streblus tepidus	<40	40–60	>60	<40
Elphidium tumidum	10–30	<10	0–20	30–50
Bolivina striatula	<10	15–20	<15	<5
Bulimenella elegantissima	x	10–30	<10	x
Quinqueloculina bellatula	20–40	10–20	<10	x
Quinqueloculina rhodiensis	x	x		
Q. rhodiensis var. *incondita*	x			
Q. subdecorata	x			
Calcituba simplex		x		
Textularia earlandi		x		x
Saccammina sphaerica				x
Ammobaculites salsus				<10
Reophax nana				x

In the Salton Sea, the water differs from sea water in many respects; the only common characteristic is the presence of chlorides, mainly sodium and magnesium chloride, which make the salinity conditions approximately similar to littoral oceanic waters. To determine the reasons for the presence of abnormal individuals, an approximate count of these was made for each sample, and the values obtained were recalculated as for 60-gram samples. Isopleths categorize the distribution of abnormal Foraminifera in several zones. The zones of high values (Fig. 23) are restricted to coastal regions, especially near estuaries of streams which bring about heterogeneous conditions of salinity, temperature, pH, turbidity, and related factors. The central part of the lake has very homogeneous conditions and does not show any abnormal individuals. However, at several stations the pH of the sediments is acidic, and the Foraminifera at these stations are either absent or show evidence of etching. Foraminifera probably have been present everywhere in the lake, but at the stations where the pH is acidic, their tests have been rapidly dissolved after their death; yet at the stations of the central region where Foraminifera are present, no abnormal specimens have been found.

Three zones of maximum values occur among the zones of high number of abnormal Foraminifera:

(1) The northern edge near a large outlet of the All American Canal. This indicates a possible marking effect of salinity variations as a factor creating abnormality.

(2) An area on the eastern side of the lake where Salton Creek enters the Salton Sea. This stream flows almost all year and contributes water of very low salinity (approximately 4-5 o/oo).

(3) The southeastern region, where the Alamo River and New River enter the lake. These two rivers bring by far the largest amount of fresh water to the Salton Sea. Because of the current pattern (Fig. 9) running counterclockwise in this region, a tongue of less saline and cooler water extends northward along the coast. In this region the greatest number of abnormal Foraminifera has been recorded and the most heterogeneous conditions exist. Because of the presence of these two rivers, a large amount of silt is deposited, and many clay particles are in suspension. The two rivers are also forming deltas and bring about an important amount of decaying organic matter of vegetable origin. The turbidity of the incoming water is also variable; during times of heavy rainfall or during periods of high winds which create a stirring of the water by wave action, the turbidity of the water may be so great that a Secchi disc disappears within a few inches from the surface, especially in coastal waters. The temperature of the water ranges from 10° C. to 33.5° C. in the lake but remains relatively cool all year in the less saline tongue of water. The salinity also is extremely variable, from fresh water to approximately 34 o/oo of total salts. The chemical composition of the water varies appreciably from that of sea water. The amount of food available for any organisms in the lake is also subject to wide variations, and its lack may be fatal, as witnessed by the thousands of *Bairdiella* (fish) found dead and washed ashore during the early months of the summer of 1954. This factor is also effective on Foraminifera and accounts for many irregularities of coiling or of size of the chambers.

The greatest number of abnormal forms occurs where fresh water flows into the lake. This, added to the effect of confined water already observed in the case of the Playa del Rey

Lagoon, undoubtedly accounts for a large number of abnormal Foraminifera. The presence of abnormal individuals is therefore a "characteristic" of environments having stagnant waters or confined waters with restricted circulation

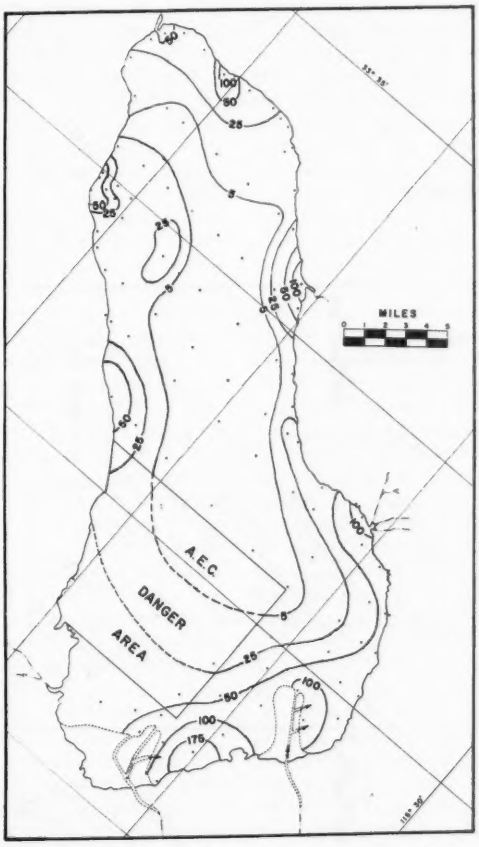

Figure 23. Number of abnormal Foraminifera per 60-gram sample

and chemical composition somewhat different from sea water. This is supported by the evidence of Le Calvez and Le Calvez (1951), who made the same observations in similar environments located several thousands of miles away from the area studied in this paper.

Foraminiferal productivity of bottom sediments. Walton (1952) used rose Bengal to determine the presence of living Foraminifera. The percentage of stained (living) individuals was computed during the frequency counts. These percentages are plotted in Figure 24A. The map is subdivided into several areas on which are indicated the months of sample collecting. This was done to determine whether productivity differs during certain periods of the year. Within each area, isopleths of percentages of living Foraminifera have been drawn to observe possible offshore variation. Such variation exists and is noticeable during any monthly period, but it varies in intensity during the year. The maximum variation occurs in June and July, which are the months showing the greatest percentages and also the greatest spread of the isopleth curves. Large areas of high percentages

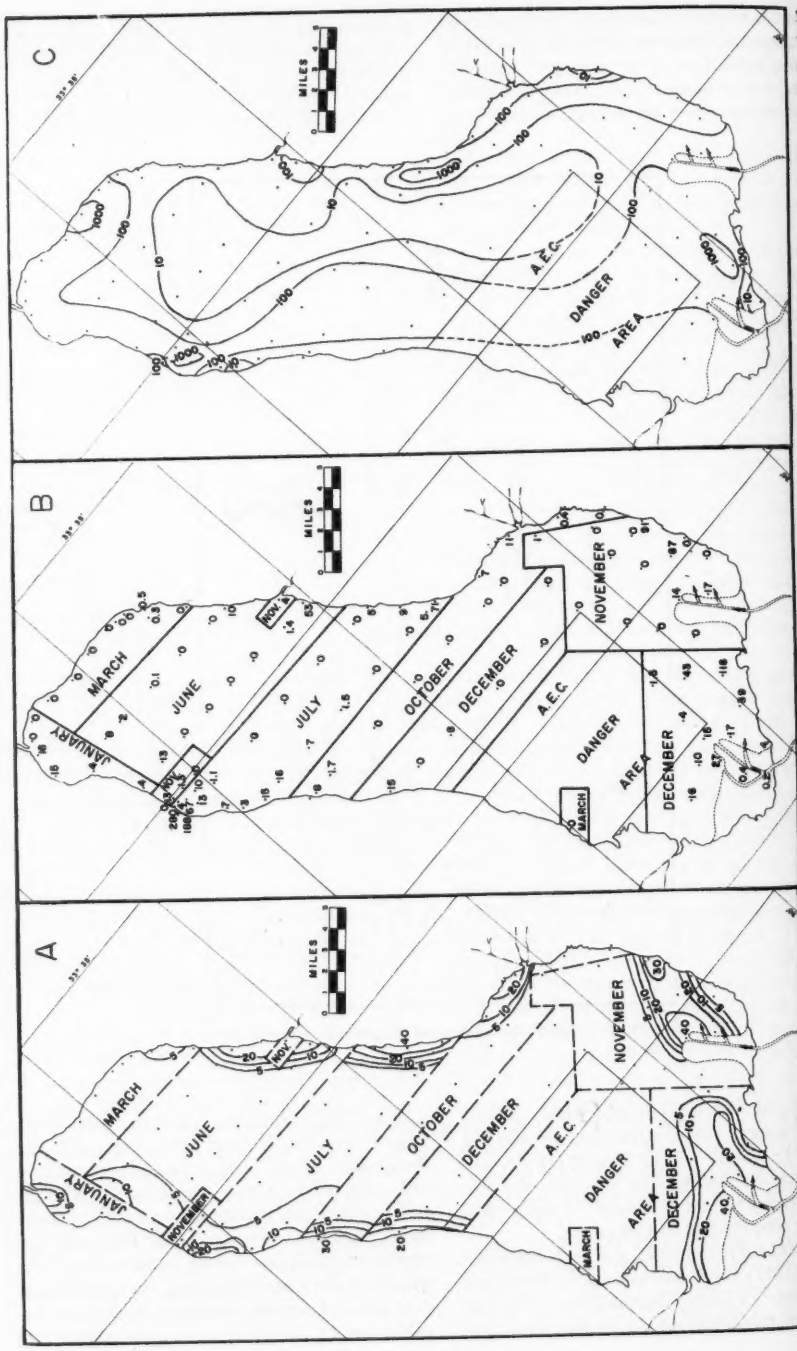

Figure 24. Foraminiferal productivity of bottom sediments. A. Percentage of living Foraminifera and month of collecting. B. Number of living Foraminifera per square centimeter of bottom surface with month of collecting. C. Distribution of the foraminiferal number

were also observed for the months of November and December (southern Salton Sea) and January (northern Salton Sea), but these are obviously related to inflow of fresh water and therefore of nutrients. This is exemplified by the position of the highest percentages and the shape of the isopleth curves, especially for the November area located around the Alamo River. Living Foraminifera are restricted in this area to the zone of inflow of fresh water and are absent in the remainder of the area. A similar pattern exists for the December area around the New River delta and around the mouth of Whitewater Creek in January.

Although the isopleth curves in the different areas cannot be correlated because of the different months of collecting, their distribution is analogous. In most areas the isopleth curves are closely spaced along the coast, and there is a rapid decrease 2–3 miles offshore. The zone of high values in the western part of the June area is an extension of that found in January at the mouth of Whitewater Creek. Since the maximum percentage is greater, although it is 3 miles offshore, June is a much more productive month than January. During the month of March, in the northern end of the sea and also in the A. E. C. danger area, almost no living Foraminifera were found; hence March appears to be the least productive month during an annual cycle. In summary, June and July are the months of foraminiferal bloom, and January to March is the period of minimum productivity. Carpelan (1955, unpublished report) observed a similar pattern for the zooplankton of the Salton Sea. Following a bloom of phytoplankton in February, March, and April, there is a maximum abundance of zooplankton in the late spring and early summer months.

A clearer concept of the productivity of the different parts of the Salton Sea may be obtained by examining the distribution of the number of living Foraminifera per surface unit of bottom sediment. Figure 24B shows the number of living Foraminifera per square centimeter of bottom surface. As the month of collecting would also influence this number, the month during which the observations were made was added to Figure 24B. This figure differs from 24A in that it shows absolute values, whereas the other gave only relative percentages regardless of the total number of living Foraminifera. The same general conclusions are drawn from the two figures—*i.e.*, that the highest productivity occurs in July. The highest number of living Foraminifera per square centimeter exists at the westerly end of the July area. This number is higher than any value found at the deltas of the Alamo and New rivers and indicates that the range of productivity from the high to the low productive month is greater than the range of productivity which exists between localities of inflow of fresh water and other regions.

The distribution of the foraminiferal number (*i.e.*, number of Foraminifera per gram of sediment) is an indication of the productivity of the sediments over a period of several years (Fig. 24C). As several annual cycles are involved, the monthly differences in productivity are compensated; therefore it is possible to draw contours of equal value over the entire area of the Salton Sea. Again the offshore decrease in productivity is evident from observation of the isopleths. Conclusions are that (1) over a period of several years the productivity is generally higher along the coast and decreases offshore; (2) the zones of highest productivity are located around the mouths of streams, and their positions are deflected as compared to the positions of the stream mouths according to the current pattern; and (3) the productivity of the central region is practically nil, and Foraminifera present in this region have been transported. A possible explanation for this transportation is presented below.

Origin of the living foraminiferal fauna. With the exception of the modern fauna, Foraminifera probably have been absent from the Salton Basin since the end of the Pliocene. What, then, is the origin of the present fauna living in the Salton Sea? Birds (sea gulls and other marine waterfowl) have been mentioned as a means of transportation; it is a possible source, but improbable because of the diversity of the fauna. The sediments containing Foraminifera that may have been caught in the feet of the birds would dry rapidly during flight and thus destroy the specimens present. A more probable explanations is accidental planting during transplantations of fishes, which have been made on several occasions by the Fish and Game Commission, or (as is probably the case for the barnacles) by naval seaplanes which often landed on the Salton Sea during World War II. Because of the amazing similarity of the fauna of the Salton Sea to that described by Parker, Phleger, and Peirson (1953) from San Antonio Bay, Texas (Arnal, 1958), I favor the last hypothesis, as such a long transportation would be possible only in the bilge water of seaplanes. However, a multiple origin (sea-

Figure 24. Foraminiferal productivity of bottom sediments. A. Percentage of living Foraminifera and month of collecting. B. Number of living Foraminifera per square centimeter of bottom surface with month of collecting. C. Distribution of the foraminiferal number

planes and transplantation of fishes from Baja California) would perhaps be a better explanation.

Other Microscopic Animal Life

Several groups of microscopic animals are well represented in the Salton Sea. Dr. A. A. Aleem of the University of Alexandria, Egypt, while at the Hancock Foundation (University of Southern California), examined plankton collections from the lake and found that "The bulk of this plankton consists of Dinoflagellates. The most common organism is probably *Exuviella compressa*. There are also species of *Peridinium*, *Gyrodinium* etc." (Carpelan, 1954, unpublished report). The plankton is also rich quantitatively and qualitatively in Radiolaria and tintinnids. Other higher organisms which may be classified as microscopic because of their size are: a copepod, *Cyclops dimorphus* (Johnson, 1953); a rotifer, *Brachionus plicatilis;* and a barnacle, *Balanus amphitrite saltonensis*, of which the naupliar and Cypris stages are planktonic (Carpelan, 1955 unpublished report). I observed seven or eight species of Ostracodes living mostly in littoral regions. These are especially abundant in the marshes of the New and Alamo rivers. The rotifer *Brachionus* and

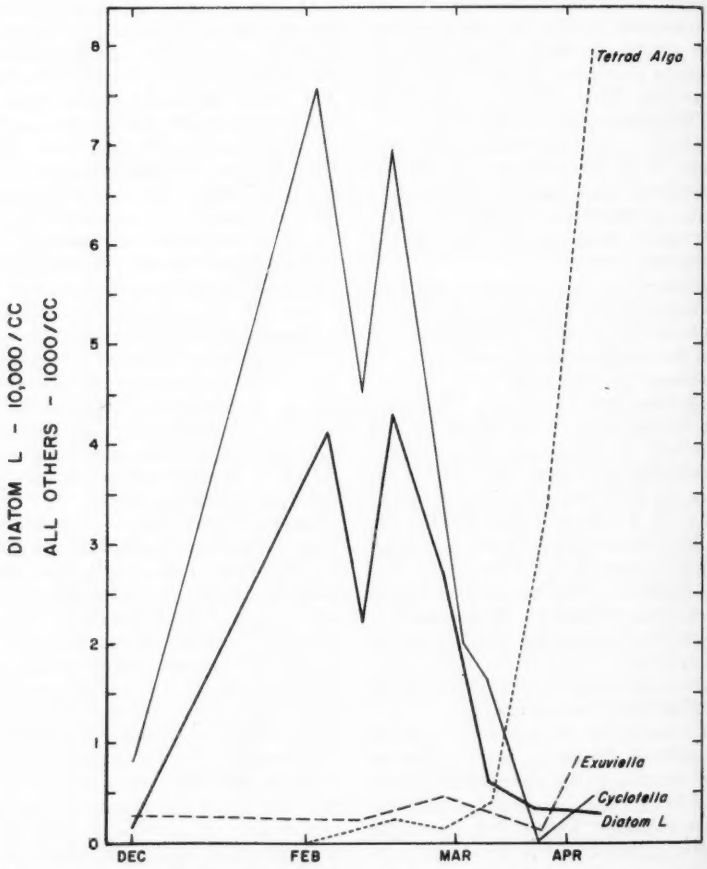

Figure 25. Phytoplankton bloom during early spring. Reproduced from Carpelan (1955, Unpublished report)

the copepod *Cyclops* are most abundant in the summer months. Other microscopic elements of the animal life of the sea are eggs and larvae of a polychaetous worm, *Neanthes succinea*. This worm spends most of its life in burrows in the mud and among the masses of barnacles. When it reaches maturity, it leaves its protective burrow at night and swims to the surface to spawn (Linsley, 1955, unpublished report). I have observed this polychaete in the sediments during the processing of the samples. A record of its presence shows that *Neanthes* lives only in littoral sediments and is restricted to fine sand and silt material. None was found in coarse sand or in fine mud in the center of the sea. In this area the acidic pH of the sediment is probably a limiting factor, as it is for other animal life.

Because *Neanthes* lives primarily in burrows and also has a swimming stage, it is probably responsible for some of the displacement of Foraminifera in the central part of the sea. When leaving its burrow, the worm may carry on its body several specimens of Foraminifera which are transported during the swimming stage and set free during that period. The Foraminifera may then drop to the bottom or be carried farther by currents. Because of the extreme abundance of this worm, which constitutes almost the entire diet of the fish population, a large number of Foraminifera may have been transported in that way to the central region where they would not be found otherwise.

Phytoplankton

Plant life in the Salton Sea is restricted to microscopic forms. The "Magdalena grass" which was present in the lake (Coleman, 1929) has now disappeared. The phytoplankton, however, is still well represented. Aleem (Personal communication) noted the presence of at least 20 species of diatoms in plankton collections he examined, and I have observed several species of diatoms in bottom samples from the marshes of the southern end of the sea. Dr. Yale Dawson of the Hancock Foundation (Personal communication) mentioned the presence of blue-green algae at shallow depths in the lake, but the most nearly complete study to date is that of Carpelan (1955, unpublished report). Carpelan studied the productivity of the Salton Sea and compared it with that of the oceans. He stated: ". . . the minimum productivity of the Salton Sea may be greater than that of the oceans during upwelling," for he found that the lowest production for the lake is 1,700,000 cells per liter, compared to 1,000,000 cells per liter in the ocean during upwelling. His results on phytoplankton bloom are particularly interesting, for they indicate a maximum during the period from February to April (Fig. 25). This bloom of the phytoplankton is followed by a bloom of Foraminifera during the late spring and early summer months, as the Foraminifera live mostly on the phytoplankton fall and therefore develop at the time of peak food abundance. The following species of algae listed by Carpelan and identified by Dawson may also form a great part of the diet of the foraminiferal population.

Phormidium tenue (Meneghini)
Plectonema calotrichoides Gomont
Spirulina major Kutzing
Spirulina subtilissima Kutzing
Calothrix seruginea (Kutzing)
Hydrocoelum sp.
Pleurococcus turgidus Trevissan
Entophysalis deusta Drouet and Daily
Oscillatoria sp. (near *O. laetevirens* Crouan)

GEOLOGIC HISTORY

Some of the conclusions drawn from the present study may be applied to the past sedimentation of the Salton Sea and thus provide additional information on the environmental conditions that existed in the Salton Basin in the past.

The oldest formation reported is the Split Mountain formation (Fig. 26). It is essentially a coarse basal conglomerate of Miocene age (Dibblee, 1954) overlying the older crystalline rocks.

Next, the Imperial formation, also of Miocene age, but younger, is represented by clays, sandstones, and calcareous shell reefs that were deposited under marine conditions in neritic water. It is too different from sediments deposited today to warrant any comparison with actual sedimentation, as the fauna is typically marine.

Overlying units are the Palm Spring and Borrego formations. Dibblee (1954) considers the Borrego formation as the lacustrine facies of the terrestrial Palm Spring formation. The latter contains a thick series of land-laid arkosic sandstones and red clays of Pliocene age. The Borrego formation represented by lacustrine and shallow marine sandstones and red clays was deposited under environmental conditions very similar to present conditions. The basin in which it was deposited was much larger, as shown by the extent of the outcrops. Partly

lacustrine and partly brackish marine sediments were deposited; the marine fauna represented by Foraminifera typical of shallow, brackish water conditions contains numerous specimens but only a few species, of which the most abundant is by far *Elphidium gunteri*. Others are *Nonion saltonensis*, *Streblus sobrinus*, and *Streblus tepidus*. A few *Chara* oögonia (an alga) are mixed with the Foraminifera, which indicates succession or alternation of fresh and brackish marine conditions. Many specimens of *Elphidium gunteri* are abnormally shaped. This, by analogy with the present conditions, suggests a large inflow of fresh water in the marine environment. Numerous specimens of the Borrego fauna are reworked throughout the lower part of the basin. These Foraminifera were at first tentatively attributed to the marine stage of Lake LeConte (Hubbs and Miller, 1948). However, they must have been reworked from the Borrego formation, for the following reasons: (1) they are distributed over the lower Salton Basin up to present sea level and are especially abundant near outcrops of

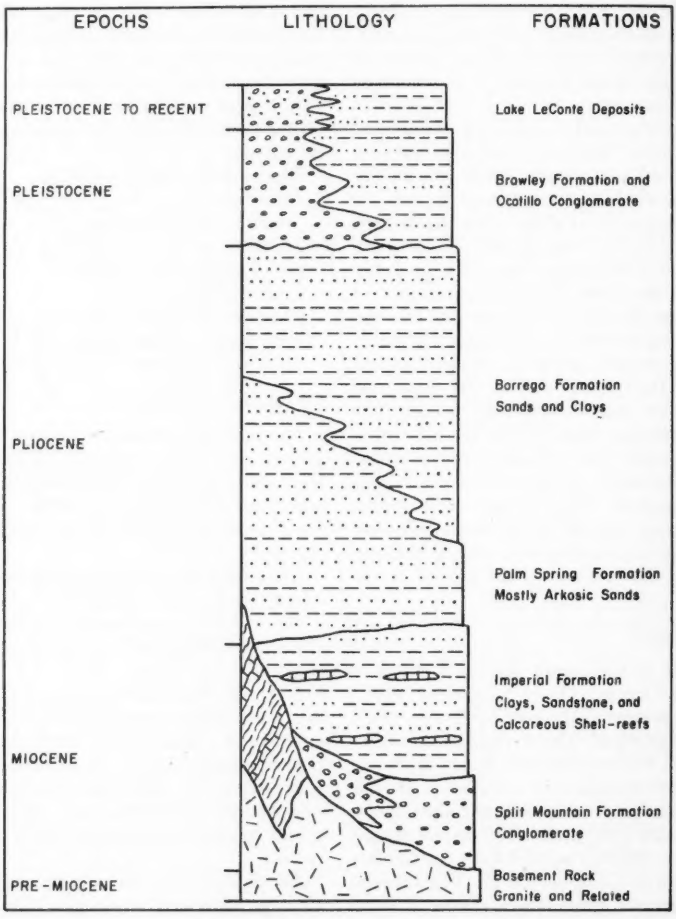

Figure 26. Columnar section in the Salton Basin. Adapted from Dibblee (1954)

the Borrego formation (*compare* Figure 27 with Dibblee's (1954) geological map of Imperial Valley); (2) many specimens are badly worn; (3) the fauna is identical with that of the Borrego formation (Tarbet and Holman, 1944);

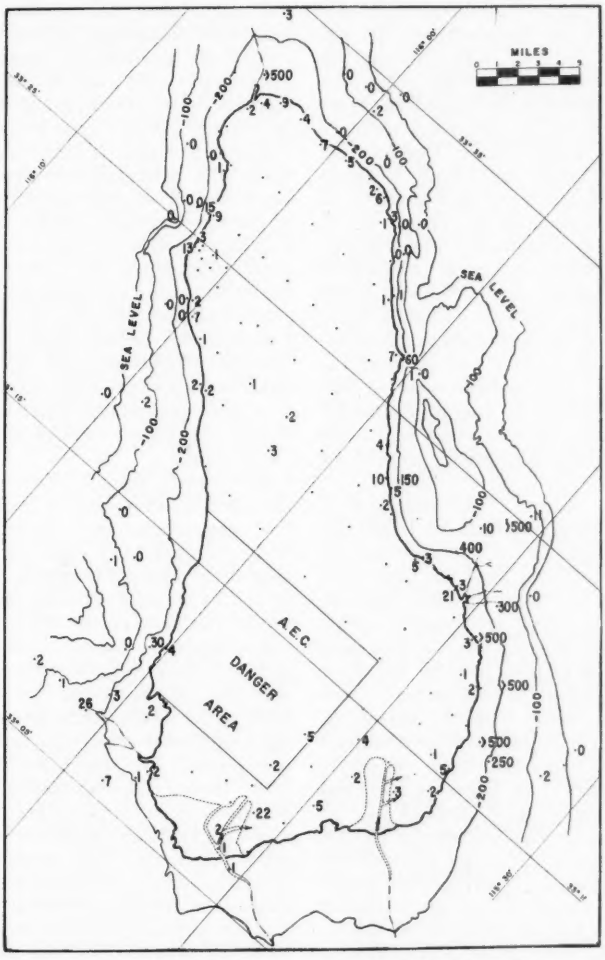

Figure 27. Number of specimens per sample reworked from the Borrego formation

(4) some specimens were found in samples from a depth of 6 feet in the sediments, and some may be found even deeper; and (5) the presence of *Elphidium gunteri* suggests a late Pliocene or early Pleistocene age for reasons subsequently explained.

The next unit is represented by the Ocotillo conglomerate of torrential origin and by the gray clays and sands of the Brawley formation which must have been deposited under conditions similar to the present ones except that the water was fresh, as indicated by the lacustrine fauna present in these sediments. The Brawley formation locally has a thickness of 2200 feet and is separated from the overlying sedimentary rocks by a local unconformity (Dibblee, 1954). Assuming that the Brawley

formation was deposited in a lake of Colorado River origin, some conclusions may be drawn about the minimum length of time that the Colorado River flowed in the Salton Basin. This would permit knowledge of the approximate age of the Brawley formation by comparison with conditions of sedimentation known today. The Colorado River average load was estimated (*see* Rate of Sedimentation) at 210,000,000 tons, or about 95,000 acre-feet, per year. The areal extent of the Salton Basin at sea level was estimated by planimeter measurements to be 1,367,000 acres. Dividing the volume of the annual load of the Colorado River by the surface of the basin indicates an annual rate of sedimentation which was calculated to be 0.83 inch per year. Thus deposition of the 2200-foot maximum thickness of the Brawley formation would take about 32,000 years. This implies that the Colorado River carried its load to the lake without any interruption. However, even if it were assumed that the river discharge in the basin occurred only once every 10 years, the length of time for deposition of the 2200 feet would be 320,000 years, which is still well within the range of the Pleistocene.

The last unit exposed in the lower part of the basin has a maximum thickness of 300 feet and is made of alluvial material derived from older sediments. It represents the fresh-water Lake LeConte, or Lake Cahuilla, deposits. Hubbs and Miller (1948) have made a comprehensive study of these sediments and suggests that they are of probable Pluvial age (Late Pleistocene to Recent). Several species of fresh-water mollusks suggest lacustrine deposition. The tufa deposit at Travertine Rock must have been deposited under conditions similar to other tufa deposits in the Lahontan Basin and is probably of similar age. Carbon-14 data for tufa of the Lahontan Basin indicates (Phil Orr, personal communication) an age range of 0 to 37,000 years, which is in good agreement with the late Pleistocene to Recent age attributed to the Lake LeConte deposits. In the deposition of the tufa, wave action is purported to have played an important role in releasing carbon dioxide and helping precipitation of calcium carbonate from the original calcium bicarbonate in the water (Twenhofel, 1950). This may have been the case in Lake LeConte, as the tufa deposits are noticeable only on masses of rocks which must have been obstacles to waves and increased the turbulence of the water there. Such rock masses—*i.e.*, Travertine Rock to the northwest and the Pumice and Obsidian buttes to the south—were projecting from the surface of Lake LeConte and were well exposed to wave action.

The water in which the calcareous tufa was deposited was certainly different from the water of the present Salton Sea. The salinity was much lower, since it was inhabited by fresh-water gastropods, and the chemical composition also was different. Important elements in the water were calcium, carbonates (probably mostly bicarbonate), and silica, as shown by examination of a thin section of the tufa deposits. The rock is botryoidal and reveals under the petrographic microscope definite laminations of concretionary appearance. Bands of calcium carbonate contain, and are intercalated with, very fine particles of chalcedony (cryptocrystalline) and opal. Larger detrital quartz fragments and some shells of *Hydrobia protea*, the most abundant gastropod of Lake LeConte, may be seen embedded in the tufa material. Chalcedony and opal compose as much as 50 per cent of the material and must have been precipitated with the calcium carbonate which forms most of the remainder of the material.

In summary, from Miocene to the present time, sedimentation has undergone a progressive change from marine to lacustrine conditions; the break occurs slightly after the deposition of the Borrego formation. As mentioned earlier, I favor a late Pliocene-early Pleistocene age for this formation on the basis of the presence of *Elphidium gunteri* because, although this species is known to be living today, many specimens of the Salton Sea sediments are badly worn, which indicates reworking and an age considerably older than that of the forms now present. The species was described originally from a Pliocene marl of Florida, and abundant specimens have been found associated with *Elphidium hughesi* in late Pliocene or early Pleistocene well samples from other regions of southern California—*e.g.*, at some localities in the Ventura Basin. Since Borrego time no continuous marine occupation of the basin has occurred, and the presence in the Salton Sea of living Foraminifera (of accidental introduction) certainly does not constitute proof of recent occupancy of the present basin by the Gulf of California, as proposed in the literature.

SUMMARY

The following statements summarize the present study:

(1) In the Salton Sea, the lowest elevation is

−276.7 feet, only 4 feet higher than the lowest point in the western hemisphere, in Death Valley, California.

(2) The yearly temperature range of the Salton Sea is from 10° C. to 34.5° C., and the salinity (about 34.00 o/oo) approximates closely that of the oceans.

(3) In the future, the height of stabilization of the lake level will probably occur between −210 and −200 feet.

(4) The chemical composition of Salton Sea water differs markedly from ocean water and is in constant evolution. Of the salts present in solution in the water, 113 million tons was redissolved from salts present on the floor of the basin before the flood of 1905. The remainder, about 140 million tons, has been concentrated by evaporation from Colorado River water used for irrigation purposes. The percentage of sulfates will probably increase in the future.

(5) Currents in the Salton Sea have been determined from salinity measurements and direct observation. They move in a counterclockwise gyral around the lake because of the influence of the prevailing winds. The distribution of pumice transported by longshore currents indicates that the current pattern for Lake LeConte was similar to the current pattern of the Salton Sea.

(6) The water content of the sediments varies in inverse ratio to the grain size. It is high in places of clay deposition and low where sands are deposited; the water content decreases with depth of burial.

(7) Hydrogen-ion concentration, or pH, is low in very fine material and influences directly the pH of the overlying bottom water. Strong etching of calcareous shells was observed in sediments having a pH of less than 7.2.

(8) Clays, silts, and fine sands are being deposited in the Salton Sea. With a few exceptions, grain size decreases basinward throughout the basin. The median diameter of Salton Sea sediments compares well with that of the sediments in suspension in Colorado River water; it is a little larger because the sediments contributed by the Salton Basin are predominantly sands.

(9) Offshore increase in percentage of calcium carbonate is more closely related to a slow rate of sedimentation than to a larger amount of shell fragments or calcareous tests. The sediments deposited during the past 50 years contain approximately 70 million tons of calcium carbonate, of which about 27 million tons has been precipitated from the water, either chemically or by organisms.

(10) Distribution of heavy residues and mineralogical composition suggest local sources for the origin of some of the present sediments; however, a greater part (about 75 per cent) has been transported by Colorado River water into the Salton Sea.

(11) Rates of deposition vary greatly within the Salton Sea. The extreme values recorded were 2 inches per year off the mouths of the rivers and two hundredths of an inch per year in the central part of the lake. Computations of rates of sedimentation by direct measurements, by comparison of percentages of living to total Foraminifera, and by weight estimate of transported sediments give analogous results.

Among the organisms living in the Salton Sea, the microorganisms are the most abundant. Detailed study of the Foraminifera shows that:

(1) There are three main environments in the Salton Sea: the coastal facies, the central facies, and the deltaic facies. Each is characterized by a specific assemblage and a well-defined depth of occurrence. The coastal facies is characterized by a great abundance of *Elphidium tumidum* and *Quinqueloculina bellatula* (inner part of this facies). An abundance of *Streblus tepidus* and *Bolivina striatula* is typical of the outer part of that facies. A great variety of arenaceous Foraminifera exists in deltaic areas. Porcellaneous Foraminifera are restricted to coastal regions, whereas hyaline species are most abundant in the central portion of the lake.

(2) Comparison of frequency distribution with ecologic factors existing in the lake suggests that (a) the observed chlorinity and temperature characters of bottom water do not influence the distribution of Foraminifera; (b) depth may be important by its effect on other ecologic factors; and (c) the variation in pH of the sediments is significant and regulates the distribution of living and dead populations to a large extent; *i.e.*, abundance of individuals is very low where the pH of the sediments is below 7.2.

(3) In contrast to marine conditions, species abundance decreases offshore. The percentage of all species diminishes away from the shore except that of *Streblus tepidus*. *Bolivina striatula* shows a peak abundance at a depth of about 30 feet. *Buliminella elegantissima* and *Quinqueloculina bellatula* are strongly dependent on food related to abundant nutrients.

(4) The fauna of the Salton Sea is dwarfed, and many tests are malformed. Most of these abnormal specimens occur where fresh water flows into the sea and represent one of the gen-

eral characteristics of the foraminiferal fauna. Living specimens are most abundant in the late spring and early summer months, following a phytoplankton bloom during the early spring. The fauna of the Salton Sea was introduced accidentally into the lake.

(5) The productivity of the Salton Sea is generally higher than that of the ocean, even in regions where upwelling occurs. The Salton Sea supports an abundant microscopic life other than Foraminifera. Ostracoda are most prevalent in coastal regions. Diatoms are represented by many species of fresh-water and marine types. Dinoflagellates, Radiolaria, and tintinnids are also present in the plankton of the lake.

Comparison of present and past environmental conditions suggests that the Borrego formation was deposited under conditions similar to the present, but with a connection to the open sea. A Pleistocene age is suggested for the lacustrine sediments of the Brawley formation. The geologic history of the Salton Basin is dominated by a change from marine to lacustrine conditions at the end of the deposition of the sediments of the Borrego formation in late Pliocene to early Pleistocene time.

BIBLIOGRAPHY

Allison, L. E., 1935, Organic carbon by reduction of chromic acid: Soil Sci., v. 40, p. 311–320

Arnal, R. E., 1954, Preliminary report on the sediments and Foraminifera of the Salton Sea, Southern California (Abstract): Geol. Soc. America Bull., v. 65, p. 1227–1228

—— 1955, Significance of abnormal Foraminifera (Abstract): Geol. Soc. America Bull., v. 66, p. 1641

—— 1958, Rhizopoda from the Salton Sea, California: Cushman Found. for Foram. Research, v. 9, no. 2, p. 36–45

Bailey, G. E., 1902, The saline deposits of California: Calif. State Min. Bur. Bull., v. 24, 216 p.

Bandy, O. L., 1954, Distribution of some shallow water Foraminifera in the Gulf of Mexico: U. S. Geol. Survey Prof. Paper 254-F, p. 125–141

Blake, W. P., 1854, Ancient lake of the Colorado Desert: Am. Jour. Sci., v. 17, p. 435–438

—— 1907, Lake Cahuilla. The ancient lake of the Colorado Desert: Natl. Geog. Mag., v. 18, p. 830

Blaney, H. F., 1955, Evaporation from and stabilization of Salton Sea water surface: Am. Geophys. Union Trans., v. 36, p. 633–640

Brown, J. S., 1922, Fault features of the Salton Basin in California: Jour. Geology, v. 30, p. 217–228

Buwalda, J. P., and Stanton, W. L., 1930, Geological events in the history of the Indio Hills and Salton Basin, Southern California: Science, v. 71, p. 104–106

Cockerell, T. D., 1945, The Colorado Desert of California: Its origin and biota: Kans. Acad. Sci. Trans., v. 48, no. 1, p. 1–59

Coleman, G. A., 1929, A biological survey of the Salton Sea: Calif. Fish and Game, v. 15, no. 2, p. 218–227

Dibblee, T. W., 1954, Geology of the Imperial Valley region, California: Calif. Div. Mines Bull. 170, p. 21–28

Emery, K. O., 1938, Rapid method of mechanical analysis of sands: Jour. Sed. Petrology, v. 8, p. 105–111

Emery, K. O., and Rittenberg, S. C., 1952, Early diagenesis of California basin sediments in relation to origin of oil: Am. Assoc. Petroleum Geologists, v. 36, p. 735–806

Gautier-Lievre, L., 1935, Sur une des singularités de l'Oued Rhir; des Foraminiféres Thalassoides vivant dans les eaux sahariennes: Soc. Hist. Nat. Afr. Nord Bull., no. 26, p. 142–147

Gould, H. R., 1954, Lake Mead comprehensive survey of 1948–49. Sedimentology, amount of sediments: U. S. Geol. Survey Advance Rept. for Official Use and Rev. by Cooperative Agencies and Others Concerned, v. 3, p. 211–329

Hubbs, C. L., and Miller, R. R., 1948, The Great Basin. Part II, The zoological evidence: Univ. Utah Bull., v. 38, no. 20, p. 103–113

Johnson, M. W., 1953, The copepod *Cyclops dimorphus* from the Salton Sea: Am. Midland Naturalist, v. 49, p. 188–192

Le Calvez, J., and Le Calvez, Y., 1951, Contribution a l'étude des Foraminiféres des eaux saumatres: Vie et Milieu, T. 2, Fasc. 2, p. 237–254

MacDougal, D. T., 1907, Desert basins of the Colorado Delta: Am. Geog. Soc. Bull., v. 39, p. 705–729

MacDougal, D. T., and others, 1914, The Salton Sea: Carnegie Inst. Washington Pub. 193, 250 p.

Mendenhall, W. C., 1909, Ground water of the Indio region, Calif., with a sketch of the Colorado Desert: U. S. Geol. Survey Water Supply Paper 225, 56 p.

Milner, H. B., 1952, Sedimentary petrography: London, Thomas Murby and Co., 666 p.

Myers, E. H., 1942, Rate at which Foraminifera are contributed to marine sediments: Jour. Sed. Petrology, v. 12, p. 92–95

Parker, F. L., Phleger, F. B, and Peirson, J. F., 1953, Ecology of Foraminifera from San Antonio Bay and environs, Southwest Texas: Cushman Found. for Foram. Research Special Pub. 2, 75 p.

Rogers, F. L., 1949, Three new subspecies of *Balanus:* Jour. Entomology and Zoology, v. 41, no. 2, p. 342–346

Salma, D. C., 1954, Arenaceous tests in Foraminifera—an experiment: The Micropaleontologist, v. 8, p. 29–30

Sverdrup, H. U., Johnson, M. W., and Fleming, R. H., 1942, The oceans: New York, Prentice-Hall Co., 1087 p.

Sykes, G., 1937, The Colorado delta: Am. Geog. Soc. Special Pub. 19, p. 132–133

Tarbet, L. A., and Holman, W. H., 1944, Stratigraphy and micropaleontology of the west side of Imperial Valley, California: Am. Assoc. Petroleum Geologists Bull., v. 28, p. 1781–1782

Thomas, H. E., Gould, H. R., and Langbein, W. B., 1954, Lake Mead comprehensive survey of 1948–49. Life of the reservoir: U. S. Geol. Survey Advance Rept. for Official Use and Rev. by Cooperative Agencies and Others Concerned, v. 3, p. 330–350

Trask, P. D., 1932, Origin and environment of source sediments of petroleum: Houston, Texas, Gulf Publishing Co., p. 1–97

Trask, P. D., *Editor*, 1955, Recent marine sediments. New edition: Soc. Econ. Paleontologists and Mineralogists Special Pub. 4, 736 p.

Twenhofel, W. H., 1950, Principles of sedimentation: 2d ed., New York, McGraw-Hill Book Co., 673 p.

U. S. Bureau of Reclamation, 1947, Lake Mead density currents investigations: Washington, D. C., 897 p., 3 volumes

U. S. Geological Survey, 1928, Salton Sea reconnaissance map: Washington, D. C.

Walton, W. R., 1952, Techniques for the recognition of living Foraminifera: Contr. Cushman Found. Foram. Research, v. 3, Pt. 2, p. 56–60

—— 1955, Ecology of living benthonic Foraminifera, Todos Santos Bay, Baja California: Jour. Paleontology, v. 29, p. 952–1018

Manuscript Received by the Secretary of the Society, October 13, 1958

APPENDIX. WATER-BUDGET DATA

Year	Elevation (in feet)	Precipitation (in acre-feet)	Evaporation (in acre-feet)	Runoff (in acre-feet)	Balance − loss or + gain (in acre-feet)
1908	−202	85,700	1,932,000	880,300	− 966,000
1909	−207.5	81,100	1,830,000	71,400	−1,677,500
1910	−212.5	77,700	1,752,000	214,300	−1,460,000
1911	−216.5	74,700	1,686,000	487,300	−1,124,000
1912	−220	72,100	1,626,000	605,400	− 948,500
1913	−224	69,200	1,560,000	480,000	−1,040,000
1914	−228	66,200	1,494,000	431,800	− 996,000
1915	−233	62,200	1,404,000	171,800	−1,170,000
1916	−237	59,100	1,332,000	384,900	− 888,000
1917	−240.5	56,400	1,272,000	473,600	− 742,000
1918	−244.5	52,100	1,176,000	339,900	− 784,000
1919	−247.5	49,200	1,110,000	505,800	− 555,000
1920	−248.5	48,400	1,092,000	861,600	− 182,000
1921	−249	47,900	1,080,000	942,100	− 90,000
1922	−249.5	47,300	1,068,000	931,100	− 89,000
1923	−250	46,600	1,050,000	916,000	− 87,500
1924	−250	46,600	1,050,000	1,003,500	0
1925	−249.5	47,300	1,068,000	1,109,700	+ 89,000
1926	−248	48,900	1,104,000	1,331,100	+ 276,000
1927	−247	49,700	1,122,000	1,259,300	+ 187,000
1928	−246	50,500	1,140,000	1,279,500	+ 190,000
1929	−245	51,600	1,164,000	1,306,400	+ 194,000
1930	−244	52,700	1,188,000	1,333,300	+ 198,000
1931	−244	52,700	1,188,000	1,135,300	0
1932	−244	52,700	1,188,000	1,135,300	0
1933	−245	51,600	1,164,000	918,400	− 194,000
1934	−246.5	50,000	1,128,000	795,000	− 282,000
1935	−247.5	49,200	1,110,000	875,800	− 185,000
1936	−247	49,700	1,122,000	1,165,800	+ 93,500
1937	−245.5	51,100	1,152,000	1,388,900	+ 288,000
1938	−244.0	52,700	1,188,000	1,432,300	+ 297,000
1939	−243	53,700	1,212,000	1,360,300	+ 202,000
1940	−241.5	55,300	1,248,000	1,504,700	+ 312,000
1941	−241	55,900	1,260,000	1,309,100	+ 105,000
1942	−240.5	56,400	1,272,000	1,321,600	+ 106,000
1943	−240.5	56,400	1,272,000	1,215,600	0
1944	−240	56,900	1,284,000	1,334,100	+ 107,000
1945	−240	56,900	1,284,000	1,227,100	0
1946	−240	56,900	1,284,000	1,227,100	0
1947	−240.5	56,400	1,272,000	1,109,600	− 106,000
1948	−240	56,900	1,284,000	1,334,100	+ 107,000
1949	−240	56,900	1,284,000	1,227,100	0
1950	−239.5	57,500	1,296,000	1,346,500	+ 108,000
1951	−239	57,700	1,302,000	1,352,800	+ 108,500
1952	−237.5	58,500	1,320,000	1,591,500	+ 330,000
1953	−236.5	59,100	1,332,000	1,494,900	+ 222,000
1954	−235.5	60,400	1,362,000	1,528,900	+ 227,000
1955	−235	60,600	1,368,000	1,466,800	+ 114,000

Short Notes

JOAN B. SNELL

METHOD FOR PREDICTING LINE-OF-SIGHT CAPABILITIES: PRELIMINARY INVESTIGATIONS

Abstract: A mathematical terrain model, from which it is possible to predict the number of valleys visible from the highest elevation within an area, has been applied to the New England physiographic province and to an area in the Colorado Plateau. Correlation between the predicted and actual number of visible valleys for two areas is good.

Recent developments in communications and transportation, both civilian and military, have placed increasing emphasis on the phenomena referred to as "line of sight." The term denotes a straight line along which vision and light, or other electro-magnetic waves, travel from a point of origin. Such waves continue to travel in a straight line until they are refracted by the medium through which they pass, or meet an obstacle high enough or dense enough to obstruct their courses. A variety of factors determine whether or not one point on the surface of the earth is in direct line of sight from another point, but on a large scale the most significant obstacle to line of sight is the terrain.

The extent to which points lie in direct line of sight from one another generally has been determined by drawing profiles of the surface over which a single line of sight would travel. Now that rapid analysis of many and large areas must be undertaken, however, the well-established methods of profile drawing are not adequate. New methods are needed to answer quickly such questions as "Can equipment and tactics which depend on line of sight be advantageously used in a particular area?" The results of studies conducted by our group indicate that prediction techniques can provide quick and accurate evaluations of areas in terms of line of sight.

In seeking a method for predicting line-of-sight information, the preliminary investigations have been limited to consideration of that type of equipment which would have line-of-sight capabilities for 20 miles over smooth earth, and to the ability to see into valleys at specified distances from a single point.

Whether or not valleys are visible from a point will depend on the various terrain dimensions: distance from the point to a valley, difference in elevations between these two points, depth of valley, width of valley, orientation of valley, slope of the land surface, and heights of peaks and ridges. A mathematical terrain model that incorporates these dimensions was devised and showed promise as a feasible method for predicting valley visibility. To construct this model, certain assumptions about the landscape were made; then, by using a few actual dimensions, easily obtained from topographic maps, other pertinent terrain dimensions were calculated. Thus, through a series of computations, a simplified description of an existing landscape was created.

For this problem, it was assumed that all the valleys within an area are of equal depth and have the same side slope, all are parallel, all are equally spaced, and the ridges between valleys are the same distance apart as the valleys themselves. It was further assumed that angles made by the intersection of lines of sight and any given valley are equally likely within the range of 0° and 90°. Measurements of relief, average slope, and valley spacing constituted the basic data necessary to construct the model. From these, other dimensions of ridge-valley distance, valley depth, angle of sight, ridge-interference distance, and angle-of-valley entrance were computed. A prediction of valley visibility was made by converting the computed angle-of-valley entrance to a percentage of valleys that could be seen from a single point.

This mathematical model has been applied to two different physiographic provinces: New England and the Colorado Plateau. The Glens Falls, New York, sheet of the 1:250,000 Army Map Service series was chosen to represent

Geological Society of America Bulletin, v. 72, p. 479–484, 3 figs., March 1961

New England, a mountainous area with many deep, closely spaced valleys and steep slopes. In contrast, the Colorado Plateau, as represented on the Grand Canyon, Arizona, sheet of the same map series, is plateau country with fewer widely spaced valleys and less steep slopes.

the number of valleys that actually are visible from the viewing point was determined. These figures of valley visibility were later compared with those predicted from the model.

To construct the model and thereby determine the dimensions of an average valley for the individual circles, a data sheet was ar-

TABLE 1.—TERRAIN MODEL TO PREDICT NUMBER OF VISIBLE VALLEYS

Terrain Factors	Formulae	Computations	Results
A. Radius of circle			20 mi.
B. Circumference	$2\pi r$	6.2832×20	125.66 mi.
C. Number of valleys			41
D. Relief (in feet)	highest elevation —lowest elevation	4000 feet —300 feet	
		3670 feet	
(miles)	relief ÷ 5280	3670 ÷ 5280	.6951 mi.
E. Average slope	contour counts per mile × contour interval	4.84×100 feet	
(tangent)	3361	3361	.1440
F. Valley spacing	traverse ÷ valley number	125.66 ÷ 41	
	1.57	1.57	1.9512 mi.
G. Ridge-valley distance	valley spacing ÷ 2	1.9512 ÷ 2	.9756 mi.
H. Valley depth	average slope × ridge-valley distance	.1440 × .9756	.1405 mi.
I. Angle of sight (tangent)	relief / radius	.6951 / 20	.0348
J. Ridge—interference distance	valley depth / angle of sight	.1405 / .0348	4.0374 mi.
K. Angle of valley entrance (sine)	ridge—valley distance / ridge—interference distance	.9756 / 4.0374	.2416
(degrees)			13.98°
L. Percent of visible valleys	angle of valley entrance / 90°	13.98 / 90	15.53%
M. Predicted number of visible valleys	% visible valleys × number of valleys	15.53 × 41	6

For both areas, the highest elevation on the sheet was selected as the point from which to project lines of sight to the valleys. This point is referred to as "the viewing point." The studies were contained within a circle having a radius of 20 miles, with the viewing point as the center. From this point, 20 concentric circles were drawn at 1-mile intervals. Every stream, indicated by a blue line on the map, that crossed these circles was considered a valley entering the area under observation. By projecting lines of sight from the high point to each of the valleys where it crossed the circle, and examining the terrain by profile method,

ranged on which to make computations and record information (Table 1). In the first column were listed the terrain factors considered, next the formulae for computing the various dimensions, and in the third column the actual computations. The results were recorded in the last column. During the following explanation specific references will be to the 20-mile circle of the Glens Falls sheet.

a. The first dimension recorded is the RADIUS of the circle, which is also the distance between the viewing point and the valleys. In this case, the radius is 20 miles.

b. The CIRCUMFERENCE delineates the

edge of the circle. Computation for this dimension is by the well-known formula $2\pi r$. With a radius of 20 miles the circumference is $2 \times 3.14 \times 20$ or 125.66 miles.

c. The NUMBER OF VALLEYS is determined by counting the streams that cross the circumference line of the circle; 41 valleys cross the 20-mile circle.

d. RELIEF is the difference in elevation between the highest and lowest points within a unit area. In this area the viewing point, 4000 feet, is the highest point, and the elevation of the lowest valley, 330 feet, is the lowest point. The relief, then, is 3670 feet. All the dimensions are expressed in the same unit, so this figure is converted to miles and becomes .6951 mile.

e. AVERAGE SLOPE TANGENT, which is used to represent the valley side slope, is obtained by counting the number of contour lines crossed on a random traverse and processing this information by the Wentworth equation: average slope tangent equals contour

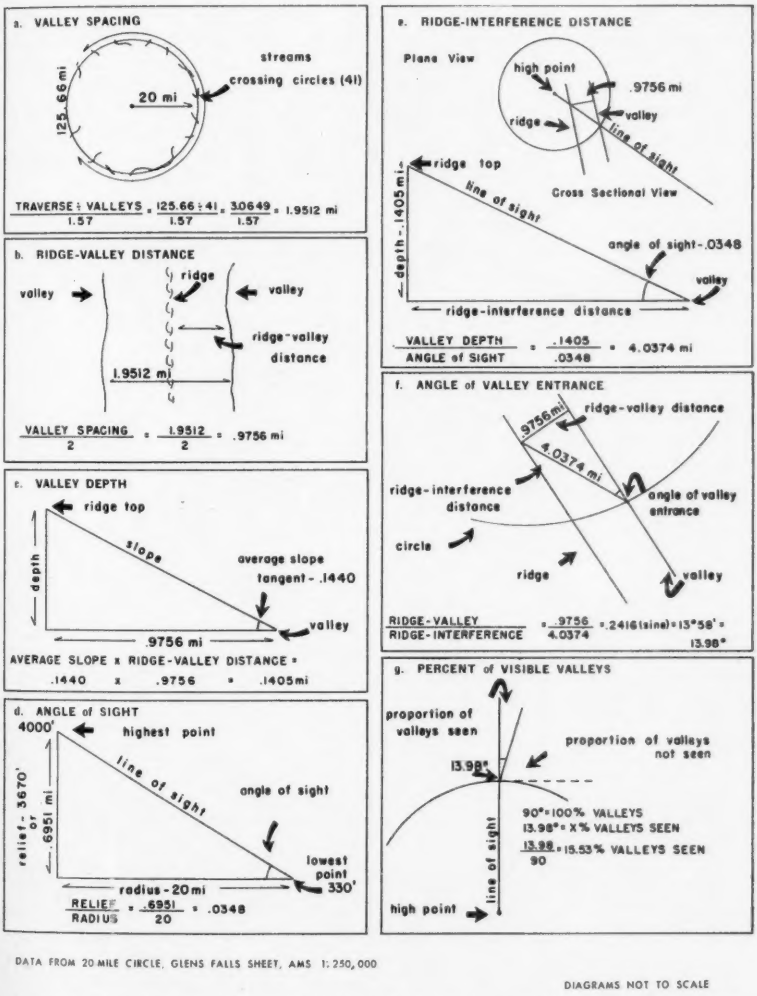

DATA FROM 20 MILE CIRCLE, GLENS FALLS SHEET, AMS 1:250,000

DIAGRAMS NOT TO SCALE

Figure 1. Graphic presentation of terrain model to predict number of protected valleys

counts per mile times contour interval of the map ÷ 3361. For the 20-mile circle, there were 4.84 contour counts per mile; this figure multiplied by the contour interval of the map, 100 feet, equals 484; 484 ÷ 3361 results in an average slope tangent of .1440.

f. VALLEY SPACING (Fig. 1a) denotes the average distance between valleys. This is computed by counting the number of valleys along a random traverse, in this case the circumference of the circle, and substituting in the equation: traverse ÷ valley number ÷ 1.57 or 125.66 ÷ 41 ÷ 1.57 = 1.9512 miles.

g. RIDGE-VALLEY DISTANCE (Fig. 1b). Since it has been assumed that the ridges are the same distance apart as the valleys, the distance from a ridge to a valley will be half the valley spacing. In other words, the valley spacing of 1.9512, derived in step F, ÷ 2 = .9756 mile.

h. VALLEY DEPTH refers to the perpendicular distance between the top of a ridge and the bottom of a valley (Fig. 1c). Visualizing the cross section of a valley as a right triangle, the valley side slope is the hypotenuse, the ridge-valley distance the base of the triangle, and the valley depth the short leg of the triangle. Thus, if certain dimensions of this triangle are known, others can be computed by the standard formulae for a right triangle. The tangent of one angle is known, the average slope tangent, .1440, and the length of the base is known, the ridge-valley distance computed in step G, .9756 mile. To calculate the length of the other leg of the triangle, the depth of the valley, multiply the tangent .1440 by the length .9756. This will result in an average valley depth of .1405 mile.

i. ANGLE OF SIGHT (Fig. 1d) designates the angle a line of sight makes between the viewing point and a valley at a given distance. The lowest valley on the circle was used to calculate an angle of sight. Again, the cross-sectional view of this situation can be visualized as a right triangle with the line of sight connecting the high and low points of the hypotenuse, the distance between the two points (the radius of the circle) the base of the triangle, and the difference in elevation between the two points (the relief) the other leg. The tangent of the angle formed by the line of sight between the two points is computed by dividing the relief by the radius, or .6951 mile by 20 miles. The tangent then is .0348.

j. RIDGE-INTERFERENCE DISTANCE (Fig. 1e) is the distance from a valley to its parallel ridge along a line of sight. This distance will be greater than the straight-line distance between ridge and valley, as computed in step G, and will depend on the angle at which a valley crosses the circle. In plan view the situation will be like the diagram at the top of Figure 1e. The valley crosses the circle at a particular angle, the ridge parallels this valley at a distance of .9756 mile. A line of sight is projected from the high point at the center of the circle to the place where the valley crosses the circle. The distance from the point at which the valley enters the circle to the ridge along the line of sight is the ridge-interference distance. In cross section, as in the lower diagram, the angle of sight is the hypotenuse of a right triangle, the ridge-interference distance the base of the triangle, and the valley depth the opposite leg. The value for ridge-interference distance is obtained by dividing the valley depth by the angle of sight, or .1405 ÷ .0348 = 4.0374 miles.

k. ANGLE OF VALLEY ENTRANCE (Fig. 1f). When all valleys have the same depth and spacing and are assumed to be parallel, only one other variable will determine whether or not a given valley is seen from a particular point—the angle at which the valley enters the area under observation. This diagram is an enlargement of the plan view in Figure 1e. If the geometric properties of the average valley are still in terms of a right triangle, the sine of the angle of valley entrance is computed by dividing the ridge-valley distance by the ridge-interference distance. Thus, .9756 ÷ 4.0374 = .2416. The sine expressed in degrees is 13° 59′ or, to facilitate further computations, 13.98°.

l. PER CENT OF VISIBLE VALLEYS (Fig. 1g). Through steps a–k, a mathematical model that gives the dimensions of an average valley has now been constructed. To predict the number of valleys that can be seen, the angle of valley entrance will be converted to a percentage of visible valleys.

The valley that enters an area directly toward the point from which a line of sight is projected—that is, the valley that is an extension of the line of sight and therefore has an angle of 0°—will always be seen. The valley tangent to the circle and at a right angle to the line of sight—in other words, the valley that forms a 90° angle with the line of sight—will not be seen. Between these two extremes there is an angle at which a valley can just barely be seen. This angle is referred to as the "limiting angle" and is governed by the valley dimensions. Valleys forming angles more acute than

the limiting angle would, in all likelihood, be seen, but valleys forming angles greater than the limiting angle probably would not be seen. In the model, the computed angle of valley entrance represents the limiting angle.

Since it has been assumed that angles are equally likely between 0° and 90°, it can be said that a right triangle contains all the valleys in a given area. If this right triangle is divided into two parts by the entrance angle of the average valley, the section of the triangle that lies to one side of the line formed by this angle is analogous to the proportion of valleys seen in that area; the section of the triangle that lies to the other side of this line is analogous to the proportion of valleys that cannot be seen.

In step k the angle of valley entrance for the 20-mile circle was found to be 13.98°. A triangle that contains 90° is said to represent 100 per cent of the valleys. In other words, 90° is equal to 100 per cent. When 13.98° of the total 90° forms the dividing line between the seen and unseen valleys, a percentage can be determined by simple arithmetic. If 90° =100%, 13.98°=x%; 13.98÷90=15.53%. Therefore, 15.53% of the valleys are visible, 84.47% are not. To convert the percentage to an actual number of valleys, multiply the number of valleys that crossed the circle, in this case 41, by this percentage, 41×15.53% =6. From the model it is predicted that on the Glens Falls sheet 15.53%, or 6, of the valleys that cross a circle 20 miles from the viewing point will be visible from that point.

A number of visible valleys were predicted for each of the 40 experimental circles in this same manner, and the predicted number was compared with the actual number previously determined by profile.

Figure 2 shows the comparison for the Glens Falls sheet. Correlation of the predicted with the actual number of visible valleys results in a correlation coefficient of .4414. The significance of the "r" is revealed by the F value 4.35. According to significance tables, the least significant value for F, at the 5 per cent level, is 3.49.

The same type of graph for the Grand Canyon sheet appears in Figure 3. This graph also shows that the two lines follow the same trend. Here the correlation results in an "r" of .8605 with a significance value of 51.36. As in the other case, the least significant value for F at the 5 per cent level is 3.49.

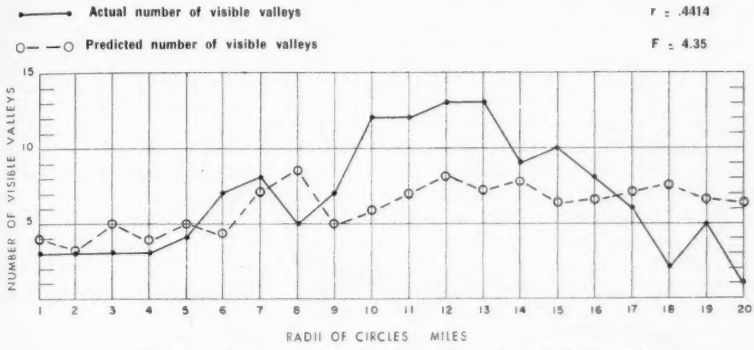
Actual number of visible valleys
Predicted number of visible valleys
r = .4414
F = 4.35
NUMBER OF VISIBLE VALLEYS
15
10
5
1 2 3 4 5 6 7 8 9 10 11 12 13 14 15 16 17 18 19 20
RADII OF CIRCLES MILES

Figure 2. Comparison of predicted and actual number of visible valleys

These results are encouraging and suggest that the concept of a mathematical terrain model to predict line-of-sight information is valid, that the model is realistic, and that it will be applicable in different types of terrain. Possible areas for improvement of the model are under consideration, but to date no final conclusions have been reached. Some thought has been given to the following as possibilities for overcoming the existing error.

The construction of the model and subsequent predictions are based on the assumption that the angles at which valleys intercept a line of sight are equally likely between 0° and 90°. Theoretically, an infinite number of angles can intersect a line at a point, and no two of these angles can be equal; therefore, the assumption should be valid. However, the actual angles at which the streams cross the circles on the Glens Falls sheet are not randomly distributed.

The mean angle here is 28° rather than 45° which would be the case if the angles were equally likely between 0° and 90°. Because the viewing point was placed subjectively on the highest elevation and is the center of the circles, bias may have been introduced unwittingly, and possibly a random distribution of stream angles on which to base predictions can no longer be assumed. Clearly the distribution of stream angles requires further detailed study.

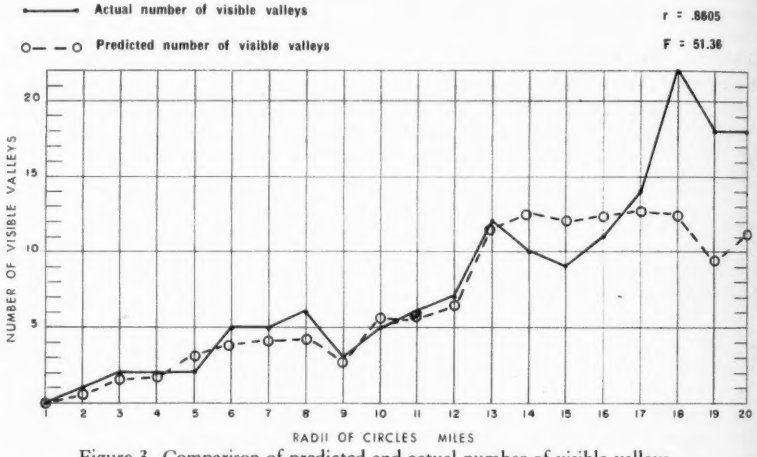
Actual number of visible valleys
Predicted number of visible valleys
r = .8605
F = 51.36
NUMBER OF VISIBLE VALLEYS
RADII OF CIRCLES MILES

Figure 3. Comparison of predicted and actual number of visible valleys

The extent to which peaks and ridges at some distance from a valley interfere with lines of sight should be investigated. In developing the model the only height of land considered capable of blocking a line of sight was the ridge nearest the valley, but it is possible that a peak or ridge farther from the valley would cause interference. The pattern of prediction errors leads us to believe that the grain of the landscape contributes to this blocking effect. Landscape grain is indicative of the spacing of the major ridges and valleys. In the Glens Falls area, grain is at 7 miles—that is, 7 miles from the highest point there is another ridge of essentially the same elevation. On the graph of prediction errors it has been noted that, up to 7 miles, the predicted number of visible valleys follows the actual number quite closely, and the error is small. Beyond the 7-mile circle, there is a tendency toward underprediction, and the error increases. The grain of the Grand Canyon was found to be at the 14-mile circle, and, here again, for the first 14 miles the predicted and actual number of valleys are very close. At grain size, the predictions tend to change to less than actual, while the error increases.

Angle of sight also deserves more attention. For the model, an angle of sight was formed between the viewing point and the deepest valley on the circle. Cursory examination shows that a line of sight projected from the viewing point to the elevation of an average valley (the mean elevation of all the valleys on the circle) would give an angle of sight smaller than that already computed. A smaller angle of sight would result in fewer predicted visible valleys. This in turn should bias the predictions toward underprediction and hence might simplify the task of correcting the error.

One other aspect of the model that must be scrutinized is the fact that the highest point on the sheet was selected as the viewing point. This point is presumably the optimum location from which to keep the entire area under surveillance, but how effective lines of sight are when projected from a point other than the highest point has yet to be discovered. Some changes in the existing model will probably be necessary in order to predict valley visibility when the viewing point is not the highest point.

This study was based in part on Research Study Report EA-10: *Preliminary investigation of a method to predict line-of-sight capabilities:* HQ, QM R&E Center, Natick, Mass., July 1959.

Quartermaster Research and Engineering Center, Natick, Mass.

JOHN E. SANDERS
LUCIAN PLATT
R. W. POWERS

BALD MOUNTAIN LIMESTONE, NEW YORK: NEW FACTS AND INTERPRETATIONS RELATIVE TO TACONIC GEOLOGY

Abstract: The "Bald Mountain limestone" of Ruedemann has been found to consist of the upper part of the autochthonous carbonate-rock sequence of the Champlain-Hudson valleys and not to be part of the Taconic sequence. At Bald Mountain this carbonate-rock sequence is overlain unconformably by the Snake Hill shale, with local basal limestone-pebble conglomerate (Rysedorph Hill conglomerate of Ruedemann). The Taconic thrust is present; along it the fossiliferous Lower Cambrian and younger fine-grained terrigenous rocks of the allochthonous sequence have been thrust over the autochthonous Middle Ordovician graptolite-bearing black shale.

In connection with geologic mapping of the Cossayuna 7½-minute quadrangle, Washington County, New York, by Lucian Platt in 1958 and 1959 (1960, Ph.D. dissertation, Yale Univ.), a Yale Expedition to Bald Mountain, in the town of Greenwich, Washington County, New York, was organized under the leadership of Visiting Professor S. W. Carey.[1] On November 14–15, 1959, a party of 14, including 11 graduate students, Platt, Sanders, and Carey, made a detailed study and plane-table map of the abandoned Bald Mountain quarry and vicinity. The authors of this paper studied the carbonate rocks and examined all the localities mentioned by Ruedemann (1914) within the area shown on his geologic map as "Bald Mountain limestone."

Bald Mountain has long been a classic locality for Taconic geology; fossiliferous Ordovician limestones are here exposed in the abandoned quarry along the western base of the hill, whereas fossiliferous Lower Cambrian and younger fine-grained terrigenous rocks of the Taconic sequence lie structurally above the limestones and cap the hill. The limestones form part of an outcrop belt which is nearly 5 miles long and half a mile wide and extends from approximately 1 mile north of Bald Mountain to a point 3½ miles south of the town of Middle Falls.

Two other rock units are locally present and are significant in this discussion: a limestone-pebble conglomerate containing Trenton-age fossils in both pebbles and matrix (Rysedorph Hill conglomerate of Ruedemann) and an upper Middle Ordovician graptolite-bearing black shale (Snake Hill shale of Ruedemann).

Present understanding of the Bald Mountain limestone is derived from Ruedemann (1914), who published the most detailed map of the area, summarized previous work, and proposed the name Bald Mountain limestone for the belt of carbonate rocks that includes the exposures in the abandoned quarry. Ruedemann considered the Bald Mountain limestone to be a single formation of Early Ordovician age in the Taconic sequence; he dismissed reports by earlier workers of Trenton-age fossils from limestones near Bald Mountain and regarded these fossils as having come from pebbles of fossiliferous limestone in the Rysedorph Hill conglomerate.

We have found the following units in the belt of "Bald Mountain limestone" of Ruedemann's map (from youngest to oldest):

Unit 6: Thin-bedded black limestone; fossiliferous, with abundant brachiopods, *Cryptolithus*, *Prasopora*, and other fossils. At least 40 feet thick, with top not seen in section that exposes base. Tentatively assigned to the lower Trentonian (= Shoreham member of Glens Falls limestone of Kay, 1937, p. 264–265)

Unit 5: Thicker-bedded gray aphanitic limestone; nonfossiliferous, 1–2 feet thick (thinned extension of a limestone of Black River age?)

Unit 4: Thick-bedded light-gray nonsandy dolostone; nonfossiliferous; thickness not measured; similar to the rock quarried at Middle Falls

Unit 3: Thick-bedded light-gray limestone, estimated to be approximately 200 feet thick; gastropods, fossils locally abundant; quarry

[1] Supported by a grant from the Shell Fund for Fundamental Research at Yale University

rock of Bald Mountain ("Bald Mountain limestone" of Ruedemann's fossils and the classical concept in the literature, but only part of the "Bald Mountain limestone" of Ruedemann's map)

Unit 2: Very sandy dolostone-dolomitic sandstone, light-gray, cross-stratified, with current flow indicated from the west; nonfossiliferous; at least 250 feet thick by our incomplete detailed measurements in the woods just south of the Bald Mountain quarry south face ("Calciferous sandstone" of early classifications?)

Unit 1: Laminated dolostone, outcrops showing distinctive "striped" appearance; only the upper few feet observed beneath Unit 2. (Exposed on New York Route 40 west of Schuyler Mountain and half a mile north of the section containing Units 4–6; also present as a fault slice along the Taconic thrust and visible in the south quarry face at Bald Mountain)

This section is confirmed by the order of beds in several small folds that occur on the west face of Schuyler Mountain (Schuylerville 15-minute quadrangle; Louse Hill of Ruedemann's map). Units 4–6 are well shown in road cuts on the east side of State Route 40, 2.1 miles south of Middle Falls. Unit 4 also crops out in the woods west of the Bald Mountain quarry.

According to John Rodgers (personal communication), Marshall Kay had earlier observed the presence of the Trentonian-age limestone in this belt at the Route 40 cut, but we are not aware that Kay published this discovery.

We are indebted to Terry Offield for drawing our attention to the similarity between this sequence and the upper two-thirds or so of the Valley or autochthonous carbonate-rock sequence, known in the areas to the south as the "Wappinger" or "Kittatinny" in older literature, and the similarity to the sequence worked out by E. B. Knopf (1927; 1946; 1956) near Stissing Mountain, Dutchess County, New York.

We consider that the Bald Mountain limestone represents the upper part of the autochthonous carbonate-rock terrane that extends from the Champlain Valley southwestward into New Jersey, as contended by the first geologists who studied it. This terrane is critical for the concept of a Taconic allochthone, for it consists entirely of carbonate rocks that range in age from Early Cambrian to Early Trentonian ("Trenton" is used here in the sense of Kay, 1937, not of Cooper, 1956). At Bald Mountain these carbonate rocks lie structurally below the Lower Cambrian and younger fine-grained terrigenous rocks of the Taconic sequence, hence a thrust must be present.

An unconformity with karst topography occurs between these autochthonous carbonate rocks and the overlying Rysedorph Hill conglomerate and Snake Hill shale; this is part of the same regional unconformity emphasized by Bucher (1957). On the other hand, our concept that the Bald Mountain limestone coincides with the upper part of the autochthonous carbonate sequence is diametrically opposed to Bucher's interpretation that the "Bald Mountain limestone" underlies the Schaghticoke shale (part of the "Taconic" sequence), and the structural, stratigraphic, and paleontologic relationships at Bald Mountain (Lower Cambrian beds thrust on Middle Ordovician beds) deny Bucher's and others' proposed alternatives to a Taconic thrust. The relationships at Bald Mountain exactly coincide with those found by Kaiser (1945), Fowler (1950), Zen (1959a), and others at the northeastern end of the Taconic belt; they indicate that the autochthonous carbonates were faulted, folded, and eroded in the middle Trenton (Vermontian disturbance of Kay, 1937) and afterwards buried by autochthonous "shales" of later Trenton age. The Rysedorph Hill conglomerate is a local limestone-pebble conglomerate in this younger autochthonous fine-grained terrigenous sequence; as pointed out by Kay (1937, p. 266–267) these limestone-pebble conglomerates cannot be related to the advancing Taconic thrust, for the Taconic sequence contains no such carbonate rocks as are found among these pebbles. Zen (1959b) has indicated that the Taconic thrust mass was emplaced during deposition of the Snake Hill shale, the upper unit of the autochthonous "shales" which unconformably overlies the previously deformed and eroded autochthonous carbonates.

Carbonate rocks occur in a continuous belt along the lowland east of the Taconic upland as well as along the west side of this upland. This relationship demands the existence of a Taconic allochthone; it cannot be explained by facies changes or imbricate thrusts.

References Cited

Bucher, W. H., 1957, Taconic klippe: a stratigraphic-structural problem: Geol. Soc. America Bull., v. 68, p. 657–674

Cooper, G. A., 1956, Chazyan and related brachiopods: Smithsonian Misc. Coll., v. 127, pt. 1, 1024 p.

Fowler, Philip, 1950, Stratigraphy and structure of the Castleton area, Vermont: Vt. Geol. Survey Bull. 2, 83 p.

Kaiser, E. P., 1945, Northern end of the Taconic thrust sheet in western Vermont; Geol. Soc. America Bull., v. 56, p. 1079–1098

Kay, G. M., 1937, Stratigraphy of the Trenton group: Geol. Soc. America Bull., v. 48, p. 233–302

Knopf, E. B., 1927, Some results of recent work in the southern Taconic area: Am. Jour. Sci., 5th ser., v. 14, p. 429–458

— 1946, Stratigraphy of the lower Paleozoic rocks surrounding Stissing Mountain, Dutchess County, N. Y. (Abstract): Geol. Soc. America Bull., v. 57, p. 1211–1212

— 1956, Stratigraphy and structure of the Stissing area, Dutchess County, New York (Abstract): Geol. Soc. America Bull., v. 67, p. 1817–1818

Ruedemann, Rudolf, 1914, *in* Cushing, H. P., and Ruedemann, Rudolf, Geology of Saratoga Springs and vicinity: New York State Mus. Bull. 169, 177 p.

— 1942, Cambrian and Ordovician geology of the Catskill quadrangle: New York State Mus. Bull. 331, 251 p.

Zen, E-an, 1959a, Stratigraphy and structure at the north end of the Taconic Range and adjacent areas: New England Intercollegiate Geol. Conf. 51st Meeting Guidebook, p. 1–13

— 1959b, Problem of the "Hortonville formation" in west-central Vermont (Abstract): Geol. Soc. America Bull., v. 70, p. 1705

Dept. Geology, Yale University, New Haven, Conn.

Manuscript Received by the Secretary of the Society, June 2, 1960

THEODORE R. WALKER

GROUND-WATER CONTAMINATION IN THE ROCKY MOUNTAIN ARSENAL AREA, DENVER, COLORADO

Abstract: Improper waste-disposal practices at the Rocky Mountain Arsenal have seriously damaged the free ground-water aquifer throughout an area of approximately 6½ square miles. Contaminants include chlorates and 2,4-D-type compounds, both of which are effective herbicides. Contaminated ground water within the affected area is toxic to agricultural crops and unpotable for humans. Corrective measures have been taken to halt further contamination, but the area of toxicity is expanding owing to migration of the body of ground water already contaminated.

Since 1943, chemical factories at the Rocky Mountain Arsenal, northeast of Denver, Colorado (Fig. 1), have manufactured materials for chemical warfare and other chemical products. Between 1943 and 1957, waste products from these operations were dumped into artificial reservoirs that were located above the water table and separated from it by permeable sediments. When the reservoirs were constructed no attempt was made to seal them, and consequently conditions favored infiltration of the waste water into the subsurface throughout the 14 years that the reservoirs were used as waste basins.

These waste-disposal practices have seriously contaminated the underlying free ground-water aquifer in a large area that extends northwest from the waste basins. This aquifer, because it is highly permeable and can be penetrated at a shallow depth, is used extensively as a source of water for domestic and livestock use. In addition, it is the only aquifer in the area that can yield the large quantities of water needed for irrigation purposes. Owing to contamination from the Arsenal, however, approximately 6½ square miles of this aquifer now contains ground water that generally is toxic to plants, unpotable for humans, and apparently injurious to livestock.

Alternate supplies of water are not readily accessible in the area. Good-quality ground water in quantities adequate for domestic and livestock use can be obtained from deep bedrock aquifers, but many residents in the affected area do not have deep wells, and the high cost of new wells has forced many of these residents to import water. Furthermore, the deep bedrock aquifers are not permeable enough to supply the large quantities of water that are needed for irrigation purposes. Irrigation ditches traverse the affected area, but, because farmers here have low priorities on ditch water, this source of water is inadequate; since no other source of irrigation water is available, the farmers have been forced to decrease the number of acres they cultivate.

Contamination of the ground-water supplies has caused decline in property values. Qualified land appraisers have estimated that, owing solely to the loss of usable ground water, land formerly valued at $500 per acre now is worth only $250 per acre. Additional damage also has resulted from continued crop loss owing to prolonged retention of the toxic substances by soils. In some places, land that was irrigated with toxic water in 1954 did not yield normal crops in 1960, although toxic water has not been applied to the soil since the initial irrigation in 1954.

Arsenal authorities first became aware of the problem in 1954, and in 1955 measures were taken to halt further contamination of the aquifer. The volume of waste produced by Arsenal operations was greatly reduced, and a reservoir with an asphalt-sealed bottom was constructed for waste disposal. This reservoir, which was completed in 1957, has received all the waste produced since that time. Plans also are in progress for construction of a well 10,000 to 12,000 feet deep that will permit injection of the waste water into deep bedrock formations that cannot be used for water supplies. It is hoped that these corrective measures will prevent further contamination of the shallow aquifer. However, extensive damage already has occurred; the front of the toxic ground water has migrated 5 miles from the waste basins, and continued migration can be anticipated.

Investigation of this problem began in June

Geological Society of America Bulletin, v. 72, p. 489–494, 2 figs., March 1961

1954, when a complaint of crop damage was made to Arsenal authorities by Mr. Jesse E. Powers, owner of a farm located northwest of the Arsenal boundary (Fig. 2). Since that time various aspects of the problem have been investigated by private consultants, university research groups, and several government agencies, including the U. S. Geological Survey (Petri and Smith, 1956). This paper summarizes the hydrogeologic aspects of an investigation of the problem that was carried on by three members of the University of Colorado faculty between 1956 and 1960. Three aspects of the problem were investigated in the study: (1) a botanical and chemical phase for the purpose of identifying the phytotoxic materials (those poisonous to plants) in the ground water; (2) a chemical and botanical phase to determine methods of removing or neutralizing the phytotoxic substances; (3) a geologic phase to determine the path of migration of water seeping into the subsurface from the Arsenal waste basins, and its relationship to areas of phytotoxic ground water northwest of the Arsenal. The botanical research was directed by Dr. Erik Bonde of the Biology department.

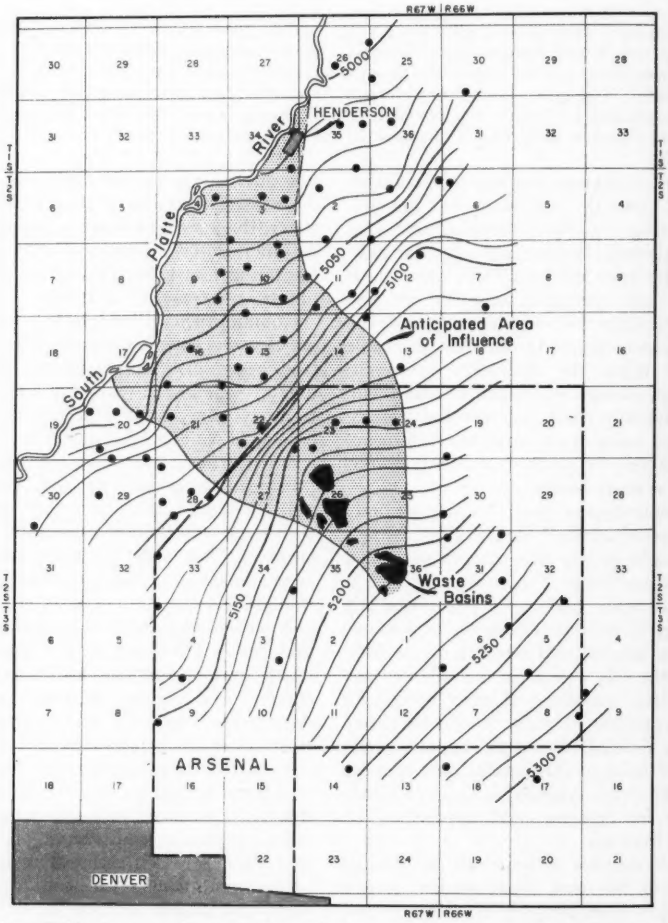

Figure 1. Water-Table Contours for April 1956. Showing anticipated area of influence of Arsenal waste basins. Water-table elevations at control points are taken from Petri and Smith (1956).

the chemical research by Dr. Paul Urone of the Chemistry department. The details of the results of these phases of the investigation will be published separately. The geologic phase was the responsibility of the writer, and the results of that study are presented here.

The Arsenal, including the area in the vicinity of the waste basins, is underlain by permeable surficial deposits consisting of upland alluvium and eolian sand and silt of Pleistocene and Recent age. These deposits in turn are underlain by bedrock sediments composed of poorly consolidated sandstone, siltstone, conglomerate, and mudstone of Cretaceous and Tertiary age. Regardless of age, all the interconnected permeable sediments above the highest continuous bed of impermeable material behave as a hydrologic unit and contain free ground water that migrates under the influence of the water-table gradient. These permeable sediments have a maximum thickness of about 75 feet and an average thickness of about 40 feet, the lower part of which is saturated and forms the shallow aquifer in the area. Owing to relief on the bedrock surface the thickness of the saturated zone ranges from 0 to about 50 feet.

At present ground-water contamination generally is limited to this shallow aquifer. Deeper bedrock aquifers occur in the area, but these contain confined ground water that is separated from the contaminated water by impermeable clay layers. These aquifers have been contaminated only where old wells have been abandoned, or where damaged or improperly sealed well casings have locally permitted infiltration of the toxic water through the confining layers.

The configuration of the water table (Fig. 1) indicates that ground water migrates beneath the Arsenal waste basins in a generally northwest direction toward the South Platte River valley. These data indicate that any water recharged to the aquifer from the waste basins also will migrate northwestward. The area affected by such recharge should lie generally within the anticipated area of influence shown on the map, the boundaries of which have been determined by constructing lines that originate at the edge of the waste basins and extend in a downslope direction perpendicular to the water-table contours. The actual area of influence of the Arsenal waste basins, however, can be expected to vary somewhat from the anticipated area shown in Figure 1 because local inaccuracies may exist in the interpolated positions of the water-table contours, and because lateral diffusion may carry some of the dissolved toxic materials beyond the borders of the anticipated area. Nevertheless, in a general way the migration of water that seeps into the subsurface from the waste basins should follow the path outlined (Fig. 1).

That the predicted migration has occurred is evident from Figure 2, which shows a striking correlation between the anticipated area of influence of the waste basins and the actual area of phytotoxic ground water. The boundary of the latter has been determined from data collected in the botanical phase of the study in which water samples from selected wells throughout the area were used to irrigate test plants grown in University greenhouses. The boundary is generalized, but it reasonably delineates the area that presently contains phytotoxic ground water, and it shows the direction toward which the contaminated water is moving, where additional crop damage may occur in the future if irrigation with ground water is continued.

The ground water is not consistently phytotoxic everywhere within the affected area. Water from some wells has not caused plant damage in the greenhouse experiments, and water from other wells has caused plant damage in some experiments and produced normal plant growth in others. These differences in toxicity from place to place and from time to time are caused in part by variations in the permeability of the sediments and in part by variations in the amount of dilution by uncontaminated recharge from such sources as rainfall, irrigation ditches, and underflow in the South Platte alluvium. In spite of these local variations in toxicity, however, the evidence indicates that ground water in the shallow aquifer is potentially toxic to plants throughout the area shown to be phytotoxic in Figure 2, and plant damage can be expected wherever this water is used for irrigation.

Studies made in the chemical and botanical phases of the investigation have determined that at least two phytotoxic substances are present in the contaminated water. Each toxicant tends to be concentrated in a separate part of the contaminated area (Fig. 2), and each is related to a separate type of industrial effluent. In the area farthest from the Arsenal waste basins, the phytotoxicity is caused by dissolved chlorate, and is related to waste products that were dumped into the basins between 1944 and 1950 (Weintraub, 1959, p. 4–6). These waste

products have not recently been a part of the industrial effluent. The migration front of this type of toxic ground water lies about 5 miles from the waste basins, and the total area presently affected is about 3 square miles. Nearer the waste basins the phytotoxicity is caused by either 2,4-dichlorophenoxyacetic acid (2,4-D) or a closely related compound and is related to wastes produced at the Arsenal since 1950 (Weintraub, 1959, p. 8–10). At the time of this writing, ground water containing 2,4-D-type toxicity has migrated about 3½ miles from the basins and has contaminated an area of about 3½ square miles, making a combined area of about 6½ square miles that is underlain by generally phytotoxic ground water.

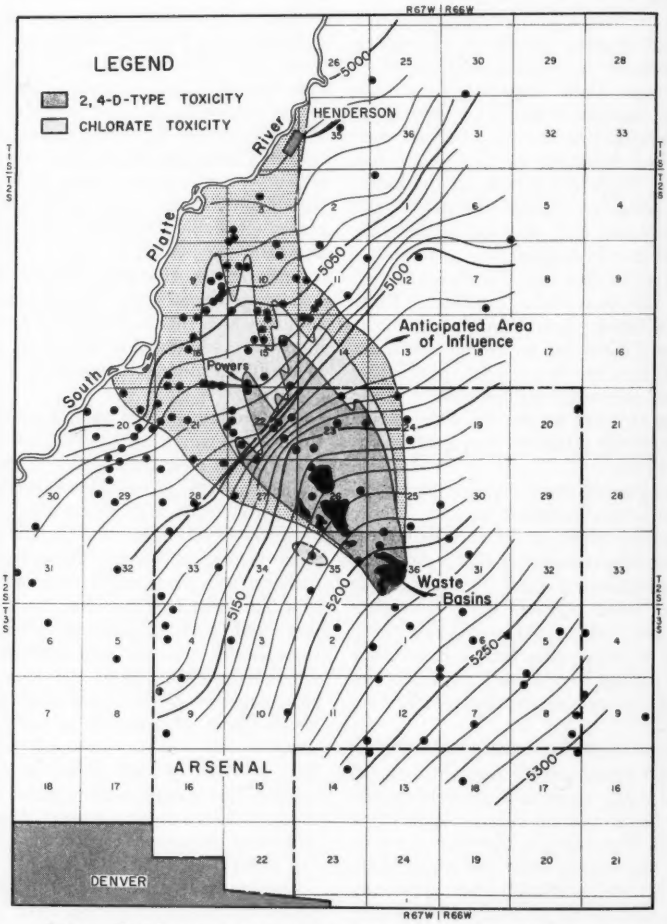

Figure 2. Areas of Generally Phytotoxic Ground Water. Control points show locations of samples tested in greenhouse experiments.

Available Arsenal records indicate that chlorates and 2,4-D-type compounds were at no time direct waste products of any of the Arsenal operations. These toxicants appear to have originated as a result of chemical reactions that occurred within the waste basins where

effluent from different types of operations became mixed.

The present body of phytotoxic ground water will probably continue to move in the direction of the water-table gradient, and the area of toxicity will continue to expand. The configuration of the water-table contours and the shape of the west boundary of the phytotoxic area shown in Figure 2 indicate that the direction of ground-water migration changes from northwest to northeast as the water moves into the alluvium of the South Platte River valley. Hence future expansion of the phytotoxic area can be expected in a northeast direction within the South Platte River valley, toward the town of Henderson. In addition, continued expansion may eventually carry the toxicants into the surface water of the South Platte River, but dilution here will probably be great enough to prevent the river water from becoming phytotoxic.

The rate of migration of the front of the body of phytotoxic water is governed by permeability of the aquifer, water-table gradient, amount of recharge of phytotoxic materials, and amount of dilution by uncontaminated water. Because these are variable factors, the migration rate of the front is not the same everywhere. Based on the time required for the phytotoxic waste water to reach control points in the affected area, the maximum migration rate along the front is estimated to be less than 3 feet per day. The initial migration of the chlorate front across the area between the waste basins and the Powers farm (Fig. 2) was at a rate of approximately 3 feet per day, and the front of the area of 2,4-D-type toxicity migrated across the same area at a similar rate. The present migration rate of the phytotoxic front, however, probably is somewhat slower than when the front was near the Powers farm because of the increased tendency for dilution along the more extended front, and because recharge of significant amounts of chlorates to the aquifer has been eliminated since 1950.

The front of the area of 2,4-D-type toxicity steadily is encroaching upon the area of chlorate toxicity, and some wells that formerly yielded chlorate water now yield water that causes 2,4-D-type damage to plants. This encroachment probably will continue, but whether or not the 2,4-D front will eventually overtake the more slowly moving chlorate front is problematical.

The extent of the area that ultimately will be affected by phytotoxic ground water will depend in part on the amount of dilution needed to reduce both the chlorate and 2,4-D-type toxicants to nontoxic concentrations, and in part on how effectively the asphalt membrane in the bottom of the present waste basin prevents further recharge of the toxicants. Assuming that the source of contamination has been effectively sealed, the concentration of the contaminants at the toxic front eventually will reach nontoxic levels owing to mixing with uncontaminated water, and expansion of the phytotoxic area will cease. Adequate dilution, however, may not occur until the fronts of both types of phytotoxic ground water have migrated to the South Platte River. Meanwhile, the toxicity of the entire body of contaminated water should gradually decrease owing to dilution by continued recharge from uncontaminated surface sources such as rainfall and irrigation ditches and from the uncontaminated underflow in the South Platte alluvium. The time necessary to dilute the phytotoxic water effectively, however, is not known. It will probably take many years to dilute all the water in the affected area to the extent that it will be consistently safe for use, because chlorate and 2,4-D are toxic to plants in concentrations of only a few parts per million, and both substances appear to be chemically stable under the natural conditions in the aquifer.

Restoration of the normal ground-water quality in the affected area will be aided by any measure that will help to speed natural dilution, such as excessive irrigation of the area with uncontaminated surface water. At present, however, excessive irrigation does not seem practicable because in the affected area the existing supplies of uncontaminated water from both surface and subsurface sources are inadequate even for normal needs. Moreover, it is unlikely that additional water can be imported into the area because all available surface water in this semiarid region has been previously allocated to other uses.

Possibly the existing toxicity also could be diminished by artificially recharging the aquifer with a neutralizing agent, but as yet no safe and economical substance has been determined.

This study provides a noteworthy example of the damage that results to ground-water supplies from improper methods of industrial waste disposal. Furthermore, it typifies a commonplace problem. The use of basins for waste-disposal purposes is common practice, but there is wisdom in such practice only if infiltration of

contaminated water into usable aquifers can be effectively prevented. Where unsealed waste basins containing toxic waters are located on permeable material, as at the Rocky Mountain Arsenal, they serve the unintended function of infiltration basins that provide local sources of contaminated recharge. Damage to the aquifer becomes inevitable because the soluble toxic compounds readily pass through soils into the underlying ground water. Once these compounds are present in ground water they are difficult to remove; natural dilution is slow, and treatment or artificial flushing generally is impractical. Moreover, because the rate of ground-water migration generally is slow, large areas may be affected before the damage is detected, and many years may be required before the aquifer can be restored to its normal quality.

The only reasonable cure for such problems is the prevention of contamination. This requires knowledge of the hydrogeologic conditions at proposed sites of waste-disposal basins. With adequate investigation, problems such as those that now exist near the Rocky Mountain Arsenal are readily anticipated before they occur, and measures can be taken to avoid them.

Acknowledgments

This investigation was sponsored by the United States Army Chemical Corps under research contract DA-05-021-CML-10,092. Expenses for preparation of the manuscript were financed by a grant from the Council on Research and Creative Work at the University of Colorado. James McConaghy, Edward Moulder, and Paul Schneider, members of the staff of the Ground-Water Branch of the U. S. Geological Survey, critically read the manuscript and made many helpful suggestions.

References Cited

Petri, L. R., and Smith, R. O., 1956, Investigation of quality of ground water in the vicinity of Derby, Colorado: U. S. Geol. Survey Open-File Rept., 56 p., 7 pls., 5 figs., 13 tables

Weintraub, R. L., 1959, Toxicity of Rocky Mountain Arsenal waste: U. S. Army Chemical Corps Status Rept. (unpublished)

University of Colorado, Boulder, Colo.
Manuscript Received by the Secretary of the Society, June 30, 1960

A. R. McBIRNEY
MYRON G. BEST

EXPERIMENTAL DEFORMATION OF VISCOUS LAYERS IN OBLIQUE STRESS FIELDS

Abstract: Alternating layers of soft viscous wax and asphalt were squeezed in various orientations within a constant-strain squeeze box. Compression produced folds and small wrinkles whose axial orientation is determined solely by the intersection of the plane normal to the direction of maximum shortening with the layer surface. Formation of folds in viscous materials appears to be a function of the strain rate.

Many structural features of folded rocks have been used to interpret the stress systems responsible for their deformation without any real assurance of the geometrical relations involved. Although much work has been done on the orientation of fractures in known stress fields, little has been done on folded structures, and the dynamic interpretation of folds remains one of the most difficult problems of structural geology. Bucher (1956) and others have produced folds in flat-lying layered materials, but, to our knowledge, no attempt has been made to find the nature of non-elastic deformation when layers have other orientations with respect to the principal stresses. In the case of highly deformed strata, folding by compression in a direction parallel to a horizontal layering is merely a special case, which may, in fact, be far from common.

In order to determine the nature of deformation when layered, viscous materials are subjected to a simple set of stresses at various orientations with respect to the layers, we have performed a series of experiments using materials whose properties resemble those of rocks over prolonged periods of geologic time. Assuming elasticoviscous behavior in rocks, model theory (*cf.* Hubbert, 1937; Bucher, 1956) indicates that a suitable material for tectonic experiments must have a low elastic strength and a viscosity of about 10^7 poises. These properties are characteristic of substances that flow slowly under small differential stresses. The purposes of the experiments further required the use of substances whose relative competencies could be varied.

A satisfactory combination of these requirements was found in common asphalt and miscible mixtures of clear mineral oil and low-melting wax. By varying the proportions of wax and oil we obtained a range of viscosities. An added advantage is the sharp color contrast between the black asphalt and white wax mixture. Alternating, molded layers of these materials were placed in a squeeze box and compressed from an original length of about 25 cm to about 10 cm. This amounted to a horizontal shortening of approximately 60 per cent, which was compensated by a corresponding vertical elongation. In the initial experiments a box (Pl. 1, fig. 2) was used in which a fairly constant stress was applied through a system of weights and levers. This proved to have serious mechanical disadvantages and was replaced by

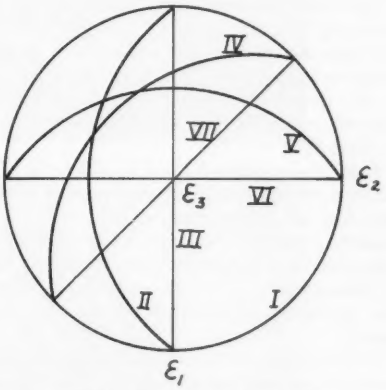

Figure 1. Orientation of layering in different experiments shown in stereographic projection (looking down into box). ϵ_1, ϵ_2, and ϵ_3 are principal strain axes in the deformed block. The $\epsilon_2\epsilon_3$ plane is normal to the direction of maximum shortening, and ϵ_2 is the direction of no strain.

Geological Society of America Bulletin, v. 72, p. 495–498, 2 figs., 2 pls., March 1961

another (Pl. 1, fig. 1) which was powered by an electric motor driving the piston through a gear reduction. By changing gears, reductions of 200,000 to 1 and 25,000 to 1 and corresponding strain rates of 7 mm and 57 mm per hour were produced.

A series of blocks with layers at the orientations shown in Figure 1 were used to determine the nature and orientation of folds produced by compression. In the simplest case, where the layering was initially horizontal (Case 1), the result was a set of folds with horizontal axes and vertical axial planes normal to the direction of compression (Pl. 1, fig. 2). The folds had an amplitude that increased upward, because of the cumulative effect of the vertical movement. Geometrically, they were neither parallel nor concentric, and genetically they cannot be classed as strictly flexural or shear folds because they appear to contain elements of both. A strong linear wrinkling measuring about 1–2 mm from crest to trough paralleled the fold axes in both the asphalt and wax layers.

This same block was then rotated 90° about a vertical axis and squeezed a second time in the direction of the first fold axis. A second lineation was produced, which was again normal to the direction of shortening. A portion of this twice-deformed block is shown in Figure 3 of Plate 1.

Case III represents a block in which the layers were oriented vertically and parallel to the direction of compression. Again, folds and wrinkling were produced, and in this case their axes were vertical. Despite marginal effects, the wrinkling and folds in the central portion of the specimen were essentially straight and parallel.

In some tests in which a more brittle wax mixture was used a parting or cleavage developed in a plane normal to the compression (Pl. 2, fig. 2). This parting did not extend through the asphalt.

In all other cases, except Case VI (where the only deformation was a vertical extension and layer thinning), compression produced folds and parallel wrinkling. The orientation of these linear features was defined by the intersection of the layering with a plane normal to the direction of maximum shortening.

To test the general case of layers inclined at

Figure 2. Schematic diagram illustrating the original orientation of pre-formed folds before deformation. σ_1, σ_2, and σ_3 are principal stress axes. Compression of the block was parallel to σ_1. The folds were nearly isoclinal and plunged at angles to all three stress axes.

various attitudes to the three principal stress axes a block was prepared with two nearly isoclinal folds, as shown in Figure 2. The preformed folds also served to overcome interlayer slip and rotation which were particularly troublesome in blocks with planar layers oblique to the compression.

A compression of about 50 per cent resulted in a very uniform bulk strain. The results are shown in Figure 3 of Plate 2, in which the wax medium has been removed, leaving a skeleton of asphalt layers. Several well-developed folds with parallel wrinkles were superposed on the

PLATE 1. DEFORMATION APPARATUS AND RESULTS OF CASE I

Figure 1. View of constant-strain squeeze box showing drive mechanism. One side of plate has been removed to show interior dimensions of the box. Position of the back plate is adjustable.

Figure 2. Alternating layers of asphalt and wax in an earlier model box folded by compression parallel to the horizontal layers. Note the cumulative effect of the folding and thickening of fold hinges. Asphalt-wax block measures 5 inches by 7 inches.

Figure 3. Result of second deformation of same block shown in Figure 2. Note primary lineation parallel to the large fold axes from the first deformation. The strong lineation on the limbs is the result of squeezing the block a second time in a direction parallel to the first fold axes.

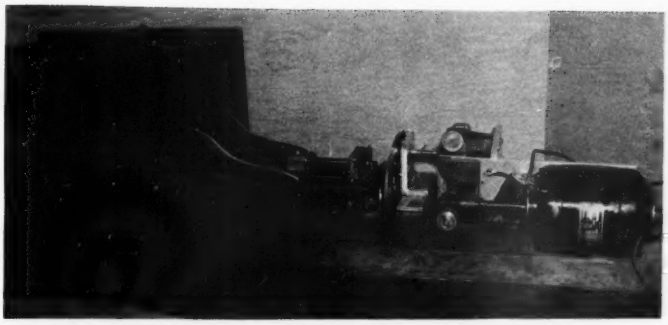

Figure 1

Figure 2

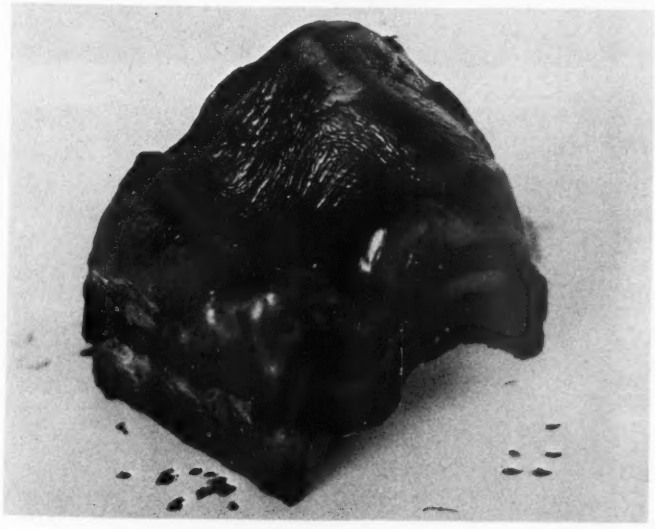

Figure 3

DEFORMATION APPARATUS AND RESULTS OF CASE I

McBIRNEY AND BEST, PLATE 1
Geological Society of America Bulletin, volume 72

Figure 1

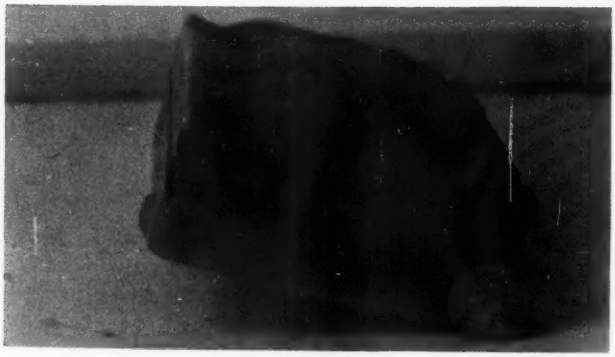

Figure 2

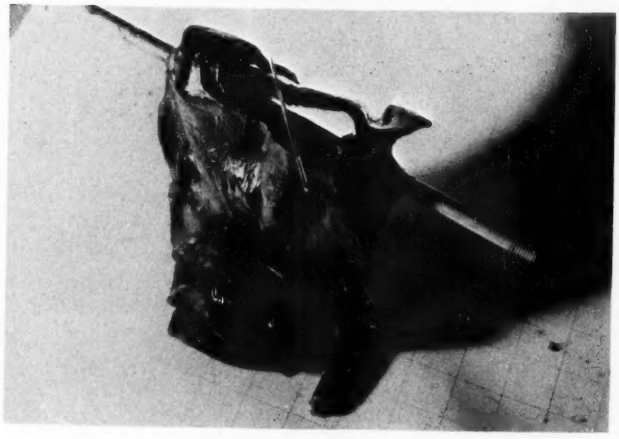

Figure 3

EXPERIMENTAL RESULTS

original isoclinal folds. Regardless of their plunge, the fold axes and wrinkles tended to lie in a plane normal to the direction of compression, and fold axial planes generally coincided with the same normal plane.

In all the experiments the linear fold elements lie within the plane normal to the maximum shortening, but their plunge is independent of the position of intermediate and minimum strain axes. The maximum component of elongation or flow may be oriented at any angle to the fold axes. Thus the orientation of stress and strain axes in a deformed body cannot be inferred from the trend and plunge of fold axes or lineations alone. Although expressed implicitly in the works of Sander (1926), E. Cloos (1946), and others, this principle is often ignored. The only conclusion we can safely draw from the orientation of these linear features is that they lie in a plane normal to the direction of compression and maximum shortening.

A second objective of the experiments was to determine the relationship between the size of folds and such factors as the rate of strain and the relative thickness and viscosity of the layers. Goguel (1948) and, more recently, Ramberg (1960) have analyzed this problem theoretically. Using a simplified model of a single buckled plate in a medium of lower viscosity, Ramberg found that the initial wave length or length of arc, λ, measured *in* the folded surface would be determined by the relation:

$$\lambda = 2\pi h \left(\frac{2\mu_1}{3\mu_2}\right)^{1/3}$$

where h is half the plate thickness, and μ_1 and μ_2 are the viscosities of the plate and enclosing medium respectively. In effect, this relation states that the length of arc of folds varies directly with the thickness of the stiff layer and a function of the ratio of viscosities and is independent of the rate of strain. It is interesting to note that only the relative viscosities and not their absolute values enter this relation. One can expect, therefore, the same fold dimensions in deformed experimental materials as in actual rocks, provided the ratio of viscosities is the same, and corrections for the short time and small dimensions of the model are unnecessary in Ramberg's formula.

TABLE 1.—EXPERIMENTAL VALUES OF PARAMETERS IN RAMBERG'S (1960) EQUATION RELATED TO CALCULATED AND OBSERVED LENGTH OF ARC OF FOLDS

h mm	μ_1 (poises)	μ_2 (poises)	rate (mm/hr.)	λ mm calc.	λ mm obs.
5	1×10^8	5×10^5	57	160	50
15	1×10^8	5×10^5	57	481	320
5	1×10^8	5×10^4	57	345	60
15	1×10^8	5×10^4	57	1035	380
5	1×10^8	5×10^5	7	160	8
15	1×10^8	5×10^5	7	481	*
5	1×10^8	5×10^4	7	345	36
15	1×10^8	5×10^4	7	1035	*

* No folding

In order to test the effects of varying the thickness, relative viscosities, and rate of strain, single layers of asphalt were placed vertically in a uniform medium of lower viscosity and compressed in the direction of their longest dimension. Successive tests were run with different combinations of thick or thin layers of asphalt in low- or high-viscosity wax at fast and slow rates of deformation. Results of eight of these tests are tabulated in Table 1.

Increase in the thickness of the resistant layer and the ratio of viscosities causes an increased length of fold arc, as Goguel and Ramberg predicted. Although the measured lengths of arc differ from those predicted mathematically, they are of the same order of magnitude and vary in the same direction. Effects of pre-existing irregularities in the layers and the inhomogeneous nature of the strain may account for some of the difference between the measured and calculated values, but it appears that the formula of Ramberg, which is necessarily based on several assumptions and simplifica-

PLATE 2. EXPERIMENTAL RESULTS

Figure 1. Result of deforming vertical layers by compression parallel to the layers (Case III)

Figure 2. Weak axial-plane parting in wax layers from same deformation

Figure 3. Result of deforming block sketched in Figure 2. Wax layers have been removed to show the asphalt skeleton of the block. A small glass rod lies along the horizontal trace of the plane normal to the direction of compression, and the steel rod is nearly coincident with the axis of the original folds. Note that folds and wrinkles produced by the deformation are not restricted to previously planar surfaces but also wrap around hinge areas of the original folds (left of knife and in extreme upper left).

tions, is inexact. (Goguel, after considering the problem in more detail, concluded that a single, precise equation cannot be written.)

At slow rates of strain no folding occurred in the thick asphalt layer, and only minor, small-scale wrinkling was produced in a thinner layer. In these cases it appeared that the rate of compression was too low to produce folding, and we concluded that the asphalt was able to take up the strain by viscous flow without buckling. These limited tests suggest that the rate of strain must be great enough to produce a stress in the resistant layer greater than some critical-strength value at which failure by buckling occurs. This value would probably be a function of the viscosity, thickness, and inclination of the layer, as well as of the confining pressure of the surrounding medium.

The fact that rocks are buckled in nature suggests that the rate of deformation exceeded the limits of viscous flow and might offer a means of estimating a minimum rate of deformation that is required in this type of folding.

Conclusions

We believe the experiments warrant the following conclusions:

(1) The orientation of linear features and fold axes produced by deformation of viscous materials is determined by the intersection of the layered surface and a plane normal to the direction of maximum shortening and is independent of the orientation of the minimum and intermediate bulk strain axes. Large components of strain are possible in the direction of fold axes.

(2) The size of folds is a function of the relative viscosities and thickness of layers. Before folding will occur, the rate of strain must exceed a certain minimum value. At slower rates, no folding occurs, and strain is expressed only by thickening and elongation of the layers.

Acknowledgments

We thank L. E. Weiss for many stimulating discussions of fold tectonics related to these experiments and for his critical comments on the manuscript. Many associates in the Geology Department of the University of California gave material assistance which expedited the work. Viscosity measurements were made under the direction of C. Monismith at the Asphalt Products Laboratory, Richmond Field Station of the University of California.

References Cited

Bucher, W. H., 1956, Role of gravity in orogenesis: Geol. Soc. America Bull., v. 67, p. 1295–1313

Cloos, E., 1946, Lineation: Geol. Soc. America Mem. 18, 122 p.

Goguel, 1948, Introduction a l'étude mécanique des déformations de l'écorce terrestre: Mem. Serv. Corte Géol. France, 530 p.

Hubbert, M. K., 1937, Theory of scale models as applied to the study of geologic structures: Geol. Soc. America Bull., v. 48, p. 1459–1520

Ramberg, H., 1960, Relationships between length of arc and thickness of ptygmatically folded veins: Am. Jour. Sci., v. 258, p. 36–46

Sander, B., 1926, Rückblick auf die Entwicklung einiger Begriffe der neuren Gesteinskunde: Geol. Archiv. Jahrg., v. 4, p. 141–150

Dept. Geology, Univ. California, Berkeley, Calif.
Manuscript Received by the Secretary of the Society, June 20, 1960